Univerzita Karlova v Praze

1. lékařská fakulta

Studijní program: Biomedicína

Studijní obor: Imunologie

RNDr. Jan Svoboda

NK buňky a jejich receptory v imunitní regulaci – možné cíle pro imunomodulaci

NK cells and their receptors in immune regulation – possible targets for immunomodulation

Dizertační práce
(zkrácená)

Ph.D. dissertation thesis

Vedoucí závěrečné práce/školitel: MUDr. Anna Fišerová, CSc.

Praha, 2013

Prohlášení:

Prohlašuji, že jsem závěrečnou práci zpracoval samostatně a že jsem řádně uvedl a citoval všechny použité prameny a literaturu. Současně prohlašuji, že práce nebyla využita k získání jiného nebo stejného titulu

Souhlasím s trvalým uložením elektronické verze mé práce v databázi systému meziuniverzitního projektu Theses.cz za účelem soustavné kontroly podobnosti kvalifikačních prací.

V Praze, Jan Svoboda

Podpis

Poděkování:

Chtěl bych poděkovat své školitelce MUDr. Anně Fišerové, CSc. za odborné vedení mé práce a dobré pracovní podmínky při jejím vypracování a za psychickou i profesionální podporu po celou dobu mého studia. Dále bych chtěl poděkovat všem kolegům z Laboratoře Přirozené Imunity za příjemné pracovní prostředí a atmosféru, odbornou i neodbornou pomoc po celou dobu mé práce a v neposlední řadě Prof. RNDr. Blance Říhové, DrSc. a RNDr. Martinu Bilejovi, DrSc. za umožnění pokračování mého postgraduálního studia ve složité osobní i profesionální situaci.

Identifikační záznam:

SVOBODA, Jan. *NK buňky a jejich receptory v imunitní regulaci – možné cíle pro imunomodulaci.[NK cells and their receptors in immune regulation – possible targets for immunomodulation]*.Praha, 2013. 45 s., 7 příl. v textu, Dizertační práce (PhD.), zkrácená. Univerzita Karlova v Praze, 1. lékařská fakulta, 1. LF UK 2008.Vedoucí práce: MUDr. Anna Fišerová, CSc.

Klíčová slova:

Imunomodulace, NK buňky, receptory, cytotoxicita, efektorová funkce, průtoková cytometrie

Immunomodulation, NK cells, receptors, cytotoxicity, effector function, flow cytometry

Contents

Introduction

NK cells

Natural killer (NK) cells are a subset of leucocytes, which is capable of direct target cell lysis without the need of previous activation. Despite the fact that NK cells are primarily known to serve as the first line of defense against virus–infected (reviewed in (1)) and malignant transformed cells (reviewed in (2)), they are also known to be able to recruit non–specific lineages of cells (neutrophils, macrophages), activate dendritic cells (DCs) (3), prime adaptive lymphocytes (T and B cells) (4, 5) and secrete cytokines (6). *Malhotra et al.* further review the NK cell cross–talk with other cell populations as an important mechanism for therapeutic implications, like during viral infections, autoimmunity or tumor therapy (5). It was also reported, that NK cells stimulated with recombinant IL–2, poly (I:C), *Trypanosoma cruzi* infection or certain tumor cell lines are able to up–regulate IgG2a levels (7-9) produced by B cells. Aside from viral infection and malignant transformation, NK cells were also reported to play important roles in autoimmunity (10, 11), pregnancy (12), transplantation immunology (13) and microbial infection clearance (14). Such a wide spectrum of processes in which NK cells are involved implies even wider range of effector functions NK cells are able to perform and specific subpopulations into which they can differentiate.

NK cell subpopulations

In humans, there are two major NK cell subpopulations present in the peripheral blood, based on the presence and the expression level of two specific surface markers – CD56 and CD16. Low CD56 expressing NK cells, termed $CD56^{dim}$ (CD16+) have high cytotoxic capability and are prevalent in peripheral blood, while the high–density CD56 ($CD56^{bright}$ – comprising approximately 1% of peripheral blood lymphocytes (CD16-)) have only marginal cytotoxic activity, and produce high amounts of IFNγ and TNFα (reviewed in (15)). In addition, these two subpopulations differ in the expression of over 400 other gene transcripts (16).

Murine NK cells lack the expression of CD56 or other ortholog, but based on the expression of CD27, it is believed to distinguish the cytokine producer (CD27+) and cytotoxic NK cell subpopulations in mice (17, 18) as well, despite this division is not as clear–cut as in humans. Murine NK cells express CD49b, which could also be used to define NK cell populations in mice (15), and more recently a more suitable marker, NKp46, was described (19). The prototype murine NK cell marker NK1.1, which was frequently used in the past to define NK cells, is not even detectable on many murine strains due to the distinct allele expression in these strains (20). Nevertheless, only two distinct NK cell populations are not enough to describe all the various effector functions exerted by NK cells. Thus the wide array of responses to outer stimuli must be established by the numerous NK cell receptors signaling pathways.

NK cell receptors

Unlike T or B cells, NK cells do not express clonally distributed receptor for antigen (6, 21). Instead, they are believed to act upon weighing the balance of many different inputs before they decide whether to kill a target (22, 23). To understand this moment of decision, one must realize that there are many different receptors on the surface of NK cells – some deliver activating and others inhibiting signals, while some may deliver both, depending on the circumstances and on the activation state of the cell (24). Inhibitory receptors are usually determined by the presence of immunoreceptor tyrosine–based inhibition motif (ITIM) sequence in their cytoplasmic tail, which recruits protein tyrosine phosphatase SHP–1 (25). It was proposed by Ljunggren and Kärre that the expression of self MHC molecules protects healthy cells from NK cell lysis and its absence or aberrant expression promotes the NK cell–mediated cytotoxicity (26). Thus malignant or virus–infected cells, which try to evade the T–cell recognition via MHC are attacked by NK cells (27). This would imply, that there has to be an "on" signal, whenever NK cells interact with a potential target (28). Activating receptors lack the ITIM sequence and rather associate via charged residue in the cytoplasmic tail with adaptor proteins (23). These proteins contain activation motifs (ITAMs) and are able to recruit protein tyrosine kinases and subsequently activate transcription (24).

Activating NK cell receptors

Activating NK cell receptors have no means of transducing the outer signal into the cell and instead associate with adaptor proteins. The family of transmembrane adaptor proteins that contains ITAMs includes CD3γ, CD3δ, CD3ε, ζ, Igα, Igβ, FcεRIγ and DAP12 (29). They are all characterized by a small extracellular region, an aspartic acid (D) in the transmembrane segment and a cytoplasmic domain that contains one or more ITAMs. The acidic amino acid in the transmembrane region is required for association of these proteins with their ligand–binding receptor subunit, which typically has a basic amino acid (arginine or lysine) in its transmembrane region. When these receptor complexes engage their ligands, the tyrosines in the ITAM are phosphorylated–often by Src family kinases–which, in turn, results in recruitment through SH2–domain binding and activation of the Syk or ZAP–70 cytoplasmic tyrosine kinases (23). These events represent the immediate and proximal signals that ultimately result in cellular activation.

NK cells express three of the ITAM–bearing transmembrane adaptor proteins: ζ, FcεRIγ and DAP12. In NK cells, ζ and FcεRIγ are present as either disulfide–bonded homodimers or heterodimers (30), whereas DAP12 is exclusively a disulfide–bonded homodimer (31). On NK cells, FcεRIγ and ζ associate with CD16, the low affinity Fc receptor for IgG which is responsible for antibody–dependent cellular cytotoxicity (ADCC) (23). Cross–linking CD16 on NK cells results in: the association of the receptor complex with the $p56^{lck}$ tyrosine kinase; tyrosine phosphorylation of FcεRIγ and ζ; the activation of Syk and ZAP–70 (both of which are expressed by NK cells); the induction of phospholipase C1γ tyrosine phosphorylation; and the activation of phosphatidylinositol–3 kinase (PI3K), mitogen–activated protein kinase (MAPK),

p21^{ras}, nuclear factor Atp (NFATp) and NFATc (reviewed in (32)). Signaling via CD16 causes degranulation and cytokine production (33) but may also lead to apoptosis in NK cells (34). NK cells in FcεRIγ–deficient mice do not mediate ADCC (35) and these mice were unable to reject melanoma cells in the presence of antibodies that provided anti–tumor protection in wild–type mice (36). In mice, CD16 associates with FcεRIγ but not ζ, whereas in humans FcεRIγ and ζ are both able to pair with CD16 (23). Although immune receptors that signal through ITAM are the best characterized, there are alternative pathways also implicated in NK cell and T cell stimulation, which include the activation of PI3K. Previous studies have indicated that a Ras-independent, PI3K pathway may be critically involved in NK cell−mediated cytotoxicity (37). This raises the question of which NK cell receptors are linked to PI3K activation. A strong candidate is the DAP10 transmembrane adaptor protein, which is associated with the NKG2D receptor (38). Like the ITAM–containing adaptors, DAP10 has a small extracellular region, a transmembrane domain that contains an acidic amino acid and a cytoplasmic domain that is responsible for signal transduction. Instead of an ITAM, DAP10 contains the sequence YINM, which fits the consensus motif for binding the p85 subunit of PI3K (23). Ligation of the NKG2D–DAP10 receptor complex on NK cells triggers cell–mediated cytotoxicity (39) and can augment cytokine production initiated by signaling *via* the DAP12–associated receptors (31). Other adaptor molecules and receptors associating with these proteins are listed in Table 1.

Table 1: **NK cell activation receptors and ligands**					
Gene	***Known as***	***Species***	***Structure***	***Signaling***	***Ligand***
Klra4	Ly49D	Mouse	C-lectin homodimer	DAP12	H2-D^{d}
Klra8	Ly49H	Mouse	C-lectin homodimer	DAP12	MCMV m157
Klra16	Ly49P	Mouse	C-lectin homodimer	DAP12	MCMV?
Klrb1c	NKR-P1C, NK1.1	Mouse	C-lectin homodimer	FcεRIγ	?
Klrb1f	NKR-P1F	Mouse	C-lectin homodimer	FcεRIγ?	Clr–g
Pilrb1	PILRβ	Mouse	Ig monomer	DAP12	CD99
CD244	2B4	Mouse, Human	Ig monomer	ITSM, SAP	CD48
KLRD1-KLRC2	CD94-NKG2C (CD159c)	Mouse, Human	C-lectin homodimer	DAP12	Mouse Qa1^{b}, human HLA-E
KLRK1	NKG2D, CD314	Mouse, Human	C-lectin homodimer	Mouse DAP10 or DAP12, human DAP10	Mouse Rae-1, H60, MULT1 human MICA, MICB, ULBP1-4
KLRF1	NKp80, CLEC5C	Human	C-lectin homodimer	?	AICL
KIR2DS1	CD158h	Human	Ig monomer	DAP12	HLA-C N77/K80
KIR2DS2	CD158j	Human	Ig monomer	DAP12	HLA-C1 family
KIR2DS4	CD158i	Human	Ig monomer	DAP12	HLA-Cw4
KIR3DS1	CD158e2	Human	Ig monomer	DAP12	HLA-Bw4
KIR2DL4	CD158d	Human	Ig monomer	FcεRIγ	HLA-G
NCR1	NKp46, CD335	Mouse, Human	Ig monomer	FcεRIγ, CD3ζ	heparan sulfate
NCR2	NKp44, CD336	Human	Ig monomer	DAP12	PCNA - Proliferating Cell Nuclear Antigen
NCR3	NKp30, 1C7, CD337	Human	Ig monomer	FcεRIγ, CD3ζ	B7-H6
FCGR3	CD16	Mouse, Human	Ig monomer	Mouse FcεRIγ, human FcεRIγ or CD3ζ	IgG
CD226	DNAM-1, TLisa1	Mouse, Human	Ig monomer	Protein kinase C	CD112, CD155
SLAMF7	CRACC, CD319	Human	Ig monomer	ITSM, EAT2	CRACC
SLAMF6	NTB-A	Human	Ig monomer	ITSM, SAP, EAT2	NTB-A

Inhibitory NK cell receptors

Two types of inhibitory processes regulate cellular activation by ITAM–coupled receptors. The first of these is mediated by members of the C–terminal Src kinase (Csk) family, which phosphorylate the tyrosine residue at the C–terminus of Src family kinases (SFKs), thereby enabling an intramolecular association that suppresses SFK activity (40). The second mechanism is mediated by immunoreceptor tyrosine–based inhibitory motif (ITIM)–containing inhibitory receptors (41). The inhibition requires phosphorylation of ITIM tyrosine residues, which enables recruitment and activation of SH2 domain–containing inositol and tyrosine phosphatases that, upon binding, interfere with signaling by ITAM–coupled receptors. However, the precise phosphorylation events for which SFKs are required are not known (42).

Despite the structural differences between the human KIR, human CD94/NKG2A, and mouse Ly49 receptors, all NK cell inhibitory receptors appear to use a common strategy to inhibit effector activation. The unifying characteristic is the presence of ITIM sequences in the cytoplasmic domain of these receptors that upon tyrosine phosphorylation are able to recruit SHP–1, and possibly SHP–2, to mediate the inhibitory function (reviewed in (43)). The precise sequence of biochemical events may involve Src family kinases, phosphorylating the C–terminal ITIM, thereby enabling phosphorylation of the N–terminal ITIM, which was described recently in the case of platelet endothelial cell adhesion molecule 1 (PECAM–1) (41). KIR, Ly49, and CD94/NKG2A receptors regulate not only cytotoxicity but can also inhibit cytokine production by T and NK cells (44).

NK cell stimulation induced by exposure to NK–sensitive target cells or by ADCC via CD16 results in the immediate activation of tyrosine kinases, PLC–γ induced generation of phosphoinositides, and increases in intracellular Ca^{2+} levels (45). If KIR are engaged either by their natural class I ligands on the potential target cells or by agonistic anti–KIR mAb, the tyrosine residues in the ITIM (I/VxYxxL/V) are phosphorylated, possibly by *src* family kinases, and SHP–1 is recruited to the receptor complex (reviewed in (45, 46)). In NK cell–mediated cytotoxicity against EBV–transformed B lymphoblastoid cell lines, Valiante *et al*. (47) have shown that recognition of an appropriate HLA allotype on the target cells prevents the generation of inositol 1,4,5–trisphosphate and intracellular Ca^{2+} elevations. However, KIR ligation did not affect phosphorylation of PLC1–γ or PLC2–γ but apparently inhibited activation by preventing the association of an adapter protein, pp36, with PLC–γ or Grb2. In this experimental system, pp36 might be the critical substrate for activated SHP–1 that is recruited by the phosphorylated ITIM in the KIR cytoplasmic domain. By contrast, when NK cells are stimulated via CD16 to trigger ADCC, activation of KIR or the CD94/NKG2A receptor inhibits phosphorylation of PLC–γ, ζ chain, and the protein tyrosine kinase ZAP70 (48). Nonetheless, the critical event in all of these pathways is the recruitment and enzymatic activity of the tyrosine phosphatase, SHP–1. NK cells transfected with enzymatically inactive SHP–1 mutant are unable to transmit negative signals via KIR (49). Similarly, SHP–1 mutant mice demonstrate defects in Ly49A receptor signaling, although inhibitory function is not completely absent, suggesting a potential role for

other phosphatases, possibly SHP–2 (50). SHIP, a polyphosphate inositol 5–phosphatase implicated in the inhibitory function of FcγRIIB (51), does not appear to participate in KIR–induced negative signaling (52). Receptors containing ITIM sequence are listed in Table 2.

Table 2: **NK cell inhibitory receptors and ligands**					
Gene	***Known as***	***Species***	***Structure***	***Signaling***	***Ligand***
Klra1	Ly49a	Mouse	C-lectin homodimer	1 ITIM	H2-D^d , -D^k
Klra3	Ly49c	Mouse	C-lectin homodimer	1 ITIM	H2-K^b , -K^d , -D^d, -D^k
Klra5	Ly49e	Mouse	C-lectin homodimer	1 ITIM	?
Klra6	Ly49f	Mouse	C-lectin homodimer	1 ITIM	$H2^d$
Klra7	Ly49g	Mouse	C-lectin homodimer	1 ITIM	H2-D^d
Klra9	Ly49i	Mouse	C-lectin homodimer	1 ITIM	H2-D^k
Klrb1a	NKR-P1A	Mouse	C-lectin homodimer	1 ITIM	?
Klrb1b	NKR-P1B	Mouse	C-lectin homodimer	1 ITIM	Ocil (Clrb)
Lilrb4	gp49b1	Mouse	Ig monomer	2 ITIM	αv β3
Pilra	PILRA	Mouse	Ig monomer	1 ITIM	CD99
CD244	2B4	Mouse, human	Ig monomer	0 ITIM (4 ITSM)	CD48
KLRG1	Mafa	Mouse, human	C-lectin homodimer	1 ITIM	E-, N-, R-cadherin
KLRD1-KLRC1	CD94-NKG2A (CD159a)	Mouse, human	C-lectin heterodimer	1 ITIM	Mouse $Qa1^b$, Human HLA-E
LAIR1	LAIR-1, CD305	Mouse, human	Ig monomer	2 ITIM	Collagen
KLRB1	NKR-P1A, CD161	Human	C-lectin homodimer	1 ITIM	LLT1 (OCIL, CLEC2D)
LILRB1	ILT2, LIR1, CD85j	Human	Ig monomer	4 ITIM	HLA class I
KIR2DL3	CD158b2	Human	Ig monomer	2 ITIM	HLA-C S77/N80
KIR2DL2	CD158b1	Human	Ig monomer	2 ITIM	HLA-C S77/N80
KIR2DL1	CD158b	Human	Ig monomer	2 ITIM	HLA-C N77/K80
KIR3DL1	CD158e1	Human	Ig monomer	2 ITIM	HLA-Bw4
KIR2DL5A KIR2DL5b	CD158f	Human	Ig monomer	2 ITIM	?
KIR3DL2	CD158k	Human	Ig homodimer	2 ITIM	HLA-A3, HLA-A11
CEACAM1	CD66a	Human	Ig monomer	2 ITIM	CD66
SIGLEC7	CDw328, p75	Human	Ig monomer	1 ITIM	α-2,8 disialic acid

Target structures recognized by NK cells

NK cell receptors are able to respond to great numbers of target structures which are either directly associated with given pathogen infected or transformed cell, or indirectly by co–stimulation by cell population recognizing and presenting the pathogen–associated structure. Since NK cells are primarily designed to destroy malignant, infected, transformed or stress–damaged cells, they seldom recognize the exogenous pathogens themselves. While they can be directly activated by virus–derived proteins via their NKp (53) or Ly49H receptors (54), it only occurs when these proteins are expressed on the surface of the infected cell. As of yet, little conclusive evidence was presented to suggest direct NK cell activation by bacteria, or protozoan parasites (reviewed in (14)). Despite their inability to recognize such pathogens directly, NK cells still play critical role in their clearance. Indirect activation of NK cells by bacteria is well–documented in numerous bacterial models and generally requires TLR–mediated activation of mDCs and monocytes or macrophages to secrete IL–12, IL–18 and type–1 interferons (55). More recent studies also pointed to the necessity of direct DC–NK cell contact for activation of effector function (56), suggesting DC–mediated antigen presentation and recognition by NK cells.

Classical MHC class I glycoproteins

Primarily, NK cells are well equipped to recognize classical MHC class I molecules on the target cell surface and if those are presented in sufficient amount, they attenuate the NK cell activation potential. This inhibition of NK cell function can nevertheless be overcome when multiple activating receptors are engaged simultaneously (57) or when a sufficiently potent activating receptor is stimulated (58). Thus MHC–I inhibitory receptors rather dampen, than completely terminate NK cell function, pointing to a more analogue, not binary process of signal interpretation (59). While classical MHC–I glycoproteins are the main ligands of inhibitory NK cell receptors (lectin–like Ly49 in mice and Ig–like KIRs in humans), several activating isoforms of these receptors exist in both species. The most notable are the mouse Ly49D and human KIR2DS or KIR3DS molecules, that bind MHC I with much weaker affinity, despite having very high sequential homology to their inhibitory counterparts (59). Another KIR molecule with activating capabilities is KIR2DL4, which is shared by all haplotypes (59). It is the most distinct gene in the KIR family, since it associates with the activating FcεRIγ adaptor protein while having a functional ITIM in its cytoplasmic domain (60). Despite the ITIM presence, mAb cross–linking of KIR2DL4 induces IFNγ production by resting NK cells and cytotoxicity and IFNγ production in IL–2 activated NK cells (61, 62).

Non–classical MHC class I glycoproteins

Human HLA–E and mouse $Qa1^b$ belong to the nonconventional MHC class Ib family and are recognized by the lectin–like CD94/NKG2 receptors in both humans and mice (63-65).

Unlike in the case of Ly49 and KIR, the CD94/NKG2 receptors do not demonstrate high polymorphism, probably due to their ligands little allelic variation (59). Non–classical MHC–I receptors also have activating (CD94/NKG2C or NKG2E) (66) and inhibitory (CD94/NKGA) isoforms (67) and usually are present in the form of heterodimers, since CD94 alone lacks a signal–transducing cytoplasmic domain. The question then is why activating and inhibitory receptors both seemingly bind the same ligands. As with KIR and Ly49, the inhibitory CD94/NKG2A binds the ligand with higher affinity than the activating CD94/NKG2C and the peptides bound to HLA–E or $Qa1^b$ can differentially affect their recognition (68). Since HLA–E and $Qa1^b$ bind most abundantly the leading peptides provided by HLA–A, –B, –C, –G or H–2 respectively (69), the CD94/NKG2 receptors are, through HLA–E or $Qa1^b$, able to monitor the status of classical MHC class I glycoproteins in the target cell.

MHC class I–related ligands

NKG2D, the lectin–like receptor of NK cells, recognizes cell surface MHC–I–related glycoproteins, and is encoded in NKC (NK cell receptor complex) domain. It is a type II activating homodimeric receptor highly conserved in mice or in humans (70, 71). Among others, it binds the stress–inducible proteins MICA, MICB and ULBP in humans and Rae–1 and H60 in mice (reviewed in (59)). Despite very low sequential homology between MIC and ULPB or Rae–1 and H60, these ligands all bind with high affinity to NKG2D. They are often appearing on the cell surface under stress conditions evoked by cancer transformation or viral infection, but there were also reports of CMV and tumor immune–escape strategies, involving these ligands retention or shedding (72, 73). Several of these ligands were also reported to be increasingly expressed in tumor cells subjected to heat shock or ionizing radiation (74), thus increasing the tumor immunogenicity. Heat shock protein 70 (Hsp70) was also reported to be involved in increased NKG2D ligand expression (75), pointing to important role of this receptor in heat–induced cell stress. Although NKG2D–mediated responses are beneficial in immune responses against tumors and pathogens, evidence was provided that this system may also be deleterious by contributing to autoimmunity. In humans, MICA has been detected on synoviocytes in the joints of patients with rheumatoid arthritis, accompanied by the presence of an unusual subset of $CD4^+$ T cells that lack CD28 but express NKG2D (76).

Endogenous MHC non–related ligands

Clr or C–type lectin–like receptor related glycoproteins, are a family of proteins encoded by the NK cell receptor complex genes localized between mouse *Nkr–p1a* and *Cd69* (77). Clr–b, which is expressed on the surface of virtually all hematopoietic cells (78), is recognized by the inhibitory lectin–like receptor NKR–P1D in mice and renders the target cell resistant to NK–cell mediated lysis (79). With the exception of Clr–g, which is expressed preferentially on the surface of activated NK cells and is recognized by the activating NKR–P1F, no other members of the Clr

family as of yet have been linked to their putative NKR–P1 receptors in mice (77). As only one *Nkr–p1* gene exists in humans, only one mouse *Clr* ortholog exists: LLT1. It is being transcribed by human NK cells and it was confirmed to bind to the single human NKR–P1A (59, 80, 81). The ligands of the activating members of the murine NKR–P1 family (e.g. NKR–P1A and C) of Clr remain to be identified, since these receptors show a high activation potential (82).

Endogenous adenosine

Adenosine, produced in high amounts in hypoxic tissue such as in tumor sites, is an endogenous modulator of innate immune system and is being recognized by many cell types, including NK cells (reviewed in (83)). Adenosine receptors (AR) A_1, A_{2A}, A_{2B} and A_3, vary in the nature of the transmitted signal and the resulting effector reaction. While A_{2A} adenosine receptor was reported to inhibit the cytotoxicity of activated NK cells (84) upon its agonist binding, A3 increased the synthesis of IL–12 in the tumor microenvironment, stimulating the NK cell activity and IFNγ production (85). Activation of the A_{2A}AR also results in inhibition of the immune response to tumors via suppression of T regulatory cell function and inhibition of natural killer cell cytotoxicity and tumor–specific CD4+/CD8+ activity. Therefore, it is suggested that pharmacological inhibition of A_{2A}AR activation by specific antagonists may enhance immunotherapeutics in cancer therapy as well as its stimulation by agonists could be used in transplantation immunology. Therefore, the inhibitory and stimulatory action of adenosine on NK cells depends on its binding to the different types of adenosine receptors and specific receptor agonists need to be designed (83). In addition, such compound's effect universality needs to be confirmed, since different species may react in different ways to a specific receptor agonist.

NK cell–based immunotherapeutic approaches

NK cells are involved in almost all aspects of immune response – aside from viral infection and malignant transformation in autoimmunity (10, 11), pregnancy (12) and transplantation immunology (13) not only by their cytotoxic effector function, but also as powerful cytokine producers. This makes NK cells excellent candidates for immune modulation and vaccine development (86). Among such development belong the recently emerging synthetic carbohydrate–based vaccines (87), which use multivalent glycans as mimetics of common antigens in a diverse set of pathologies (reviewed in (88)). Aberrant glycosylation with branched *N*–Acetyl–glucosamine (GlcNAc) subunits, among others, was also associated with ongoing oncogenesis and metastatic potential (reviewed in (89)). Tumor associated carbohydrate antigens (TACAs) are overexpressed on a variety of cancer cell surfaces, which present tempting targets for anticancer vaccine development. The local density of antigen rather than the total amount of antigen administered was found to be crucial for induction of high Tn antigen (*N*-acetyl-galactosamine-serin-threonine)–specific IgG titers (90). Globo H (GH), for instance, is a hexasaccharide specifically overexpressed on a variety of cancer cells and therefore, a good

candidate for cancer vaccine development (91). Glucosamine oligosaccharides corresponding to fragments of the bacterial surface poly–*N*–Acetyl–glucosamine were also previously synthesized to mimic the bacterial antigen (92) as well as other, dendrimeric GlcNAc structures (93). Saccharide structures are also emerging to be useful targeting tools to affect only selected tissues or cell subpopulations (94), or as anti–pathogenic structures (95). Multivalency plays a major role in biological processes and particularly in the relationship between pathogenic microorganisms and their host that involves protein–glycan recognition. These interactions occur during the first steps of infection, for specific recognition between host and bacteria, but also at different stages of the immune response. The search for high–affinity ligands for studying such interactions involves the combination of carbohydrate head groups with different scaffolds and linkers, generating multivalent glycocompounds with controlled spatial and topology parameters. By interfering with pathogen adhesion, such glycocompounds, including glycopolymers, glycoclusters, glyconanoparticles and glycodendrimers have the potential to improve or replace antibiotic treatments that are now being subverted by resistance. Bacteria present on their surfaces natural multivalent glycoconjugates such as lipopolysaccharides and S-layers that can also be exploited or targeted in anti–infectious strategies. Multivalent glycoconjugates have also been used for stimulating the innate and adaptive immune systems, for example with carbohydrate–based vaccines.

As the understanding of the molecular mechanisms involved in NK cell activation and effector function grows, the expectations concerning NK cell–based immunotherapeutic approaches (*in vivo* modulation of NK cell activity, purification/expansion, adoptive transfer) increase (96). As shown earlier, determination of the NK cell numbers in the periphery or in the affected tissue is not as reliable a marker for disease progression or immune response, as when assessing the NK cell activation and differentiation state markers (97). Thus, the levels of expression for different activating and inhibitory receptors from NKR–P1, NKG2, KIR families, and others are being determined in order to ascertain the effect of diverse mediators (neurotransmitter, purine nucleotides, and hormones) on NK cells function (97).

Aims

The goal of this work was to provide new insights and applications for NK cell–mediated immune modulation and on the receptors involved in these processes. Such data can provide the basis for more precise and balanced strategies of immune response alteration toward the desired effects. In order to provide such tool, it was first needed to study the receptors and their isoforms involved in both activation and inhibition of NK cell effector function upon stimulation – which are involved in direct cytotoxicity triggering and which tend to polarize the target cells toward cytokine production. It was also necessary to study the possible mediators and receptor ligands and whether they exert the same effect in different species, since many human immune disorders are studied in animal models. Thus, we focused at the following points:

- Analyze the involvement of NKR-P1 receptor recognition systems in human autoimmune disorders and mouse tumor models employing synthetic glycan mimetics.
- Study the involvement of KIR2DL4 receptor in hormonal ovarian hyperstimulation protocol in assisted reproduction and its effect on the implantation rate.
- Determine the role of adenosine receptors in various species in antitumor immune response.
- Evaluation of therapeutic implication of local hyperthermia on NK cell effector function in cancer models and the establishing of versatile targeting platform using ferritin nanoparticles.

Publication 1: CD161 is involved in NK cell cytotoxicity downmodulation in response to glycan mimetic and vimentin in human autoimmunity.

Overview

Innate immunity is likely to play a critical role in the development and regulation of autoimmunity. The cell populations and receptors involved in various autoimmune diseases may vary significantly and a more general approach should be devised in order to influence the involved processes. Rheumatoid arthritis (RA) is a chronic inflammatory disease mediated by the activation of T cells, which leads to the activation of macrophages and subsequent production of proinflammatory cytokines, resulting in the destruction of cartilage and bone tissue. The related production of proteinases, which degrade collagen and proteoglycans, further compromises the immune system by the release of carbohydrate and other autoantigens. Alterations in N–glycan branching and the presence of endogenous glycan–specific autoantibodies is associated with autoimmune disorders (98). Since NK cells are key players in innate immunity which are able to influence the components of adaptive cellular response, their activity and involvement in autoimmune processes needs to be evaluated. CD161 (human NKR–P1A) is a bifunctional lectin–like receptor on the surface of NK cells, which was primarily designated in humans as an activating receptor (99), and is now being reported to have inhibitory functions (80).

Aims and methods

In this study, we investigated the mechanisms of NK cell functional impairment, which was described previously in systemic autoimmune diseases (100). We focused on the involvement of CD161 in this process, specifically on its response to synthetic saccharide mimetic, octavalent *N*–acetyl–β–D–glucosamine–terminated dendrimer (GN8P) and endogenous RA–specific marker, mutated citrullinated vimentin (MCV). Patients with RA, polymyositis (PM) and dermatomyositis (DM) were compared to patients with osteoarthritis (OA) and healthy donors.

Results and discussion

Here we confirmed the highly significant impairment of NK–mediated cytotoxicity in patients with autoimmune disorders (RA, PM, DM) compared to healthy donors or patients with OA. This impairment was accompanied with only slight decrease in the number of cytotoxic ($CD56^{dim}$) NK cell subpopulation. Thus, we tested the NK cell activity after 30–minute preincubation with the synthetic GN8P. We found that NK cells were divided into two groups – either they were unaffected by the GN8P glycomimetic, or their activity was impaired by the preincubation. The GN8P–inhibited group exerted significantly higher expression of CD161 on $CD56^{dim}$ NK cells in both HD and RA patient groups. When we assessed the CD161 expression

on the mRNA level, RA patients had significantly more CD161–mRNA, which further increased after incubation with MCV.

We can thus conclude that there is a subset of NK cells (~50%), which react to GN8P glycomimetic by impaired cytotoxic effector function and this subpopulation can be identified by the elevated amount of CD161 expression. This expression can be further increased by MCV in both RA patients and in healthy donors, pointing to a more universal effect of MCV. In addition, these results make us believe, that the impaired NK cell cytotoxicity in autoimmune patients is caused by ligand binding to CD161, which is in accordance with the findings of Rosen et al. (80).

The effect of synthetic mediators (GN8P) on NK cell activity may not be the same in murine immune models, since rodents express various activating/inhibitory isoforms of NKR–P1 (A, B, C, D, E and F) when compared to single human *Nkr–p1a* gene (101). And since human NKR–P1A (CD161) was reported to have both inhibitory (102) and stimulatory (103, 104) properties it was needed to further confirm, whether the same GN8P–mediated inhibitory effect will be observed in mice with various isoforms of NKR–P1.

Clinical Immunology (2010) **136**, 139–147

available at www.sciencedirect.com

Clinical Immunology

www.elsevier.com/locate/yclim

CD161 receptor participates in both impairing NK cell cytotoxicity and the response to glycans and vimentin in patients with rheumatoid arthritis

J. Richter [a], V. Benson [a], V. Grobarova [a], J. Svoboda [a], J. Vencovsky [b], R. Svobodova [b], A. Fiserova [a,*]

[a] *Laboratory of Natural Cell Immunity, Section of Immunology and Gnotobiology, Institute of Microbiology, Videnska 1083, 14220 Prague 4, Czech Republic*
[b] *Institute of Rheumatology, Na Slupi 4, 12850 Prague 2, Czech Republic*

Received 16 December 2009; accepted with revision 10 March 2010
Available online 31 March 2010

KEYWORDS
CD161;
Rheumatoid arthritis;
NK cells;
MCV;
PAD4;
Glycosylation;
MGAT5

Abstract We investigated the role of natural killer (NK) cells and CD161, their primary C-type-lectin-like receptor in rheumatoid arthritis (RA). Samples were compared with healthy donors (HD), dermatomyositic (DM), polymyositic (PM), and osteoarthritic (OA) patients. RA, PM, and DM NK cell cytotoxicities significantly decreased relative to the HD and OA NK cells ($p<0.0001$). These results correlated with an increased expression of NK cell inhibitory receptor CD161, in active disease RA patients. We demonstrated that NK cells are able to respond to mutated citrullinated vimentin (MCV), an RA-specific autoantigen, leading to increases in both PAD4 enzyme and CD161 mRNA expression. MGAT5 glycosidase involvement was detected in GlcNAc metabolism within the synoviocytes of RA patients. Our findings reveal a functional relationship between CD161 expression and NK cell cytotoxicity as well as reactivity to glycans and MCV, thus providing new insight into the pathogenesis of RA and confirming the involvement of surface glycosylation.

Introduction

Rheumatoid arthritis (RA) is a chronic inflammatory disease that affects the synovial tissue in multiple joints. Inflammation in RA and other rheumatoid diseases is mediated by activation of T cells, leading to activation of macrophages and fibroblast-like synoviocytes that subsequently produce proinflammatory cytokines. Synovial tissue proliferation is associated with destruction of cartilage and bone; the closely related production of proteinases (MMPs), which degrade collagen and proteoglycans, serves to further antigenically challenge the immune system [1].

Innate immunity is likely to be of critical importance in the development and regulation of autoimmunity. However, the cells, receptors, and mediators involved in various autoimmune conditions are mostly unknown. Natural killer

* Corresponding author. Laboratory of Natural Cell Immunity, Department of Immunology and Gnotobiology, Institute of Microbiology AS CR v. v. i., Videnska 1083, 14220, Prague 4, Czech Republic. Fax: +420 296 442 106.
E-mail address: fiserova@biomed.cas.cz (A. Fiserova).

1521-6616/$ - see front matter © 2010 Elsevier Inc. All rights reserved.
doi:10.1016/j.clim.2010.03.005

(NK) cells are the key players in innate immunity; in addition to their primary function of killing virally infected or transformed cells, they also assist in the initiation and development of adaptive immune responses by producing cytokines or by direct cell-to-cell interactions. Reduced numbers or impaired functioning of NK cells could lead to the persistence of autoreactive T cells. Therefore, it is important to identify NK cell activity and related molecular events in RA patients. NK cell function is tightly regulated by activating and inhibitory signals that are delivered by a diverse array of cell surface receptors [2]. One important inhibitory receptor on human NK cells is CD161 (NKR-P1A), which belongs to the C-type lectin family that preferentially binds carbohydrate-bearing structures. In a previous study, we determined that CD161 binds to an N-acetylglucosamine (GlcNAc)-containing glycoconjugate [3].One of the described natural glycoprotein ligands of CD161 is LLT1 (osteoclast inhibitory lectin or CLEC2D) that is known to inhibit in vitro osteoclastogenesis [4,5]. LLT1 is present on the surfaces of dendritic and activated B cells, and plays a role in mediating direct interactions between these cells and NK cells [6]. Although previous studies have investigated the role of some CD161 ligands, little is known about the function of the CD161 receptor and its role in autoimmune diseases.

RA is, at least in part, a deregulated glycosylation disease, and cells from patients with the disease display changes in the glycosylation of cartilage and synoviocytes. Changes appear also in the glycosylation or expression of galectins, lectins, acute-phase proteins, IgG, and other unidentified plasma proteins [7–10]. Dense, complex glycan structures are the most abundant and diverse molecules on cell surfaces. The glycoprotein pattern is modified by Golgi-resident glycosyltransferases such as MGAT5, which is required for the generation of N-glycan complexes. These enzymes are regulated and expressed in a tissue-specific manner that enables them to rapidly modify the glycan profile in response to physiological or pathological changes. Alterations in protein N-glycan branching, together with the presence of antibodies that recognize endogenous glycans, is associated with autoimmune disorders [11–13]. MGAT5-deficient mice have increased spontaneous kidney autoimmunity and increased susceptibility to experimental autoimmune encephalomyelitis [14]. Knowledge of Golgi-resident enzymes operating in glycan synthesis pathways could provide further insights into the pathogenesis of autoimmune diseases [15–17].

Currently, the only specific marker for RA is the presence of citrullinated proteins, which are produced in inflamed synovium and function as autoantigens (cit [18,19]). Anti-citrullinated protein antibodies circulating in the peripheral blood of RA patients can serve as highly specific markers for early detection of RA, and can be used to predict disease outcome [20–24]. Proteins are citrullinated by peptidylarginine deiminase enzymes (PADs). PAD2 and PAD4 are predominantly expressed in CD14+ macrophages and, to a lesser extent, in CD56+ cells [25]. Under normal conditions, PAD enzymes are located intracellularly; however, in inflamed synovium, they can leak from damaged cells and become active due to high extracellular Ca^{2+} levels [26].

Although it is known that NK cell-mediated cytotoxicity is downmodulated in systemic rheumatoid diseases [27], the molecular mechanism is not fully understood. Thus, we investigated the NK cell functional impairment that persists even after patients have received classical therapies to treat RA. We focused on the role of NK cells and CD161 in patients with RA, polymyositis (PM) and dermatomyositis (DM), and compared it with their roles in patients with osteoarthritis (OA), and in healthy donors (HD). Specifically, we evaluated saccharide recognition of the CD161 inhibitory receptor using synthetic N-acetyl-β-D-glucosamine-terminated glycoconjugates, as well as the possible interaction between CD161 and modified citrullinated vimentin (MCV).

Patients and methods

Patients and healthy donors

The study population comprised 86 patients (5 men and 81 women) followed by the Institute of Rheumatology in Prague, Czech Republic, and 60 healthy donors (HD, 24 men and 36 women, mean age 46.1 ± 9.2 years) from the Blood Transfusion Department of Thomayer University Hospital in Prague. Patients had the following diagnoses: RA (n = 50, mean age 59.3 ± 10.3 years), OA (n = 19, mean age 66.7 ± 6.3 years), DM (n = 12, mean age 61.4 ± 4.8 years), and PM (n = 5, mean age 60 ± 4.9 years). Patients with DM, or PM were diagnosed using valid criteria including MRI [28–30]. Patients with RA met the 1987 revised criteria of the American College of Rheumatology (ACR) [31]. Patients with OA were diagnosed according to the ACR Subcommittee on Osteoarthritis [32].

Peripheral blood or synovial fluid from patients and healthy donors was drawn after we obtained an informed consent agreement. Therapy involved the use of glucocorticoids, immunosuppressives (cyclosporin A, methotrexate, azathioprine, and leflunomide), TNF antagonists, and non-steroidal anti-inflammatory drugs. To exclude the influence of therapy on the immune parameters that we investigated, four untreated RA patients were also enrolled in the study.

Cell separation and glycoconjugate or vimentin treatment

Citrated blood samples from patients and healthy donors were separated by Ficoll-Hypaque 1077 (Sigma-Aldrich, St. Louis, MO, USA) density centrifugation for 40 min to obtain the peripheral blood mononuclear cell (PBMC) fraction. Synovial fluid including synoviocytes was obtained from patients with RA. Purified human CD56+CD3− NK cells (>98%) were sorted with a FACS Vantage SE (BD Bioscience, Heidelberg, Germany) using antibodies CD3-FITC (Dako, Glostrup, Denmark) and CD56-PE (Immunotech, Marseille, France).

A glycoconjugate–polyamidoamine core with eight terminal *N*-acetyl-β-D-glucosamine moieties (GN8P) was synthesized and kindly provided by Vladimir Kren (Academy of Sciences, Prague, Czech Republic). The synthesis and dose-dependent effects of this glycoconjugate on human PBMCs were described previously [33,34]. Purified NK cells were incubated with GN8P (10 nM), RA-specific autoantigen MCV (Orgentec, Mainz, Germany), and recombinant human vimentin (VIM, 10 mM; Progen Biotechnik, Heidelberg, Germany) at 37 °C for 24 h. GN8P and VIM were added to the cells in solution, and MCV was coated to microtitre

plates. Cell lysis was performed after incubation directly on the plates.

Cytotoxicity assay

In vitro NK cell-mediated cytotoxicity was determined using a standard ^{51}Cr-release assay with PBMCs from patients and healthy donors in the presence or absence of GN8P. We used the NK cell-sensitive K562 (CCL-243, ATCC) erythroleukemia cell line. Effector cells at a concentration of 1.6×10^5/well were incubated with 10^4 target cells (labeled for 60 min with $Na_2^{51}CrO_4$), in round-bottomed 96-well microtitre plates (NUNC) at 37 °C in a humidified atmosphere containing 5% CO_2. NK cell activity was evaluated after 18 h of incubation and was calculated as described previously [35].

Flow cytometry

The fluorochrome-conjugated antibodies CD3-Pacific Blue (clone UCHT1), CD56-APC (clone MEM-188), and CD161-FITC (clone B199.2) were obtained from Dako (Glostrup, Denmark), Exbio (Prague, Czech Republic), and Serotec (Raleigh, NC, USA), respectively. Optimal staining concentrations were determined by single-stain titration of antibodies prior to experimental use.

PBMCs (5×10^5 cells/well) were stained with the antibody mixture for 30 min on ice, washed, and measured with a Becton Dickinson (Franklin Lakes, NJ, USA) LSRII instrument. We included single-stain controls for further offline compensation. Measurement and subsequent analysis was performed using FACSDiva and TreeStar FlowJo 8 software, respectively.

Reverse transcriptase PCR and real-time reverse transcriptase PCR analyses

Total RNA from purified NK cells and PBMC was isolated with RNeasy Micro and Mini Kits (Qiagen, Hilden, Germany), respectively. Five micrograms of RNA were transcribed into cDNA using the cDNA Archive Kit (Applied Biosystem, Foster City, CA, USA). Reverse transcriptase PCR (RT-PCR) was carried out with HotStarTaq DNA Polymerase (Qiagen) and an iCycler5 (Bio-Rad, Philadelphia, PA, USA). Real-time RT-PCR was performed with PowerSybr Green Master Mix (Applied Biosystems) and an iCycler5. PCR product specificity was checked by melt curve analysis. The sequences of the primers used to amplify human β-2-microglobulin (B2M) and PAD4 were described previously [36,37]. The primers designed by us with Primer3 Input software were: MGAT5 F, 5′-CTTCTTTCTTCCAGCACCTCAAC; MGAT5 R, 5′-AAACACACAGTGCTTATTCTTAGGG; NKR-P1A F, 5′-TCTTCCTCGGGATGTCTGTC; and NKR-P1A R, 5′-CCTGCTCTGTTGAATGTCCA. The gene of interest was normalized to the control gene β-2-microglobulin and differences in gene expression between the treated cells and the appropriate control cells were evaluated with Bio-Rad iQ5 2.0 software.

ELISA to detect MCV and CCP antibodies

An anti-MCV ELISA kit (Orgentec, Mainz, Germany) was employed to detect antibodies against MCV. Antibody amounts were calculated as pg/ml on the basis of the standard curve. Antibodies to citrullinated peptides (anti-CCP) were detected by commercially available ELISA for anti-CCP2 (Immunoscan RA; Euro-Diagnostica, Malmoe, Sweden). The results are expressed in U/ml with the cut-off for normal levels at 25 U/ml. Plasma from patients and healthy donors was diluted 100-fold, and ELISAs were performed according to the manufacturers' protocols.

Statistical analysis

Differences in NK cell phenotypes and numbers among patients grouped by disease were analyzed using the nonparametric Mann-Whitney test with a confidence interval of 95%. The significance of NK cell cytotoxicity in the presence or absence of GN8P was evaluated with the paired one-tailed Student's *t*-test. Values of $p\le0.05$ (*), $p\le0.01$ (**), and $p\le0.001$ (***) were considered to be statistically significant.

Results

Reduced NK cell number and effector function in patients with autoimmune diseases

To compare the cytolytic function of NK cells in patients with autoimmune diseases to their function in those with OA and in HD, we examined PBMCs from RA, DM, PM, and OA patients, and from HD using a standard 18-h ^{51}Cr-release assay. There was a highly significant decrease in NK cell cytotoxicity in both RA (32.53%±15.64%, $p<0.0001$) and PM/DM patients (27.81%±14.07%, $p<0.0001$), but not in OA patients (45.61%±19.32%, $p=0.365$) compared to HD (49.76%±15.82%) (Fig. 1A). Thus, NK cell function was impaired only in patients suffering from autoimmune diseases (i.e., RA, PM, and DM).

Because decreased cytotoxicity can be caused by either impaired NK cell function or a lower number of functional NK cells, we correlated our functional assay results with FACS analysis of NK cell percentages. There are two main populations of NK cells that are distinguished by their level of CD56 expression: CD3−CD56high (NK1 type synthesizing TH1 cytokines and NK2 synthesizing TH2 cytokines) and CD3−CD56low (killer-type NK cells); we concentrated on the CD3−CD56low subpopulation. We found a highly significant decrease in the percentage of killer NK cells in PM/DM patients (4.92%±3.0%, $p=0.0006$); however, the NK cell percentage was only slightly decreased in RA patients (6.58%±4.4%, $p=0.003$) compared to HD (8.62%±3.8%) (Fig. 1B). OA patients showed no significant change in the percentage of NK cells (10.39%±3.4%, $p=0.11$). We did not find any significant differences in NK cell activity impairment when comparing different therapeutic interventions or disease stages.

Differences in reactivity to GN8P

Differences in NK cell distribution between RA and HD did not sufficiently explain the highly significant decrease of cytotoxic activity. Therefore, we evaluated the relationship between the impaired function of NK cells and inhibitory activity of CD161 receptor triggered by ligand binding. We used the GN8P glycoconjugate in a 30-min preincubation with PBMC samples as a prototype ligand of CD161 [3] to

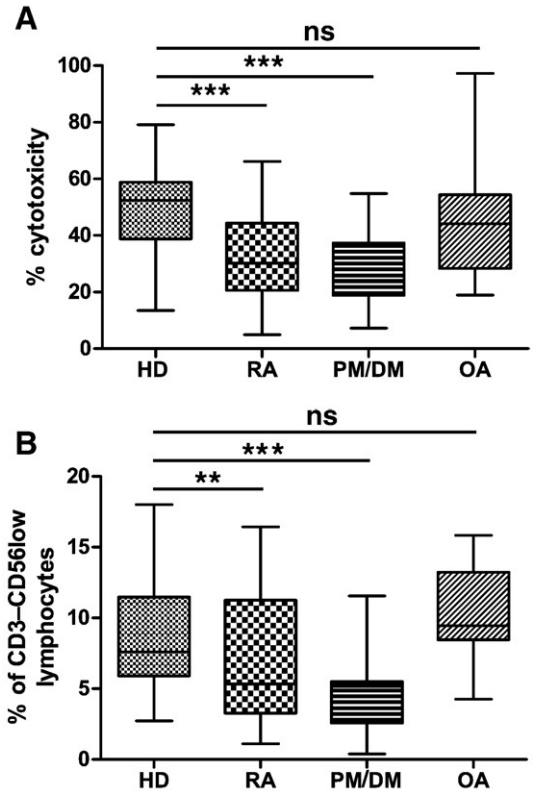

Figure 1 Comparison of NK cell-mediated cytotoxicity and NK cell distribution in the autoimmune diseases RA, PM, and DM with OA and HD. (A) Standard 18-h ^{51}Cr-release cytotoxicity assay was performed with an effector: NK-sensitive K562 target cell ratio of 16:1. Cytotoxicity was significantly impaired in all of the samples from patients with autoimmune disease. OA patient samples had normal cytotoxic activity that was not significantly different from HD. (B) Percentage of NK cells among lymphocytes. The data shown represent the percentage of CD3−CD56low NK cells in patient samples with the same diseases measured in the cytotoxicity assay (**A**). A lower number of killer NK cells corresponded with lower cytotoxicity. Statistical significance according to the Mann−Whitney test is indicated by ** ($p \leq 0.01$), *** ($p \leq 0.001$). ns, not significant ($p > 0.05$). RA $n = 50$, PM $n = 5$, DM $n = 12$, OA $n = 19$, HD $n = 60$.

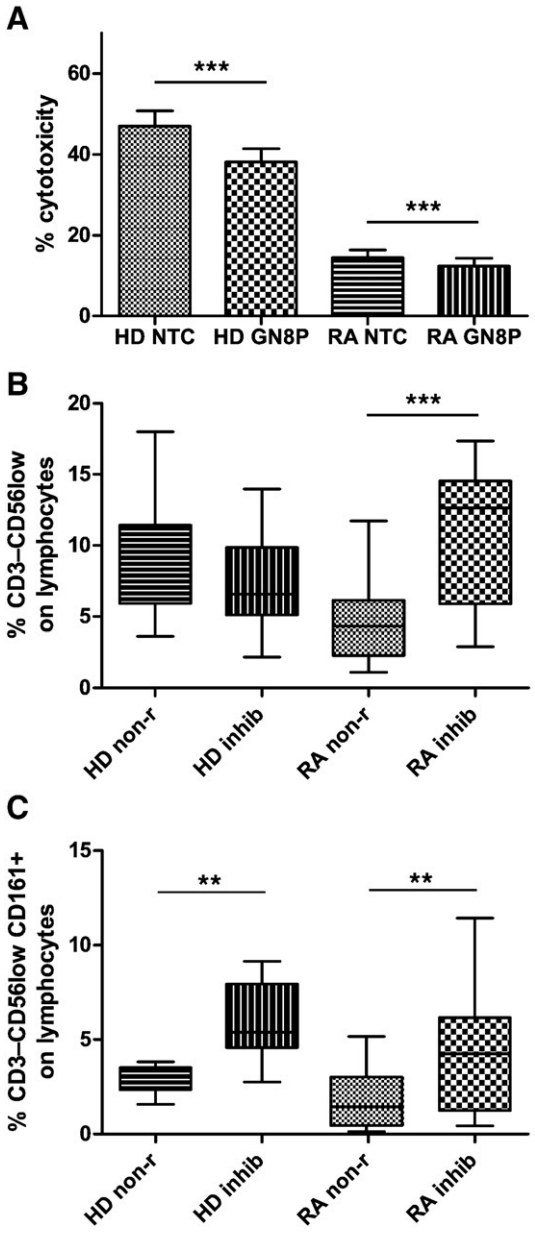

Figure 2 Cytotoxicity, distribution, and phenotype of NK cells in RA patients and HD grouped according to GN8P sensitivity. (A) Cytotoxic activity of GN8P-inhibited samples. NK cell activity measured by 18-h ^{51}Cr-release cytotoxicity assay in the presence or absence (NTC) of GN8P. 50% of RA patient samples were inhibited by GN8P pretreatment, and 50% were GN8P-nonreactive. (B) Percentage of CD3-CD56low NK cells. The plot shows the number of NK cells among lymphocytes divided according GN8P reactivity in HD and RA patients. **C,** Percentage of CD161-positive NK cells (CD3−CD56low CD161+). Significantly higher levels of the CD161+ NK cell subset in GN8P-inhibited samples from both HD and RA patients corresponded with impaired cytotoxicity in the same sample groups. inhib, GN8P-inhibited samples; non-r, GN8P-nonreactive samples. Statistical significance is indicated by ** ($p \leq 0.01$) and *** ($p \leq 0.001$).

investigate how ligand binding affects NK cell functional activity.

We separated the RA patients and HD into GN8P inhibited and non-reactive (data not shown) groups on the basis of differences from control, untreated values. We have taken 5% tolerance, so values under 95% of the untreated controls were taken as inhibited. We found that PBMCs from 50% of the RA patients ($n = 25/50$) *in vitro* responded to GN8P pretreatment by inhibition of NK cell cytotoxicity (Fig. 2A). The mean percentage of cytotoxicity in patients PBMCs not treated with GN8P was 14.44%±8.5%, compared to 12.37%± 7.8% in the GN8P-pretreated PBMCs ($p < 0.0001$). Similarly, in 42% of HD ($n = 26/56$) PBMCs, incubation with GN8P down-modulated the NK cell activity from 46.96%±16.28% to 38.15%±13.8% ($p < 0.0001$), as evaluated by paired, one-tailed Student's *t*-test. However, 50.0% of RA patient PBMCs and 58% of HD PBMCs did not exhibit any significant reaction to GN8P. As we expected, based on what is known about the inhibitory function of the CD161 receptor, the NK cells that

reacted to GN8P showed decreased cytotoxic activity. We found that there was a slightly higher percentage of GN8P-inhibited samples from RA patients compared to HD (50% vs. 42%, respectively). Thus, we next investigated whether the GN8P-mediated decrease in cytotoxicity was caused by a lower number of NK cells, or the inhibitory activity of CD161.

Distribution of NK cells according to reactivity to GN8P

We compared the percentages of NK cells from the two groups of RA patients and HD that were either GN8P inhibited or nonreactive. We found that the percentage of killer NK cells (CD3−CD56low) did not correlate with the difference in cytotoxicity of HD (8.46%±3.7% and 7.44%±3.6%, in nonreactive vs. inhibited, respectively), moreover, in the samples from RA patients, we observed a significant indirect relationship between NK cell percentages and the cytotoxicity assay results: 7.75%±2.8% and 10.98%±4.7% in GN8P-nonreactive and -inhibited samples, respectively ($p=0.0003$) (Fig. 2B). Once we had determined that the percentage of NK cells did not have a direct effect on cytotoxicity as measured by the GN8P assay, we verified the expression of CD161. The total number of CD161-expressing lymphocytes, unlike the percentage of NK cells, correlated indirectly with the cytotoxicity assay results in both HD (15.18%±7.9% vs. 24.92%±7.5% for GN8P-nonreactive and -inhibited samples, respectively; $p=0.005$) and RA patients (12.95%±4.3% vs. 19.80%±5.8% for GN8P-nonreactive and -inhibited samples, respectively; $p=0.0002$). The effect of GN8P on cytotoxicity was likely mediated by binding to CD161 receptors expressed on CD3−CD56low NK cells; ligand binding to CD161 inhibited effector function. Those samples that were inhibited by GN8P had significantly higher percentages of CD161-positive NK cells: HD, 15.18%±7.9% and 24.92%±7.5% in nonreactive and inhibited samples, respectively ($p=0.005$); RA, 1.94%±1.6% and 4.21%±2.1% in nonreactive and inhibited samples, respectively ($p<0.01$) (Fig. 2C).

FACS analysis of CD161-positive lymphocytes showed that RA samples inhibited by GN8P pretreatment even expressed higher levels of CD161 (4300 mean fluorescence intensity [MFI]±304.3 MFI; $p=0.003$) compared to GN8P-inhibited HD samples (2,802 MFI±177.9 MFI). CD161 expression in GN8P-nonreactive HD and RA samples was not significantly different (3,620 MFI±237.3 MFI and 2,991 MFI±224.2MFI, respectively). These findings support the hypothesis that CD161 plays an important role in regulation of NK cell recognition and effector functions.

When we grouped RA patients ($n=50$) according to the therapy that they received (Table 1A), we found that samples from patients receiving either glucocorticoids or immunosuppressives were GN8P inhibited (expressed high levels of CD161): 63% ($n=7/11$) and 66% ($n=6/9$), respectively. In contrast, 70% ($n=14/20$) of the samples from RA patients treated with a combination of glucocorticoids and immunosuppressives were GN8P nonreactive (expressed low levels of CD161). There was no difference in the number of GN8P-nonreactive and -inhibited samples from untreated and TNF antagonist-treated patients (50%). Differentiation of samples from patients according to disease stage revealed that the majority of patients with stage I and II RA fell into the GN8P-inhibited group, while a majority of the samples from patients with stage III and IV RA [31] were nonreactive. All of the samples from patients with active arthritis and inflamed joints (synovial fluid-positive) were GN8P nonreactive (Table 1B).

Table 1 Reactivity of RA patient PBMCs to GN8P according to therapy (A) or disease stage (B).

A			
Therapy	GN8P nonreactive	GN8P inhibited	Total
	Low CD161 expression	High CD161 expression	No. of patients
Glucocorticoids	37%	**63%**	11
Immunosuppresives	34%	66%	9
Glucocorticoids and immunosuppressives	**70%**	30%	20
TNF-antagonists	50%	50%	6
No therapy	25%	**75%**	4
B			
Disease stage	GN8P nonreactive	GN8P inhibited	Total
	Low CD161 expression	High CD161 expression	No. of subjects
I	36%	64%	14
II	44%	56%	9
III	58%	42%	12
IV	60%	40%	10
SF positive	60%	40%	5
Healthy donors	**58%**	**42%**	56

Legend: SF = synovial fluid.

CD161 gene expression in response to GN8P

As NK cells showed major changes in their cytotoxic activity after treatment with GN8P, we wanted to describe this phenomenon in a more detailed manner. We thus investigated the changes that occurred intracellularly following ligand binding by evaluating CD161 – the responsible receptor – expression in purified NK cells. FACS analysis of HD NK cells revealed that untreated HD NK cells fell into two groups: the first group had high numbers of NK cells expressing CD161 receptor, and the second group had low numbers of NK cells expressing CD161 receptor (Fig. 3A).

NK cell reactivity to GN8P correlated with the cytotoxic response of the donor cells. In response to GN8P, subjects with higher numbers of NK cells (CD56+CD3−) expressing CD161 protein showed a slight reduction in CD161 mRNA expression, as measured by RT-PCR. However, the donors with low numbers of CD161+ NK cells resulted in a slight increase in CD161 mRNA expression (Fig. 3B).

MGAT5 gene expression in response GN8P

The role of the glycosyltransferase MGAT5, a key glycan metabolism enzyme, in autoimmune disease was previously

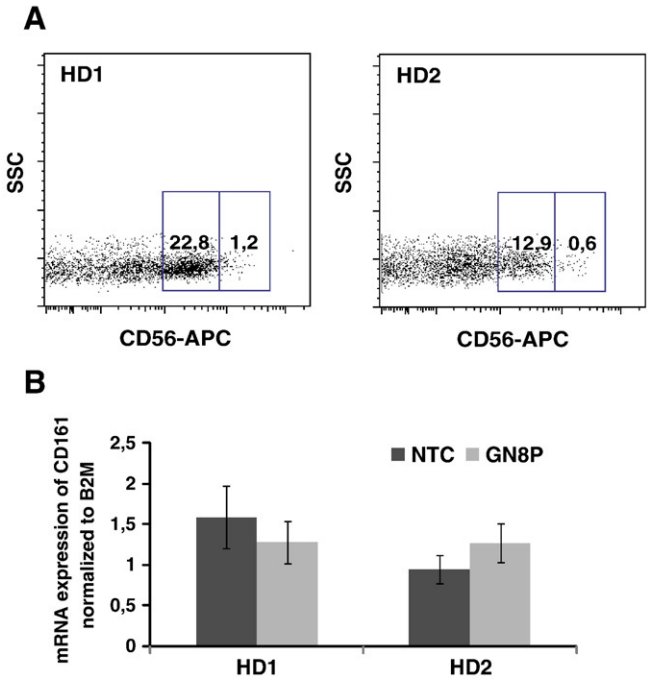

Figure 3 CD161 mRNA expression by purified NK cells incubated with GN8P. (A) Distribution of cell populations (percentage) in representative HD with a higher percentage of CD3−CD56low NK cells (HD1) and a lower proportion of CD3−CD56low NK (HD2). The dotplots show CD56/SSC gated on CD161 positive cells. (B) CD161 mRNA expression detected by RT-PCR and normalized to control gene β-2-microglobulin (B2M). Purified NK cells (CD56+CD3−) were incubated in the presence or absence (NTC) of GN8P. Two different patterns were identified in response to GN8P: a group ($n=6$) in which CD161 mRNA expression was inhibited by GN8P (HD1), and a group ($n=7$) that did not exhibit GN8P-mediated inhibition (HD2).

studied in a mouse model. Demetriou et al. [14] have found that a deficiency in MGAT5 lowers T-cell activation thresholds by directly enhancing TCR clustering. MGAT-5-deficient mice showed kidney autoimmunity as well as an increased susceptibility to experimental autoimmune encephalomyelitis. We have thus wanted to elucidate the role of MGAT5 under the conditions of human RA. To determine if MGAT5 expression differs between PBMCs from RA patients and HD, or between PBMCs and synoviocytes from RA patients, we performed real-time RT-PCR. PBMCs from HD expressed lower levels of MGAT5 mRNA than did PBMCs from RA patients. Synoviocytes, the adherent cell population within synovial fluid extracted from the joints of RA patients, expressed significantly higher levels of MGAT5 than did PBMCs from RA patients.

Because GlcNAc compounds similar to synthetic GN8P are involved in modulation of the glycan profile in RA, we investigated whether GN8P modulated the expression of MGAT5 mRNA. GN8P significantly downregulated the expression of MGAT5 mRNA in synoviocytes ($p=0.05$). However, GN8P did not affect MGAT5 mRNA expression in either the HD or the RA patient samples ($p=0.35$ and $p=0.5$, respectively) (Fig. 4A and B).

CD161 and PAD4 gene expression in response to MCV autoantigen

We next evaluated changes in the CD161 and PAD4 mRNA expressions of purified NK cells from RA patients or HD in response to incubation with either the RA-specific autoantigen MCV or non-citrullinated vimentin (VIM, data not shown). NK cells from HD expressed significantly less CD161 mRNA than NK cells from RA patients ($p=0.0171$). Incubation of HD NK with VIM or MCV led to a significant increase in CD161

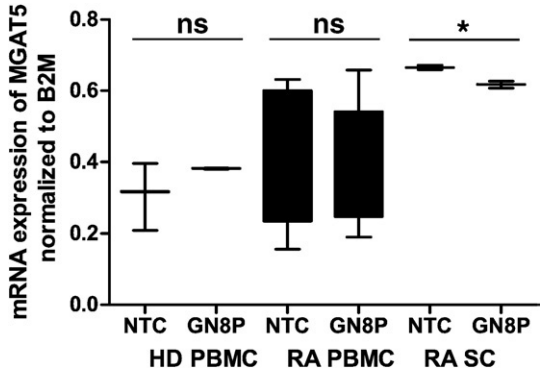

Figure 4 MGAT5 mRNA expression in PBMCs and synoviocytes. MGAT5 mRNA expression in PBMCs from HD (HD PBMC), RA patients (RA PBMC), and synoviocytes extracted from the synovial fluid of RA patients (RA SC). Cells were incubated in the presence or absence (NTC) of GN8P and gene expression was detected by real-time RT-PCR represented as the mean ± max/min values of 5–7 samples. β-2-microglobulin (B2M) was used for PCR normalization. Synoviocytes from RA patients expressed high levels of MGAT5 mRNA, and incubation with GN8P led to a decrease in MGAT5 mRNA expression. Statistical significance is indicated by * ($p \leq 0.05$). ns, not significant ($p > 0.05$).

mRNA expression ($p=0.0083$ and 0.0088, respectively). NK cells from RA patients did not exhibit a similar increase in CD161 mRNA expression following incubation with MCV ($p=0.2$) (Fig. 5A). Because HD NK cells responded to MCV or VIM treatment but RA NK cells did not, we next investigated whether there were differences in the expression of PAD4, the enzyme responsible for citrullination, in RA patient and HD NK cells, and whether incubation with MCV or VIM affected PAD4 expression levels. Equal levels of PAD4 mRNA were expressed in purified NK cells from HD and RA patients ($p=0.41$). Incubation of HD NK cells with VIM or MCV resulted in a significant increase in PAD4 mRNA ($p=0.0083$ and 0.0025, respectively). This upregulation in PAD4 expression did not occur when NK cells from RA patients were incubated with MCV ($p=0.5$) (Fig. 5B).

To determine the level of disease activity in RA patients that were used in mRNA analysis, we tested for the presence of anti-MCV and anti-CCP antibodies. As shown in Fig. 5C, all of the RA samples contained high levels of anti-MCV and anti-CCP antibodies. HD and OA patients (non-RA) had antibody levels that were within normal limits (Fig. 5C).

Discussion

NK cells participate in preserving immunological tolerance by providing negative feedback to activated macrophages as well by influencing other cell types. NK cells can suppress autoreactive B or T lymphocytes, which may explain the protective role of NK cells in some autoimmune diseases [38,39].

We found that NK cell-mediated cytotoxicity was impaired in RA and PM/DM patients in contrast to OA patients and HD. In contrast to PM/DM patients, who exhibited both decreased cytotoxicity and lower NK cell numbers, the percentage of killer NK cells in RA patient samples did not correlate well with decreased cytotoxicity levels. Thus, we further explored the role of NK cells in patients with RA.

Because a previous study proposed that glycosylation plays an important role in the pathogenesis of autoimmunity [1], we focused on expression of the lectin receptor CD161, which recognizes and binds glycoproteins with GlcNAc moieties [3]. We used GN8P as a prototype ligand to determine how glycan recognition inhibits NK cell function in RA patients and HD. We divided the patients into GN8P-inhibited and -nonreactive groups depending upon how NK cell cytotoxicity responded to incubation with GN8P. We believe that the inhibitory effect was caused by ligand binding to CD161, which is in agreement with the findings of Rosen et al. [4]. This hypothesis was supported by the results of FACS analysis, which showed a correlation between increased CD161 expression on NK cells and decreased cytotoxicity. Upregulation of CD161 mRNA expression in purified NK cells after ligand induction was confirmed by RT-PCR (Fig. 3).

The differences between CD161 low and high expressers according to the disease stage correlate with the seriousness of the illness that corresponded as well with the therapeutic protocols (Table 1A, B). Majority of the patients with severe stages of illness undergo more powerful therapeutic procedures, either combination of glucocorticoids and immunosuppressant or TNF antagonist treatment. Further possible explanation of higher proportion of GN8P nonresponsive NK cells in patients with the exacerbation of arthritic symptoms could be their recruitment into the joint microenvironment and their consequent absence in peripheral blood.

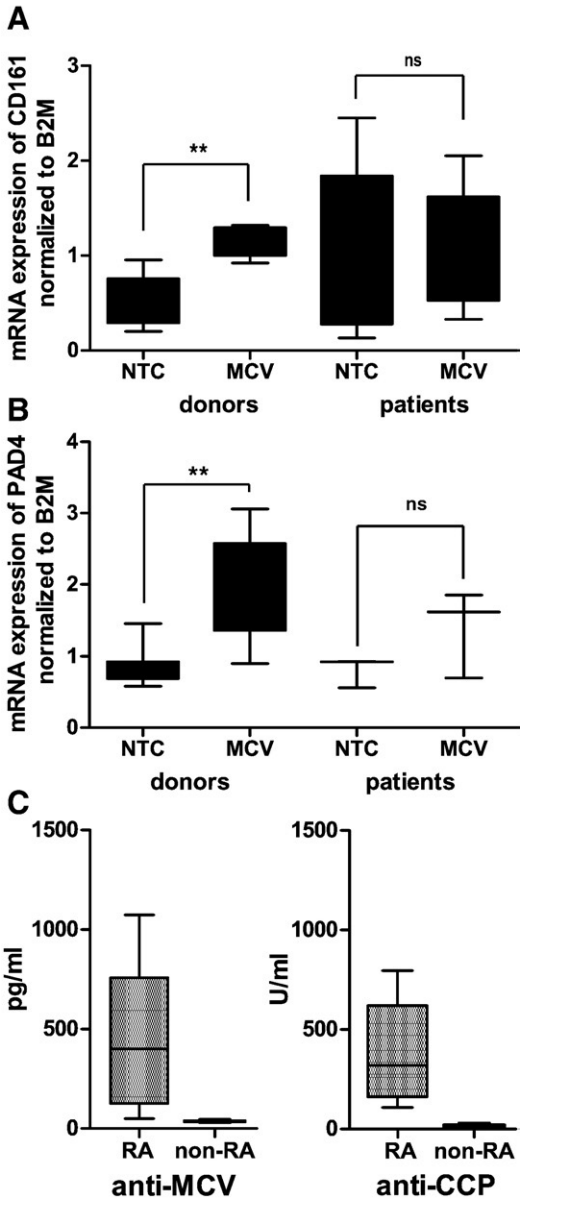

Figure 5 CD161 and PAD4 mRNA expression in NK cells from HD and RA patients. CD161 (A) and PAD4 (B) mRNA expression detected by RT-PCR and normalized to the control gene β-2-microglobulin (B2M). Purified NK cells were incubated in the presence or absence of MCV. Nontreated controls (NTC) were cells incubated without MCV. Statistical significance is indicated by ** ($p \leq 0.01$). ns, not significant ($p > 0.05$). (C) Determination of anti-MCV and anti-CCP antibodies in plasma samples from RA patients and HD/OA selected for mRNA analyses (A, B). RA, patients with active disease; non-RA, HD and OA patients. Plasma samples from RA patients had high levels of anti-MCV and anti-CCP antibodies in contrast to healthy donors. NK cells from healthy donors, but not RA patients, responded to incubation with MCV by increased expression of CD161 and PAD4 mRNA.

In the active disease 2/3 of patients fall into the group GN8P inhibited, CD161 high expressing NK cells that supports the hypothesis about the importance of CD161 molecule in the course of RA and the sensitivity of patients to the inhibitory action of glycans produced on the surface of synoviocytes [9,10,14].

From the therapeutic point of view the best results were achieved by the combined treatment with glucocorticoids and immunosuppressive drugs (70%) followed by TNF antagonist treatment (50%). The single glucocorticoid or immunosuppressive therapy was less effective, 37% and 34%, respectively, as depicted in the Table 1A.

We found that CD161 expression was increased not only on NK cells, but also on other type of lymphocytes from RA patients, including T and NKT cells, which, when activated, could deepen the severity of the disease (data not shown). Exley et al. [40] showed that CD161 can act as a specific costimulatory molecule for TCR-mediated proliferation and cytokine secretion by $V_{\alpha}24^{invt}$ T cells. Ligation of CD161 in the absence of TCR stimulation does not result in $V_{\alpha}24^{invt}$ T cell activation, and costimulation through CD161 does not cause polarization of the cytokine secretion pattern. However, CD161 signaling events remain unclear.

A number of enzymes that synthesize N- and O-linked oligosaccharides are active in synoviocytes ([41], for review see [42]). To explore the molecular events underlying glycosylation pathways in the synovium of RA patients, we examined the effect of GN8P on expression of the glycosyltransferase MGAT5. The synthetic glycoconjugate GN8P can serve as a substrate for MGAT5, which is responsible for GlcNAc branching. GlcNAc branching plays a key role in NK cell recognition in autoimmune conditions [43–45]. We found that MGAT5 was involved in GlcNAc metabolism in the synoviocytes of RA patients with active disease, but not in their PBMCs. Metabolic regulation of GlcNAc branching on synoviocytes, but not on peripheral blood immune cells, may indicate genetic predisposition to RA susceptibility. GlcNAc-terminated glycans may be involved in upregulation of CD161 expression, resulting in downmodulation of NK cell function in patients with RA. Similarly, GN8P, acting as a substrate for synoviocytes, may reduce MGAT5 mRNA expression.

A characteristic feature of RA is the reaction of lymphocytes to the autoantigens MCV and VIM. We tested the effect of human MCV and recombinant VIM on CD161 expression in NK cells derived from HD and RA patients. Both MCV and VIM led to a significant increase in CD161 mRNA levels in NK cells from HD. In RA patients, where MCV and VIM expression is elevated; we found that NK cells did not exhibit any further change in CD161 expression levels when incubated with MCV or VIM in vitro. Thus, the increased expression of CD161 seen in RA patient NK cells may be due to continual stimulation by citrullinated VIM or to higher levels of free VIM from damaged cells.

In this study, we showed, to our knowledge for the first time, that in addition to macrophages and granulocytes, the main producers of PAD4 enzyme [25], NK cells are also able to activate the PAD4 in response to VIM or MCV. Incubation of HD NK cells with either VIM or MCV led to upregulation of PAD4 mRNA. This was not observed in NK cells derived from RA patients, which had already been exposed to the MCV autoantigen. Thus, we deduce that NK cells may be involved in the citrullination of vimentin in patients with RA.

Conclusions

We discovered that NK cells of healthy donors recognize the RA autoantigen MCV. Exposure to MCV may serve as the triggering mechanism for induction of CD161, as well as increased expression of the citrullination enzyme PAD4. We also provide evidence, for the first time to our knowledge, that high levels of CD161 receptor on NK cells are correlated with impairment of NK cytotoxic activity in RA patients. We propose that MCV plays an important role in RA by increasing expression of CD161, which leads to inhibition of NK cell activity and, consequently, insufficient downregulation of autoreactive T cells, thus accelerating disease progression.

Acknowledgments

We thank Vladimir Kren (Institute of Microbiology ASCR, Prague) for providing the GN8P glycoconjugate, Sarka Ruzickova (Institute of Rheumatology, Prague) for providing the RA patient samples and clinical data, and Katerina Fiserova and Zdenek Cimburek for excellent technical assistance.

The work contained herein was supported by grants 310/06/0477 and 310/08/H077 from the Czech Science Foundation, grant NR/9106-3 from the Grant Agency of the Czech Ministry of Health, grant IAA500200620 from the Grant Agency of the Czech Academy of Sciences, and grant AV0Z50200510 from Institutional Research Concepts (Czech Academy of Sciences).

References

[1] L.A. Walakovits, V.L. Moore, N. Bhardwaj, G.S. Gallick, M.W. Lark, Detection of stromelysin and collagenase in synovial fluid from patients with rheumatoid arthritis and posttraumatic knee injury, Arthritis Rheum. 35 (1992) 35–42.

[2] C. Bottino, R. Castriconi, L. Moretta, A. Moretta, Cellular ligands of activating NK eceptors, Trends Immunol. 26 (2005) 221–226.

[3] K. Bezouska, C.T. Yuen, J. O'Brien, R.A. Childs, W. Chai, A.M. Lawson, et al., Oligosaccharide ligands for NKR-P1 protein activate NK cells and cytotoxicity, Nature 372 (1994) 150–157.

[4] D.B. Rosen, J. Bettadapura, M. Alsharifi, P.A. Mathew, H.S. Warren, L.L. Lanier, Cutting edge: lectin-like transcript-1 is a ligand for the inhibitory human NKR-P1A receptor, J. Immunol. 175 (2005) 7796–7799.

[5] Y.S. Hu, H. Zhou, D. Myers, J.M. Quinn, G.J. Atkins, C. Ly, et al., Isolation of a human homolog of osteoclast inhibitory lectin that inhibits the formation and function of osteoclasts, J. Bone Miner. Res. 19 (2004) 89–99.

[6] D.B. Rosen, W. Cao, D.T. Avery, S.G. Tangye, Y.J. Liu, J.P. Houchins, et al., Functional consequences of interactions between human NKR-P1A and its ligand LLT1 expressed on activated dendritic cells and B cells, J. Immunol. 180 (2008) 6508–6517.

[7] A. Alavi, N. Arden, T.D. Spector, J.S. Axford, Immunoglobulin G glycosylation and clinical outcome in rheumatoid arthritis during pregnancy, J. Rheumatol. 27 (2000) 1379–1385.

[8] E. Gindzienska-Sieskiewicz, P.A. Klimiuk, D.G. Kisiel, A. Gindzienski, S. Sierakowski, The changes in monosaccharide composition of immunoglobulin G in the course of rheumatoid arthritis, Clin. Rheumatol. 26 (2007) 685–690.

[9] L.N. Troelsen, P. Garred, H.O. Madsen, S. Jacobsen, Genetically determined high serum levels of mannose-binding lectin and agalactosyl IgG are associated with ischemic heart disease in rheumatoid arthritis, Arthritis Rheum. 26 (2007) 21–29.

[10] M. Watson, P.M. Rudd, M. Bland, R.A. Dwek, J.S. Axford, Sugar printing rheumatic diseases: a potential method for disease differentiation using immunoglobulin G oligosaccharides, Arthritis Rheum. 42 (1999) 1682–1690.
[11] P.J. Delves, The role of glycosylation in autoimmune disease, Autoimmunity 27 (1998) 239–253.
[12] G. Dighiero, N.R. Rose, Critical self-epitopes are key to the understanding of self-tolerance and autoimmunity, Immunol. Today 20 (1999) 423–428.
[13] A.K. Nyame, R. Bose-Boyd, T.D. Long, V.C. Tsang, R.D. Cummings, Expression of Lex antigen in Schistosoma japonicum and S.haematobium and immune responses to Lex in infected animals: lack of Lex expression in other trematodes and nematodes, Glycobiology 8 (1998) 615–624.
[14] M. Demetriou, M. Granovsky, S. Quaggin, J.W. Dennis, Negative regulation of T-cell activation and autoimmunity by Mgat5 N-glycosylation, Nature 409 (2001) 733–739.
[15] D. Chui, M. Oh-Eda, Y.F. Liao, K. Panneerselvam, A. Lal, K.W. Marek, et al., Alpha-mannosidase-II deficiency results in dyserythropoiesis and unveils an alternate pathway in oligosaccharide biosynthesis, Cell 90 (1997) 157–167.
[16] K.W. Moremen, R.B. Trimble, A. Herscovics, Glycosidases of the asparagine-linked oligosaccharide processing pathway, Glycobiology 4 (1994) 113–125.
[17] H. Schachter, The 'yellow brick road' to branched complex N-glycans, Glycobiology 1 (1991) 453–461.
[18] A. Kinloch, K. Lundberg, R. Wait, N. Wegner, N.H. Lim, A.J. Zendman, T. Saxne, V. Malmström, P.J. Venables, Synovial fluid is a site of citrullination of autoantigens in inflammatory arthritis, Arthritis Rheum. 58 (2008) 2287–2295.
[19] Y. Tabushi, T. Nakanishi, T. Takeuchi, M. Nakajima, K. Ueda, T. Kotani, S. Makino, A. Shimizu, T. Hanafusa, T. Takubo, Detection of citrullinated proteins in synovial fluids derived from patients with rheumatoid arthritis by proteomics-based analysis, Ann. Clin. Biochem. 45 (2008) 413–417.
[20] M.A. van Boekel, E.R. Vossenaar, F.H. van den Hoogen, W.J. van Venrooij, Autoantibody systems in rheumatoid arthritis: specificity, sensitivity and diagnostic value, Arthritis Res. 4 (2002) 87–93.
[21] O. Meyer, C. Labarre, M. Dougados, P. Goupille, A. Cantagrel, A. Dubois, et al., Anticitrullinated protein/peptide antibody assays in early rheumatoid arthritis for predicting five year radiographic damage, Ann. Rheum. Dis. 62 (2003) 120–126.
[22] H. Visser, C.S. Le, K. Vos, F.C. Breedveld, J.M. Hazes, How to diagnose rheumatoid arthritis early: a prediction model for persistent (erosive) arthritis, Arthritis Rheum. 46 (2002) 357–365.
[23] H. Uysal, R. Bockermann, K.S. Nandakumar, B. Sehnert, E. Bajtner, A. Engström, G. Serre, H. Burkhardt, M.M. Thunnissen, R. Holmdahl, Structure and pathogenicity of antibodies specific for citrullinated collagen type II in experimental arthritis, J. Exp. Med. 206 (2009) 449–462.
[24] R.P. Nicaise, M.S. Grootenboer, A. Bruns, M. Hurtado, E. Palazzo, G. Hayem, P. Dieudé, O. Meyer, M.S. Chollet, Antibodies to mutated citrullinated vimentin for diagnosing rheumatoid arthritis in anti-CCP-negative patients and for monitoring infliximab therapy, Arthritis Res. Ther. 10 (2008) R142.
[25] E.R. Vossenaar, T.R. Radstake, A. van der Heijden, M.A. van Mansum, C. Dieteren, D.J. de Rooij, et al., Expression and activity of citrullinating peptidylarginine deiminase enzymes in monocytes and macrophages, Ann. Rheum. Dis. 63 (2004) 373–381.
[26] C. Masson-Bessiere, M. Sebbag, E. Girbal-Neuhauser, L. Nogueira, C. Vincent, T. Senshu, et al., The major synovial targets of the rheumatoid arthritis-specific antifilaggrin autoantibodies are deiminated forms of the alpha- and beta-chains of fibrin, J. Immunol. 166 (2001) 4177–4184.
[27] Y.W. Park, S.J. Kee, Y.N. Cho, E.H. Lee, H.Y. Lee, E.M. Kim, et al., Impaired differentiation and cytotoxicity of natural killer cells in systemic lupus erythematosus, Arthritis Rheum. 60 (2009) 1753–1763.
[28] A. Bohan, J.B. Peter, Polymyositis and dermatomyositis (second of two parts), N. Engl. J. Med. 292 (1975) 403–407.
[29] A. Bohan, J.B. Peter, Polymyositis and dermatomyositis (first of two parts), N. Engl. J. Med. 292 (1975) 344–347.
[30] S.J. Tomasova, F. Charvat, K. Jarosova, J. Vencovsky, The role of MRI in the assessment of polymyositis and dermatomyositis, Rheumatology (Oxford) 46 (2007) 1174–1179.
[31] F.C. Arnett, S.M. Edworthy, D.A. Bloch, D.J. McShane, J.F. Fries, N.S. Cooper, et al., The American Rheumatism Association 1987 revised criteria for the classification of rheumatoid arthritis, Arthritis Rheum. 31 (1988) 315–324.
[32] R. Altman, E. Asch, D. Bloch, G. Bole, D. Borenstein, K. Brandt, et al., Development of criteria for the classification and reporting of osteoarthritis. Classification of osteoarthritis of the knee. Diagnostic and Therapeutic Criteria Committee of the American Rheumatism Association, Arthritis Rheum. 29 (1986) 1039–1049.
[33] K. Bezouska, V. Kren, C. Kieburg, T.K. Lindhorst, GlcNAc-terminated glycodendrimers form defined precipitates with the soluble dimeric receptor of rat natural killer cells, sNKR-P1A, FEBS Lett. 426 (1998) 243–247.
[34] T.K. Lindhorst, C. Kieburg, Glycocoating of oligovalent amines: synthesis of thiourea-bridged cluster glycosides from glycosyl isothiocyanates, Angew. Chem. Int. Ed. Engl. 35 (1996) 1953–1956.
[35] A. Fiserova, H. Kovaru, Z. Hajduova, V. Mares, M. Starec, V. Kren, et al., Neuroimmunomodulation of natural killer (NK) cells by ergot alkaloid derivatives, Physiol. Res. 46 (1997) 119–125.
[36] R. Nachat, M.C. Mechin, H. Takahara, S. Chavanas, M. Charveron, G. Serre, et al., Peptidylarginine deiminase isoforms 1-3 are expressed in the epidermis and involved in the deimination of K1 and filaggrin, J. Invest. Dermatol. 124 (2005) 384–393.
[37] V. Ullmannova, P. Stockbauer, M. Hradcova, J. Soucek, C. Haskovec, Relationship between cyclin D1 and p21(Waf1/Cip1) during differentiation of human myeloid leukemia cell lines, Leuk. Res. 27 (2003) 1115–1123.
[38] H. Ji, K. Ohmura, U. Mahmood, D.M. Lee, F.M. Hofhuis, S.A. Boackle, et al., Arthritis critically dependent on innate immune system players, Immunity 16 (2002) 157–168.
[39] S. Johansson, L. Berg, H. Hall, P. Hoglund, NK cells: elusive players in autoimmunity, Trends Immunol. 26 (2005) 613–618.
[40] M. Exley, S. Porcelli, M. Furman, J. Garcia, S. Balk, CD161 (NKR-P1A) costimulation of CD1d-dependent activation of human T cells expressing invariant V alpha 24 J alpha Q T cell receptor alpha chains, J. Exp. Med. 188 (1998) 867–876.
[41] X. Yang, M. Lehotay, T. Anastassiades, M. Harrison, I. Brockhausen, The effect of TNF-alpha on glycosylation pathways in bovine synoviocytes, Biochem. Cell Biol. 82 (2004) 559–568.
[42] A. Alavi, J.S. Axford, Sweet and sour: the impact of sugars on dinase, Rheumatology 47 (2008) 760–770.
[43] A. Grigorian, S.U. Lee, W. Tian, I.J. Chen, G. Gao, R. Mendelsohn, et al., Control of T cell-mediated autoimmunity by metabolite flux to N-glycan biosynthesis, J. Biol. Chem. 282 (2007) 20027–20035.
[44] L. Ma, W.A. Rudert, J. Harnaha, M. Wright, J. Machen, R. Lakomy, et al., Immunosuppressive effects of glucosamine, J. Biol. Chem. 277 (2002) 39343–39349.
[45] G.X. Zhang, S. Yu, B. Gran, A. Rostami, Glucosamine abrogates the acute phase of experimental autoimmune encephalomyelitis by induction of Th2 response, J. Immunol. 175 (2005) 7202–7208.

Publication 2: GN8P glycomimetic induces antibody formation via NK1.1 positive cell activation in mice.

Overview

Since the involvement of NKR–P1 was obvious in human autoimmune models in reaction to synthetic GN8P mimetic (105), we needed to study its effect in mice. Rodents in general and mice in particular have different isoforms of NKR–P1 in their receptor repertoire (20). While NKR–P1A, C and F are considered activating, NKR–P1B and D are reported to have inhibitory properties (106). The prototype murine NK–cell defining antigen NK1.1 (107) is detected by PK136 mAb which reacts exclusively with the product of *Nkr–p1c* (108), though it was reported to react with Swiss.NIH mouse *Nkr–p1b* transcript (109). NK1.1 is via this mAb detected on CE, B6, NZB, C58, Ma/My, ST, SJL, FVB, and Swiss outbred mice, but not on the surface of BALB/c, AKR, CBA, C3H, DBA, or 129 mice NK cells (20). It has been shown, that BALB/c NK cells (NK1.1–) have otherwise normal *Nkr–p1* expression, when compared to C57BL/6 (NK1.1+) and that the absent NK1.1 reactivity is explained by allelic divergence – specifically a single amino acid substitution (S191T) in the *Nkr–p1c* gene (20). In humans, we observed direct proportion of GN8P–reactivity to the level of NKR–P1 expression. In mice, we confirmed previously the beneficial antitumor effect of GN8P administration (110), but the exact mechanism of effect and whether NKR–P1 is involved in this process would not be clear, unless various mouse strains with different *Nkr–p1* genes are compared. Tumor associated carbohydrate antigens (TACAs) are overexpressed on a variety of cancer cell surfaces, which present tempting targets for anticancer vaccine development. The local density of antigen rather than the total amount of antigen administered was found to be crucial for induction of high antigen–specific IgG titers (90, 91).

Aims and methods

Since NK cells are known to mediate IgG production (111), we investigated whether GN8P modulates antibody response specific for T–independent and T–dependent (soluble as well as corpuscular) antigen in C57BL/6 mice. To prove the involvement of NK and NKT cells and particularly NK1.1 receptor in the mechanism of GN8P effect, we determined Ig levels *in vitro* in supernatants of spleen mononuclear cells (SMCs) depleted of CD49b–positive or NK1.1–positive subpopulations. Finally, we examined whether GN8P increases antigen–specific IgG2a levels in DBA/2 and BALB/c mice, which are considered NK1.1–negative based on FACS analysis.

Results and discussion

The GN8P mimetic significantly elevated the relative number of plasma cells and CD80/CD86/MHC–II expressing B cells in C57BL/6 mice, which are the basis of antigen

presentation and antibody formation. In addition, we detected significantly higher serum levels of IgG2a specific for both T–independent and T–dependent antigen after GN8P administration, when compared with the response to the antigen alone.

In DBA/2 and BALB/c mice, unlike in C57BL/6, GN8P treatment did not influence serum antigen–specific IgG2a levels. Therefore, we suggest that GN8P effect on antibody formation in mice might be dependent on the presence of NKR–P1C isoform encoded by *Nkr–p1c(T)* gene allelic form present in C57BL/6 strain. We do not expect involvement of NKR–P1A and NKR–P1F isoforms (activating receptors) as their genes are present in DBA/2 and BALB/c as well as in C57BL/6 mice. As for NKR–P1B and NKR–P1D isoforms, *Nkr–p1b* gene in DBA/2 and BALB/c mice exerted 94.9% homology with *Nkr–p1d* in C57BL/6 mice. In addition, they both have inhibitory function (20) and have a mutual ligand, Clr–b (78).

To further solidify the conclusion that NK cells are involved in the GN8P–induced antibody formation, IgM levels were measured in response to DNP–LPS antigen (2,4–dinitrophenylated lipopolysaccharide). SMC, CD49b–negative or NK1.1–negative cells were cultured with DNP–LPS in the presence or absence of the glycomimetic for 5 days. While in SMC, the IgM level was significantly increased in the presence of the glycomimetic, we observed no such change in either CD49b–negative or NK1.1–negative populations. Since most CD49b–positive NK cells are also NK1.1–positive, this does not come as a surprise.

In conclusion, GN8P has shown a potential to modulate specific antibody formation via NK cell stimulation. This stimulation seems to be dependent on the surface expression of NKR–P1C isoform encoded by C57BL/6 *Nkr–p1c(T)* gene allele.

However, this study is limited by its focus on the administration of synthetic, exogenous antigens against which GN8P glycomimetic mounts increased antibody response. The practical applications in tumor or immune therapy needed further investigation in the *in vivo* models.

International Immunopharmacology 9 (2009) 792–799

Contents lists available at ScienceDirect

International Immunopharmacology

journal homepage: www.elsevier.com/locate/intimp

N-Acetyl-D-glucosamine-coated polyamidoamine dendrimer modulates antibody formation via natural killer cell activation

Katarina Hulikova [a,b], Veronika Benson [a], Jan Svoboda [a], Petr Sima [a], Anna Fiserova [a,*]

[a] Institute of Microbiology, Academy of Sciences of the Czech Republic, Videnska 1083, 142 20 Prague 4, Czech Republic
[b] Third Faculty of Medicine, Charles University, Ruska 87, 100 00 Prague 10, Czech Republic

ARTICLE INFO

Article history:
Received 1 December 2008
Received in revised form 12 February 2009
Accepted 3 March 2009

Keywords:
$GlcNAc_8$
Antibody formation
NK cells
NKR-P1 (NK1.1) receptor
IgG2a

ABSTRACT

N-Acetyl-D-glucosamine-coated polyamidoamine dendrimer ($GlcNAc_8$) was shown previously to exhibit binding affinity to the rat recombinant NKR-P1 molecule (known in mice also as NK1.1) and to induce NK cell-mediated cytotoxicity. In this study, we investigated whether $GlcNAc_8$ modulates antibody formation as activated NK cells were reported to participate in its regulation. C57BL/6 mice treated with $GlcNAc_8$ and intact controls were immunized either with sheep red blood cells (SRBCs), 2,4-dinitrophenylated-lipopolysaccharide (DNP-LPS) or keyhole limpet hemocyanin (KLH) for evaluation of splenic antibody forming cell counts and serum immunoglobulin (Ig) levels. *In vitro* Ig formation was determined using supernatants of spleen mononuclear cells (SMCs) and CD49b or NK1.1-depleted SMC subpopulations. Serum antigen-specific IgG2a levels were also measured in DBA/2 and BALB/c mice (NK1.1-negative mouse strains on the basis of flow cytometric analysis) which possess different *Nkr-p1c* gene form than C57BL/6 ones. A significant increase in anti-SRBC IgG forming cells, serum levels of anti-KLH as well as anti-DNP IgG and IgG2a was observed after $GlcNAc_8$ administration in C57BL/6 mice. IgM levels in supernatants of SMCs stimulated *in vitro* simultaneously with DNP-LPS and $GlcNAc_8$ were significantly mounted compared with supernatants of SMCs primed with the antigen alone, but this enhancement was blocked after depletion of CD49b-positive or NK1.1-positive cells. In DBA/2 and BALB/c mice, $GlcNAc_8$ influenced neither serum levels of anti-KLH nor anti-DNP IgG2a. These results indicate that $GlcNAc_8$-induced upregulation of antibody formation is triggered by NK cell stimulation and depends on expressed NKR-P1 isoforms, particularly NKR-P1C.

1. Introduction

Oligosaccharide components of glycoproteins and glycolipids are involved in molecular interactions essential for intercellular communication and immune recognition [1–2]. NK and NKT cells express wide repertoire of carbohydrate-binding surface receptors belonging to C-type lectin family (e.g. rat NKR-P1 known in mice also as NK1.1) [3–4].

Carbohydrate sequences based on *N*-acetyl-D-glucosamine were shown previously to be capable of binding to the rat recombinant NKR-P1 molecule and inducing NK cell-mediated cytotoxicity [5–6]. Structural studies of NK cell receptors and their carbohydrate recognition domains brought results indicating that multiple copies of saccharide epitopes presented on a suitable scaffold (molecular, dendritic, polymeric) exerted higher binding affinity to NKR-P1 receptor, which contributed to the synthesis of functionally more effective NKR-P1 ligands such as glycodendrimers [7–8].

Our initial experiments confirmed that the octavalent glycodendrimer displaying simple *N*-acetyl-D-glucosamine substituents clustered on a polyamidoamine core ($GlcNAc_8$) bound strongly to the recombinant NKR-P1 molecule and activated natural killing of tumor cell targets *in vitro* [9–10]. Furthermore, $GlcNAc_8$ delayed appearance of B16F10 murine melanoma and colorectal carcinoma in rat, reduced their growth, and prolonged survival time of treated animals [11].

Although NK cells are primarily known to serve as the first line of defense against malignant transformed and virus-infected cells (reviewed in Ref. [12]), if activated, they were also reported to regulate antibody formation via direct contact with B cells [13–16] and cytokine secretion [17–20]. It was demonstrated that NK cell stimulation by recombinant interleukin-2 [21], polyriboinosinic polyribocytidylic acid (poly (I:C)) [22], certain tumors [23], *Trypanosoma cruzi* [24] or Ribi adjuvant [25] led to the shift in the distribution of antigen-specific immunoglobulin (Ig) isotypes (preferential increase in IgG2a serum level).

In this study, we investigated whether $GlcNAc_8$ modulates antibody response specific for T-independent (2,4-dinitrophenylated lipopolysaccharide, DNP-LPS) and T-dependent soluble (keyhole limpet hemocyanin, KLH) as well as corpuscular antigen (sheep red blood cells, SRBCs) in C57BL/6 mice. To prove the involvement of NK and NKT cells or particularly NK1.1 receptor in the mechanism of $GlcNAc_8$ effect, we determined Ig levels *in vitro* in supernatants of

* Corresponding author. Tel.: +420 296 442 107.
E-mail address: fiserova@biomed.cas.cz (A. Fiserova).

1567-5769/$ – see front matter © 2009 Elsevier B.V. All rights reserved.
doi:10.1016/j.intimp.2009.03.007

spleen mononuclear cells (SMCs) depleted of CD49b-positive or NK1.1-positive subpopulations. Changes in B, T, NK, and NKT cell relative numbers in the spleen and the expression of their activation markers induced by $GlcNAc_8$ were evaluated as well. Finally, we examined whether $GlcNAc_8$ increases antigen-specific IgG2a levels in DBA/2 and BALB/c mice which are considered to be NK1.1-negative on the basis of FACS analysis, whereas PCR genotyping revealed that they possessed different set of NKR-P1 isoforms than C57BL/6 mice (varying in *Nkr-p1b*, *Nkr-p1d* genes, and *Nkr-p1c* alleles) [26].

2. Materials and methods

2.1. Stimuli

N-Acetyl-D-glucosamine-coated polyamidoamine dendrimer (Scheme 1) kindly provided by Prof. T.K. Lindhorst (from Christiana Albertina University in Kiel, Germany) was synthesized as described previously [27]. Briefly, the reaction between polyamidoamine dendrimer of generation 1 bearing eight peripheral amino groups and 2,3,4,6-tetra-O-acetyl-β-*N*-acetyl-glucosaminyl isothiocyanate resulted in O-acetylated isothiourea-bridged glycodendrimer formation. After deacetylation using MeONa in MeOH and subsequent purification by gel permeation chromatography, $GlcNAc_8$ was obtained as a white water-soluble lyophilisate. The structure and purity of the prepared compound were confirmed by electrospray ionization mass spectrometry (ESI-MS) and nuclear magnetic resonance (NMR), (Supplementary material). SRBCs were obtained from Biotest (Prague, the Czech Republic) and washed three times in phosphate buffered saline (PBS) before use. KLH and poly (I:C) were purchased from Sigma-Aldrich (St. Louis, MO, USA) and DNP-LPS from Biosearch Technologies (Novato, CA, USA). All substances used in this study are endotoxin free.

2.2. Experimental animals

Eight-week-old inbred female C57BL/6, DBA/2, and BALB/c mice were purchased from AnLab (Prague, the Czech Republic). The mice were housed under natural day/night conditions (22 °C, 55% relative humidity) and fed on a commercial ST1 diet (Velaz, Prague, the Czech Republic) *ad libitum*. All procedures were conducted in accordance with the European Convention for the Care and Use of Laboratory Animals as approved by the Czech Animal Care and Use Committee.

2.3. Isolation of spleen mononuclear cells (SMCs)

Spleens were squeezed through a nylon mesh and separated on Ficoll-Hypaque (Sigma-Aldrich) density gradient (1.086). SMCs were washed tree times in H-MEMd (Sebac, Aidenbach, Germany) and used immediately for assays.

2.4. Flow cytometric analysis (FACS)

Cell suspensions prepared from spleens of individual mice (as described above) were resuspended in PBS with 0.02% cold water fish skin gelatin (Sigma-Aldrich) and 0.01% sodium azide (Sigma-Aldrich). The phenotype of cells was determined using the following monoclonal antibodies (mAbs) against surface markers of B cells: anti-CD45R/B220-Alexa405 (RA3-6B2), anti-CD19-APC-Cy5.5 (6D5), anti-IgM-FITC, plasma cells: anti-CD138-biotin (281-2), T cells: anti-CD3-PECy5 (17A2), anti-CD8a-Alexa405, anti-CD4-biotin (H129.19), NK and NKT cells: anti-CD49b-FITC (DX5), anti-NK1.1-PECy7 (PK136). The expression of activation antigens on B cells was evaluated by means of anti-CD80-biotin (1G10), anti-CD86-APC (RMMP-2), anti-I-A/I-E-PE (anti-MHC class II molecules, 2G9), and anti-IgG-PE mAbs. Four to six color staining was performed according to the manufacturer's

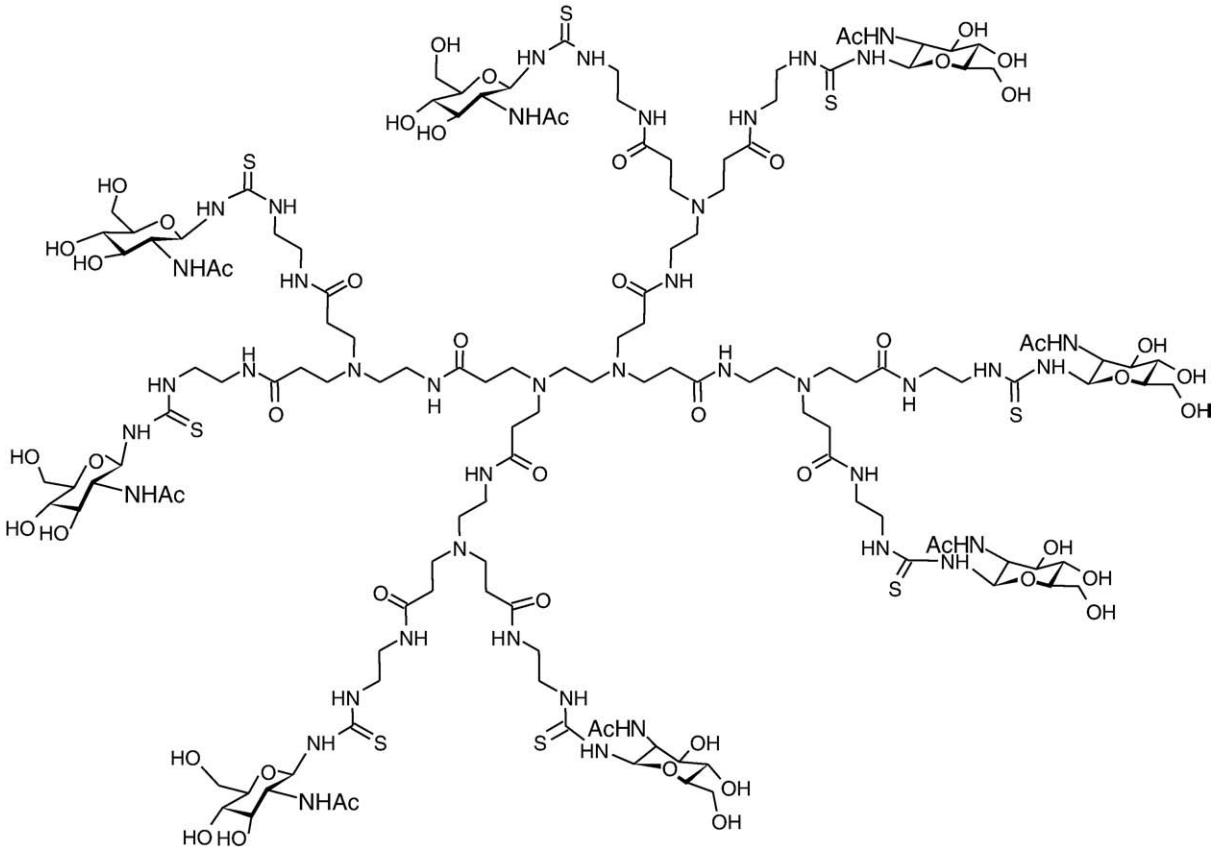

Scheme 1. *N*-Acetyl-D-glucosamine-coated polyamidoamine dendrimer ($GlcNAc_8$).

Table 1
Distribution of T and B cells in the spleen. Significant changes were not observed comparing $GlcNAc_8$ treated mice with controls (PBS group).

		PBS (%)	$GlcNAc_8$ (%)	*p* value
T cells	CD3+	42.07 ± 3.37	40.88 ± 2.11	0.5519
Helper T cells	CD4+/CD8− (out of CD3+ cells)	54.47 ± 1.69	56.96 ± 1.56	0.0592
Cytotoxic T cells	CD8+/CD4− (out of CD3+ cells)	33.22 ± 1.12	31.96 ± 1.33	0.1581
B cells	CD45R/B220+	51.47 ± 1.36	55.32 ± 1.86	0.0772
	CD19+	51.54 ± 1.65	56.22 ± 1.75	0.0562

The data represent average ± standard deviation of values from three performed experiments.

standard protocol. All mAbs were purchased either from Pharmingen (San Diego, CA, USA) or Caltag (San Francisco, CA, USA). Cell surface markers labeled with biotinylated mAbs in the first step were detected with streptavidine-APC-Cy7 (Pharmingen). Samples were analyzed by FACS LSRII (Becton–Dickinson, Franklin Lakes, NJ, USA). The evaluation of measured data was performed using FlowJo version 6.1.1 software (Tree Star, Ashland, OR, USA). The percentage of positive cells was calculated from propidium iodide (Becton–Dickinson) negative cell population (live cells).

2.5. Plaque forming cell (PFC) assay

Five days before the end of experiment, mice (five per group) were immunized i.p. with 5% SRBCs in 0.5 ml PBS. The first dose of $GlcNAc_8$ (0.075 mg/kg) or PBS (in control animals) was administered on the day of immunization. The total treatment comprised two doses (on day 1 and 4). The absolute number of antibody forming cells in the spleen was evaluated by modified Jerne's plaque assay [28]. Briefly, isolated SMCs (2.5×10^6 cells/ml) in RPMI-1640 medium (Sebac) were added to the mixture (42 °C) composed of melted agarose (Fluka Chemie AG, Buchs, Switzerland), 5% HSA (Sigma-Aldrich), and 5% SRBC suspension and then pipetted onto Petri dishes, which were subsequently incubated at 37 °C for 2 h. Hemolytic plaques were counted after incubation (37 °C, 30 min) with 1:9 diluted guinea pig complement (Sigma-Aldrich). To assess the number of IgG forming cells, anti-mouse IgG serum (Sigma-Aldrich) was added to Petri dishes prior to guinea pig complement. The results are expressed as the number of PFCs per spleen (10^8 splenocytes).

2.6. Immunoglobulin ELISA

2.6.1. Ex vivo experiments

Mice (five per group) were immunized i.p. with KLH (5 mg/kg) or DNP-LPS (2.5 mg/kg). Three doses of $GlcNAc_8$ (0.075 mg/kg) were administered every three days starting on the day of immunization. Control animals were treated with PBS in the same intervals. Poly (I:C) treated mice were injected i.p. on day 1 (5.5 mg/kg). Animals were bled 8 days after antigen injection. Sera were collected and stored at −20 °C until levels of anti-KLH or anti-DNP specific antibodies were measured by ELISA. Briefly, flat-bottom, 96-well microtiter plates were coated with either KLH or DNP-BSA at the concentration of 10 μg/ml in 0.1 M $NaHCO_3$ (100 μl/well) and incubated overnight at 4 °C. Then plates were blocked with 5% BSA-PBS (22 °C, 2 h). Subsequently, three dilutions of each serum sample were added to the

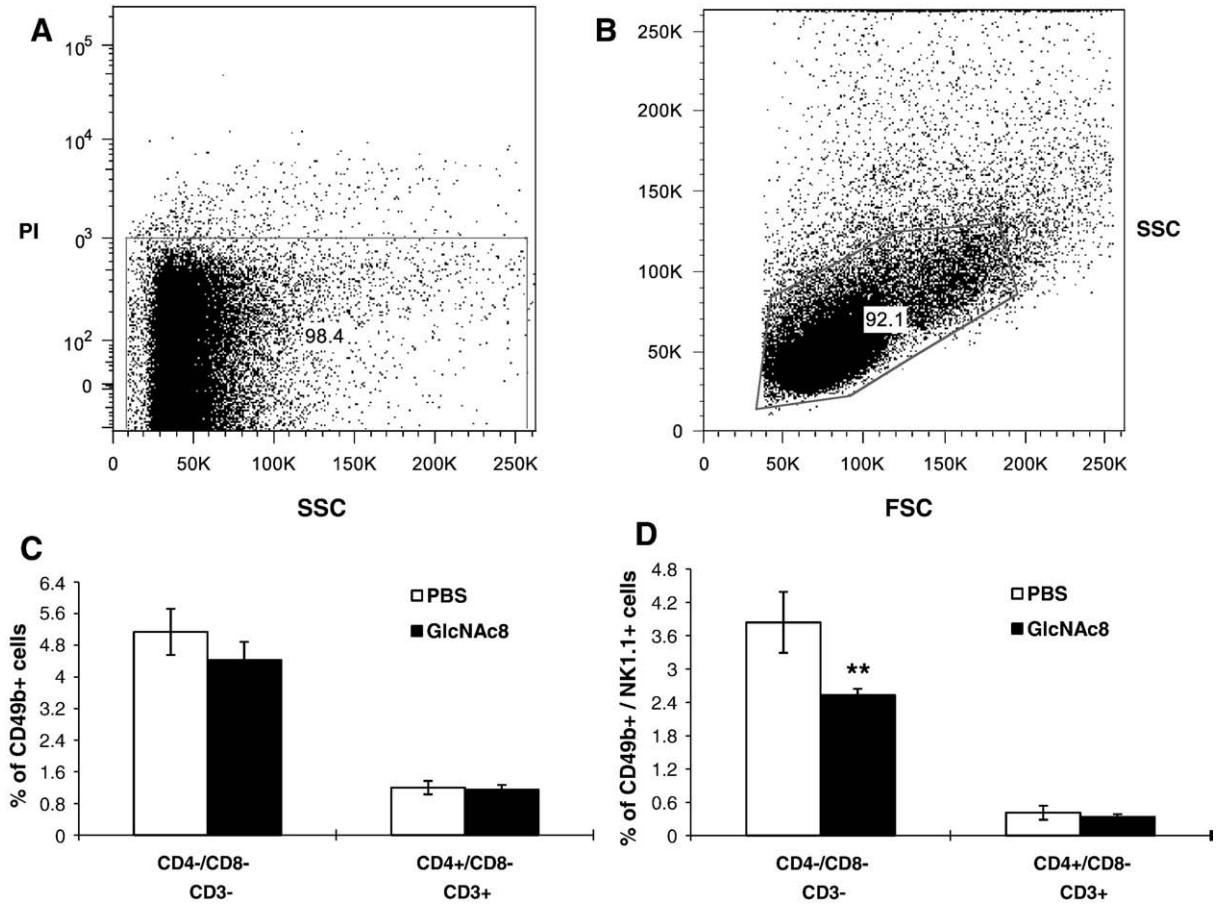

Fig. 1. Distribution of NK and NKT cells in the spleen (C) and their NK1.1 expression (D). Live (propidium iodide (PI) negative) cells (A) with lymphocyte/monocyte morphology gated on the basis of Forward and Side Scatter (FSC/SSC) (B) were at first analyzed for CD3 expression. CD3-negative or CD3-positive subpopulations were further analyzed for CD4 and CD8 expression. NK cells were defined as CD49b-positive cells out of CD3−/CD4−/CD8− cell subpopulation, whereas NKT cells as CD49b-positive cells out of CD3+/CD4+/CD8− cell subpopulation (C). The percentage of NK1.1-positive NK cells was significantly decreased (** $p \leq 0.01$) comparing $GlcNAc_8$ treated mice with controls (PBS group) (D). The data represent average ± standard deviation of values from three performed experiments.

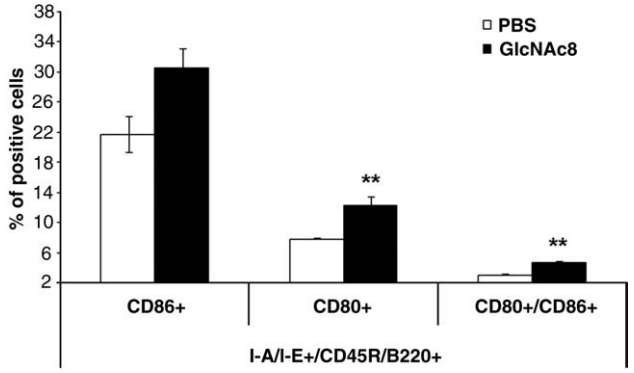

Fig. 2. Proportion of antigen presenting B cells in the spleen. Live (propidium iodide negative) cells with lymphocyte/monocyte morphology gated on the basis of Forward and Side Scatter (FSC/SSC) were at first analyzed for I-A/I-E expression (MHC class II molecules). Then the percentage of B cells (CD45R/B220+) out of I-A/I-E-positive cells was determined. This B cell subpopulation was further analyzed for expression of costimulatory molecules CD80 and CD86. Increase in counts of I-A/I-E+/CD80+ and I-A/I-E+/CD80+/CD86+ antigen-presenting B cells was statistically significant ($p \leq 0.01$) comparing $GlcNAc_8$ treated mice with controls (PBS group). The data represent average ± standard deviation of values from three performed experiments.

plate in duplicate (100 µl/well). After overnight incubation (4 °C) and extensive washing, Igs were detected with horseradish peroxidase-conjugated goat anti-mouse IgM, IgG or IgG2a (Jackson Immunoresearch Laboratories, West Grove, PA, USA). Plates were developed using TMB substrate (Kirkegaard and Perry Laboratories, Gaithersburg, MD, USA) and read at OD 450 nm by an automated ELISA reader (Rainbow Thermo, Tecan Spectra, Salzburg, Austria). Nonimmunized mice were bled to obtain control serum.

2.6.2. In vitro experiments

SMCs from intact C57BL/6 mice (prepared as describe above) were collected and depleted of CD49b-positive or NK1.1-positive cell subpopulations by FACS Vantage SE (Becton–Dickinson) using anti-CD49b-FITC or anti-NK1.1-PECy7 mAb. SMCs, CD49b-negative, and NK1.1-negative cells were cultured in triplicate with DNP-LPS (1 µg/ml) in the presence or absence of 10 nM $GlcNAc_8$ in RPMI-1640 medium supplemented with 2 mM L-glutamine, gentamycin, 10% heat-inactivated fetal calf serum and essential amminoacids (Gibco, Grand Island, NY, USA). Supernatants were harvested after a 5 day-long incubation at 37 °C in a humidified atmosphere containing 5% CO_2 (CO_2 incubator, Jouan, St. Herblain, France). IgM levels were determined by ELISA (as described above).

2.7. PCR genotyping

Genomic DNA for genotyping was obtained from mice tails. Typical 3 mm of mice tails were incubated with lysis buffer containing 100 mM Tris–HCl, 5 mM EDTA, 0.5% SDS, 200 mM NaCl, 40 µg ProteinaseK per tail (Qiagen, Hilden, Germany) in 55 °C for 4 h. Homogenous samples were boiled in 95 °C for 10 min, diluted by water and used as a template for PCR. Amplification was carried out with 0.5 U of HotStarTaq® DNA polymerase (Qiagen), 400 nM primers, and an iCycler5 (Bio-Rad, Hercules, CA, USA). Gene for β-actin was used as a load control. Primers for amplification were following *β-actin* F: 5'*agagggaaatcgtgcgtgac* 3', *β-actin* R: 5' *acggccaggtcatcactattg* 3', *Nkr-p1a* F: *acaagtaggggctgtgatgg* 3', *Nkr-p1a* R: 5'*ctgaaaaccctgctgaaagc* 3', *Nkr-p1b* and *d* F: *agggagcaggaagagaggac* 3', *Nkr-p1b* R: *agtcttgtgggcactctaaa* 3', *Nkr-p1d* R: *agtcttgtgggcactctagc* 3', *Nkr-p1f* F: *tctgaaatctggctgtgctg* 3', and *Nkr-p1f* R: *tgggacttttgggttctttg* 3'. Two alleles of *Nkr-p1c* (allele *(A)* in BALB/c and *(T)* in C57BL/6 mice) were distinguished by allele-specific PCR using common reverse primer: 5'*tgctttcagagtccatgtgc* 3', forward primer for *Nkr-p1c(A)*: 5' *gaaaatggcagctgtgcca* 3', and forward primer for *Nkr-p1c(T)*: 5'gaaaatggcagctgtgcct 3'. Primers were designed in our laboratory using Primer3 Input software.

2.8. Statistical analysis

Statistical significance of differences between two groups was calculated by Student's *t*-test and between more groups by one-way analysis of variance (ANOVA). *p* values ≤ 0.05 were considered as significant (* $p \leq 0.05$, ** $p \leq 0.01$).

3. Results

3.1. Effect of $GlcNAc_8$ on distribution and activation state of SMC subpopulations

The expression of specific and activation markers on SMC subpopulations was evaluated using FACS analysis to reveal the effect of $GlcNAc_8$ on their proportion and activation state. We did not observe significant changes in the relative number of B cells (CD45R/B220+, CD19+), cytotoxic (CD3+/CD8+/CD4−) and helper (CD3+/CD4+/CD8−) T cells (Table 1), NK cells (CD3−/CD4−/CD8−/CD49b+), and NKT cells (CD3+/CD4+/CD8−/CD49b+) (Fig. 1C) comparing $GlcNAc_8$ treated mice with controls (PBS group). The expression of NK1.1 receptor (Fig. 1D) on NK and NKT cells was decreased by $GlcNAc_8$ ($p<0.01$ and $p>0.05$). Results depicted in Fig. 2 demonstrate that $GlcNAc_8$ elevated the counts of I-A/I-E+/CD86+, I-A/I-E+/CD80+, and I-A/I-E+/CD86+/80+ B cells by 41% ($p>0.05$), 58%

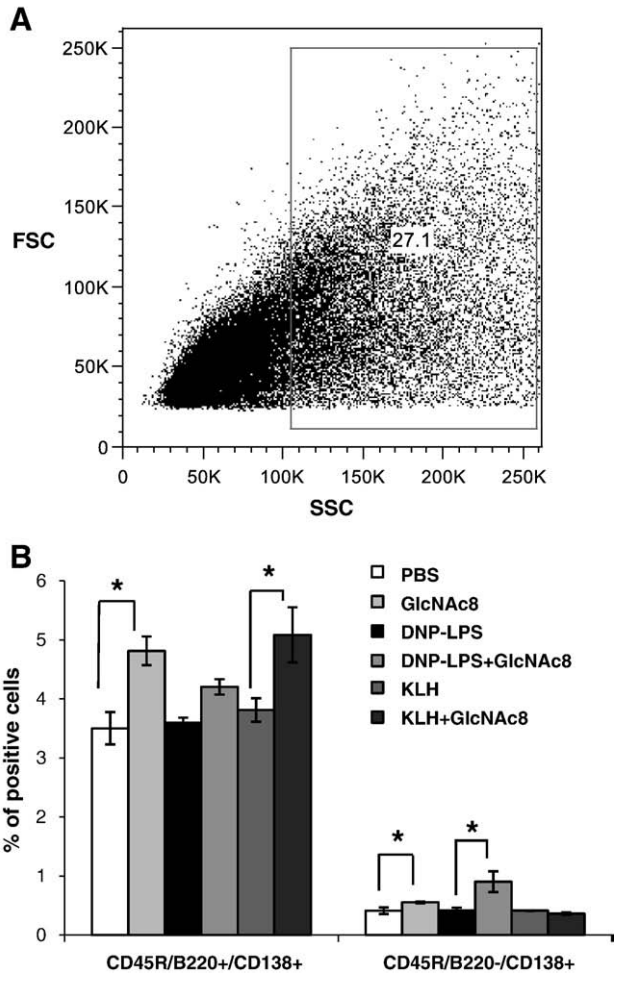

Fig. 3. Distribution of plasma cells in the spleen. Live (propidium iodide negative) cells with monocyte/granulocyte morphology gated on the basis of Forward and Side Scatter (FSC/SSC) (A) were analyzed for CD45R/B220 and CD138 expression. The significant changes in counts of CD45R/B220+/CD138+ and CD45R/B220−/CD138+ plasma cells (B) are marked by asterisk * $p \leq 0.05$. The data represent average ± standard deviation of values from three performed experiments.

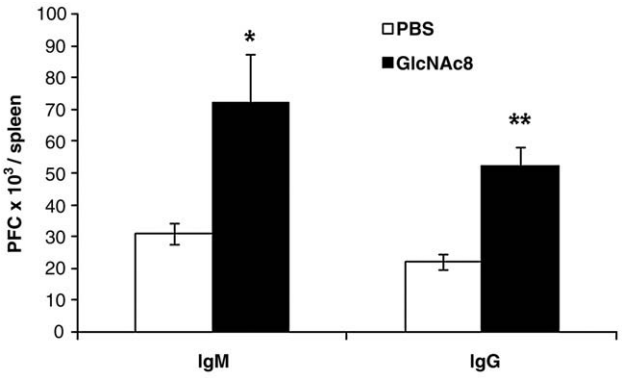

Fig. 4. Effect of $GlcNAc_8$ on the absolute number of antibody forming cells in the spleen. Mice were immunized with SRBC on day 1 and treated with two doses of $GlcNAc_8$ or PBS (controls). PFC assay was performed on day 6. Results are expressed as the number of antibody forming cells (PFC) $\times 10^3$/spleen (10^8 cells). The data represent the average ± standard deviation of values from three independent experiments. Significant changes relative to controls (PBS group) are marked by asterisk (* $p \leq 0.05$, ** $p \leq 0.01$).

($p<0.01$), and 53% ($p<0.01$), respectively. Furthermore, $GlcNAc_8$ treated mice showed nonsignificant 14% and 24% increase in the occurrence of IgM+/IgG+ and I-A/I-E+ B cells, respectively, when compared with controls (data not shown). Plasma cells (CD45R/B220+/CD138+ and CD45R/B220−/CD138+) enhanced their counts after $GlcNAc_8$ administration by 37% ($p<0.05$) and 34% ($p<0.05$), respectively (Fig. 3B).

3.2. Effect of $GlcNAc_8$ on the absolute number of splenic antibody forming cells

We investigated whether $GlcNAc_8$ influences anti-SRBC antibody response by means of PFC assay, which enables to determine the absolute number of IgM and IgG forming cells in the spleen. We found a significant increase in anti-SRBC IgG ($p<0.01$) as well as IgM ($p<0.05$) forming cell counts in spleens of $GlcNAc_8$ treated mice, when compared with immunized controls (SRBC group), (Fig. 4).

3.3. Serum Ig levels in C57BL/6 mice treated with $GlcNAc_8$

To find out whether $GlcNAc_8$ modulates serum levels of antigen-specific Igs, we determined IgM, IgG and IgG2a response by isotype-specific ELISA after immunization of C57BL/6 mice with either KLH (T-dependent antigen) or DNP-LPS (T-independent antigen) in the presence or absence of $GlcNAc_8$. We chose to measure IgG2a levels because the formation of this antibody isotype was reported to be mostly regulated by activated NK cells. We did not observe significant changes in either anti-KLH (Fig. 5A) nor anti-DNP (Fig. 5B) IgM levels between $GlcNAc_8$ treated mice and controls primed with the antigen alone. However, anti-KLH (Fig. 5C) as well as anti-DNP (Fig. 5D) IgG formation was significantly increased after $GlcNAc_8$ administration. Both anti-DNP and anti-KLH IgG2a levels in $GlcNAc_8$ treated mice were significantly enhanced compared with immunized controls and almost reach IgG2a levels in poly (I:C) treated mice (Fig. 6).

3.4. Effect of $GlcNAc_8$ on in vitro antibody formation

The effect of $GlcNAc_8$ on *in vitro* antibody formation was determined by ELISA in supernatants of SMCs after a 5 day-long incubation with DNP-LPS in the presence or absence of $GlcNAc_8$. We observed significant increase ($p<0.05$) in anti-DNP IgM levels measured in supernatants of SMCs which were incubated simultaneously with DNP-LPS and $GlcNAc_8$ compared with controls cultured with DNP-LPS alone. In order to evaluate the involvement of NK and NKT cells or particularly NK1.1 receptor in $GlcNAc_8$ induced *in vitro* IgM formation, we repeated the experiment after depletion of CD49b-positive or NK1.1-positive SMC subpopulations, which blocked the enhancement

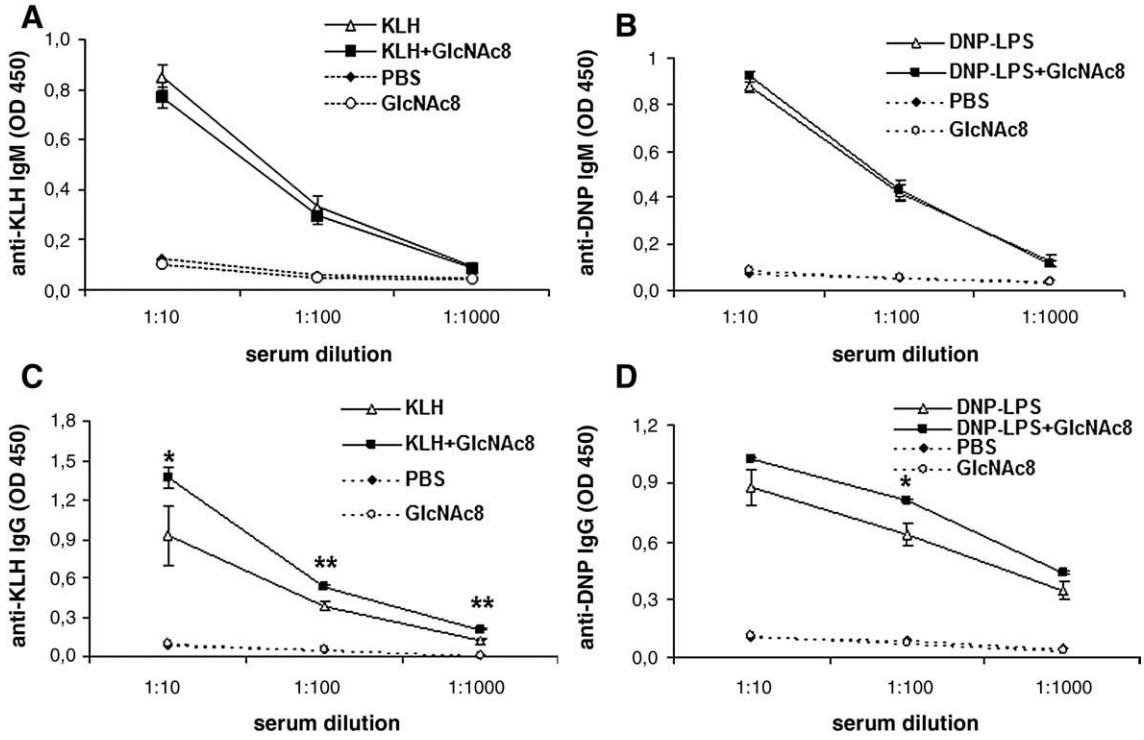

Fig. 5. Antigen-specific IgM and IgG levels in the serum. Mice were primed with KLH or DNP–LPS and treated with 3 doses of $GlcNAc_8$ (on day 1, 4, 7) or PBS. Sera were collected 8 days after immunization. Anti-KLH IgM (A) and IgG (C) or anti-DNP IgM (B) and IgG (D) levels were measured by ELISA. Nonimmunized mice were bled to obtain control serum (dashed lines). Figure shows an illustrative example of three consecutive experiments with similar results. The data represent the average ± standard deviation of values from individual mice (five per group). The level of significance for immunized mice treated with $GlcNAc_8$ (KLH+$GlcNAc_8$ and DNP–LPS+$GlcNAc_8$ group) *vs* immunized controls (KLH and DNP–LPS group) are indicated as follows * $p \leq 0.05$, ** $p \leq 0.01$.

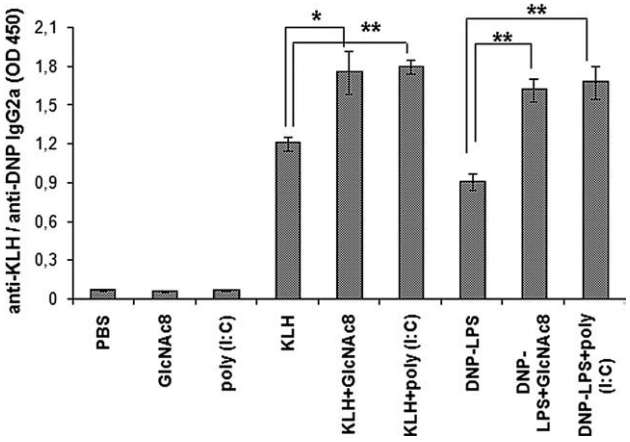

Fig. 6. Serum levels of antigen-specific IgG2a in C57BL/6 mice. Animals were immunized with KLH or DNP–LPS and treated with either poly (I:C), $GlcNAc_8$ or PBS. ELISA for antigen-specific IgG2a was performed 8 days later. Nonimmunized mice were bled to obtain control serum. Figure shows data for 1:10 serum dilution which are representative of three independent experiments with similar results. The statistical analysis was performed by ANOVA and Student's *t*-test for comparison between immunized mice treated with $GlcNAc_8$ or poly (I:C) and immunized controls (KLH and DNP–LPS group). The significant changes are marked by asterisk * $p \leq 0.05$, ** $p \leq 0.01$.

of anti-DNP IgM levels (Fig. 7). IgG levels were not detectable in supernatants of SMCs after a 5 day-long incubation.

3.5. *Nkr-p1* gene family distribution and NK1.1 expression in C57BL/6, DBA/2, and BALB/c mice

Distribution of Nkr-p1 gene family (encoding individual NKR-P1 isoforms) and NK1.1 expression in mice used in the experiments were verified by PCR genotyping and FACS analysis, respectively. *Nkr-p1a* and *Nkr-p1f* genes were identified in all mouse strains. *Nkr-p1b* was of BALB/c and DBA/2, whereas *Nkr-p1d* of C57BL/6 origin. *Nkr-p1c* was present in two distinct gene forms indicated as allele A (*Nkr-p1c(A)*) in BALB/c as well as DBA/2 and as allele T (*Nkr-p1c(T)*) in C57BL/6 mice (Table 2). FACS analysis showed that DBA/2 and BALB/c mice were NK1.1-negative (Fig. 8) as they did not express the product of *Nkr-p1c (T)* gene form which is recognized by anti-NK1.1 (PK136) mAb.

3.6. Serum IgG2a levels in DBA/2 and BALB/c mice treated with $GlcNAc_8$

To assess whether $GlcNAc_8$ increases serum antigen-specific IgG2a levels in NK1.1-negative mouse strains (on the basis of FACS analysis),

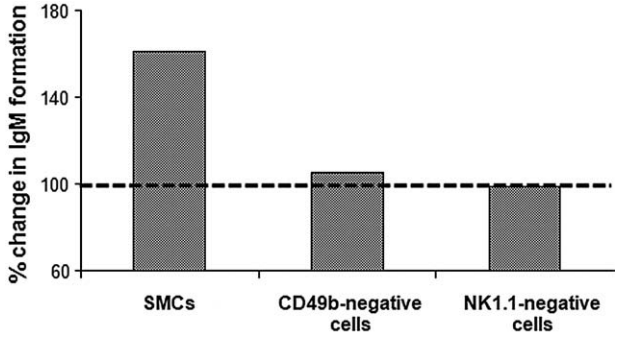

Fig. 7. IgM formation *in vitro*. Isolated SMCs, CD49b-negative or NK1.1-negative cells were cultured with DNP–LPS in the presence or absence of $GlcNAc_8$ for 5 days. Subsequently, anti-DNP IgM levels in supernatants were measured by ELISA. The data are presented as percentage changes in IgM levels (OD 450 nm) comparing supernatants of cells cultured simultaneously with DNP–LPS and $GlcNAc_8$ with those stimulated with DNP–LPS alone (stated as 100%, dashed line). Figure shows an illustrative example of three performed experiments with similar results. Significant difference ($p > 0.05$) was observed only in case of SMCs (undepleted cells).

Table 2
The relationship between distribution of *Nkr-p1* gene family members and NK1.1 expression in C57BL/6, DBA/2, and BALB/c mice.

Mouse strain	*NK1.1* expression by FACS (PK136 mAb)	*Nkr-pl* gene family members					
		a	*b*	*c*(A)	*c*(T)	*d*	*f*
C57BL/6	High	+	−	−	+	+	+
BALB/c	Negative	+	+	+	−	−	+
DBA/2	Negative	+	+	+	−	−	+

Presence and absence of *Nkr-p1* genes for individual NKR-P1 isoforms are indicated with + or −, respectively.

we immunized DBA/2 and BALB/c mice possessing different *Nkr-p1c* gene form than C57BL/6 ones. In DBA/2 and BALB/c mice, unlike in C57BL/6 ones, neither anti-DNP nor anti-KLH IgG2a levels were influenced by $GlcNAc_8$ treatment (Fig. 9A, B).

4. Discussion

It is generally accepted that Ig isotypes and their subclasses contribute to protection against viral and bacterial infection or tumor spreading. Namely, increased IgG2a levels significantly augment antibody-dependent cellular cytotoxicity mediated by NK cells both *in vivo* and *in vitro* [29].

In this study, we demonstrated that $GlcNAc_8$ administration in C57BL/6 mice (NK1.1-positive strain on the basis of FACS analysis) significantly mounted serum levels of IgG2a specific for both T-independent (DNP-LPS) and T-dependent (KLH) antigen (Fig. 6), when compared with controls primed with the antigen alone. As $GlcNAc_8$ activates NK cells [10–11], this finding is in agreement with previous reports showing that resting NK cells fail to modulate antibody response, but if activated (e.g. by poly (I:C)), they preferentially upregulate IgG2a formation [21–25]. In addition, serum levels of IgG2a in mice treated with $GlcNAc_8$ and poly (I:C) were comparable (Fig. 6).

Furthermore, a significant enhancement in serum anti-KLH (Fig. 5C) as well as anti-DNP (Fig. 5D) IgG levels and in the absolute number of anti-SRBC IgG forming cells (Fig. 4) was observed after $GlcNAc_8$ injections. Similarly, it was documented that oral administration of simple D-glucosamine in mice resulted in a significant raise in serum anti-SRBC Ig levels [30]. On the other hand, Reynolds et al. reported that activated NK cells suppressed antibody response to SRBC, probably by interferon-γ secretion [31]. However, on the day when PFC assay was performed (day 6), we did not detect significantly higher levels of this cytokine in supernatants of SMCs isolated from mice treated with $GlcNAc_8$ alone or in combination with SRBC than in those from intact controls (data not shown).

Significant increase in the relative number of plasma cells revealed by FACS analysis (Fig. 3B) confirmed the modulatory effect of $GlcNAc_8$ on antibody formation. Furthermore, $GlcNAc_8$ elevated counts of B cells expressing CD80, CD86, and I-A/I-E molecules (MHC class II), (Fig. 2), which are important for the antigen presentation.

Studies in both murine and human systems showed that activated NK cells did not significantly influence serum IgM levels after immunization with both T-independent and T-dependent antigens [32], which correlates with our results. However, *in vitro* IgM formation can be induced by activated NK cells [22, 33], although further differentiation by switching to downstream isotypes was not reported [33]. We found out that IgM levels in supernatants of SMCs stimulated *in vitro* simultaneously with DNP-LPS and $GlcNAc_8$ were significantly mounted comparing with those primed with the antigen alone, but this enhancement was blocked after depletion of CD49b-positive or NK1.1-positive cell subpopulations (Fig. 7). Anti-DNP IgG levels were not detectable in supernatants of SMCs after a 5 day-long incubation. These observations show that in C57BL/6 mice NK and NKT cells (CD49b-positive cells with high expression of NK1.1 receptor) play a

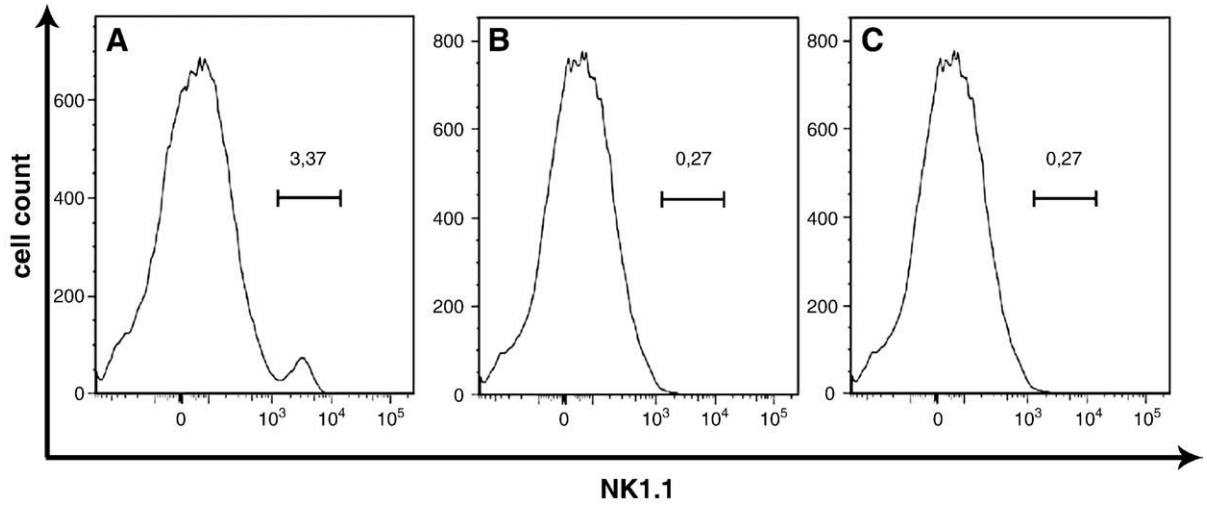

Fig. 8. NK1.1 expression in C57BL/6 (A), DBA/2 (B), and BALB/c (C) mice evaluated by FACS analysis. Live (propidium iodide negative) cells with lymphocyte/monocyte morphology gated on the basis of Forward and Side Scatter were analyzed for NK1.1 expression (cell labeling with PK136 mAb). Figure shows an illustrative example of performed experiments.

crucial role in modulation of antibody formation by $GlcNAc_8$ exerting binding affinity to the recombinant rat NKR-P1 molecule (NK1.1 in mice) [9]. Using FACS analysis, we observed that although $GlcNAc_8$ did not influence the relative number of NK and NKT cells in the spleen (Fig. 1C), it induced a decrease in their NK1.1 expression (statistically significant only in NK cells), (Fig. 1D). This might indicate that $GlcNAc_8$ is uptaken by NK and NKT cells in a complex with NK1.1 receptor.

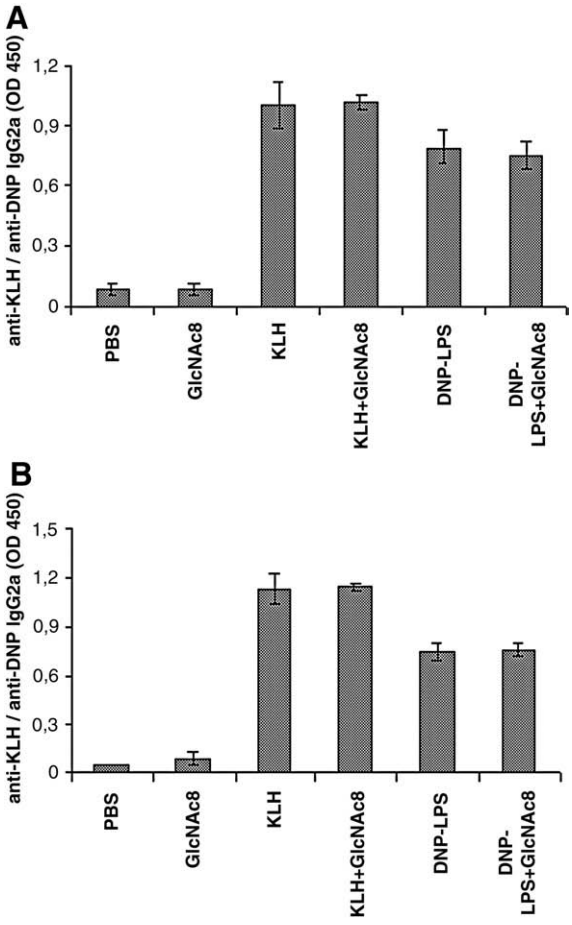

Fig. 9. Serum levels of antigen-specific IgG2a in DBA/2 (A) and BALB/c (B) mice. Animals were immunized with KLH or DNP–LPS and treated with $GlcNAc_8$ or PBS. ELISA for antigen-specific IgG2a was performed 8 days later. Nonimmunized mice were bled to obtain control serum. Figure shows data for 1:10 serum dilution which are representative of three independent experiments with similar results. The statistical analysis was performed by Student's *t*-test for comparison between immunized mice treated with $GlcNAc_8$ and immunized controls (KLH and DNP–LPS group).

NK1.1 is referred to as an antigen defining NK cells in C57BL/6 mice, where it is encoded by several members of *Nkr-p1* gene family (*Nkr-p1a, c, d,* and *f*), [reviewed in Ref. [34]]. On the other hand, DBA/2 and BALB/c mouse strains with *Nkr-p1a, b, c,* and *f* genes are NK1.1-negative on the basis of FACS analysis (Fig. 8) as anti-NK1.1 mAb (PK136) recognizes NKR-P1C of C57BL/6 and NKR-P1B of SJL and Sw mice [35–36]. We demonstrated by PCR genotyping that DBA/2 and BALB/c mice possessed *Nkr-p1c(A)* gene form, whereas C57BL/6 mice had *Nkr-p1c(T)* (Table 2), which is in agreement with results obtained earlier by Carlyle et al. [26]. In DBA/2 and BALB/c mice, unlike in C57BL/6 ones, $GlcNAc_8$ treatment did not influence serum antigen-specific IgG2a levels (Fig. 9A, B). Therefore, we suggest that $GlcNAc_8$ effect on antibody formation in mice might be dependent on the presence of NKR-P1C isoform encoded by *Nkr-p1c(T)* gene form. We do not expect involvement of NKR-P1A and NKR-P1F isoforms (activating receptors) as their genes are present in DBA/2 and BALB/c as well as in C57BL/6 mice. As for NKR-P1B and NKR-P1D isoforms, *Nkr-p1b* gene in DBA/2 and BALB/c mice exerted 94.9% homology with *Nkr-p1d* in C57BL/6 mice. In addition, they both have inhibitory function [26].

In conclusion, $GlcNAc_8$ has a potential to modulate antibody formation via NK cell stimulation. This is probably dependent on expression of NKR-P1C isoform encoded by *Nkr-p1(T)* gene form.

Acknowledgements

We thank Prof. Thisbe K. Lindhorst for kindly providing us $GlcNAc_8$ and its ESI-MS as well as NMR spectra, and Prof. Karel Bezouska for his helpful discussion. This work was supported by the Czech Science Foundation — 310/06/0477, Ministry of Education, Youth and Sports of the Czech Republic – MSM 21620808, the Grant Agency of the AS CR — IAA500200509, IAA500200620, and Institutional Research Concept AV0Z50200510.

Appendix A. Supplementary data

Supplementary data associated with this article can be found, in the online version, at doi:10.1016/j.intimp.2009.03.007.

References

[1] Feizi T, Childs RA. Carbohydrates as antigenic determinants of glycoproteins. Biochem J 1987;245:1–11.
[2] Muraille E, Pajak B, Urbain J, Leo L. Carbohydrate-bearing cell surface receptors involved in innate immunity: interleukin-12 induction by mitogenic and nonmitogenic lectins. Cell Immunol 1999;191:1–9.
[3] Yokoyama WM. Wayne M. Recognition structures on natural killer cells. Curr Opin Immun 1993;5:67–73.
[4] Ryan JC, Seaman WE. Divergent functions of lectin-like receptors on NK cells. Immunol Rev 1997;155:79–89.
[5] Bezouska K, Vlahas G, Horvath O, Jinochova G, Fiserova A, Giorda R, et al. Rat natural killer cell antigen, NKR-P1, related to C-type animal lectins is a carbohydrate-binding protein. J Biol Chem 1994;269:16945–52.
[6] Pospisil M, Vannucci L, Horvath O, Fiserova A, Krausova K, Bezouska K, et al. Cancer immunomodulation by carbohydrate ligands for the lymphocyte receptor NKR-P1. Int J Oncol 2000;16:267–76.
[7] Bezouska K. Design, functional evaluation and biomedical applications of carbohydrate dendrimers (glycodendrimers). J Biotechnol 2002;90:269–90.
[8] Lindhorst TK. Artificial multivalent sugar ligands to understand and manipulate carbohydrate–protein interactions. Host-Guest Chem 2002;218:201–35.
[9] Bezouska K, Kren V, Kieburg C, Lindhorst TK. GlcNAc-terminated glycodendrimers form defined precipitates with the soluble dimeric receptor of rat natural killer cells, sNKR-P1A. FEBS Lett 1998;426:243–7.
[10] Fiserova A, Bezouska K, Svabova L, Jedelsky P, Pucova A, Luptovcova M, et al. Analysis of glycodendrimers effect(s) in tumor microenviroment. Immunol Lett 2003;87:206–10.
[11] Vannucci L, Fiserova A, Sadalapure K, Lindhorst TK, Kuldova M, Rossmann P, et al. Effects of N-acetyl-glucosamine-coated glycodendrimers as biological modulators in the B16F10 melanoma model *in vivo*. Int J Oncol 2003;23:285–96.
[12] Herberman RB, Numm ME, Holdern AT. Natural killer (NK) cells. Prog Clin Biol Res 1976;58:33–43.
[13] Gray J, Horwitz D. Activated human NK cells can stimulate resting B cells to secrete immunoglobulin. J Immunol 1995;154:5656–64.
[14] Cheung JC, Koh CY, Gordon BE, Wilder JA, Yuan D. The mechanism of activation of NK-cell IFN-γ production by ligation of CD28. Mol Immunol 1999;36:361–72.
[15] Blanca IR, Bere EW, Young HA, Ortaldo JR. Human B cell activation by autologous NK cells is regulated by CD40–CD40 ligand interaction: role of memory B cells and CD5+ B cells. J Immunol 2001;167:6132–9.
[16] Gao N, Dang T, Dunnick WA, Collins JT, Blazar RB, Yuan D. Receptors and counterreceptors involved in NK-B cell interactions. J Immunol 2005;174:4113–9.
[17] Becker JC, Kolanus W, Lonnemann C, Schmidt RE. Human natural killer clones enhance *in vitro* antibody production by tumor necrosis factor alpha and gamma interferon. Scand J Immunol 1990;32:153–62.
[18] Michael A, Shao A, Yuan D. Productive interactions between B and NK cells. Nat Immun Cell Growth Regul 1991;218:71–82.
[19] Yuan D, Wilder J, Dang T, Bennett M, Kumar V. Activation of B lymphocytes by NK cells. Int Immunol 1992;4:1373–80.
[20] Snapper CM, Hamaguchi H, Moorman MA, Sneed R, Smoot D, Mond JJ. Natural killer cells induce activated murine B cells to secrete Ig. J Immunol 1994;151: 5251–60.
[21] Amigorena S, Bonnerot C, Fridman WH, Teillaud JL. Recombinant interleukin-2-activated natural killer cells regulate IgG2a production. Eur J Immunol 1990;20: 1781–7.
[22] Wilder JA, Koh CY, Yuan D. The role of NK cells during *in vivo* antigen-specific antibody response. J Immunol 1996;156:146–52.
[23] Koh CY, Yuan D. The effect of NK cell activation by tumor cells on antigen-specific antibody responses. J Immunol 1997;159:4745–52.
[24] De Arruda Hinds LB, Alexandre-Moreira MS, Decote-Ricardo D, Nunes MP, Peçantha MT. Increased immunoglobulin secretion by B lymphocytes from *Trypanosoma cruzi* infected mice after B lymphocytes–natural killer cell interaction. Parasite Immunol 2001;23:581–6.
[25] Yuan D, Bibi R, Dang T. The role of adjuvant on the regulatory effects on NK cells on B cell responses as revealed by a new model of NK cell deficiency. Int Immunol 2004;5:707–16.
[26] Carlyle JR, Mesci A, Ljutic B, Belanger S, Tai LH, Rousselle E, et al. Molecular and genetic basis for strain-dependent NK1.1 alloreactivity of mouse NK cells. J Immunol 2006;176:7511–24.
[27] Lindhorst TK, Kieburg C. Glycocoating of oligovalent amines: synthesis of thiourea-bridged cluster glycosides from glycosyl isothiocyanates. Angew Chem Int Ed Engl 1996;35:1953–6.
[28] Sterzl J, Mandel L. Estimation of the inductive phase of antibody formation by plaque technique. Folia Microbiol 1964;14:173–6.
[29] Koh CY, Yuan D. The functional relevance of NK-cell-mediated upregulation of antigen-specific IgG2a responses. Cell Immunol 2000;204:135–42.
[30] Yan Y, Wanshun L, Baoqin H, Changhong W, Chenwei F, Bing L, et al. The antioxidative and immunostimulating properties of D-glucosamine. Int Immunopharmacol 2006;7:29–35.
[31] Reynolds DS, Boom WH, Abbas AK. Inhibition of B lymphocyte activation by interferon-gamma. J Immunol 1987;139:767–73.
[32] Yuan D. Interactions between NK cells and B lymphocytes. Adv Immunol 2004;84: 1–37.
[33] Vos Q, Ortaldo JR, Conan-Cibotti M, Vos MD, Young HA, Anderson SK, et al. Phenotypic and functional characterization of a panel of cytotoxic murine NK cell clones that are heterogeneous in their enhancement of Ig secretion *in vitro*. Int Immunol 1998;10:1093–101.
[34] Lanier LL. NK cell recognition. Annu Rev Immunol 2005;23:225–74.
[35] Carlyle JR, Martin A, Mehra A, Attisano L, Tsui FW, Zuniga-Pflucker. Mouse NKR-P1B, a novel NK1.1 antigen with inhibitory function. J Immunol 1999;162:5917–23.
[36] Kung SK, Su RC, Shannon J, Miller RG. The NKR-P1B gene product is an inhibitory receptor on SJL/J NK cells. J Immunol 1999;162:5876–87.

Publication 3: GN8P glycomimetic induces tumor–specific antibody response and ADCC via NK cells in tumor–bearing mice.

Overview

We demonstrated previously that repeated GN8P administrations to C57BL/6 mice significantly elevated the number of anti–SRBC (anti–sheep red blood cell) antibody forming cells, serum IgG, and particularly IgG2a, levels specific for both T–independent (2,4–dinitrophenylated lipopolysaccharide, DNP–LPS) and T–dependent (keyhole limpet hemocyanin, KLH) antigen, when compared with controls primed with the antigen alone. Furthermore, depleting CD49b–positive or NK1.1–positive cells from spleen mononuclear cell (SMC) population, we proved that GN8P–induced upregulation of *in vitro* antibody formation was dependent on the presence of NK1.1 expressing NK, eventually NKT cells (112). Many such studies however deal with artificial and simulated conditions and rely on the administration of synthetic exogenous antigens into otherwise healthy immune system. While instrumental in describing the undergoing mechanisms, the practical applications remain elusive, unless proven in immune–compromised conditions, such as tumor–growth or autoimmunity. In order to prove the usefulness of the GN8P glycomimetic administrations we had to confirm its beneficial effect in tumor–bearing mice.

Aims and methods

To evaluate possible GN8P–mediated anti–tumor immune response, several different parameters needed to be investigated. For this purpose, we determined serum anti–B16F10 melanoma IgG levels, IgG2a mRNA expression, and antibody dependent cell–mediated cytotoxicity (ADCC) in tumor–bearing C57BL/6 mice. Changes in counts of basic lymphocyte populations in the spleen evoked by GN8P were followed, with focus on B cells and their differentiation stages as well. Finally, we estimated the synthesis of interferon–gamma (IFNγ) and IL–4, cytokines involved in the regulation of immunoglobulin class switch (111, 113), to reveal the mechanism of NK–mediated glycomimetic effects.

Results and discussion

GN8P administration to tumor–bearing animals did not significantly change the percentual distribution of basic immune cell populations as T helper, T cytotoxic, B cells or NK cells. However, there was a significant increase in CD80/CD86/MHC–II expressing B cell population levels, as well as increased counts of CD138 positive plasma cells, which was previously observed in healthy animals (112).

Serum tumor–specific IgG levels were naturally significantly higher in melanoma–bearing mice when compared to healthy animals, but this increase was further augmented by GN8P administration. This increase was represented not only by the number of IgG positive

B16F10 melanoma cells, but also by the level of coverage by the IgG on these cells. To determine, whether these IgG antibodies had any impact on tumor clearance, we performed the antibody–dependent cell cytotoxicity assay, using B16F10 melanomas as targets – preincubated with sera of GN8P or PBS treated melanoma–bearing mice. Significant increase in cytotoxicity was achieved with sera of GN8P–treated animals. IgG2a antibodies were reported previously to represent the most efficient IgG subclass in mediating ADCC reaction (8) and when tested here, their mRNA expression levels were increased several–fold after the glycomimetic administration, indicating this subclass to be the major one of the IgG detected before.

Since IgG2a–oriented class switch does not usually occur in B cells by itself, but under the effect of IFN–γ or IL–4 (8, 113), we investigated the fate of these two cytokines as well. Both exerted significant increases in expression on the mRNA level and IFNγ was almost exclusively produced by NK cells after GN8P administration, which points to a positive feedback loop established by NK cells. Natural killers, upon interaction with GN8P, increased the production of IFNγ, thus induced the IgG2a class switch in B cells and their differentiation into plasma cells and then used the provided tumor–specific IgG2a for enhanced tumor clearing via ADCC, releasing more tumor–associated antigenic material in the process.

In conclusion, GN8P–activated NK cells potentiate tumor–specific IgG formation, triggering ADCC reaction as well as antigen presentation by B cells. These results illustrate the importance of carbohydrate recognition in NK cell–mediated regulation of adaptive immunity, with benefit for anticancer immune responses.

International Immunopharmacology 11 (2011) 955–961

Contents lists available at ScienceDirect

International Immunopharmacology

journal homepage: www.elsevier.com/locate/intimp

N-Acetyl-D-glucosamine-coated polyamidoamine dendrimer promotes tumor-specific B cell responses via natural killer cell activation

Katarina Hulikova, Jan Svoboda, Veronika Benson, Valeria Grobarova, Anna Fiserova *

Laboratory of Natural Cell Immunity, Department of Immunology and Gnotobiology, Institute of Microbiology, Academy of Sciences of the Czech Republic, v.v.i., Videnska 1083, 142 20 Prague 4, Czech Republic

ARTICLE INFO

Article history:
Received 13 August 2010
Received in revised form 31 January 2011
Accepted 8 February 2011
Available online 22 February 2011

Keywords:
GN8P
B16F10 melanoma
Antibody formation
NK cells
ADCC reaction
IFN-γ

ABSTRACT

N-Acetyl-D-glucosamine-coated polyamidoamine dendrimer (GN8P), exerting high binding affinity to rodent recombinant NKR-P1A and NKR-P1C activating proteins, was shown previously to delay the development of rat colorectal carcinoma as well as mouse B16F10 melanoma, and to potentiate antigen-specific antibody formation in healthy C57BL/6 mice via NK cell stimulation. In this study, we investigated whether GN8P also modulates tumor-specific B cell responses. Serum anti-B16F10 melanoma IgG levels, IgG2a mRNA expression, antibody dependent cell-mediated cytotoxicity (ADCC), and counts of plasma as well as antigen presenting B cells were evaluated in tumor-bearing C57BL/6 mice treated with GN8P and in respective controls. To reveal the mechanism of GN8P effects, the synthesis of interferon-gamma (IFN-γ) and interleukin-4 (IL-4), cytokines involved in regulation of immunoglobulin class switch, was determined. The GN8P treatment significantly elevated IgG, and particularly IgG2a, response against B16F10 melanoma, which led to augmented ADCC reaction. The significant increase in production of IFN-γ, which is known to support IgG2a secretion, was observed solely in NK1.1 expressing cell populations, predominantly in NK cells. Moreover, GN8P raised the number of plasma cells, and promoted antigen presenting capacity of I-A/I-E-positive B lymphocytes by up-regulation of their CD80 and CD86 co-stimulatory molecule expression. These results indicate that GN8P-induced enhancement of tumor-specific antibody formation is triggered by NK cell activation, and contributes to complexity of anticancer immune response involving lectin–saccharide interaction.

1. Introduction

The C-type lectin receptors, predominantly expressed by cells of the innate immunity e.g. natural killer cells (NK cells), are involved in recognition of pathogen associated and/or endogenous carbohydrate structures, including aberrant glycosylation patterns of cancer cells [1–3]. The NK cell receptor protein 1 (NKR-P1) is present in rodents in several isoforms that are encoded by genes located within the natural killer gene complex [4]. While the physiological ligands for NKR-P1B/D, and F were identified as products of the osteoclast inhibitory lectin/C-type lectin related (*Ocil*/*Clr*) gene family, which is interspersed among the *Nkr-p1* genes themselves, those for NKR-P1A and C remain still unknown [5,6].

The synthetic octavalent glycoconjugate with terminal *N*-acetyl-β-D-glucosamine substituents clustered on the polyamidoamine scaffold (GN8P) exerted high binding affinity to activating rat recombinant NKR-P1A [7] and C57BL/6 mouse NKR-P1C (NK1.1) proteins (Bezouska, unpublished experiments), representing orthologous molecules [8]. The GN8P promoted natural killing of tumor targets *in vitro*, delayed incidence of colorectal carcinoma in rats as well as reduced the tumor growth and prolonged survival time in B16F10 melanoma-bearing C57BL/6 mice [9–11].

Although NK cells are primarily known to participate in surveillance against virus-infected and malignant transformed cells (reviewed in Ref. [12]) if activated they were also reported to regulate antibody response via cytokine secretion and/or direct intercellular contact with B lymphocytes [13–21]. Namely, NK cell stimulation by recombinant interleukin-2 [13], polyriboinosinic polyribocytidylic acid (poly (I:C)) [16], certain tumors [17] or *Trypanosoma cruzi* infection [19] led to the shift in the distribution of antigen-specific immunoglobulin (Ig) isotypes with preferential increase of IgG2a secretion.

We demonstrated previously that repeated GN8P administrations to C57BL/6 mice significantly elevated the number of anti-SRBC (anti-sheep red blood cell) antibody forming cells, serum IgG, and particularly IgG2a, levels specific for both T-independent (2,4-dinitrophenylated lipopolysaccharide, DNP-LPS) and T-dependent (keyhole limpet hemocyanin, KLH) antigen, when compared with controls primed with the antigen alone. Furthermore, depleting CD49b-positive or NK1.1-positive cells from spleen mononuclear cell (SMC) subpopulation, we proved that GN8P-induced up-regulation of *in vitro* antibody formation was dependent on the presence of NK1.1 expressing NK, eventually NKT cells [22].

* Corresponding author. Tel.: +420 296 442 107.
E-mail address: fiserova@biomed.cas.cz (A. Fiserova).

1567-5769/$ – see front matter © 2011 Elsevier B.V. All rights reserved.
doi:10.1016/j.intimp.2011.02.009

In this study, we investigated whether GN8P is also able to modulate tumor-specific antibody response. For this purpose, we determined serum anti-B16F10 melanoma IgG levels, IgG2a mRNA expression, and antibody dependent cell-mediated cytotoxicity (ADCC) in tumor-bearing C57BL/6 mice. Changes in counts of basic lymphocyte populations in the spleen evoked by GN8P, with focus on B cells and their differentiation stages were evaluated as well. Finally, we estimated the synthesis of interferon-gamma (IFN-γ) and IL-4, cytokines involved in regulation of immunoglobulin class switch [16,17,23], to reveal the mechanism of GN8P effects.

2. Materials and methods

2.1. Glycodendrimer (GN8P)

N-Acetyl-D-glucosamine-coated polyamidoamine dendrimer (GN8P) kindly provided by Prof. T.K. Lindhorst (Christiana Albertina University in Kiel, Germany) and Prof. V. Kren (Institute of Microbiology, Academy of Sciences of the Czech Republic, Prague, Czech Republic) was synthesized as described previously [24]. Briefly, the reaction between polyamidoamine dendrimer of generation 1, bearing eight peripheral amino groups, and 2,3,4,6-tetra-*O*-acetyl-β-*N*-acetyl-glucosaminyl isothiocyanate resulted in *O*-acetylated isothiourea-bridged glycodendrimer formation. After deacetylation, using sodium methoxide in methanol, and subsequent purification by gel permeation chromatography, GN8P was obtained as a white water-soluble lyophilisate. The structure and purity of the prepared compound were confirmed by electrospray ionization mass spectrometry and nuclear magnetic resonance. Furthermore, GN8P was purified on a reversed phase column to assure that it is endotoxin/LPS free [22].

2.2. Experimental animals

Eight-week-old inbred female C57BL/6 mice (AnLab, Prague, Czech Republic) were housed under natural day/night conditions (22 °C, 55% relative humidity), and fed on a commercial ST1 diet (Velaz, Prague, Czech Republic) *ad libitum*. All procedures were conducted in accordance with the European Convention for the Care and Use of Laboratory Animals as approved by the Czech Animal Care and Use Committee.

2.3. Tumor cells

Established B16F10 cell line (mouse melanoma), purchased from American Type Culture Collection (via Teddington, UK), was cultivated in RPMI-1640 medium (Sigma-Aldrich, St. Luis, MO, USA) supplemented with 2 mM L-glutamine, 1 mM sodium pyruvate, 0.05 mM 2-sulfanylethanol (2-mercaptoethanol), antibiotics (0.05 mg/ml gentamycin, 25 mg/ml amphotericin B), and 10% heat-inactivated fetal calf serum (Gibco, Grand Island, NY, USA) in humidified atmosphere containing 5% CO_2 (CO_2 incubator; Jouan, St. Herblain, France).

2.4. Design of experiments

The mice (5 per group) were injected subcutaneously with 10^6 B16F10 cells/mouse in 0.1 ml phosphate buffered saline (PBS) into the lower back on day 0. Three doses of GN8P or PBS (controls) were administrated intraperitoneally every 3 days starting on day 11 after the tumor inoculation. The animals were bled 24 h after the last treatment (day 18). The GN8P concentration used in this study (0.15 mg/kg of mouse) was chosen on the basis of our previous experiments with doses 7.5–0.0075 mg/kg [11].

2.5. Isolation of spleen mononuclear cells (SMCs)

Spleens were harvested, squeezed through a nylon mesh, and separated on Ficoll-Hypaque (Sigma-Aldrich) density gradient (1.086) to obtain SMCs, which were washed three times in H-MEMd medium (Sebac, Aidenbach, Germany) and used immediately for assays.

2.6. Cell surface marker expression

Cell suspensions prepared from spleens of individual mice (as described above) were re-suspended in PBS with 0.02% cold water fish skin gelatin (Sigma-Aldrich) and 0.01% sodium azide (Sigma-Aldrich). The phenotype of cells was determined using the following monoclonal antibodies (mAbs) against surface markers of B cells: anti-CD45R/B220-Alexa405 (RA3-6B2); plasma cells: anti-CD138-biotin (281-2); T cells: anti-CD3-PECy5 (17A2), anti-CD8a-Alexa405 (5H10), anti-CD4-biotin (H129.19); NK and NKT cells: anti-CD49b-FITC (DX5), anti-NK1.1-PECy7 (PK136). The expression of activation antigens on B cells was evaluated by means of anti-CD80-biotin (1G10), anti-CD86-APC (RMMP-2), and anti-I-A/I-E-PE (anti-MHC class II molecules; 2G9) mAbs. Four to six color staining was performed according to the manufacturer's standard protocol. Monoclonal antibodies were purchased either from Pharmingen (San Diego, CA, USA) or Caltag (San Francisco, CA, USA). The cell surface markers labeled with biotinylated mAbs in the first step were detected with streptavidine-APC-Cy7 (Pharmingen). The samples were analyzed by LSRII cytometer (Becton-Dickinson, Franklin Lakes, NJ, USA). The evaluation of measured data was performed using FlowJo software (Tree Star, Ashland, OR, USA). The percentage of positive cells was calculated from live cell population (propidium iodide-negative; Becton-Dickinson).

2.7. Tumor cell-specific antibodies

2.7.1. Flow cytometric analysis

B16F10 cells were seeded into round-bottomed 96-well microtiter plates (2×10^5cells/well; NUNC, Roskilde, Denmark). Subsequently, 1:10 diluted sera from individual tumor-bearing mice (GN8P or PBS-treated) were added (100 μl/well, 30 min on ice). The cells were blocked with 1:99 diluted goat serum (Sigma-Aldrich), and stained with goat anti-mouse IgG-PE (Immunotech, Marseille, France). B16F10 cells not incubated with serum and those incubated with sera from healthy animals were used as negative controls. The samples were analyzed by LSRII cytometer. The evaluation of measured data was performed using FlowJo software. The results were expressed as mean fluorescence intensity (MFI) of the live cells (Hoechst 33342-negative; Becton-Dickinson).

2.7.2. Western blot analysis

B16F10 melanoma cells (5×10^6) were lysed using M-PER Mammalian Protein Extraction Reagent (Pierce, Rockford, IL, USA) according to the manufacturer's standard protocol. The tumor lysate and marker (pre-stained SDS-PAGE standards; Bio-Rad, Philadelphia, PA, USA) were fractionated by SDS-polyacrylamide gel electrophoresis and transferred onto nitrocellulose membranes as described previously [25]. After blocking with 5% dry milk (90 min; Bio-Rad), the membranes were incubated overnight (4 °C) with 1:10 or 1:100 diluted sera from PBS or GN8P-treated B16F10 melanoma-bearing mice and subsequently with donkey anti-mouse horseradish peroxidase-conjugated IgG (90 min; Jackson Immunoresearch Laboratories, West Grove, PA, USA). After each step, the membranes were extensively washed with TBS-T (Tris-buffered saline containing 0.05% Tween 20; Lachema, Brno, Czech Republic). Immune complexes were visualized by West Pico Chemiluminiscent Substrate Kit (Pierce).

2.8. Antibody dependent cell-mediated cytotoxicity

$Na_2^{51}CrO_4$-labeled B16F10 tumor targets were seeded in pentaplicates into round-bottomed 96-well microtiter plates (10^4 cell/well; NUNC), and pre-incubated with 1:10, 1:50 or 1:100 diluted sera from PBS or GN8P-treated B16F10 melanoma-bearing mice (37 °C, 30 min).

The antibody containing sera were washed out, and then SMCs isolated from spleens of healthy animals were added as effectors (effector to target (E:T) ratio = 64:1, 32:1, and 16:1). After 18-h incubation at 37 °C in humidified atmosphere containing 5% CO_2, the cell free supernatants were harvested (25 μl/sample), 0.1 ml of scintillation cocktail (SuperMix; Wallac, Turku, Finland) was added, and the radioactivity measured employing scintillation counter Microbeta Trilux (Wallac). The percentage of cytotoxicity was calculated as described previously [26].

2.9. Cytokine detection

2.9.1. Serum IFN-γ and IL-4 levels

For evaluation of IFN-γ and IL-4 serum levels, BD™ Cytometric Bead Array (Mouse Th1/Th2 cytokine kit; BD Bioscience, San Jose, CA, USA) was used. This assay is based on mixed bead populations with distinct fluorescence intensities, which are coated with capture antibodies specific for the individual cytokine. The samples were prepared according to manufacturer's standard protocol and measured by LSRII cytometer. The evaluation of data was performed using FlowJo software. The cytokine concentration in pg/ml was calculated from calibration curves of standards.

2.9.2. Intracellular IFN-γ levels

For intracellular detection of IFN-γ, isolated SMCs were incubated with Golgi Stop (0.7 μl/10^6 cells; Pharmingen) in humidified atmosphere containing 5% CO_2 for 6 h. Then, the cells were stained with anti-CD3-PECy5 and anti-NK1.1-PECy7 mAbs (Pharmingen), permeabilized with FACS™ permeabilizing solution (Becton-Dickinson), labeled with biotinylated anti-IFN-γ mAb and streptavidine-PE (Pharmingen), and fixed with 1% paraformaldehyde (Lachema). To evaluate IFN-γ synthesis in helper and cytotoxic T cells, SMCs were additionally *in vitro* stimulated with phorbol 12-myristate 10-acetate (PMA) and ionomycin for 4 h (at the final concentration of 50 ng/ml and 1 μg/ml, respectively, in the presence of Golgi Stop), and stained with anti-CD4-APCAlexaFluor780 and anti-CD8-PerCPCy5.5 mAbs. The samples were measured by LSRII cytometer. The data analysis was performed using FlowJo software.

2.10. Real-time reverse transcription (RT)-PCR

The total RNA was isolated from SMCs using RNeasy Mini Kit (Qiagen, Hilden, Germany). Five micrograms of RNA were transcribed into cDNA using cDNA Archive Kit (Applied Biosystem, Foster City, CA, USA). Real-time RT-PCR was carried out with FastStart SYBR Green Master (Roche, Mannheim, Germany) and iCycler5 (Bio-Rad). PCR product specificity was checked by melt curve analysis. Primer sequences used for amplification were the following *IFN-γ* Forward (F): 5′ *tcaagtggcatagatgtggaagaa* 3′, *IFN-γ* Reverse (R): 5′ *catgaaaatcctgcagagcca* 3′; *IL-4* F: 5′ *acaggagaagggacgccat* 3′, *IL-4* R: 5′ *tgagctcgtctgtagggcttc* 3′; *IgG2a* F: 5′ *tgcaaggtcaacaacagagc* 3′; and *IgG2a* R: 5′ *ggtccagtccacagcaattt* 3′. Primers were designed in our laboratory using Primer3 Input software. The gene of interest was normalized to the control gene for 18S rRNA. Differences in gene expression between individual groups of mice were evaluated with Bio-Rad iQ5 2.0 software.

2.11. Statistical analysis

The statistical significance of differences between two groups was calculated by Student's t-test and between more groups by one-way analysis of variance (ANOVA). P values ≤ 0.05 were considered as significant ($^{*}p \leq 0.05$; $^{**}p \leq 0.01$; $^{***}p \leq 0.001$).

Table 1
Percentage of helper and cytotoxic T cells, B, NK and NKT cells out of spleen mononuclear cells. The data represent average ± standard deviation of values from four performed experiments.

		PBS (%)	GN8P (%)	p value
Helper T cells	CD3+/CD4+/CD8−	20.64 ± 1.03	21.86 ± 0.54	0.0925
Cytotic T cells	CD3+/CD8+/CD4−	12.09 ± 0.69	11.2 ± 0.31	0.0871
B cells	CD45R/B220+	57.02 ± 2.28	59.6 ± 1.85	0.0778
NK cells	CD3−/CD4−/CD8−/CD49b+	3.51 ± 0.18	3.87 ± 0.22	0.1015
NKT cells	CD3+/CD4+/CD8−/CD49b+	0.28 ± 0.02	0.31 ± 0.05	0.5490

Table 2
Effect of GN8P on NK1.1 expression on NK and NKT cells in the spleen. The results represent percentage of NK1.1-positive NK and NKT cells identified as CD3−/CD4−/CD8−/CD49b+ and CD3+/CD4+/CD8−/CD49b+ subpopulations, respectively. The data are expressed as average ± standard deviation of values from three performed experiments.

	PBS	GN8P	p value
%NK1.1 + NK cells	69.00 ± 5.77	54.50 ± 6.87	0.0503
%NK1.1 + NK cells	35.4 ± 5.20	30.4 ± 5.43	0.2200

3. Results

3.1. Effect of GN8P on distribution and activation state of SMC subpopulations

The expression of membrane markers on SMC subpopulations from B16F10 melanoma-bearing mice was evaluated using flow cytometry to reveal the effect of GN8P on their proportion and activation state. We did not observe significant differences in the relative number of basic lymphocyte subpopulations i.e. B cells (CD45R/B220+), helper (CD3+/CD4+/CD8−) and cytotoxic (CD3+/CD8+/CD4−) T cells, NKT cells (CD3+/CD4+/CD8−/CD49b+), and NK cells (CD3−/CD4−/CD8−/CD49b+) comparing GN8P-treated mice with controls (PBS group) (Table 1). However, GN8P induced decrease in the percentage of NK1.1 expressing NK cells (Table 2). The phenotype analysis of B lymphocytes was designed to follow up their differentiation into the plasma and antigen presenting cell stage. Results depicted in Fig. 1 demonstrate that GN8P significantly elevated the counts of I-A/I-E+/CD86+ ($p<0.01$), I-A/I-E+/CD80+ ($p<0.001$), and I-A/I-E+/CD86+/CD80+ ($p<0.001$) antigen presenting B cells. Furthermore, animals injected with GN8P

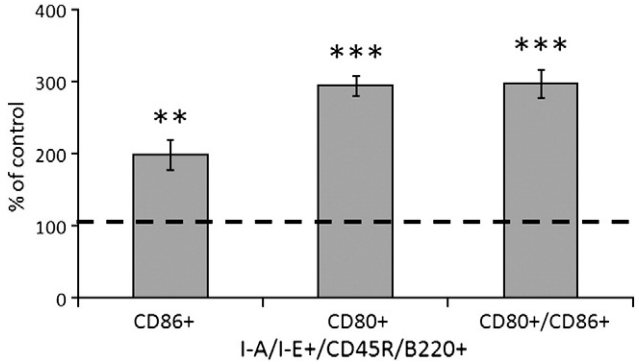

Fig. 1. Proportion of antigen presenting B cells in the spleen. Live (propidium iodide-negative) cells with lymphocyte/monocyte morphology gated on the basis of Forward and Side Scatter were at first analyzed for I-A/I-E (MHC class II) expression. Then, the percentage of B cells (CD45R/B220+) out of I-A/I-E-positive cells was determined. This B cell subpopulation was further analyzed for expression of co-stimulatory molecules CD80 and CD86. The data are presented as percentage of control (PBS group stated as 100%; dashed line; control values were 14.98 ± 3.16, 6.52 ± 0.79, and 2.02 ± 0.41 for CD86+, CD80+, and double positive CD80+ CD86+ cells, respectively). Figure shows an illustrative example of three experiments with similar results. Significant changes relative to control are marked by asterisk ($^{**}p \leq 0.01$, $^{***}p \leq 0.001$).

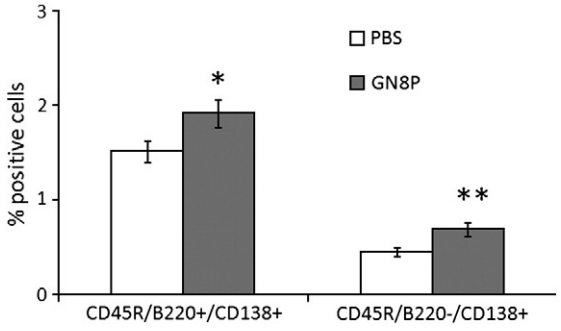

Fig. 2. Distribution of plasma cells in the spleen. Live (propidium iodide-negative) cells with lymphocyte/monocyte morphology gated on the basis of Forward and Side Scatter were analyzed for CD45R/B220 and CD138 expression. Significant changes in counts of CD45R/B220+/CD138+ and CD45R/B220−/CD138+ plasma cells relative to control (PBS group) are marked by asterisk (*$p \leq 0.05$, **$p \leq 0.01$). The data are expressed as average ± standard deviation of values from three performed experiments.

showed significantly higher proportion of plasma cells, identified as CD45R/B220+/CD138+ ($p<0.05$) and CD45R/B220−/CD138+ ($p<0.01$) cell populations, than controls (PBS group), (Fig. 2).

3.2. Serum levels of tumor-specific antibodies in B16F10 melanoma-bearing mice treated with GN8P

Results showing that GN8P mounted antigen-specific (anti-KLH and anti-DNP) IgG, and particularly IgG2a, response in healthy C57BL/6 mice [22] as well as the percentage of antigen presenting B lymphocytes (Fig. 1) and plasma cells (Fig. 2) in B16F10 melanoma-bearing counterparts, encouraged us to investigate, whether this glycoconjugate has also the potential to modulate tumor-specific antibody formation. For this purpose, serum levels of IgG antibodies, capable of specific binding to B16F10 cells, were measured in B16F10 melanoma-bearing mice after three doses of GN8P or PBS using flow cytometry. In sera of PBS-treated mice, we detected B16F10 melanoma-specific IgG levels (PBS group vs. healthy control $p<0.05$), which were further elevated by GN8P administrations (PBS vs. GN8P group $p<0.001$), (Fig. 3). To confirm these results and find out whether GN8P promotes antibody formation specific for one or more B16F10 melanoma antigens, we analyzed sera from experimental animals for reactivity against proteins of B16F10 cell lysate by Western blotting. Under our experimental conditions (West Pico Chemiluminiscent Substrate Kit), testing of 1:10 diluted sera revealed that GN8P increased antibody response against several B16F10 melanoma proteins (Fig. 4A). At 1:100 serum dilution, when only the dominant protein of molecular weight ≈ 50 kDa was visualized, sera from GN8P-treated B16F10 melanoma-bearing mice were more efficient in its recognition than those from controls (PBS group) (Fig. 4B).

3.3. Antibody dependent cell-mediated cytotoxicity in B16F10 melanoma-bearing mice treated with GN8P

To evaluate the clinical consequence of GN8P-induced enhancement in serum levels of B16F10 melanoma-specific IgG antibodies, we determined ADCC reaction performing 18-h ^{51}Cr-release assay. The

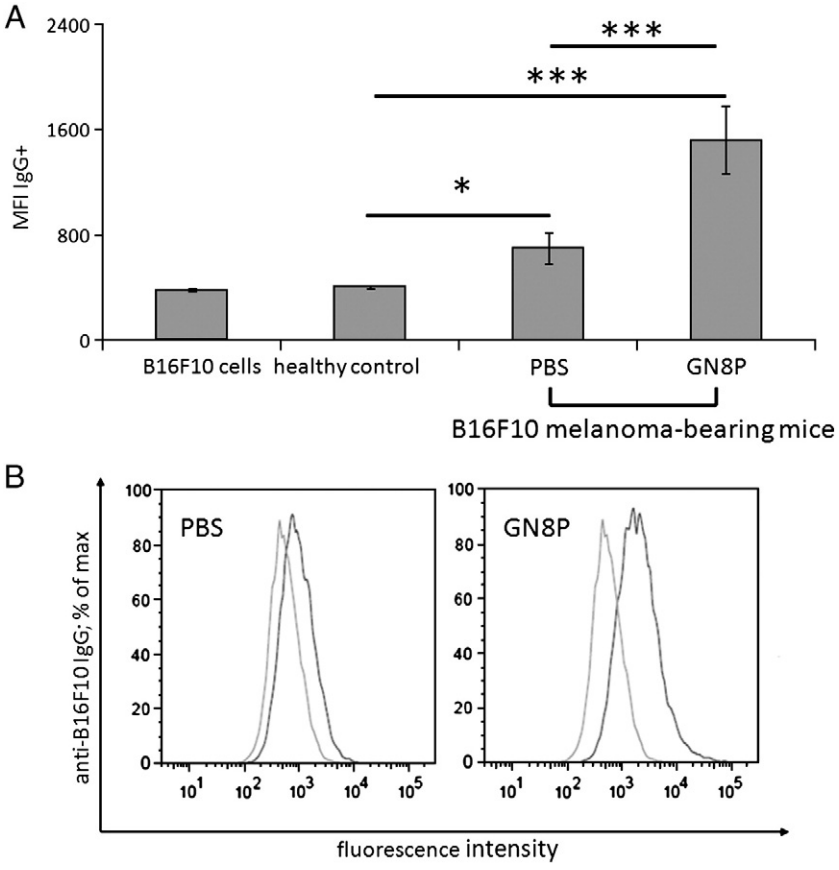

Fig. 3. Flow cytometric analysis of tumor-specific antibody formation. The mice (5 per group) were inoculated with B16F10 tumor cells and injected with 3 doses of PBS or GN8P. Sera were collected 24 h after the last treatment. To detect anti-B16F10 IgG levels, B16F10 cells were incubated with 1:10 diluted sera and anti-mouse PE-conjugated IgG as described in Materials and methods section. Intact B16F10 cells (not incubated with serum) and those incubated with sera from healthy animals were used as negative controls. The results are expressed as (A) average ± standard deviation of mean fluorescence intensity (MFI) of live B16F10 cells incubated with sera from individual mice or (B) histograms (B16F10 cells incubated with sera from healthy control are indicated in light color, whereas those incubated with sera from PBS or GN8P-treated B16F10 tumor-bearing mice in dark color). Figure shows an illustrative example of three experiments with similar results. The statistical analysis was performed by ANOVA. The significant changes are marked by asterisk (*$p \leq 0.05$, ***$p \leq 0.001$).

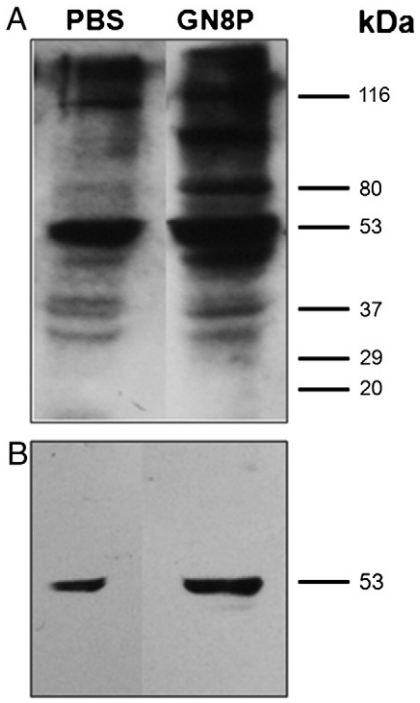

Fig. 4. Western blot analysis of tumor-specific antibody formation. The mice (5 per group) were inoculated with B16F10 tumor cells and injected with 3 doses of PBS or GN8P. Sera were collected 24 h after the last treatment. To detect anti-B16F10 IgG levels, nitrocellulose membranes with blotted proteins of B16F10 cell lysate were incubated with 1:10 (A) or 1:100 (B) diluted sera and anti-mouse horseradish peroxidase-conjugated IgG as described in Materials and Methods. Kodak films were developed after 30-min incubation with West Pico Chemiluminiscent Substrate. Figure shows an illustrative example of five experiments with similar results.

B16F10 melanoma cells pre-incubated with sera from tumor-bearing animals treated with GN8P or PBS were used as targets, while SMCs from healthy untreated C57BL/6 mice as effectors. SMCs exerted significantly higher cytotoxicity ($p<0.001$) against tumor targets pre-incubated with 1:10, 1:50 as well as 1:100 diluted sera from GN8P-treated mice than against those pre-incubated with equally diluted sera from controls (PBS group) at both 64:1 and 32:1 E:T ratios. The effect of GN8P on ADCC reaction seems to be dependent on E:T ratio (no significant differences at 16:1 E:T). The optimal E:T ratio was 32:1 (the highest significant differences), at which the lysis of B16F10 cells pre-incubated with 1:10, 1:50, and 1:100 diluted sera from B16F10 melanoma-bearing mice injected with GN8P was increased by 58.3%, 61.18%, and 50.83%, respectively, comparing to controls (PBS group) (Fig. 5).

3.4. Effect of GN8P on IgG2a mRNA expression in B16F10 melanoma-bearing mice

As IgG2a antibodies were reported to represent the most efficient IgG subclass in mediating ADCC reaction [27,28], we tested the effect of GN8P treatment on IgG2a mRNA levels. The GN8P administrations to B16F10 melanoma-bearing mice significantly augmented IgG2a mRNA expression ($p<0.01$; Fig. 6), which indicates that elevated serum levels of tumor-specific IgG antibodies (Figs. 3 and 4) triggering ADCC reaction (Fig. 5) were of IgG2a subclass.

3.5. Effect of GN8P on the cytokine synthesis

3.5.1. Serum IFN-γ and IL-4 levels

To assess whether GN8P modulates the secretion of cytokines involved in regulation of immunoglobulin class switch, we detected serum levels of IFN-γ and IL-4 (prototype Th1 and Th2-type cytokine, respectively) using the cytometric bead array. In response to GN8P

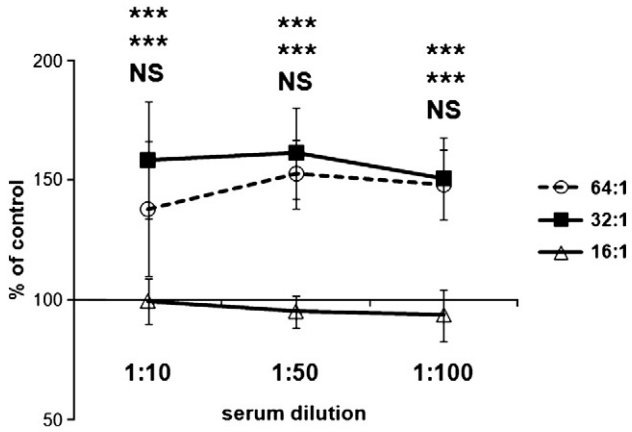

Fig. 5. Antibody-dependent cell mediated cytotoxicity (ADCC reaction). The mice (5 per group) were inoculated with B16F10 tumor cells and injected with 3 doses of PBS or GN8P. Sera were collected 24 h after the last treatment. The ADCC reaction was determined after 18-h incubation of spleen mononuclear cells from healthy mice with B16F10 tumor targets pre-incubated with sera from PBS or GN8P-treated tumor-bearing animals. The data are presented as percentage of control (PBS group stated as 100%; average control values were 14.14 ± 1.92, 11.46 ± 1.52, and 8.3 ± 1.21 for 64:1, 32:1, and 16:1 E:T ratio, respectively). Figure shows average ± standard deviation of values from three performed experiments. The significant changes relative to control ($p\leq0.001$) were observed at 64:1 and 32:1 E:T ratios at each tested serum dilution (NS = non-significant).

treatment, B16F10 melanoma-bearing mice showed significant increase ($p<0.05$) solely in IFN-γ levels (Fig. 7A).

3.5.2. IFN-γ and IL-4 mRNA expression

To confirm the above described results, we also determined expression of mRNA for the tested cytokines. Real-time RT-PCR revealed that GN8P increased IFN-γ mRNA levels to a greater extent ($p<0.001$) than those for IL-4 ($p<0.01$), (Fig. 7B). Thus, mounted IgG2a mRNA expression (Fig. 6) correlated with elevated mRNA levels for IFN-γ, which is known to support the immunoglobulin class switch to IgG2a isotype [16,17,23].

3.6. Cell subpopulations producing IFN-γ in response to GN8P treatment

To find out which cell subpopulations are involved in GN8P-induced enhancement of IFN-γ synthesis in B16F10 melanoma-bearing C57BL/6 mice, we measured intracellular levels of this cytokine using flow cytometry. Upon repeated GN8P administrations, significant increase in the percentage of IFN-γ-positive NK (CD3−/NK1.1+) as well as NKT (CD3+/NK1.1+) cells was observed ($p<0.01$

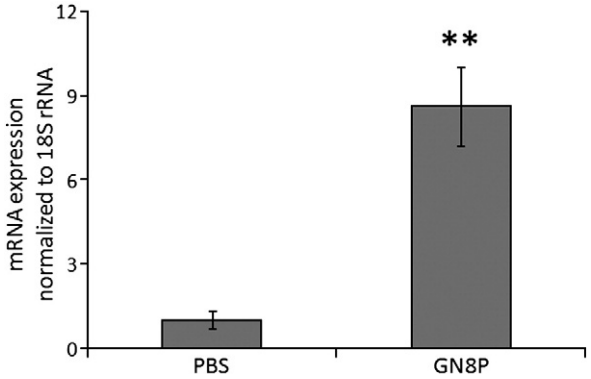

Fig. 6. IgG2a mRNA expression. The mice were inoculated with B16F10 tumor cells, injected with 3 doses of GN8P or PBS, and bled 24 h after the last treatment. The total mRNA was isolated from spleen mononuclear cells of experimental animals. IgG2a mRNA levels were determined by real-time RT-PCR and normalized to the expression of control gene for 18S rRNA. Results are expressed as average ± standard deviation of pentaplicates. Figure shows a representative example of three experiments with similar results. The significant changes are marked by asterisk (**$p\leq0.01$).

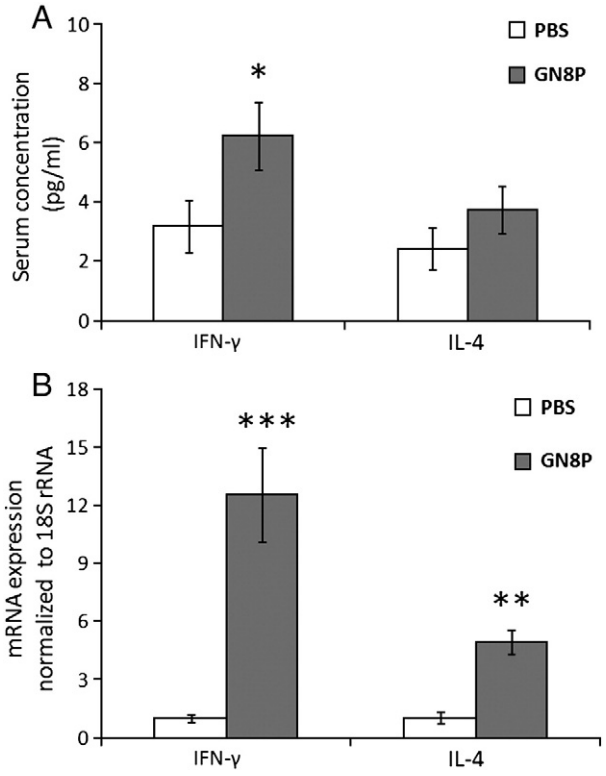

Fig. 7. IFN-γ and IL-4 synthesis. The mice (5 per group) were inoculated with B16F10 tumor cells, injected with 3 doses of GN8P or PBS, and bled 24 h after the last treatment. Serum (A) and mRNA (B) levels of IFN-γ and IL-4 were determined using BD™ Cytometric Bead Array (Mouse Th1/Th2 Cytokine Kit) and real-time RT-PCR, respectively. The total mRNA was isolated from spleen mononuclear cells of experimental animals. Results are expressed as average ± standard deviation of values from three performed experiments. Significant changes between GN8P-treated mice and controls (PBS group) are marked by asterisk (*$p \leq 0.05$, **$p \leq 0.01$, ***$p \leq 0.001$).

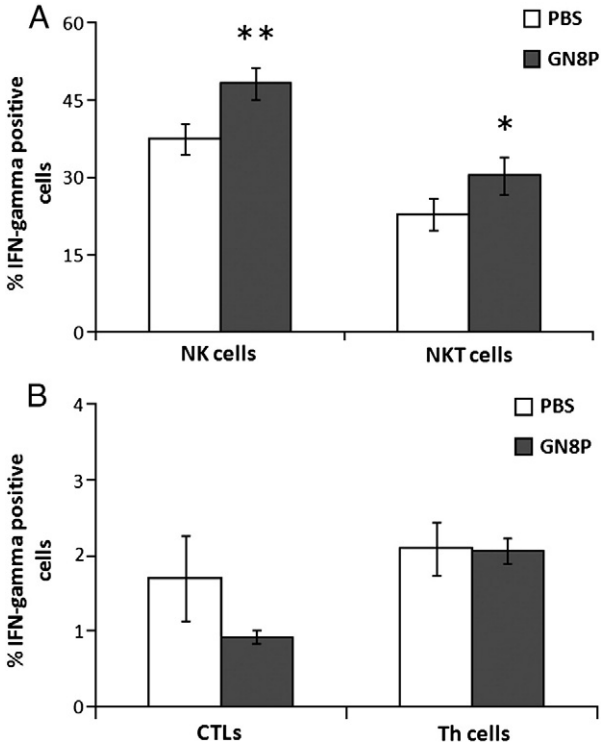

Fig. 8. Cell subpopulations producing IFN-γ. The mice (5 per group) were inoculated with B16F10 tumor cells, injected with 3 doses of GN8P or PBS, and bled 24 h after the last treatment. Spleen mononuclear cells (SMCs) were incubated with Golgi Stop in the absence (A) or presence (B) of PMA/ionomycin. SMCs with lymphocyte/monocyte morphology gated on the basis of Forward and Side Scatter were at first analyzed for CD3 and NK1.1 expression. Then, the percentage of IFN-γ-positive cells out of NK (CD3−/NK1.1+) and NKT (CD3+/NK1.1+) cells was determined (A). PMA/ionomycin-stimulated SMCs with lymphocyte/monocyte morphology were at first gated on the basis of CD3 and NK1.1 expression. Then, the percentage of cytotoxic (CD8+/CD4−) and helper (CD4+/CD8−) T lymphocytes out of CD3+/NK1.1− cells was determined. Finally, IFN-γ synthesis in these T cell subpopulations was evaluated (B). The data represent average ± standard deviation of values from 3 experiments. Significant changes between GN8P-treated mice and controls (PBS group) are marked by asterisk (*$p \leq 0.05$, **$p \leq 0.01$).

and $p < 0.05$, respectively), whereas counts of IFN-γ producing helper (CD3+/NK1.1−/CD4+/CD8−) and cytotoxic (CD3+/NK1.1−/CD8+/CD4−) T cells remained unaffected (Fig. 8B). These results proved that GN8P potentiated IFN-γ production only in NK1.1-positive cell subpopulations, predominantly in NK cells.

4. Discussion

It is generally accepted that Igs participate in protection against viral and bacterial infections. However, their role in the control of tumor spreading is not single valued. Anticancer vaccines, which are able to elicit antibody response triggering ADCC reaction and/or complement-mediated lysis of tumor cells, were successfully tested in clinical trials [28–31]. On the other hand, there are reports showing that elevated levels of tumor-specific antibodies paradoxically correlated with decreased survival of cancer patients. This can be explained by the fact that antibody functions in general, and in relation to cancer immunosurveillance depend on Ig isotype/subclass [28,32].

In this study, we demonstrated that GN8P administrations to B16F10 melanoma-bearing C57BL/6 mice evoked significant increase in anti-tumor IgG (Figs. 3 and 4), and particularly IgG2a, formation, which was confirmed at mRNA level by real-time RT-PCR (Fig. 6). IgG2a antibodies were identified as the most efficient IgG subclass in mediating ADCC reaction under both *in vitro* and *in vivo* conditions [27,28]. In accordance with this finding, we observed that SMCs isolated from healthy C57BL/6 mice showed significantly higher cytotoxic activity against B16F10 tumor targets (64:1 and 32:1 E:T) pre-incubated with sera from B16F10 melanoma-bearing mice treated with GN8P than against those pre-incubated with sera from controls (PBS group) (Fig. 5). Thus, GN8P-induced enhancement of serum anti-B16F10 melanoma IgG levels (Figs. 3 and 4) resulted in augmented ADCC reaction (Fig. 5), which might contribute to GN8P anticancer properties (i.e. reduced melanoma growth and prolonged survival time of experimental animals) described previously [11].

As GN8P promoted cytokine synthesis (Figs. 7 and 8A) as well as killing activity of NK cells derived from spleen [9,11] and peripheral blood [33], our results are in agreement with studies documenting that resting NK cells fail to modulate antibody response, but if activated (e.g. by poly (I:C)), they increase IgG2a formation [13,16,17,19]. Moreover, we reported that GN8P treatment elevated serum anti-KLH as well as anti-DNP IgG2a levels in healthy C57BL/6 mice [22]. NK cells can program B cells to switch preferentially to IgG2a isotype via IFN-γ secretion [16,17]. In our experimental model, GN8P-induced enhancement of IFN-γ production (Fig. 7) in NK cells (Fig. 8A) also represents one of the possible mechanisms involved in up-regulation of serum IgG2a levels [22] and IgG2a mRNA expression (Fig. 6).

Cross-linking of NKR-P1C receptor with anti-NK1.1 mAb was shown to trigger NK cell-mediated cytotoxicity [34] and IFN-γ release [35]. Based on these findings, we assume that GN8P-promoted IFN-γ synthesis in NK1.1-positive NK cells (Fig. 8A), that was detected neither in helper nor cytotoxic T cells (NK1.1-negative) (Fig. 8B), provides another proof of GN8P ability to effectively engage NKR-P1C isoform of C57BL/6 mice (NKR-P1C^{B6}). Although GN8P did not influence the relative number of NK cells in the spleen (Table 1), it caused decrease in their NK1.1 (NKR-P1C^{B6}) surface expression (Table 2). This might imply

that GN8P (synthetic NKR-P1C^{B6} ligand) is up-taken by NK cells in a complex with NK1.1 receptor. Similarly, Aust et al., who prepared a new panel of mAbs specific for individual isoforms of mouse NKR-P1 proteins, demonstrated that NKR-P1 expression on NK cells was down-regulated upon receptor cross-linking with the relevant mAb or physiological ligand and used this phenomenom as a functional assay for evaluation of NKR-P1 receptor–ligand interaction [6].

The modulatory effect of GN8P on B cell responses was proven by significant raise in the percentage of CD138-positive plasma cells (Fig. 2) as well as B lymphocytes expressing I-A/I-E (MHC class II), CD80, and CD86 surface markers, which are important for antigen presentation (Fig. 1). Similarly, it was reported that B cells cultured with IL-2-propagated NK cells up-regulated the expression of co-stimulatory molecule CD86 [20]. Thus, GN8P-activated NK cells are capable of promoting both of the main B cell functions, immunoglobulin secretion and antigen presentation.

Polarization of the immune system to Th1-type responses is well-known to be crucial for cancer immunosurveillance (reviewed in Ref. [32]). It is evident that the synthesis of Th1-type cytokine IFN-γ is stimulated by GN8P treatment to a greater extent than that of Th2-type IL-4 (Fig. 7). The secretion of IL-4 can be attributed to NKT cells. Michel et al. described two functionally distinct subpopulations of invariant NKT cells on the basis of NK1.1 expression (NK1.1-positive and NK1.1-negative generating IFN-γ/IL-4 and IL-17, respectively) [36]. Apart from supporting IgG2a formation (indicated as "Th1-like"), which mediates lysis of specific antibody-coated tumor targets, IFN-γ increases cancer cell apoptosis and expression of MHC class I molecules. On the other hand, it inhibits tumor cell proliferation, angiogenesis, as well as development and/or immunosuppressive effects of CD4+/CD25+ regulatory T cells [32,37,38]. Therefore, we suggest that prevalence of IFN-γ synthesis driven by GN8P is of clinical relevance.

In conclusion, GN8P-activated NK cells potentiate tumor-specific Ig formation triggering ADCC reaction as well as antigen presentation by B cells. These results illustrate the importance of carbohydrate recognition in NK cell-mediated regulation of adaptive immunity, with benefit for anticancer immune responses.

Acknowledgements

We thank Katerina Fiserova for excellent technical assistance. This work was supported by the Czech Science Foundation — 303/09/0477, 310/08/H077 the Grant Agency of the AS CR — IAA601680801, IAA500200620, and Czech Ministry of Education MSM21620808.

References

[1] McGreal EP, Martinez-Pomares L, Gordon S. Divergent roles for C-type lectins expressed by cells of the innate immune system. Mol Immunol 2004;41(11):1109–21.
[2] Garcia-Vallejo JJ, van Kooyk Y. Endogenous ligands for C-type lectin receptors: the true regulators of immune homeostasis. Immunol Rev 2009;230(1):22–37.
[3] Raulet DH, Guerra N. Oncogenic stress sensed by the immune system: role of natural killer cell receptors. Nat Rev Immunol 2009;9(8):568–80.
[4] Yokoyama WM, Seaman WE. The Ly-49 and NKR-P1 gene families encoding lectin-like receptors on natural killer cells: the NK gene complex. Annu Rev Immunol 1993;11:613–35.
[5] Iizuka K, Naidenko O, Plougastel B, Fremont D, Yokoyama WM. Genetically-linked C-type lectin-related ligands for the NKR-P1 NK cell receptors. Nat Immunol 2003;4:801–7.
[6] Aust JG, Gays F, Mickiewicz KM, Buchanan E, Brooks CG. The expression and function of the NKRP1 receptor family in C57BL/6 mice. J Immunol 2009;183:106–16.
[7] Bezouska K, Kren V, Kieburg C, Lindhorst TK. GlcNAc-terminated glycodendrimers form defined precipitates with the soluble dimeric receptor of rat natural killer cells, sNKR-P1. FEBS Lett 1998;426:243–7.
[8] Carlyle JR, Mesci A, Fine JH, Chen P, Belanger S, Tai LH, et al. Evolution of the Ly49 and Nkrp1 recognition systems. Semin Immunol 2008;20(6):321–30.
[9] Fiserova A, Bezouska K, Svabova L, Jedelsky P, Pucova A, Luptovcova M, et al. Analysis of glycodendrimers effect(s) in tumor microenvironment. Immunol Lett 2003;87:206–10.
[10] Pospisil M, Vannucci L, Fiserova A, Sadalapure K, Krausova K, Horvath O, et al. Glycodendrimeric ligands of C-type lectin receptors as therapeutic agents in experimental cancer. Adv Exp Med Biol 2001;495:343–8.
[11] Vannucci L, Fiserova A, Sadalapure K, Lindhorst TK, Kuldova M, Rossmann P, et al. Effects of N-acetyl-glucosamine-coated glycodendrimers as biological modulators in the B16F10 melanoma model *in vivo*. Int J Oncol 2003;23:285–96.
[12] Vivier E, Tomasello E, Baratin M, Walzer T, Ugolini S. Functions of natural killer cells. Nat Immunol 2008;9(5):503–10.
[13] Amigorena S, Bonnerot C, Fridman WH, Teillaud JL. Recombinant interleukin-2-activated natural killer cells regulate IgG2a production. Eur J Immunol 1990;20:1781–7.
[14] Becker JC, Kolanus W, Lonnemann C, Schmidt RE. Human natural killer clones enhance *in vitro* antibody production by tumour necrosis factor alpha and gamma interferon. Scand J Immunol 1990;32(2):153–62.
[15] Snapper CM, Hamaguchi H, Moorman MA, Sneed R, Smoot D, Mond JJ. Natural killer cells induce activated murine B cells to secrete Ig. J Immunol 1994;151:5251–60.
[16] Wilder JA, Koh CY, Yuan D. The role of NK cells during *in vivo* antigen-specific antibody response. J Immunol 1996;156:146–52.
[17] Koh CY, Yuan D. The effect of NK cell activation by tumor cells on antigen-specific antibody responses. J Immunol 1997;159:4745–52.
[18] Blanca IR, Bere EW, Young HA, Ortaldo JR. Human B cell activation by autologous NK cells is regulated by CD40–CD40L ligand interaction: role of memory B cells and CD5+ B cells. J Immunol 2001;167:6132–9.
[19] De Arruda Hinds LB, Alexandre-Moreira MS, Decote-Ricardo D, Nunes MP, Peçantha MT. Increased immunoglobulin secretion by B lymphocytes from *Trypanosoma cruzi* infected mice after B lymhocytes-natural killer cell interaction. Parasite Immunol 2001;23:581–6.
[20] Yuan D. Interactions between NK cells and B lymphocytes. Adv Immunol 2004;84:1–37.
[21] Gao N, Dang T, Dunnick WA, Collins JT, Blaazar BR, Yuan D. Receptors and counterreceptors involved in NK-B cell interactions. J Immunol 2005;174:4113–9.
[22] Hulikova K, Benson V, Svoboda J, Sima P, Fiserova A. N-acetyl-D-glucosamine-coated polyamidoamine dendrimer modulates antibody formation via natural killer cell activation. Int Immunopharmacol 2009;9:792–9.
[23] Snapper CM, Marcu KB, Zelazowski P. The immunoglobulin class switch: beyond "accessibility". Immunity 1997;6:217–23.
[24] Lindhorst TK, Kieburg C. Glycocoating of oligovalent amines. Synthesis of thiourea-bridged cluster glycosides from glycosyl isothiocyanates. Agnew Chem 1996;108:2083–6.
[25] Ullmannova V, Popescu NC. Inhibition of cell proliferation, induction of apoptosis, reactivation of DLC1, and modulation of other gene expression by dietary flavone in breast cancer cell lines. Cancer Detect Prev 2007;31(2):110–8.
[26] Fiserova A, Starec M, Kuldova M, Kovaru H, Pav M, Vannucci L, et al. Effects of $_{D2}$-dopamine and α-adrenoreceptor antagonists in stress induced changes on immune responsiveness of mice. J Neuroimmunol 2002;130:55–65.
[27] Koh CY, Yuan D. The functional relevance of NK cell-mediated upregulation of antigen-specific IgG2a responses. Cell Immunol 2000;204:135–42.
[28] Nimmerjahn F, Ravetch JV. Antibodies, Fc receptors and cancer. Curr Opin Immunol 2007;19:239–45.
[29] Sabbatini P, Kudryashov V, Ragupathi G, Danishefsky SJ, Livingston PO, Bornmann W, et al. Immunization of ovarian patients with a synthetic Lewis(y)-protein conjugate vaccine: a phase 1 trial. Int J Cancer 2000;87(1):79–85.
[30] Slovin SF, Ragupathi G, Musselli C, Fernandez C, Diani M, Verbel D, et al. Thomsen–Friedenreich (TF) antigen as a target for prostate cancer vaccine: clinical trial results with TF cluster (c)-KLH plus QS21 conjugate vaccine in patients with biochemically relapsed prostate cancer. Cancer Immunol Immunother 2005;54(7):694–702.
[31] Gilewski TA, Ragupathi G, Dickler M, Powell S, Bhuta S, Panageas K, et al. Immunization of high-risk breast cancer patients with clustered sTn-KLH conjugate plus the immunologic adjuvant QS-21. Clin Cancer Res 2007;13:2977–85.
[32] Johansson M, DeNardo DG, Coussens LM. Polarized immune responses differentially regulate cancer development. Immunol Rev 2008;222:145–54.
[33] Hulikova K, Grobarova V, Krivohlava R, Fiserova A. Antitumor activity of N-acetyl-D-glucosamine-substituted glycoconjugates and combined therapy with keyhole limpet hemocyanin in B16F10 mouse melanoma model. Folia Microbiol Praha 2010;55(5):528–32.
[34] Karlhofer FM, Yokoyama WM. Stimulation of murine natural killer (NK) cells by a monoclonal antibody specific for the NK1.1 antigen. IL-2-activated NK cells possess additional specific stimulation pathways. J Immunol 1991;146:3662–73.
[35] Arase H, Arase N, Saito T. Interferon γ production by natural killer (NK) cells and NK1.1+ T cells upon NKR-P1 cross-linking. J Exp Med 1996;183:2391–6.
[36] Michel ML, Mendes-da-Cruz D, Keller AC, Lochner M, Schneider E, Dy M, et al. Critical role of ROR-gammat in a new thymic pathway leading to IL-17-producing invariant NKT cell differentiation. Proc Natl Acad Sci USA 2008;105(50):19845–50.
[37] Dunn GP, Koebel CM, Schreiber RD. Interferons, immunity and cancer immunoediting. Nat Rev Immunol 2006;6(11):836–48.
[38] Nishikawa H, Kato T, Tawara I, Ikeda H, Kuribayashi K, Allen PM, et al. IFN-γ controls the generation/activation of CD4+ CD25+ regulatory T cells in antitumor immune response. J Immunol 2005;175:4433–40.

Publication 4: Human chorionic gonadotropin upregulates KIR2DL4 on NK cell subpopulations.

Overview

The synthetic and exogenous immune modulators as the abovementioned glycomimetic may prove economically unavailable, too difficult to synthesize and quite often impossible to predict. While volumes of different endogenous immune modulators are known, well–described and available, few have been used in such a long period of time, wide array of applications and as large a scale of population as hormones. In assisted reproduction techniques (ARTs), which partially solve the continuously growing rates of sterility of women (114), hormones are readily used for controlled ovarian hyperstimulation (COH) in order to obtain multiple fertilizable oocytes. Despite various modifications to the COH protocols have been established, gonadotropins have been used now for more than two decades. The most abundant protocol nowadays consists of the administration of gonadotropin releasing hormone (GnRH) antagonists and subsequent dose of human chorionic gonadotropin (hCG). While the effect on ovaries was intensively studied in the past, its exact effect on the immune system was studied rather marginally (115). Immune system and particularly NK cells may play a crucial role in embryo implantation, since higher levels of peripheral $CD56^{dim}$ NK cells were observed in patients with recurrent spontaneous abortions (116) or repeated IVF cycles failure (117). "Immune tolerance" to the fetus requires that uterine NK cells do not engage towards a rejection/cytotoxic pathway, thus non–classical HLA–G molecule expression is associated with placentation and protection of the allogeneic fetus from the maternal immune system (118, 119). HLA-G however cannot protect the fetus without its ligands: killer cell immunoglobulin–like receptor KIR2DL4 (120) and leukocyte immunoglobulin–like receptors LILRB1 (also known as ILT–2, CD85j), but these ligands have to be present on the surface of effector cells in order to induce the "off" signal (28). We thus aimed at the NK cell receptors and their fate during controlled ovarian hyperstimulation via hCG.

Aims and methods

While hCG is known to have immunomodulatory properties, we aimed to assess its effect on immunological changes, with respect to HLA–G binding receptors and embryo implantation success. This study involved 103 subjects, including patients undergoing COH protocols (n=66), divided on the basis of the pair's fertility disorder (FD) causes (female FD – represents immune compromised system, n=29; male FD – represents healthy immune system, n=37), and age matched healthy women (HD – represents hCG–uninfluenced healthy immune system, n=37). The relative distribution of T cell (CD3+/CD4+, CD3+/CD8+) and NK cell ($CD56^{bright}$/CD16-, $CD56^{dim}$/CD16+) populations was evaluated together with HLA–G ligands KIR2DL4 and LILRB1 expression by flow cytometry in the peripheral blood of all subjects, as well as in patient follicular fluids. CD161 and NKG2D receptor levels were also observed, but remained

unpublished for the prevailing lack of significant changes in their expression. This allowed us to sufficiently describe the effect of antagonist COH protocol on the immune system and correlate it to the implantation success rate.

Results and discussion

First, we demonstrated that while age is a known detrimental factor for the outcome of ARTs, it has no significant effect on the composition of the immune parameters observed here. Next, we compared the healthy donor samples with samples of male and female FD and revealed the massive changes in the immune system composition, mediated by the COH protocol. The CD4/CD8 ratio (or Th:CTL index) was severely pushed toward cytotoxic T–lymphocyte (CTL) preference and furthermore, those CD3/CD8 positive T cells had also significantly decreased levels of the inhibitory LILRB1 receptor. While the counts of NK cell populations were influenced only in the case of female FD ($CD56^{dim}$ NK cells upregulated), which points to COH–independent cause, the KIR2DL4 levels were significantly higher in ART patients.

These data show that hCG promotes cytotoxic T cell populations with lower inhibition potential (lack of inhibitory receptors) and NK–mediated cytokine production, since KIR2DL4 was described to activate potent cytokine production but only weak cytotoxicity (61, 62, 121). LILRB1, as an inhibitory receptor among T cells, causes impaired signaling through TCR and decreased IL–2 and IFNγ production (122, 123), further increasing the immune potential for IFNγ production. This may have a detrimental effect on embryo implantation, since $CD56^{bright}$ NK cells (124) and $CD56^{dim}$ NK cells (125) also produce IFNγ, which in high doses has detrimental effect on embryo implantation (126). We have further shown in this study, that patients with increased counts of CD8+ T cells or with higher KIR2DL4+ $CD56^{bright}$ NK cell levels have notably decreased implantation rates, further confirming the detrimental effect of hCG on ART outcome.

The CD161 receptor on either subset of NK cells did not exert any significant change upon hCG treatment and appears to be unaffected by the COH protocol. NKG2D was only slightly downmodulated on $CD56^{dim}$ cells (HD=88.8±7.9; Patients=82.2±15.6; p=0.0036) and only in the peripheral blood.

Here, follicular fluid T and NK cells, which were described previously in patients with idiopathic infertility or endometriosis (127, 128) as key players, revealed no significant differences in their relative distribution or in the expression of HLA–G ligands, when successful and failed embryotransfer groups were compared.

In conclusion, the commonly used COH protocol influences the CD4/CD8 index, promoting cytotoxic T cells and increases the expression of KIR2DL4 on NK cells, rendering them more prone for cytokine production.

These results provide another valuable modulator of the immune response, but as in previous cases, remain entirely focused on one NK cell receptor in a specific model situation.

ORIGINAL ARTICLE

Ovulation stimulation protocols utilizing GnRH-antagonist/hCG, promote cytotoxic cell populations, predominant in patients with embryo implantation complications

Jan Svoboda [1], Zaneta Ruzickova [1], Lucie Cuchalova [2], Milena Kralickova [3], Jitka Rezacova [4], Milena Vrana [5], Anna Fiserova [1], Jan Richter [1], Jindrich Madar [4]

1 Laboratory of Natural Immunity, Department of Immunology and Gnotobiology, Institute of Microbiology, ASCR v.v.i., Prague, Czech Republic
2 Institute of Macromolecular Chemistry, Academy of Sciences of the Czech Republic, Prague, Czech Republic
3 Department of Histology and Embryology, Faculty of Medicine in Pilsen, Charles University in Prague, Pilsen, Czech Republic
4 The Institute for the Care of Mother and Child, Prague, Czech Republic
5 The Institute of Hematology and Blood Transfusion, Prague, Czech Republic

Correspondence to: Anna Fiserova, MD., PhD.
Laboratory of Natural Immunity, Institute of Microbiology, ASCR v.v.i.,
1083 Videnska, Prague, 14220, Czech Republic.
TEL: +420 296 442 336; E-MAIL: fiserova@biomed.cas.cz

Submitted: 2013-03-19 Accepted: 2013-04-10 Published online: 2013-00-00

Key words: **ovulation induction; chorionic gonadotropin; gonadotropin-releasing hormone; embryo implantation; natural killer cells; T-lymphocytes; CD4/CD8 index; KIR2DL4 receptor; LILRB1 receptor**

Neuroendocrinol Lett 2013; **34**(3):101–109 **PMID:** ----- NEL340313AXX

Abstract

OBJECTIVE: Gonadotropin-releasing hormone (GnRH) antagonist combined with the human chorionic gonadotropin hormone (hCG) is commonly used in assisted reproduction techniques (ARTs) to induce controlled ovarian hyperstimulation (COH) and to synchronize oocyte maturation. While hCG is known to have immunomodulatory properties, we aimed to assess its effect on immunological changes, with respect to HLA-G binding receptors and embryo implantation success.
DESIGN: The study involved 103 subjects, including patients undergoing COH protocols (n=66), divided on the basis of the pair's fertility disorder (FD) causes (female FD, n=29; male FD, n=37), and age matched healthy women (n=37). The relative distribution of T cell (CD3+/CD4+, CD3+/CD8+) and NK cell ($CD56^{bright}$/CD16–, $CD56^{dim}$/CD16+) populations was evaluated together with HLA-G ligands KIR2DL4 and LILRB1 expression by flow cytometry in the peripheral blood of all subjects, as well as in patient follicular fluids.
RESULTS: Both groups of patients exhibited a significant decrease of their CD4/CD8 index, a down-modulation of LILRB1-positive CD8 T cells, and increased KIR2DL4-positive NK cell distribution, when compared to the healthy donors. We attribute these changes to the COH protocol, since the only significant change between the patient groups was in the number of cytotoxic $CD56^{dim}$ NK cells (elevated in the female FD group). Patients with male FD causes, having an above-average CD4/CD8 index (≥3.17) and below-average KIR2DL4+/$CD56^{bright}$ NK cell levels(≤13.3%), exhibited higher embryo implantation rates.

CONCLUSION: The GnRH antagonist/hCG protocol promotes CD3+/CD8+ and KIR2DL4+ NK cell levels, more abundant in subjects with lower implantation rates, and thus decreases the embryotransfer success in otherwise fertile women.

INTRODUCTION

The continuously growing rates of sterility of women of reproductive age in almost all developed countries represents a serious socio-economic problem (Caputo *et al.* 2008). Therefore, the development of new diagnostic and predictive tools/parameters, as well as treatment options for fertility disorders, is of great importance. Assisted reproductive technologies (ARTs) have represented a major step forward in this field (Bower & Hansen 2005).

The prerequisites of prosperous infertility treatment are the availability of multiple fertilizable oocytes of high quality (Arslan *et al.* 2005) and successful subsequent embryo implantation. Controlled ovarian hyperstimulation (COH) is an essential step to trigger oocyte maturation in an appropriate number of follicles to increase the rate of success (Arslan *et al.* 2005). However, lower implantation rates per embryo then those in natural cycles is a major limiting factor of ARTs (~30%, CDC 2010 and ESHRE 2009), (Hoozemans *et al.* 2004).

Various modifications to the hyperstimulation protocols have been established. The combination of GnRH agonist pituitary suppression and exogenous gonadotropins in ART protocols has resulted in significant beneficial effects in the past (Meldrum *et al.* 1989; Muasher 1992), while the subsequent introduction of GnRH antagonists protocols have prevented premature luteinizing hormone (LH) surges (Albano *et al.* 1997). The antagonist protocol, starting on day 6 or 7 of the menstrual cycle (fixed regimen) is now most common due to its simplicity, reduced use of gonadotropin (Arslan *et al.* 2005), and its better implantation rates (Kolibianakis *et al.* 2003).

Human chorionic gonadotropin influences many immune-cell subpopulations (Giuliani *et al.* 1998), with well described effects on dendritic cells and macrophages (Abu Alshamat *et al.* 2012; Wan *et al.* 2008). Since an immune response may play a crucial role in fertility and implantation, there is a growing interest in the examination of local innate and adaptive immunity (Chaouat *et al.* 2007a; Chaouat *et al.* 2007b).

"Immune tolerance" to the fetus requires that uNK cells do not engage towards a rejection/cytotoxic pathway. Non-classical HLA-G (human leukocyte antigen G) molecule expression is associated with placentation and protection of the allogeneic fetus from the maternal immune system (Hunt & Langat 2009; Hunt *et al.* 2005). Trophoblast mHLA-G (membrane bound HLA-G) and sHLA-G (soluble HLA-G) have been shown to provoke the deletion of activated T cells, as well as to inhibit NK cell mediated cytotoxicity (Apps *et al.* 2008; Carosella 2011; Le Bouteiller & Tabiasco 2006). HLA-G is present in human embryonic stem cells, human oocytes, and pre-implantation embryos throughout different developmental stages (Carosella 2011; Verloes *et al.* 2011).

Embryonic, as well as trophoblast HLA-G and incidentally trophoblast HLA-C, cannot exert such a set of tolerogenic functions in the absence of the proper receptors on maternal cells (Hiby *et al.* 2010). Among HLA-G ligands recently attracting the most interest are the killer cell immunoglobulin-like receptor KIR2DL4 (Middleton & Gonzelez 2010) and leukocyte immunoglobulin-like receptors LILRB1 (also known as ILT-2, CD85j) and LILRB2 (also known as ILT-4, CD85d). LILRBs are expressed by T and B lymphocytes, as well as by uterine and peripheral NK cells and mononuclear phagocytes, and generally act by interfering with activating signals (Hunt & Langat 2009). KIR2DL4, mainly restricted to $CD56^{bright}$ NK cells, exhibits the structural characteristics of both activating and inhibitory KIR (Faure & Long 2002; Kikuchi-Maki *et al.* 2003; Rajagopalan *et al.* 2001), possessing both a charged transmembrane arginine residue and a single cytoplasmic ITIM. KIR2DL4 are found on NK cells (Goodridge *et al.* 2003; Lopez-Botet *et al.* 2000) and also under certain circumstances on T cells (Tilburgs *et al.* 2009).

The majority of NK cells present in the pre/peri implantation decidua, pregnant uterus, and follicular fluid have the $CD56^{bright}$/CD16– phenotype and are endowed with immunoregulatory properties, and the production of angiogenic factors and cytokines (Bulmer *et al.* 1991; Fainaru *et al.* 2010; Loke & King 1995). On the other hand, peripheral NK cells comprise mainly the cytotoxic $CD56^{dim}$/CD16+ subpopulation (Moffett-King 2002; Saito *et al.* 2008; Trowsdale & Moffett 2008).

To elucidate the effect of the GnRH-antagonist/hCG COH protocol, we analyzed the response of NK and T cell subpopulations and the expression of their KIR2DL4 and LILRB1 receptors in patients undergoing ART, and compared their values with those of healthy donors.

MATERIALS AND METHODS

Cohort of patients and healthy donors

The analysis comprised 103 subjects. Healthy donors (n=37, age=35.5±4.1) and age matched ($p \geq 0.05$) women undergoing the GnRH-antagonist/hCG COH protocol (n=66, age=33.6±0.9), which were further divided into two groups on the basis of the cause of the pair's fertility disorder (FD) (female FD, n=29; male FD, n=37). Diagnosed male FD patients represented healthy, fertile women; while the diagnosed female FD group represented infertile women.

Healthy donor peripheral blood samples were provided by the Blood Transfusion Service of Thomayer

Hospital in Prague, Czech Republic, with informed consent of all donors. All patient samples used in this study were collected and processed with informed consent of the women undertaking the infertility treatment course at the Institute for the Care of Mother and Child in Prague, Czech Republic.

Peripheral blood samples (2–4 ml) were taken on the day of oocyte collection; and the total volume of follicular fluid (FF) varied according to the number of mature follicles (5–50 ml).

Controlled ovarian hyperstimulation protocol

Only women with the gonadotropin releasing hormone (GnRH) antagonist/hCG protocol (most common process) were enrolled for this study. Briefly, 0.25 mg of antagonist was administered at day 7 of the menstrual cycle (fixed regimen) and given daily until the day of hCG administration (6500 IUs of hCG were given to all women subcutaneously 34–36 hr before peripheral blood and oocyte collection, in order to coincide with oocyte maturation). Precise ultrasound folliculometry was performed rather than Estradiol (E2) levels measurement for COH response prediction.

Isolation of follicular fluid cells (FFC)

Centrifuged (200×g, 4 °C, 10 min) follicular fluids were subjected to a 30 sec incubation with 0.15M ACK solution (ammonium chloride with potassium: Sigma, St. Louis, MO, USA) to lyse any potential contaminating red blood cells (RBC). Afterwards, the cells were twice washed with 10ml of ice-cold PBS (200×g, 4 °C, 10 min) and resuspended in 100µl of PBS for further analysis (see section *Statistical analysis*).

Isolation of peripheral blood mononuclear cells (PBMC)

Blood samples of patients and healthy donors were transferred into heparin-supplemented H-MEMd media (blood:media=1:3, Institute of Molecular Genetics (IMG), ASCR, Prague, Czech Republic), layered by 10ml onto 3ml of Ficoll-Telebrix density gradient (1.077; Sigma and Leciva, Prague, Czech Republic) and centrifuged (400×g, 22 °C, 45 min). PBMC were collected, washed twice (300×g, 22 °C, 5 min) in H-MEMd media (IMG, ASCR), counted, resuspended in PBS, and prepared for flow cytometry (see section *Flow cytometry*).

Flow cytometry

PBMC or FFC in PBS were seeded on 96-well microtitter plates by 5×10^5 cells per well, and stained with antibodies according to the standard manufacturer protocol. A multifluorescent (9 channels; Supplementary Figure 1) staining protocol was devised to minimize sample volume requirements.

All analyzed cells were propidium iodide (PI) negative (live cells), singlet cells with standard morphology (Supplementary Figure 2, B and D), and CD45 positive (2D1, Per-CP; leukocyte common antigen) to exclude contamination by other cell types (Supplementary Figure 2, A and C). CD3 (UCHT1, Pacific Blue), CD4 (S3.5, APC-Alexa750), and CD8 (3B5, Pacific Orange) markers were used for the evaluation of T cells (Supplementary Figure 2, E and F); and CD56 (CMSSB, PE-Cy7) and CD16 (LNK16, Alexa700) were used to distinguish cytokine producing ($CD56^{bright}$/CD16–) and cytotoxic ($CD56^{dim}$/CD16+) NK cell populations (Supplementary Fig 2, H and I). The HLA-G ligands, KIR2DL4 (181703, PE) and LILRB1 (292305, APC), were assessed on NK and T cells, respectively (Supplementary Figure 2, G and J).

Monoclonal antibodies were purchased from either Becton-Dickinson (Franklin Lakes, NJ, USA), Life Technologies (Carlsbad, CA, USA), eBioscience (San Diego, CA, USA), R&D Systems (Minneapolis, MN, USA), AbD Serotec (Raleigh, NC, USA), or Exbio Praha (Vestec, Czech Republic). PBMCs (5×10^5 cells/well) were stained with the antibody mixture for 30 min on ice, washed, and measured on a BD LSR II instrument (Becton-Dickinson); and the data analysis was performed using FlowJo 7.6.5 software (Tree Star, Ashland, OR, USA).

Statistical analysis

The values presented in the figures are plotted as means with 95% confidence intervals. Due to the wide and mostly non-Gaussian distribution of human cytometry values (D'Agostino and Pearson omnibus normality test not passed), we utilized a Mann-Whitney U-test (MWU, nonparametric) instead of the more common Student's T-test to compare the two groups of samples. One-way ANOVA (Kruskal-Wallis test, not assuming Gaussian distribution) with a Dunn's post-test (95% confidence intervals) was used to establish significant differences between three or more groups. Values of $p\leq0.05$ (*), $p\leq0.01$ (**), and $p\leq0.001$ (***) were considered statistically significant as calculated and plotted by Prism 5 statistics software (GraphPad Software, La Jolla, CA, USA).

RESULTS

Patient age influences implantation success rate, but not immune cell distribution

Since age is a known detrimental factor for the outcome of ART, we intended to determine its effect on the studied cell populations. We thus divided the patient samples according to their age into groups of below and above the average value (33.2±3.8 years; Figure 1, A), and compared these groups on the basis of implantation success rate and relative distribution of T and NK cells subpopulations in male and female caused FD. Increasing age correlates with a measurable decrease in implantation success in female FD from 37.5% to 7.7%, relative to male FD (Figure 1, B; from 31.3% to 33.3%), but does not influence the proportion of the studied cell

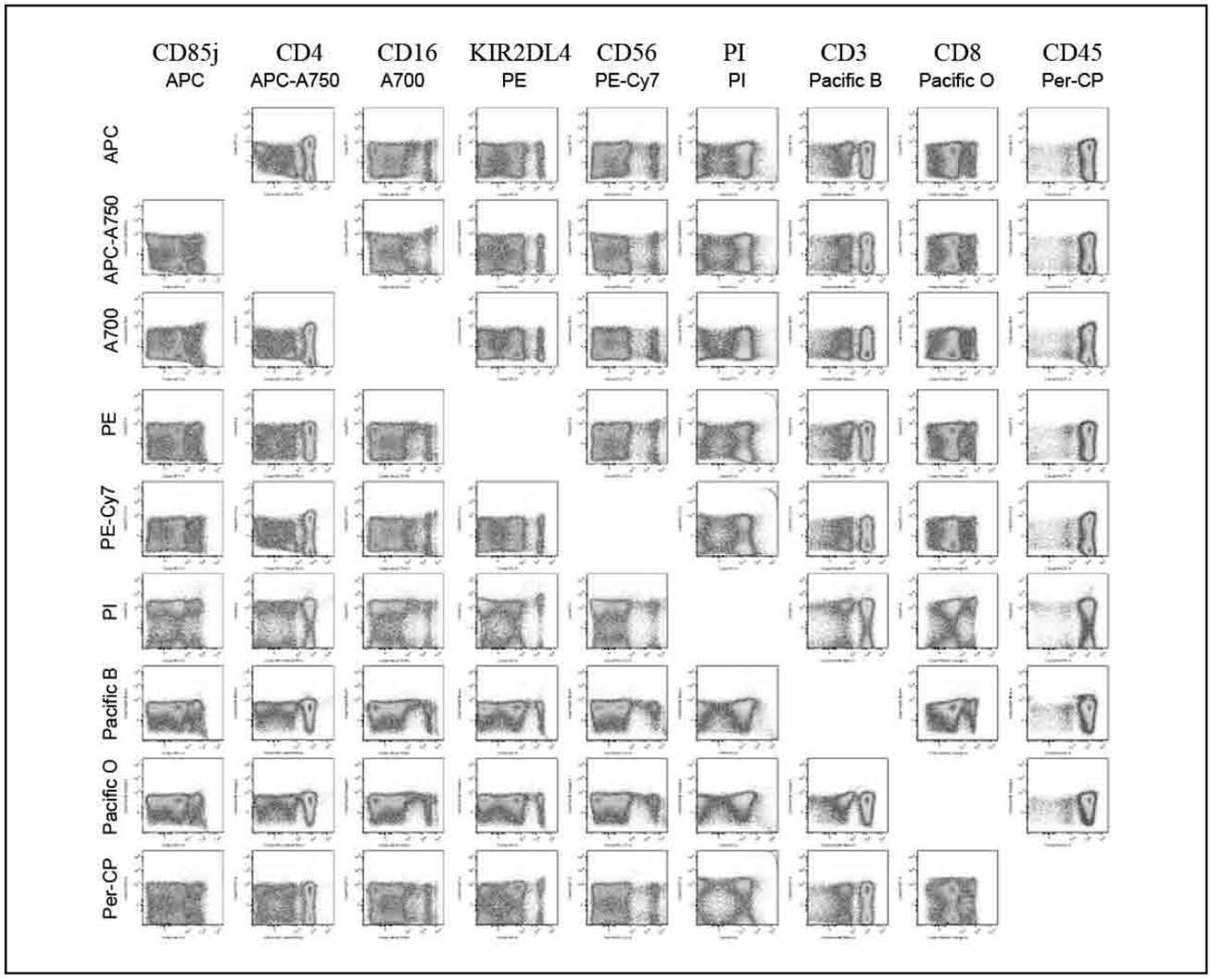

Suppl. Fig. 1. Spectral overlap compensation matrix of a 9-channel staining protocol. Columns represent single-stain controls of given fluorochromes, while rows represent their spectral overlap into all remaining channels after applied arithmetic compensation. There is no visible fluorescence overlap in the entire panel.

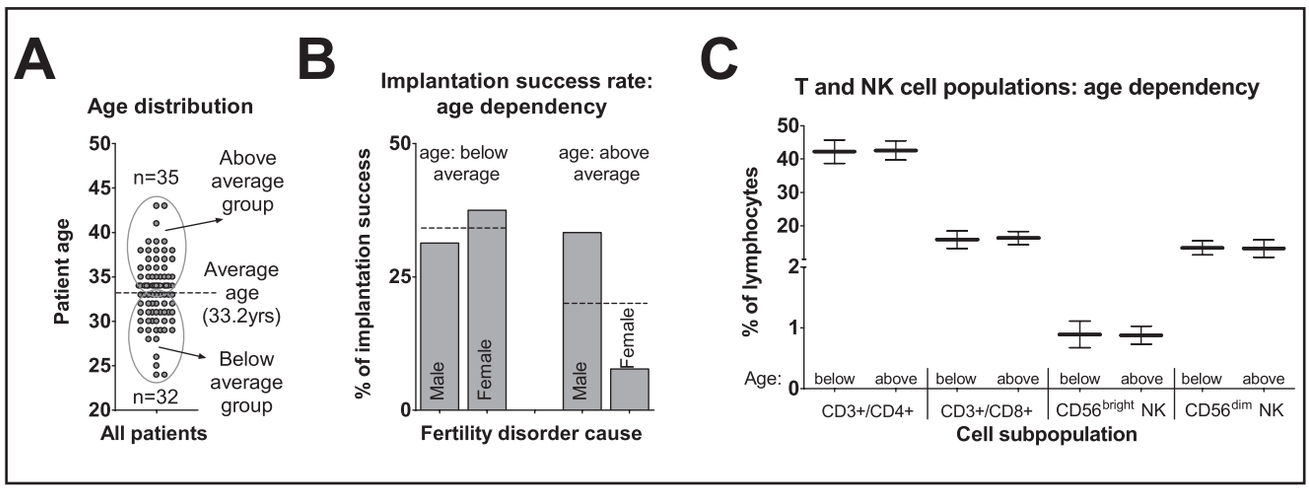

Fig. 1. Age impact on implantation success rate and immune cell populations. Patient samples were sorted into two groups according to their age at the time of ART initiation, into above and below average age (33.2±3.8 years; dashed line) (A). The evaluation of overall implantation success rates is taken from the below and above average aged male and female FD diagnosed groups. Each column represents the percentage of implantation success taken from all samples in a given group, where the dashed line represents the average of all patients (B). T and NK cell subpopulations in peripheral blood are compared on the same basis (C). Values are plotted as means with 95% confidence intervals, where Mann-Whitney p values below 0.05 were considered significant: $p \leq 0.05$ (*); $p \leq 0.01$ (**) and $p \leq 0.001$ (***).

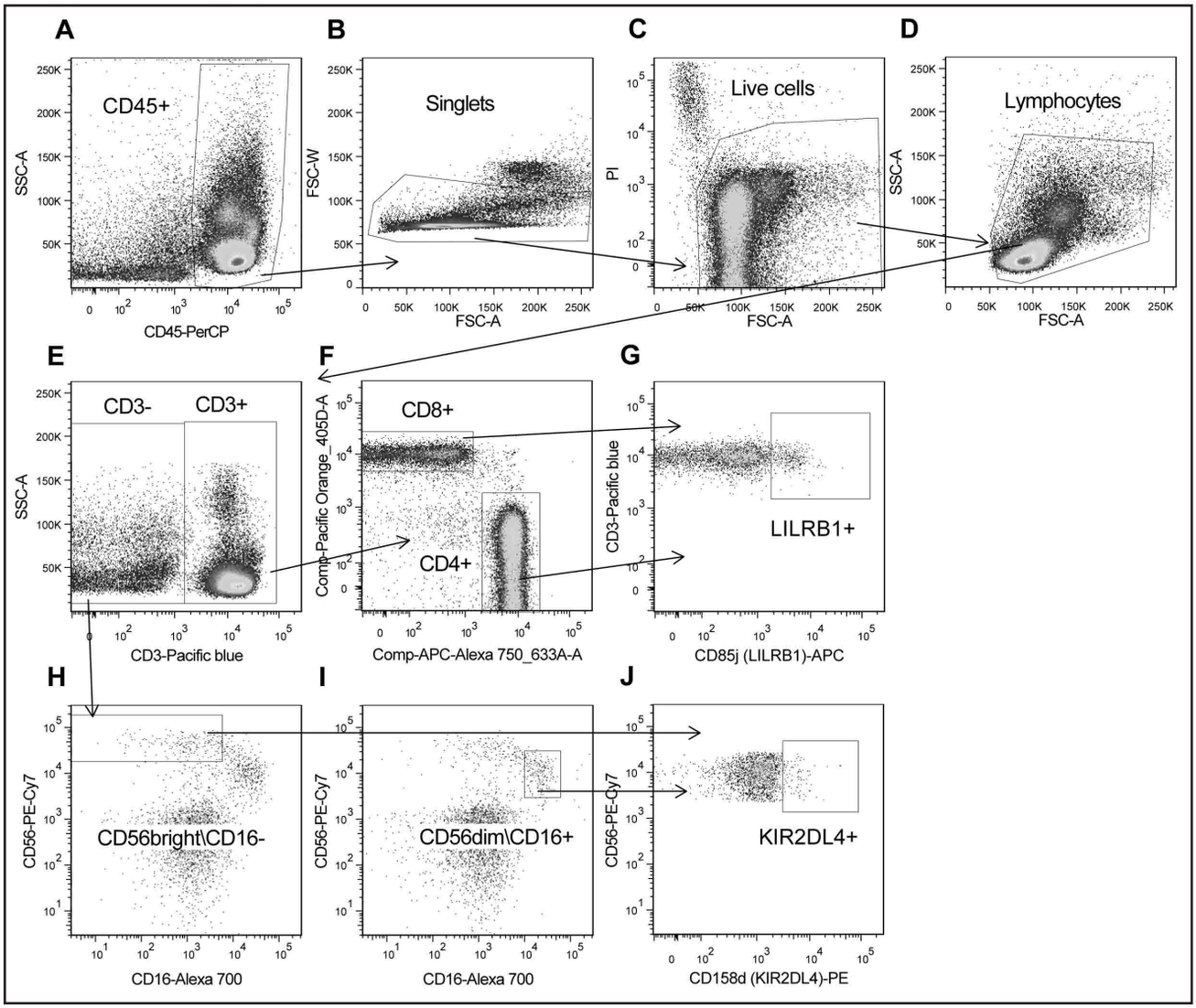

Suppl. Fig. 2. FACS data gating strategy. Gating was performed sequentially: first, CD45+ cells were selected for analysis in order to discard non-lymphocyte cells (**A**). Then doublets (**B**) and dead cells (**C**) were discarded and standard cell morphology was selected (**D**). CD3+ cells (**E**) were further divided into CD4/CD8 subpopulations (**F**) and their LILRB1 expression was analyzed (**G**). CD3- cells were divided according to their CD56/CD16 expression into $CD56^{bright}$/CD16- (**H**) and $CD56^{dim}$/CD16+ (**I**) NK cell populations - their KIR2DL4 expression was further analyzed in **J**.

populations in either PBMC (Figure 1, C) or follicular fluids (data not shown). Similarly, the LILRB1- and KIR2DL4-positive cell levels are not dependent on age either in PBMC or FFC (data not shown).

The GnRH antagonist/hCG stimulation protocol severely influences the immune cell population proportion in PMBC

To distinguish the immunological impacts evoked by the GnRH antagonist/hCG ovulation stimulation protocol from those detected in female infertility, we compared the obtained cytometry data with that of patients with male caused FD and of healthy women, in relation to embryo implantation success (Figure 2). Both male and female FD patient groups had significantly decreased CD4+ and upregulated CD8+ T cells (a lowered CD4/CD8 index), when compared to healthy donors (Figure 2, A; HD CD4/CD8 index=5.7±1.1; all patients CD4/CD8 index=3.2±0.4; $p<0.001$). LILRB1 expressing CD8+ T cell levels are also less abundant in both groups of patient PBMC samples (Figure 2, C). Cytokine producing $CD56^{bright}$ NK cell levels remain unchanged, while cytolytic $CD56^{dim}$ NK cells are upregulated significantly only in the female FD group (Figure 2, B). The relative distribution of KIR2DL4+ NK cell populations is significantly enhanced in both male and female FD patients (Figure 2, D). Thus, we could add the investigation of this phenotype to the COH treatment protocol.

A low CD4/CD8 index and augmented CD56^{dim} proportion in patient PMBC is accompanied by a decreased implantation success rate in male caused FD

The T cell ratio was significantly changed by controlled ovarian hyperstimulation (CD4/CD8 index: healthy donor (HD)=5.7±1.1; patient=3.2±0.4; $p<0.001$). To determine whether this change may have any detrimental effect on ART outcome, we divided the patient samples into two groups according to their CD4/CD8 index in PBMC, into the above-average (≥3.2) and below-average (≤3.2) ratios depicted in Figure 3, A. While the female FD group retains its implantation rate at the same level (~24%), male FD diagnosed patients have embryotransfer success repressed at below-average CD4/CD8 index values from 42.9% to 26.1% (Figure 3, B). Concurrently with the decreased CD4/CD8 index, CD56^{dim} NK cells are augmented in PBMC (Figure 3, C) and lessened in their levels in follicular fluid (from 7.5±1.5 to 5.0±1.7; $p=0.0491$) at above-average CD4/CD8 ratios. In addition, CD56^{dim} NK cells are favored only in the PBMC of the female FD group, with a high CD4/CD8 index (male FD=2.5±4.3%; female FD=18.7±3.4%; $p=0.042$). This may explain why high CD4/CD8 index bearing female FD subjects do not exhibit increased implantation rates as does the male FD group (Figure 3, B). No significant differences were observed in the LILRB1- and KIR2DL4-positive T and NK cell levels, respectively; in any of the patient follicular fluid samples (data not shown), despite the inherently low CD4/CD8 index, when compared to PBMC (FFC=2.6±0.4; PBMC=3.2±0.4; $p=0.001$).

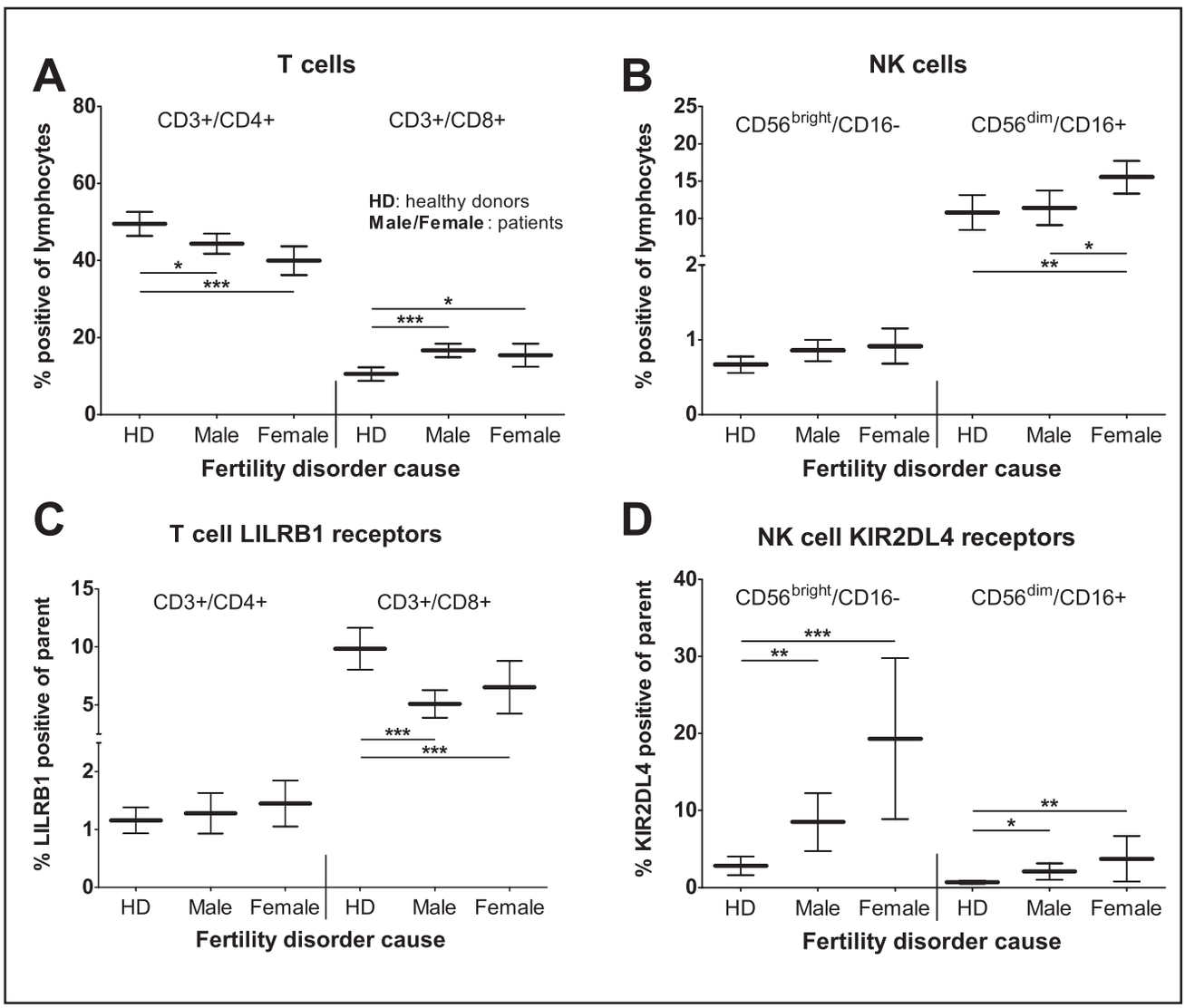

Fig. 2. Relative distribution of T and NK cell subpopulations in healthy donors and ART patients. The CD4+ and CD8+ T cell out of CD3+ lymphocytes (A) and CD56^{bright} and CD56^{dim} NK cell percentage of all lymphocyte (B) subpopulations and their respective LILRB1 (C) and KIR2DL4 (D) HLA-G ligands were compared between healthy donors (HD) and the male and female FD diagnosed patients. Values in C and D are a percentage counted from the respective parent population, as described in the figures. The data are plotted as means with 95% confidence intervals, where Mann-Whitney p values below 0.05 were considered significant: $p\leq0.05$ (*); $p\leq0.01$ (**) and $p\leq0.001$ (***).

High KIR2DL4-positive CD56^{bright} NK cell levels in PBMC are accompanied by higher KIR2DL4+/CD56^{dim} counts and decreased male FD implantation success rates

Since KIR2DL4-positive CD56^{bright} NK cell levels were significantly elevated in the ART patients, we divided their samples also on the basis of the prevalence of this population into above-average (≥13.3% KIR2DL4+) and below-average (≤13.3% KIR2DL4+) groups (Figure 4, A). Higher KIR2DL4+ levels on CD56^{bright} NK cells were accompanied only by higher KIR2DL4 levels on CD56^{dim} NK counterparts (from 1.3±0.4% to 4.9±2.8%; $p \leq 0.001$), and also by severely decreased implantation rates in the male FD group (from 37.9% to 12.5%) (Figure 4, B). CD56^{dim} NK cell levels are again favored by the female FD group with below-average KIR2DL4+CD56^{bright} levels (male FD=11.9±2.8%; female FD=16.5±2.3%; p=0.005). This may also explain why infertile women with below-average KIR2DL4+CD56^{bright} NK cells do not increase implantation rates (~24%) as in the case of the male FD group with below-average KIR2DL4+CD56^{bright} cells (Figure 4, B). No significant differences between these groups were observed in follicular fluid sample values (data not shown).

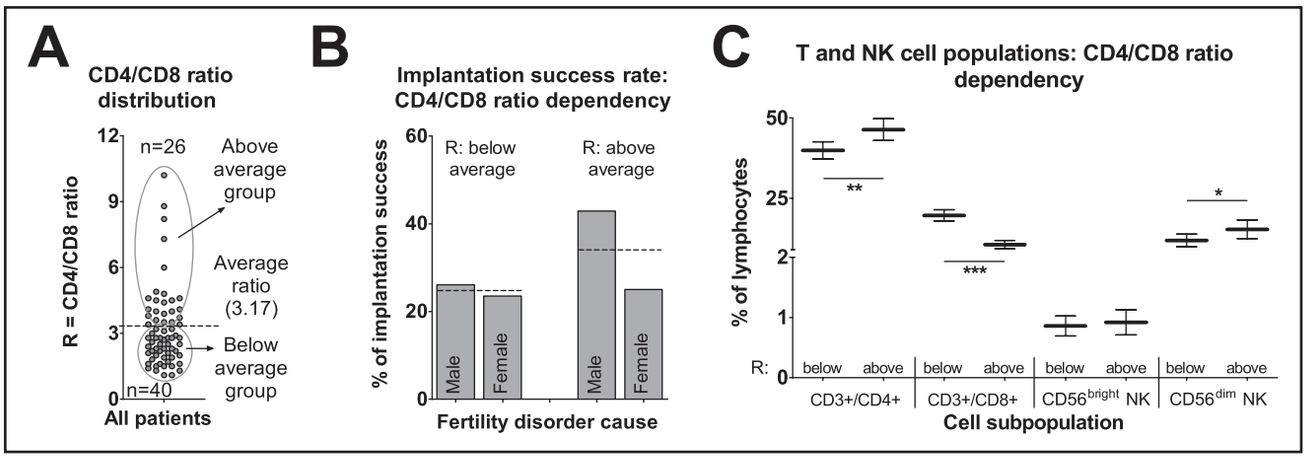

Fig. 3. Distribution of ART patient peripheral blood samples according to their CD4/CD8 index. Patient samples were distributed according to their CD4/CD8 T cell ratio and sorted into two groups of either below or above-average (average CD4/CD8 index=3.2±0.4; dashed line) values (A). The overall implantation success rates were compared on the basis of this division in the male and female FD diagnosed groups. Each column represents the percentage of implantation success, where the dashed line represents the average implantation success rate of all subjects, and the columns show the success rate proportion in male and female caused FD (B). The T and NK cells subset proportions in PBMC were analyzed relative to the CD4/CD8 index. Values are plotted as means with 95% confidence intervals, where Mann-Whitney p values below 0.05 were considered significant: $p \leq 0.05$ (*); $p \leq 0.01$ (**) and $p \leq 0.001$ (***). The significant changes in CD4 and CD8 T cell levels cannot be taken into consideration, since their levels were used to divide the patient samples.

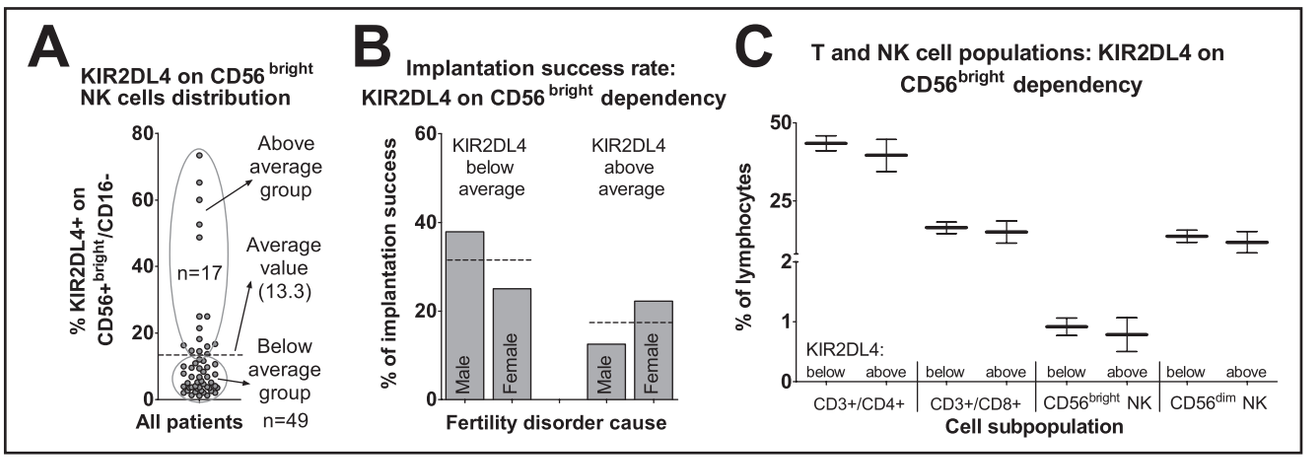

Fig. 4. Distribution of samples according to the proportion of KIR2DL4-positive CD56^{bright} NK cells in ART patient peripheral blood. Patient samples were distributed according to the levels of KIR2DL4-positive CD56^{bright} NK cells in PBMC and divided into two groups with below or above-average values (average = 13.3±5.1) (A). The values represent the percentage of the KIR2DL4-positive subset out of the CD56^{bright}/CD16- NK cells. The overall implantation success rates were compared between below and above-average KIR2DL4+CD56^{bright}/CD16- NK cells of the male and female FD diagnosed patient groups. The columns represent the percentage of implantation success rate taken from male and female FD diagnosed patients, and the dashed line represents the average of all samples (B). The T and NK cell subpopulations levels in the peripheral blood were then compared (C). Values are plotted as means with 95% confidence intervals, where Mann-Whitney p values below 0.05 were considered significant: $p \leq 0.05$ (*); $p \leq 0.01$ (**) and $p \leq 0.001$ (***).

DISCUSSION

Human chorionic gonadotropin is known to influence the composition of the immune system in general (Giuliani *et al.* 1998) with well documented effects on macrophages (Abu Alshamat *et al.* 2012; Wan *et al.* 2009) and dendritic cells (Wan *et al.* 2008) in particular. Our results show its effect on T cells, NK cells, and on their HLA-G binding receptors LILRB1 and KIR2DL4.

KIR2DL4 was described to activate cytokine production but only weakly activate cytotoxicity (Kikuchi-Maki *et al.* 2003; Miah *et al.* 2008; Rajagopalan *et al.* 2001). CD56^{bright} NK cells are known to produce TNF-α and IFN-γ (Saito *et al.* 1993); and CD56^{dim} NK cells produce IFN-γ (De Maria *et al.* 2011), which in high doses have detrimental effect on embryo implantation (Chaouat *et al.* 2007a). Thus, the increased levels of KIR2DL4 positive CD56^{bright} and CD56^{dim} NK cells induced by controlled ovarian hyperstimulation may contribute to ART failure by causing very early (immediate) post implantation embryo rejection ("occult loss"). Our study documented lower implantation rates in patients with above-average KIR2DL4-positive CD56^{bright} levels. Moreover, female FD patients with increased CD56^{dim} cell proportions, with below-average KIR2DL4, had comparable implantation rates to those of the above-average KIR2DL4 group.

LILRB1, as an inhibitory receptor among T cells, causes impaired signaling through TCR and decreased IL-2 and IFN-γ production (Brown *et al.* 2004; Moysey *et al.* 2010). Here, the GnRH-antagonist/hCG stimulation protocol decreased the levels of peripheral LILRB1-positive CD8+ T cells despite their increased overall levels, promoting cytotoxic T cells with lower inhibition potency. As shown in this study, patients with a lower CD4/CD8 index in PBMC exhibited lower implantation rates. Female FD diagnosed patients with an above-average CD4/CD8 index, on the other hand, exhibited comparable implantation rates to those of the below-average group; which could be caused by higher CD56^{dim} NK cell levels, when compared to the male FD group. Previously higher levels of peripheral CD56^{dim} NK cells were observed in patients with recurrent spontaneous abortions (Karami *et al.* 2012) or repeated IVF cycles failure (Sacks *et al.* 2012). In agreement with this published data, the COH protocol used in our study increases the levels of CD56^{dim} NK cells only in female FD diagnosed patients. In addition, higher implantation rates, accompanied by a higher CD4/CD8 index or lower KIR2DL4 levels, seen in male FD, were not observed in the female FD patients. Thus, we can deduce that an increased proportion of CD56^{dim} NK cells play the major role in embryotransfer success. Nevertheless, the female FD patients who underwent ART were further handicapped by the COH process itself. In healthy, fertile women (male FD group) cell populations associated with decreased implantation rates were promoted by the COH.

Follicular fluid T and NK cells described previously revealed no significant differences in their relative distribution or in the expression of HLA-G ligands, when successful and failed embryotransfer groups were compared in patients with idiopathic infertility or endometriosis (Lachapelle *et al.* 1996; Lukassen *et al.* 2003). The results of this study proved that the levels of these particular populations and their receptors in the follicular fluids have little or no prediction value for the actual embryotransfer outcome.

CONCLUSION

We show here that the GnRH-antagonist/hCG COH protocol promotes cell subpopulations that are undesirable for the outcome of embryotransfer, and further hinder the success rate of implantation for fertile, as well as infertile women. We thus propose the review and revision of this process, and that it most likely be widened to include other COH protocols to identify and eliminate their potential detrimental effects on embryo implantation. Our study identified a decreased CD4/CD8 index and higher populations of CD56^{dim} NK cells, together with the dysregulation of HLA-G ligands (KIR2DL and LILRB1). Thus, we also deem the above-studied cell populations and their receptors useful as diagnostic and prediction markers in future studies and clinical trials.

ACKNOWLEDGEMENT

This work was supported by a Grant Agency of the Ministry of Health of the Czech Republic grant [NR/9135-3].

REFERENCES

1 Abu Alshamat E, Al-Okla S, Soukkarieh CH, Kweider M (2012). Human chorionic gonadotrophin (hCG) enhances immunity against L. tropica by stimulating human macrophage functions. Parasite Immunol. **34**: 449–454.
2 Albano C, Smitz J, Camus M, Riethmuller-Winzen H, Van Steirteghem A, Devroey P (1997). Comparison of different doses of gonadotropin-releasing hormone antagonist Cetrorelix during controlled ovarian hyperstimulation. Fertil Steril. **67**: 917–922.
3 Apps R, Gardner L, Moffett A (2008). A critical look at HLA-G. Trends Immunol. **29**: 313–321.
4 Arslan M, Bocca S, Mirkin S, Barroso G, Stadtmauer L, Oehninger S (2005). Controlled ovarian hyperstimulation protocols for in vitro fertilization: two decades of experience after the birth of Elizabeth Carr. Fertil Steril. **84**: 555–569.
5 Bower C, Hansen M (2005). Assisted reproductive technologies and birth outcomes: overview of recent systematic reviews. Reprod Fertil Dev **17**: 329–333.
6 Brown D, Trowsdale J, Allen R (2004). The LILR family: modulators of innate and adaptive immune pathways in health and disease. Tissue Antigens. **64**: 215–225.
7 Bulmer JN, Morrison L, Longfellow M, Ritson A, Pace D (1991). Granulated lymphocytes in human endometrium: histochemical and immunohistochemical studies. Hum Reprod. **6**: 791–798.

8 Caputo M, Nicotra M, Gloria-Bottini E (2008), Fertility Transition: Forecast for Demography. Hum Biol. **80**: 359–376.
9 Carosella ED (2011). The tolerogenic molecule HLA-G. Immunol Lett. **138**: 22–24.
10 CDC (2010). http://www.cdc.gov/art/ART2010/PDFs/01_ART_2010_Clinic_Report-FM.pdf
11 Chaouat G, Dubanchet S, Ledee N (2007a). Cytokines: Important for implantation? J Assist Reprod Genet. **24**: 491–505.
12 Chaouat G, Mas AE, Petitbarat M, Dubanchet S, Ledee N (2007b). Physiology of implantation. Gynecol Obstet Fertil. **35**: 861–866.
13 De Maria A, Bozzano F, Cantoni C, Moretta L (2011). Revisiting human natural killer cell subset function revealed cytolytic CD56(dim)CD16+ NK cells as rapid producers of abundant IFN-gamma on activation. Proc Natl Acad Sci U S A. **108**: 728–732.
14 ESHRE (2009). http://www.eshre.eu/ESHRE/English/Guidelines-Legal/ART-fact-sheet/page.aspx/1061)
15 Fainaru O, Amsalem H, Bentov Y, Esfandiari N, Casper RF (2010). CD56(bright)CD16(-) natural killer cells accumulate in the ovarian follicular fluid of patients undergoing in vitro fertilization. Fertil Steril. **94**: 1918–1921.
16 Faure M, Long EO (2002). KIR2DL4 (CD158d), an NK cell-activating receptor with inhibitory potential. J Immunol. **168**: 6208–6214.
17 Giuliani A, Schoell W, Auner J, Urdl W (1998). Controlled ovarian hyperstimulation in assisted reproduction: effect on the immune system. Fertil Steril. **70**: 831–835.
18 Goodridge JP, Witt CS, Christiansen FT, Warren HS (2003). KIR2DL4 (CD158d) genotype influences expression and function in NK cells. J Immunol **171**: 1768–1774.
19 Hiby SE, Apps R, Sharkey AM, Farrell LE, Gardner L, Mulder A, Claas FH, Walker JJ, Redman CW, Morgan L, Tower C, Regan L, Moore GE, Carrington M, Moffett A (2010). Maternal activating KIRs protect against human reproductive failure mediated by fetal HLA-C2. J Clin Invest. **120**: 4102–4110.
20 Hoozemans DA, Schats R, Lambalk CB, Homburg R, Hompes PG (2004). Human embryo implantation: current knowledge and clinical implications in assisted reproductive technology. Reprod Biomed Online. **9**: 692–715.
21 Hunt JS, Langat DL (2009). HLA-G: a human pregnancy-related immunomodulator. Curr Opin Pharmacol. **9**: 462–469.
22 Hunt JS, Petroff MG, McIntire RH, Ober C (2005). HLA-G and immune tolerance in pregnancy. FASEB J. **19**: 681–693.
23 Karami N, Boroujerdnia MG, Nikbakht R, Khodadadi A (2012). Enhancement of peripheral blood CD56(dim) cell and NK cell cytotoxicity in women with recurrent spontaneous abortion or in vitro fertilization failure. J Reprod Immunol. **95**: 87–92.
24 Kikuchi-Maki A, Yusa S, Catina TL, Campbell KS (2003). KIR2DL4 is an IL-2-regulated NK cell receptor that exhibits limited expression in humans but triggers strong IFN-gamma production. J Immunol. **171**: 3415–3425.
25 Kolibianakis EM, Albano C, Kahn J, Camus M, Tournaye H, Van Steirteghem AC, Devroey P (2003). Exposure to high levels of luteinizing hormone and estradiol in the early follicular phase of gonadotropin-releasing hormone antagonist cycles is associated with a reduced chance of pregnancy. Fertil Steril. **79**: 873–880.
26 Lachapelle MH, Hemmings R, Roy DC, Falcone T, Miron P (1996). Flow cytometric evaluation of leukocyte subpopulations in the follicular fluids of infertile patients. Fertil Steril **65**: 1135–1140.
27 Le Bouteiller P, Tabiasco J (2006). Killers become builders during pregnancy. Nat Med **12**: 991–992.
28 Loke YW, King A (1995). Human implantation: cell biology and immunology. Cambridge University Press, Cambridge; New York.
29 Lopez-Botet M, Llano M, Navarro F, Bellon T (2000). NK cell recognition of non-classical HLA class I molecules. Semin Immunol. **12**: 109–119.
30 Lukassen HG, van der Meer A, van Lierop MJ, Lindeman EJ, Joosten I, Braat DD (2003). The proportion of follicular fluid CD16+CD56DIM NK cells is increased in IVF patients with idiopathic infertility. J Reprod Immunol **60**: 71–84.
31 Meldrum DR, Wisot A, Hamilton F, Gutlay AL, Kempton WF, Huynh D (1989). Routine pituitary suppression with leuprolide before ovarian stimulation for oocyte retrieval. Fertil Steril. **51**: 455–459.
32 Miah SM, Hughes TL, Campbell KS (2008). KIR2DL4 differentially signals downstream functions in human NK cells through distinct structural modules. J Immunol. **180**: 2922–2932.
33 Middleton D, Gonzelez F (2010). The extensive polymorphism of KIR genes. Immunology. **129**: 8–19.
34 Moffett-King A (2002). Natural killer cells and pregnancy. Nat Rev Immunol. **2**: 656–663.
35 Moysey RK, Li Y, Paston SJ, Baston EE, Sami MS, Cameron BJ, Gavarret J, Todorov P, Vuidepot A, Dunn SM, Pumphrey NJ, Adams KJ, Yuan F, Dennis RE, Sutton DH, Johnson AD, Brewer JE, Ashfield R, Lissin NM, Jakobsen BK (2010). High affinity soluble ILT2 receptor: a potent inhibitor of CD8(+) T cell activation. Protein Cell. **1**: 1118–1127.
36 Muasher SJ (1992). Use of gonadotrophin-releasing hormone agonists in controlled ovarian hyperstimulation for in vitro fertilization. Clin Ther. **14**(Suppl A): 74–86.
37 Rajagopalan S, Fu J, Long EO (2001). Cutting edge: induction of IFN-gamma production but not cytotoxicity by the killer cell Ig-like receptor KIR2DL4 (CD158d) in resting NK cells. J Immunol. **167**: 1877–1881.
38 Sacks G, Yang Y, Gowen E, Smith S, Fay L, Chapman M (2012). Detailed analysis of peripheral blood natural killer cells in women with repeated IVF failure. Am J Reprod Immunol. **67**: 434–442.
39 Saito S, Nakashima A, Myojo-Higuma S, Shiozaki A (2008). The balance between cytotoxic NK cells and regulatory NK cells in human pregnancy. J Reprod Immunol. **77**: 14–22.
40 Saito S, Nishikawa K, Morii T, Enomoto M, Narita N, Motoyoshi K, Ichijo M (1993). Cytokine production by CD16-CD56bright natural killer cells in the human early pregnancy decidua. Int Immunol. **5**: 559–563.
41 Tilburgs T, van der Mast BJ, Nagtzaam NM, Roelen DL, Scherjon SA, Claas FH (2009). Expression of NK cell receptors on decidual T cells in human pregnancy. J Reprod Immunol. **80**: 22–32.
42 Trowsdale J, Moffett A (2008). NK receptor interactions with MHC class I molecules in pregnancy. Semin Immunol. **20**: 317–320.
43 Verloes A, Van de Velde H, LeMaoult J, Mateizel I, Cauffman G, Horn PA, Carosella ED, Devroey P, De Waele M, Rebmann V, Vercammen M (2011). HLA-G expression in human embryonic stem cells and preimplantation embryos. J Immunol. **186**: 2663–2671.
44 Wan H, Coppens JMC, van Helden-Meeuwsen CG, Leenen PJM, van Rooijen N, Khan NA, Kiekens RCM, Benner R, Versnel MA (2009). Chorionic gonadotropin alleviates thioglycollate-induced peritonitis by affecting macrophage function. J Leukocyte Biol. **86**: 361–370.
45 Wan H, Versnel MA, Leijten LME, van Helden-Meeuwsen CG, Fekkes D, Leenen PJM, Khan NA, Benner R, Kiekens RCM (2008). Chorionic gonadotropin induces dendritic cells to express a tolerogenic phenotype. J Leukocyte Biol. **83**: 894–901.

Publication 5: A_{2A} adenosine receptor agonist impairs NK cell–mediated cytotoxicity across species.

Overview

Adenosine (purine nucleotide) is constitutively present at low concentrations virtually in all tissues. It influences many physiological functions (*e.g.*, vasodilatation, lipolysis, *etc*.) (129), and its levels are dramatically increased from nanomolar to micromolar concentrations during hypoxic conditions, tissue damage and inflammation. It inhibits inflammatory activity of neutrophils, macrophages and lymphocytes, protecting the ischemic tissues from massive damage (130). It was also reported, that adenosine receptors (AR) are involved in the inhibition of cytotoxic activity and cytokine production by activated NK cells (84, 131). There are some studies involving anti–inflammatory effects of adenosine and its ability to protect tissues from hypoxia, including developing malignant tumors. Most of these observations were carried out either in mice or on cells isolated from human blood but scarce information exists whether this effect is universal across species and in immunocompromised subjects. Four types of ARs are known: A_1, A_{2A}, A_{2B} and A_3, which are members of the G–protein coupled receptor (GPCR) family, expressed by many cell types (129). A_{2A} AR was chosen for this study, since it is the most common AR and is strongly involved in NK cell inhibition (84, 130).

Aims and methods

In this study, our goal was to provide evidence whether adenosine–mediated inhibition of NK cell function is universal among most common mammal species or whether it is specialized for humans and rodents. To achieve this goal, we used the synthetic A_2AR agonist 5'–(*N*–cyclopropyl) carboxamidoadenosine (CPCA) to *in vitro* influence the cytotoxic activity of mononuclear cells isolated from human donors, C57BL/6 mice, Wistar rats, Ladrace–Duroc pigs and White Shorthaired goats. Both healthy and tumor bearing subjects were used (except goats) to observe any tumor–mediated precoditioning of effector cells (tumor escape strategies include adenosine release) and standard ^{51}Cr–release cytotoxicity assay was performed against sepcies–specific NK–sensitive target cells (K562: human, pig, goat; C6: pig, goat rat; YAC–1: mouse, rat; B16F10: mouse)

Results and discussion

The *in vitro* addition of A_{2A}AR agonist, 10-micromolar CPCA, down-modulated the NK cell cytotoxic activity in both healthy and tumor–compromised subjects of all tested species. In several cases, even 100nM concentration was sufficient to exert significant decrease in lytic activity. A slight effector cell conditioning was visible in tumor–bearing rats, which exerted lower degree of lysis inhibition by CPCA, when compared to healthy counterparts, but overall, the effect was comparable.

In conclusion, these data, obtained by an *in vitro* stimulation of effector cells derived from different mammalian species, indicate that CPCA can be considered a universal NK cell attenuator.

A universal attenuator as CPCA could exert undesirable effects and hormones display a high degree of pleiotropy if applied systemically. Two approaches can be applied in order to circumvent systemic or pleiotropic effect: either to rely on other than chemical means of immune modulation or to use a specific–targeting platform for the delivery of chemical and biological compounds.

Folia Microbiol. **54** (4), 364–368 (2009) **http://www.biomed.cas.cz/mbu/folia/**

NK Cell-Mediated Cytotoxicity Modulation by A_2 Adenosine Receptor Agonist in Different Mammalian Species

M. KULDOVÁ[a], J. SVOBODA[a], F. KOVÁŘŮ[b], L. VANNUCCI[a], H. KOVÁŘŮ[c], A. FIŠEROVÁ[a]*

[a]*Department of Immunology and Gnotobiology, Institute of Microbiology, v.v.i., Academy of Sciences of the Czech Republic, Prague, Czech Republic*
[b]*Section of Morphology and Physiology, Veterinary and Pharmaceutical University, Brno, Czech Republic*
[c]*Department of Psychiatry, 1st Faculty of Medicine, Charles University in Prague, Czech Republic*

Received 28 April 2009
Revised version 29 May 2009

ABSTRACT. Adenosines, endogenous purine nucleosides, appear in the extracellular space under metabolically stressful conditions associated with ischemia, inflammation, and cell damage. Their activity on innate immunity is prevalently inhibitory and can develop both in infectious and neoplastic diseases. During cancer development, tumor cells that release high concentrations of adenosines can impair the function of tumor-infiltrating lymphocytes and assist tumor growth by neo-angiogenesis. We evaluated the influence of A_2 adenosine receptor (A_2AR) agonist on cytotoxic-cell response comparing human with other mammalian species (rodents, pigs, goats), both in healthy and in cancer conditions. The A_2AR agonist developed dose-dependent inhibition of the cytotoxic activity of immune effector cells in all studied species. However, variability of the response was observed in relation to the species and the target cells that were used. Altogether, our data indicate that the A_2AR plays a central role in adenosine-mediated inhibition of immune response to tumors.

Abbreviations

A_2AR	A_2 adenosine receptor	NK	natural killer cells
AR	adenosine receptor	PBMC	peripheral blood mononuclear cells
CPCA	5′-(*N*-cyclopropyl)carboxamidoadenosine	SMC	spleen mononuclear cells
FCS	fetal calf serum	TIL	tumor-infiltrating leukocyte
GPCR	G-protein-coupled receptor		

Adenosine (purine nucleotide) is constitutively present at low concentrations virtually in all tissues. It influences many physiological functions (*e.g.*, vasodilatation, lipolysis, *etc.*) (Fredholm *et al.* 2001), and its levels are dramatically increased from nanomolar to micromolar concentrations during hypoxic conditions, tissue damage and inflammation (Raskovalova *et al.* 2005; Lokshin *et al.* 2006). Adenosine inhibits inflammatory activity of neutrophils, macrophages and lymphocytes, protecting the ischemic tissues from massive damage (Ohta *et al.* 2001; Sitkovsky 2003), and distinctly reduces the damage induced by ischemia and neutrophil infiltration in many tissues, such as kidneys, lungs, brain, spinal cord and skin (Cronstein 1994; Burnstock 1997; Sitkovsky *et al.* 2004). Adenosine also reduces hypoxia by increasing the blood flow, due to its effect on vasodilatation and angiogenesis. In this way, adenosine can play an important role in the protection of tumor tissue where increased growth and insufficient vascularity induces hypoxic conditions. Hypoxic tumor tissue can protect itself by eliciting the same mechanisms applied during organism defense against damage from the immune system. In fact, accumulation of extracellular adenosine that binds to specific AR inhibits the activity of TIL (Ohta *et al.* 2001, 2006). It has been shown that extracellular adenosine inhibits the activation and effector functions of T-lymphocytes and NK cells, including their adhesion to tumor cells, cytokine production and cytotoxic activity (Hoskin *et al.* 2008).

Extracellular adenosine affects cells *via* four types of adenosine receptors (A_1, A_{2a}, A_{2b}, A_3) which are members of GPCR and are expressed by many cell types (Fredholm *et al.* 2001; Klinger *et al.* 2002). The anti-inflammatory role of adenosine is mediated mainly by its interaction with the A_{2a} AR, which is the

**Corresponding author*: Laboratory of Natural Immunity, Department of Immunology and Gnotobiology, Institute of Microbiology, Academy of Sciences of the Czech Republic, v.v.i., Vídeňská 1083, 142 20 Prague 4, Czech Republic; fax +420 296 442 107, e-mail fiserova@biomed.cas.cz.

most common within expressed AR on inflammatory cells and is also strongly involved in suppression of their effector functions (Raskovalova *et al.* 2005; Ohta *et al.* 2006).

There are some studies involving anti-inflammatory effects of adenosine and its ability to protect tissues from hypoxia, including developing malignant tumors. Most of these observations were carried out either in mice or on cells isolated from human blood but scarce information exists about effects of adenosine in other mammalian species. In this study, for the first time, we compare the effect of synthetic A_2AR agonist 5′-(*N*-cyclopropyl)carboxamidoadenosine (CPCA) on cytotoxic activity of mononuclear cells isolated from rat, pig and goat.

MATERIAL AND METHODS

Experimental individuals and sample collection. Healthy individuals and animal species. Eight-week-old inbred male C57Bl/6 mice were bled and spleens were removed. Peripheral blood (from heart) and spleens was obtained from 3-month-old Wistar rats put down under diethyl ether anesthesia. Peripheral blood from 6-month cross-breed (Landrace – Large, White – Duroc) pigs and from White Shorthaired goats was obtained by jugular vein puncture. Blood samples were heparinized with 5 IU/mL sodium heparin (*Zentiva*, Czech Republic). Human peripheral blood (citrate–EDTA) samples were collected from healthy donors from the *Blood Transfusion Service* (Prague, Czech Republic).

Tumor-bearing hosts. Blood samples were collected from patients with non-small-cell lung cancer, stage I–IIB, WHO PS 0–1, 56–70 years of age from the *Department of Thoracic Surgery at the Lower Silesian Centre in Wrocław*, Poland (Bobek *et al.* 2005). C57Bl/6 mice were injected s.c. with 10^6 syngeneic B16F10 melanoma cells, and Wistar rats were injected s.c. with 10^7 syngeneic C6 glioma cells. After 1 month the animals were sacrificed and spleens were used for experiments. Wistar rats with chemically induced colorectal carcinoma (according to Vannucci *et al*. 1994) were used for experiments at the time of well developed adenocarcinoma (6–8 months after induction). Six-month-old miniature MeLiM pigs with spontaneous hereditary malignant melanoblastoma (*Institute of Animal Physiology and Genetics AS CR*, Liběchov, Czech Republic) were used as a pig tumor model (Borovanský *et al*. 2003). Blood or spleen samples were collected by the same technique like in control healthy subjects. All animal experiments and procedures were conducted in accordance with the *European Convention for the Care and Use of Laboratory Animals* as approved by the *Czech Animal Care and Use Committee*.

Isolation of peripheral blood mononuclear cells (PBMC) and spleen mononuclear cells (SMC). PBMC and SMC were separated on Ficoll–Paque density gradient 1.077 (human, pig and goat) or 1.086 (mice and rats) (*Sigma-Aldrich*, USA) to obtain mononuclear cells, and after 3 washes by H-MEMd (*Sigma-Aldrich*) used for function assay.

Cell cultures. Established cell lines K562 (CCL-243), YAC-1 (TIB-160), B16-F10 (CRL-6475) and C6 (CCL-107) purchased from the *American Type Culture Collection* (*via* Teddington, UK) were maintained in RPMI-1640 medium (*Sigma-Aldrich*), supplemented with 2 mmol/L L-glutamine, 1 mmol/L sodium pyruvate, 0.05 mmol/L 2-sulfanylethanol ('2-mercaptoethanol'), antibiotics (0.05 mg/mL gentamicin, 25 mg/mL amphotericin B) and 10 % heat-inactivated FCS (*Gibco*, USA). Incubation was done in a humidified atmosphere (5 % CO_2) in a CO_2 incubator (*Jouan*, France) at 37 °C.

Cytotoxicity assay. The *in vitro* NK cell-mediated cytotoxicity was estimated using the standard ^{51}Cr-release assay with SMC or PBMC. Effector SMC or PBMC (3.2×10^5/100 μL per well) were seeded in tetraplicates and cultivated in the presence of A_2 AR agonist CPCA at a concentration of 10 or 0.1 μmol/L. After 18 h, 10^4 target cells labeled for 90 min with $Na_2{}^{51}CrO_4$ (YAC-1 – mouse, rat, B16F10 – mouse; C6 – rat, pig, goat; K562 – human, pig, goat) were added to the effector cells in round-bottomed 96-well microtiter plates (*Nunc*, Denmark). Evaluation of NK cell activity was performed after a 4-h incubation (humidified atmosphere containing 5 % CO_2) in the presence of target cells at 37 °C. The cell-free supernatants were harvested (250 μL per sample), 0.1 mL of scintillation cocktail (SuperMix; *Wallac*, Finland) was added, and the radioactivity measured employing scintillation counter Microbeta Trilux (*Wallac*). The percentage of cytotoxicity (ctx) was calculated according to the formula ctx [%] = 100 × (experimental cpm – spontaneous cpm)/(maximum cpm – spontaneous cpm) (Fišerová *et al*. 2002). The newly introduced cytotoxicity assay conditions for pigs and goats were established after the evaluation of commonly used NK-sensitive cell lines. The K562 and C6 cells were selected as the most sensitive targets to porcine and goat PBMC effector function.

Statistical analysis. Statistical significance of differences between groups was calculated by paired Student's *t*-test, $p < 0.05$ being considered as significant.

RESULTS

Inhibition of cytotoxic activity by CPCA in healthy individuals and animal species (Fig. 1). Human, pig and goat PBMC showed after an 18-h incubation with 10 μmol/L CPCA significantly reduced cytotoxic activities against all used target cell lines; the cytotoxic activity of human PBMC was significantly reduced by both CPCA concentrations (10 and 0.1 μmol/L). The reduction in pigs was more pronounced against C6 target cells. On the other hand, the two CPCA concentrations significantly reduced the cytotoxic activity of mononuclear cells isolated from the spleen of mice and rats. While in mice the effect was more evident against the YAC-1 target, the cytotoxicity against the syngeneic C6 target in the rat was inhibited intensively but independently of the CPCA concentration.

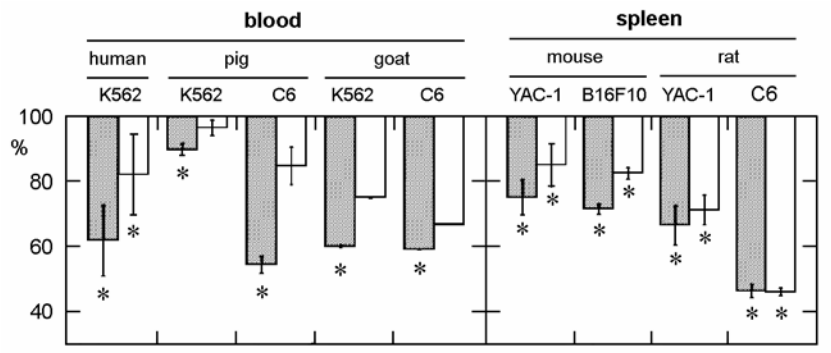

Fig. 1. The effect of CPCA on cytotoxic activity of PBMC and SMC isolated from different experimental models. The cytotoxicity after 18 h of indicated effector cell treatment is expressed as a percentage of control untreated cells; effector to target cell ratio was for all species 32:1; data represent averages ± SD of 4–6 experiments, * – $p < 0.05$; *dark columns* – 10 mmol/L, *light columns* – 0.1 mmol/L; for further details *see* the text.

Inhibition of cytotoxic activity by CPCA in tumor-bearing hosts. The effect of CPCA was evaluated on the cytotoxic activity of PBMC from patients suffering lung cancer or minipigs with hereditary melanoblastoma. The MeLiM minipigs PBMC cytotoxic activity was significantly reduced after CPCA treatments when tested against the K562 target. In humans, using the same target, the inhibition was higher at 10 μmol/L CPCA (Fig. 2, *blood*).

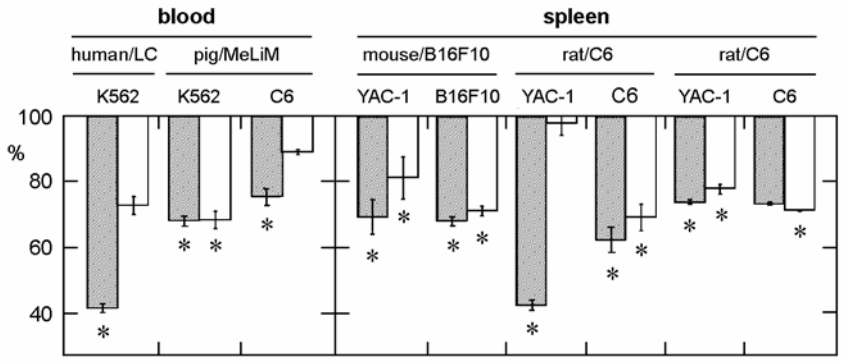

Fig. 2. The effect of CPCA on cytotoxic activity of PBMC and SMC of tumor-bearing hosts. Cytotoxic activity of cells after an 18-h incubation with CPCA is expressed as a percentage of controls untreated cells. Data are averages ± SD of 4 experiments in which 3–6 individuals were involved, * – $p < 0.05$; *dark columns* – 10 mmol/L, *light columns* – 0.1 mmol/L; LC – patients with non-small cell lung cancer; for further details *see* the text.

Using SMC isolated from syngeneic B16-F10 melanoma-bearing mice, both concentrations of the A_2AR agonist showed comparable effects on the effector cells. The same was observed in the SMC isolated from rat with syngeneic C6 glioma or chemically induced colorectal carcinoma with one exception: When

the cytotoxicity was tested in C6 glioma-bearing rat effector cells against the YAC-1 target, the lower dose (0.1 μmol/L) of CPCA had no effect while 10 μmol/L induced a 60 % inhibition (Fig. 2, *spleen*).

DISCUSSION

In humans and in mice, adenosine is indicated to be an important component of immune system regulation, especially during hypoxic conditions and inflammation and/or infection (Murphree 2005). In normal organisms, it develops a protective activity against tissue damage by enhancing blood flow and angiogenesis, and inhibiting individual components of the immune system, mainly *via* A_2AR. Study on piglets infected with *Salmonella enterica* serotype Typhimurium demonstrated reduction of NK cell activation during inflammatory response after CPCA treatment (Trebichavský *et al*. 2003). Human NK cells can be inhibited by triggering this receptor which, by adenylyl cyclase stimulation, leads to PKA I activation (Raskovalova *et al*. 2006). The same regulatory activity results in detrimental tumor microenvironment. Study of the effects and the threshold of stimulation of the A_2AR receptor can assist in better understanding its role both in physiological immune inhibition and as a therapeutic target for infection, autoimmunity, ischemia, degenerative diseases, and cancer (Haskó *et al*. 2008; Hoskin *et al*. 2008).

Our data, obtained by an *in vitro* stimulation of effector cells derived from different mammalian species, indicate that adenosine can be considered to be a universal immune system attenuator. The synthetic A_2AR agonist CPCA significantly inhibited the cytotoxic activity of mononuclear cells isolated from either peripheral blood or spleens. This effect was present in both healthy and tumor-bearing subjects, and equally pronounced in all our experimental models. Higher sensitivity of the lymphoid cells from the spleen in comparison with blood could be mediated by different microenvironmental conditions in the organ, cell activation, and possibly concentration of A_2AR on the cell surface. The literature on the argument is very poor, and further investigation would be of interest (Priebe *et al*. 1990; Hoskin *et al*. 1994). Different microenvironments and A_2AR on the cell surface expression can also explain differences about dose-dependent response and sensitivity of the used target, both in and within healthy and cancer conditions. However, independently of the complexity of this network, the response remained constantly present throughout the tested mammalian species. The results described for the first time in this, rather preliminary, report highlight the importance of this regulatory mechanism of cytotoxic cells.

This work was supported by grants of the *Grant Agency of Academy of Sciences of the Czech Republic* (KJB500200614, IAA60180801) and *Institutional Research Concept* AV 0Z 50200510.

REFERENCES

BOBEK V., BOUBELIK M., FISEROVA A., LUPTOVCOVA M., VANNUCCI L., KACPRZAK G., KOLODZEJ J., MAJEWSKI A.M., HOFFMAN R.M.: Anticoagulant drugs increase natural killer cell activity in lung cancer. *Lung Cancer* **47**, 215–223 (2005).

BOROVANSKY J., HORAK V., ELLEDER M., FORTYN K., SMITH N.P., KOLB A.M.: Biochemical characterization of a new melanoma model – the minipig MeLiM strain. *Melanoma Res.* **13**, 543–548 (2003).

BURNSTOCK G.: The past, present and future of purine nucleotides as signaling molecules. *Neuropharmacology* **36**, 1127–1139 (1997).

CRONSTEIN B.N.: Adenosine, an endogenous anti-inflammatory agent. *J.Appl.Physiol.* **76**, 5–13 (1994).

FIŠEROVÁ A., STAREC M., KULDOVÁ M., KOVÁŘŮ H., PÁV M., VANNUCCI L., POSPÍŠIL M.: Effects of D_2-dopamine and α-adrenoceptor antagonists in stress induced changes on immune responsiveness of mice. *J.Neuroimmunol.* **130**, 55–65 (2002).

FREDHOLM B.B., IJZERMAN A.P., JACOBSON K.A., KLOTZ K., LINDEN J.: *International Union of Pharmacology*. XXV. Nomenclature and classification of adenosine receptors. *Pharmacol.Rev.* **53**, 527–552 (2001).

HASKÓ G., LINDEN J., CRONSTEIN B., PACHER P.: Adenosine receptors: therapeutic aspects for inflammatory and immune diseases. *Nature Rev.Drug Discov.* **7**, 759–770 (2008).

HOSKIN D.W., REYNOLDS T., BLAY J.: 2-Chloroadenosine inhibits the MHC-unrestricted cytolytic activity of anti-CD3-activated killer cells: evidence for the involvement of a non-A_1/A_2 cell-surface adenosine receptor. *Cell.Immunol.* **159**, 85–93 (1994).

HOSKIN D.W., MADER J.S., FURLONG S.J., CONRAD D.M., BLAY J.: Inhibition of T cell and natural killer cell function by adenosine and its contribution to immune evasion by tumor cells (*review*). *Internat.J.Oncol.* **32**, 527–535 (2008).

KLINGER M., FREISSMUTH M., NANOFF C.: Adenosine receptors: G protein-mediated signaling and the role of accessory proteins. *Cell Signal.* **14**, 99–108 (2002).

LOKSHIN A., RASKOVALOVA T., HUANG X., ZACHARIA L.C., JACKSON E.K., GORELIK E.: Adenosine-mediated inhibition of the cytotoxic activity and cytokine production by activated natural killer cells. *Cancer Res.* **66**, 7758–7765 (2006).

MURPHREE L.J., SULLIVAN G.W., MARSHALL M.A., LINDEN J.: Lipopolysaccharide rapidly modifies adenosine receptor transcripts in murine and human macrophages: role of NF-κB in A_{2a} adenosine receptor induction. *Biochem.J.* **391**, 575–580 (2005).

OHTA A., SITKOVSKY M.: Role of G-protein-coupled adenosine receptors in downregulation of inflammation and protection from tissue damage. *Nature* **414**, 916–920 (2001).

OHTA A., GORELIK E., PRASAD S.J., RONCHESE F., LUKASHEV D., WONG M.K.K., HUANG X., CALDWELL S., LIU K., SMITH P., CHEN J., JACKSON E.K., APASOV S., ABRAMS S., SITKOVSKY M.V.: A_{2a} adenosine receptor protects tumors from antitumor T cells. *Proc.Nat.Acad.Sci.USA* **103**, 13132–13137 (2006).

PRIEBE T., PLATSOUCAS C.D., NELSON J.A.: Adenosine receptors and modulation of natural killer cell activity by purine nucleosides. *Cancer Res.* **50**, 4328–4331 (1990).

RASKOVALOVA T., HUANG X., SITKOVSKY M., ZACHARIA L.C., JACKSON E.K., GORELIK E.: Gs Protein-coupled adenosine receptor signaling and lytic function of activated NK cells. *J.Immunol.* **175**, 4383–4391 (2005).

RASKOVALOVA T., LOKSHIN A., HUANG X., JACKSON E.K., GORELIK E.: Adenosine-mediated inhibition of cytotoxic activity and cytokine production by IL-2/NKp46-activated NK cells: involvement of protein kinase A isozyme I (PKA I). *Immunol.Res.* **36**, 91–99 (2006).

SITKOVSKY M.V.: Use of A_{2a} adenosine receptor as a physiological immunosupressor and to engineer inflammation *in vivo*. *Biochem. Pharmacol.* **65**, 493–501 (2003).

SITKOVSKY M.V., LUKASHEV D., APASOV S., KOJIMA H., KOSHIBA M., CALDWELL C., OHTA A., THIEL M.: Physiological control of immune response and inflammatory tissue damage by hypoxia-inducible factors and adenosine A_{2a} receptors. *Ann.Rev. Immunol.* **22**, 657–682 (2004).

TREBICHAVSKÝ I., ŠPLÍCHAL I., ŠPLÍCHALOVÁ A., MUNETA Y., MORI Y.: Systemic and local cytokine response of young piglets to oral infection with *Salmonella enterica* serotype Typhimurium. *Folia Microbiol.* **48**, 403–407 (2003).

VANNUCCI L., HUGGINS C.B., MOSCA F.: A new experimental model for colorectal carcinogenesis in the rat. *J.Environ.Pathol.Toxicol. Oncol.* **13**, 59–61 (1994).

Publication 6: Local hyperthermia induces NK cell–mediated response.

Overview

Hyperthermia is a process of artificial heating of tissue or the entire organism to temperatures above normal ranges. Its advantages lie in the contact–less application (microwave generators with adjustable effective aperture and focal localization), well–defined targeting and real–time application temperature monitoring. Hyperthermia can be applied either as whole body hyperthermia (WBH), which is usually applied in the fever–range of temperatures (39–42°C) with beneficial immunoregulatory effects (132) or locally. While higher temperatures (≥42°C) have directly cytotoxic and immunogenic effect on malignant tissue (133), they tend to render the host immune system ineffective (134). Thus, if properly localized and focused only on the affected tissue, local hyperthermia (LHT) can provide tumoricidal temperature in the tumor itself, while maintaining febrile temperature range in the surrounding tissue. This could prove very beneficial, since such range was reported previously to activate spleen cells (135), NK cells (136), cytotoxic T cells and T helper cells (137, 138).

Aims and methods

In this study, we investigated the effect of LHT on *in vivo* and *in vitro* induction of NK and CTL–mediated cytotoxicity and on the changes in effector cell subpopulation proportions and activation state in LHT–treated B16F10 melanoma–bearing C57BL/6 mice. These mice were first inoculated with B16F10 melanoma cells, and after palpable tumors were developed, underwent LHT under anesthesia. Furthermore, to distinguish the effect of HT on effector cells and tumors, we incubated either effectors or targets in 42°C prior to a standard ^{51}Cr–release assay.

Results and discussion

As for spleen immune cell subpopulations, neither CTL nor NK cells exerted significant changes in their occurrence induced by the local hyperthermia *in vivo*. Their activation state, indicated by the presence of the very early activation antigen CD69, was also unaltered. The only change observed was in the higher counts of CD69 positive CD11b+ cell population in the tumor site – other changes were ascribed to the anesthesia itself.

The functional assay pointed to increased effector lytic activity against NK–sensitive YAC–1 target cells after *in vivo* applied LHT. When *in vitro* HT of 42°C was applied to target cells only, healthy mice–derived effectors exerted significantly decreased lytic activity (probably due to the tumor cell–mediated release of adenosines). Tumor–compromised effectors exerted a slight increase in cytotoxicity against *in vitro* hyperthermed targets, pointing to an unknown melanoma–based preconditioning of the effector cells. Effector cells after *in vitro* HT exerted

slight, but significant decreases of lytic activity, probably due to the temperature reaching the limit of beneficial febrile response.

In conclusion, *in vivo* LHT proved to have beneficial effect on NK cell–mediated lytic activity, despite NK cell numbers or receptors repertoire remained unchanged. This, together with *in vitro* HT data suggests indirect effect on NK cells and the linking elements identification would require further study in more precisely controlled conditions.

Despite the simplicity and benefits of hyperthermia, its effects are systemic, despite its localized application. Also its application is limited to solid or localized tumors, leaving metastatic loci or leukemia outside the tumoricidal temperature range. Most immune–related problems and immune–modulating applications require specific targeting to achieve even measurable effectiveness. An answer may be in the recent development of nanoparticular targeting platforms discussed below, which have the potential to be loaded with heat–generating particles (139) and specific targeting molecules and/or mediators, affecting selectively only specific cell populations.

Physiol. Res. 57: 459-465, 2008

Immunological Response in the Mouse Melanoma Model after Local Hyperthermia

J. KUBEŠ[1], J. SVOBODA[2], J. ROSINA[3], M. STAREC[3], A. FIŠEROVÁ[2]

[1]Department of Radiation Oncology, Faculty Hospital in Ostrava, [2]Institute of Microbiology of the Academy of Sciences, Prague, [3]Third Faculty of Medicine, Charles University, Prague, Czech Republic.

Received February 15, 2007
Accepted April 18, 2007
On-line May 30, 2007

Summary

Our study was aimed to characterize the phenotype and functional endpoints of local microwave hyperthermia (LHT, 42 °C) on tumor infiltrating and spleen leukocytes. The effectiveness of LHT applied into the tumor of B16F10 melanoma-bearing C57/BL6 mice was compared with anesthetized and non-treated animals. Subpopulations of leukocytes were analyzed using the flow cytometry, and the cytotoxic activity of splenocytes against syngeneic B16F10 melanoma and NK-sensitive YAC-1 tumor cell lines was evaluated in ^{51}Cr-release assay. Similarly, the *in vitro* modification of the heat treatment was performed using healthy and melanoma-bearing splenocytes. We found a 40 % increase of activated monocytes (CD11b+CD69+) infiltration into the tumor microenvironment. In the spleen of experimental animals, the numbers of cytotoxic T lymphocytes (CTLs-CD3+CD8+) and NK cell (CD49b+NK1.1+) raised by 22 % and 14 %, respectively, while the NK1.1+ monocytes decreases by 37 %. This was accompanied by an enhancement of cytotoxic effector function against B16F10 and YAC-1 targets in both *in vivo* and *in vitro* conditions. These results demonstrate that LHT induces better killing of syngeneic melanoma targets. Furthermore, LHT evokes the homing of activated monocytes into the tumor microenvironment and increases the counts of NK cells and CTL in the spleen.

Key words

Local hyperthermia • Melanoma • Cytotoxic cells • Monocytes • CD69

Corresponding author

Jiri Kubes, Department of Radiation Oncology, Faculty Hospital in Ostrava, 17. listopadu 1790, 708 52, Ostrava, Czech Republic. E-mail: jiri.kubes@fnb.cz

Introduction

The use of hyperthermia (HT – heating of tissue to 41-44 ºC) is one of the promising methods in cancer treatment (Van der Zee 2002, Baronzio *et al.* 2006). Although the molecular mechanisms of this process are not fully understood yet, possible effects are: 1) direct cytotoxicity (Milani and Noessner 2006), 2) inhibition of DNA-repair procedures (Kampinga *et al.* 2004), 3) changes in capillary blood flow and microvessels (Emami *et al.* 1980) and 4) immunomodulatory effects (Hildebrandt *et al.* 2002). Relative contributions of the above stated effects are still not fully clarified and are presumably dependent on tumor type (Ostapenko *et al.* 2005).

Hyperthermia is being introduced either as localized (LHT) or as a whole body hyperthermia (WBH) in various temperature ranges. During WBH, the elevation of temperature near tumoricidal levels (T≥42 ºC) leads to the inhibition of host immunocompetence (Huang *et al.* 1996, Shen *et al.* 1994), making such arrangement unsuitable for immunological studies. On the other hand, the fever-range temperatures (39-41 ºC) show an immuno-regulatory advantage by enhanced secretion of immuno-globulins (Ostapenko *et al.* 2005).

In case of LHT, even if the heating of tumor exceeds 42 ºC, the surrounding healthy tissue usually remains at fever-range temperatures (39-41 ºC). This selectivity is beneficial, because LHT combines the tumoricidal effect of the heating with the fever-induced immunostimulation.

Immunomodulatory effect of HT can consist of augmenting of antigenicity of tumor cells, followed by induction of the immune response. More efficient antigen presentation on tumor cells and stimulation of immunocompetent cells was demonstrated *in vitro* (Ito *et al.* 2001) and *in vivo* using LHT (Basu and Srivastava 2003) or WBH (Atanackovic *et al.* 2002). The current knowledge of the LHT influence on immunological changes encompasses the activation of spleen cells (Vartak *et al.* 1996), natural killer (NK) cells (Szmigielski *et al.* 1991), CD8+ (Tc or CTL) cells (Ostapenko *et al.* 2005) and CD4+ (Th) cells (Stawarz *et al.* 1993) at temperatures within the fever-range (39-41 ºC).

In our study, we investigated the effect of LHT on *in vivo* and *in vitro* induction of NK and CTL-mediated cytotoxic activity against B16F10 melanoma targets. We evaluated changes in effector cell numbers, activation, and killing activity in the spleen and the tumor site after *in vivo* LHT application. To distinguish effects on effector and target cells, we examined the LHT impact *in vitro*, with consequent functional studies. We demonstrated that the response to LHT is not a single-step event, but a cascade of actions ranging from tumor infiltration, possible augmentation of antigen presentation and effector cells proliferation to the activation of terminal cytotoxic cell function.

Methods

Experimental animals

Eight-week-old inbred male C57/BL6 mice were purchased from Charles River (D). The mice were housed under natural day/night conditions (22 °C, 55 % humidity) and fed a commercial pelleted diet (ST1, Velaz, Prague) *ad libitum*. The *ex vivo* experiments started at least 2 weeks after the arrival of the animals to avoid immunological changes caused by transportation stress. The mouse melanoma cell line – B16F10 derived from C57/BL6 mice (kindly donated by Weizmann Institute, Rehovot, Israel) was used in the syngeneic tumor model. B16F10 cells (10^6/mouse in 0.1 ml PBS) were inoculated subcutaneously (*s.c.*) into the lower back at day 0. Mice with tumors reaching 1-2 cm in greatest dimension were randomly divided into three groups: 1) anesthetized mice treated with hyperthermia (HT), 2) anesthetized mice (anest), and 3) non-treated controls (control). All procedures were conducted in accordance with the European Convention for the Care and Use of Laboratory Animals as approved by the Czech Animal Care and Use Committee.

Hyperthermia

Local hyperthermia was performed under anesthesia (ketamine: 1.9 mg/mouse and xylazine: 0.25 mg/mouse weighing 25-30 g, *i.p.*). A microwave generator with working frequency 2450 MHz and power 10 W was used for tumor heating, in connection with the applicator constructed at the Czech Technical University (Prague, CZ) based on conventional waveguide, with the effective aperture 2x2 cm. The superficial, intra-tumor and rectal temperature of mice was monitored during the whole period of HT application by the fluoro-optic thermometer (LUXTRON, Luxtron Corporation CA). Target temperature (42 ºC) in the tumor was reached during one minute and was maintained using pulses of microwaves for 7 min. Rectal temperature did not surpass 38 ºC. We performed three consecutive heatings in the hyperthermia group at days 10, 14 and 17 after tumor cells inoculation. Animals in the anesthesia group were anesthetized in the same time intervals as mice in the HT group, but without hyperthermia. Twelve hours after the third session of hyperthermia all mice were euthanized and tumors and spleens were removed for further separation.

Isolation of mouse spleen cells (SC) and tumor infiltrating leukocytes (TIL)

Spleens were dissociated through a nylon mesh, repeatedly washed and used immediately for flow cytometry (FACS) or *in vitro* experiments. Tumor infiltrating leukocytes (TILs) were prepared from individual melanomas minced with scissors, eluted by repeated pipetting, and mononuclear cells separated on Ficoll-Hypaque density gradient (1.086). Freshly separated mononuclear cells were used for further phenotype and functional assays.

Cell cultures and in vitro experiments

Established cell lines YAC-1 (mouse NK-sensitive T lymphoma) and B16F10 (mouse melanoma) were maintained in RPMI-1640 medium supplemented with 2 mM L-glutamine, 1 mM sodium pyruvate, 0.05 mM 2-mercaptoethanol, antibiotics (0.05 mg/ml gentamycin, 25 mg/ml amphotericin B) and 10 % heat-inactivated fetal calf serum - FCS (Gibco, Grand Island, NY, USA).

The cytotoxic activity assays of mouse spleen

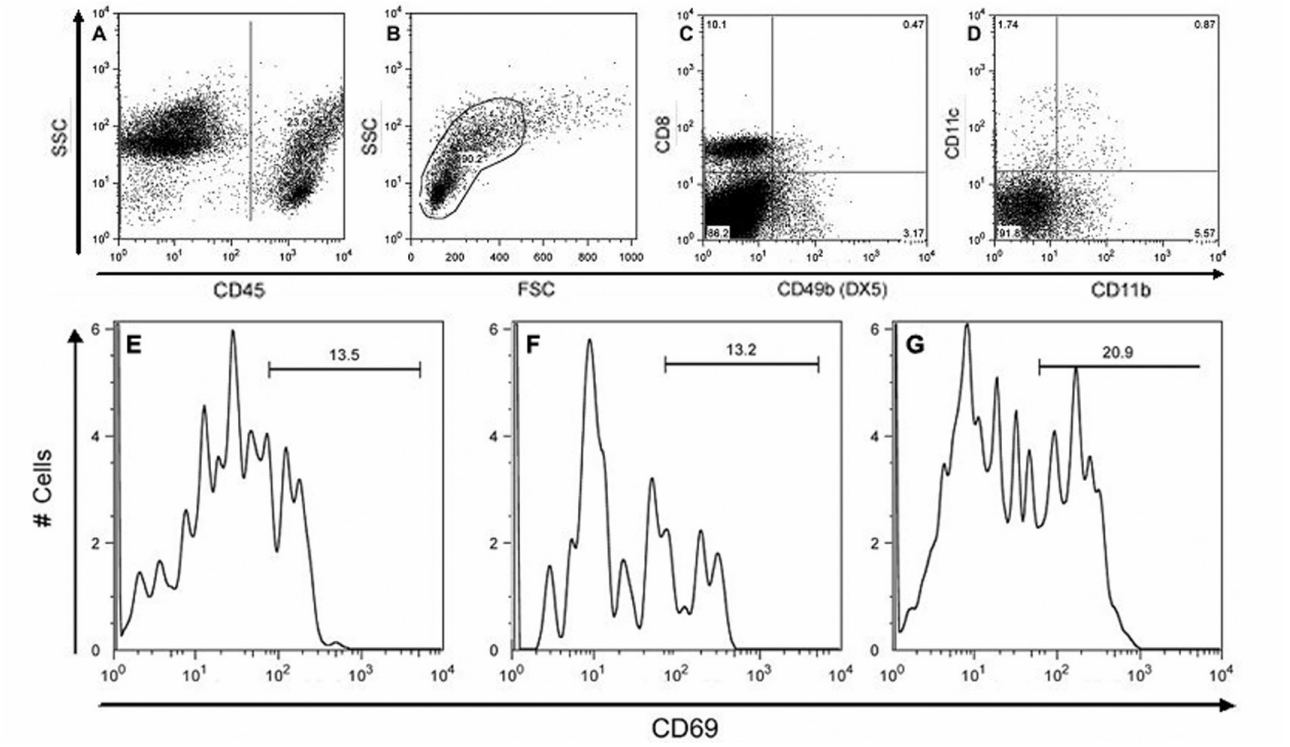

Fig. 1. Cell surface markers FACS analysis. PI negative (not shown) and CD45 positive cells (A), with lymphocyte/monocyte morphology (B), were analyzed for expression of surface markers of NK/CTL cells (C) and monocyte/DC subpopulation (D). These subsets were further analyzed for CD69 expression (E, F, G), which changed significantly only in case of CD45+/CD49b-CD8-/CD11b+CD11c- cells (monocytes) comparing the hyperthermed animals (G) to controls (E) and anesthetized groups (F). Histograms (E, F, G) represent the percentage of CD69 positive cells out of the gated parental population (CD45+, CD49b-/CD8-/CD11b+/CD11c-). Figure shows an illustrative example of four consecutive experiments with similar results.

cells were performed in RPMI 1640 medium supplemented with L-glutamine, gentamycin and 5 % FCS. Incubation was carried out at 37 °C in a humidified atmosphere containing 5 % CO_2 in a CO_2 incubator (Jouan, France).

For *in vitro* modification of hyperthermia, B16F10 cell line (as target) and splenocytes (as effectors) were cultivated at 37 °C or 42 °C, in a humidified atmosphere, and 5 % CO_2. The effector or target cells were transferred into prewarmed cultivation medium for the heat treatment and the incubation at 42 °C for 10 min followed, once or three times in the same schedule as in the *in vivo* model. The melanoma cells were then harvested and used as targets in cytotoxic assays.

Flow cytometry

Individual cell suspensions prepared from the spleen and tumor were resuspended in PBS with 0.1 % gelatin (gelatin from cold water fish skin – Sigma) and 0.01 % sodium azide. Phenotypes of cells were determined using specific surface markers for T lymphocytes – CD3-PECy5 (17A2), CD4-FITC (H129.19), CD8-PE (53-6.7), B-lymphocytes –CD45R/B220-Alexa405 (RA3-6B2), monocytes, APCs - CD11b-Pacific Blue (M1/70.15), CD11c-FITC (HL3), NK cells – CD49b-FITC (DX5), activation antigens NK1.1-PECy7 (PK136), CD69-PECy5 (H1.2F3) and analysis was performed by FACS LSR II (Becton-Dickinson, USA). Five- or six-color staining was performed according to the manufacturer's standard protocol. The CD45-PECy7 (30-F11) leukocyte common antigen (LCA) staining was applied to distinguish the leukocytes from residual melanoma cells in TIL fraction. Further, the PI negative (live) CD45 positive (leukocytes, Fig. 1A) cells with lymphocyte and monocyte morphology were gated (large lymphomonogate, SSC *vs* FSC, Fig. 1B) and analyzed for surface markers expression (Fig. 1C,D). Monoclonal antibodies were purchased either from Pharmingen (San Diego, CA, USA) or Caltag (San Francisco, CA). Evaluation of data was performed using FlowJo version 6.1.1 software (Tree Star Inc., Ashland, OR, USA).

Cytotoxicity assay

Cell-mediated cytotoxicity was estimated using standard ^{51}Cr-release assay with splenocytes of experimental animals as effectors. YAC-1, mouse NK-

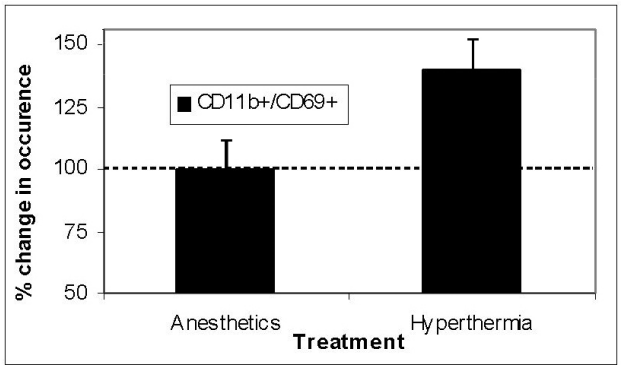

Fig. 2. Proportion of activated monocytes (CD11b+/CD69+) occurrence in TIL fraction. Both control and anesthetized groups showed 12±1.7 % of CD11b+/CD69+, while HT treated group had 17±2.6 % of CD11b+/CD69+, showing a 40 % increase. The percentage was counted from CD45 positive cells in the TIL fraction and is shown as percentage change relative to control stated as 100 % (dashed line).

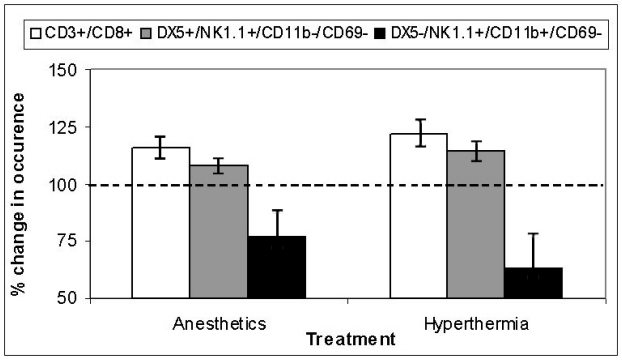

Fig. 3. Distribution of immune cell subpopulations in the spleen after local hyperthermia. The values are presented as percentage changes in occurrence relative to individual controls. The control values (stated as 100 %, dashed line) were for CTLs – 55 % (CD8+ out of CD3+); for NK cells – 36 % (NK1.1+ out of CD49b+); for NK1.1 positive monocytes – 17.5 % (NK1.1+ out of CD11b+). The data represent mean ± S.D. of three performed experiments (5-7 animals per group).

sensitive, and B16F10 melanoma cell lines were used as target cells and were labeled by 60-min incubation with $Na_2{}^{51}CrO_4$ in round-bottomed 96-well microtiter plates (NUNC), at 37 °C in a humidified atmosphere containing 5 % CO_2. Evaluation of effector cell lytic activity against 10^4 target cells was performed after 4 h of incubation as described previously (Fišerová *et al.* 1997). The cell free supernatants were harvested (0.025ml/sample), 0.1ml of scintillation cocktail (SuperMix, Wallac, Finland) was added, and radioactivity was measured using scintillation counter Microbeta Trilux (Wallac, Finland).

Statistical analysis

Results in groups were analyzed using one-way analysis of variance (ANOVA), P≤0.05 values were considered significant.

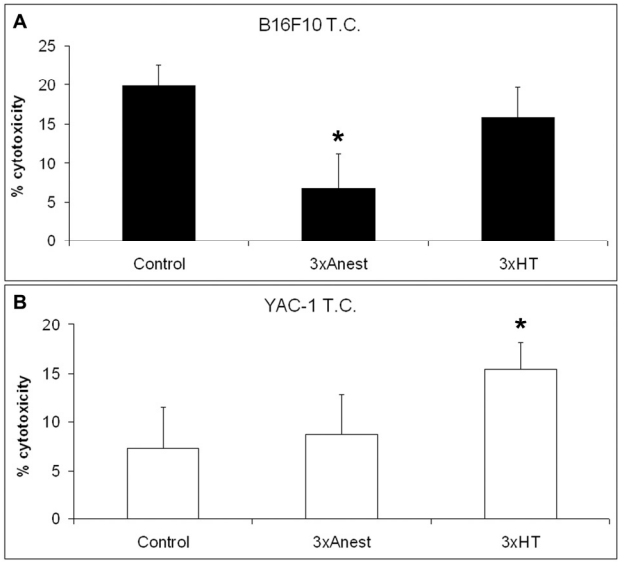

Fig. 4. The specific (A) and natural (B) cytotoxic activity of splenocytes against syngeneic B16F10 melanoma or NK-sensitive YAC-1 target cells in E:T ratio of 32:1 after *in vivo* applied local hyperthermia. Specific cytotoxicity against B16F10 melanomas was impaired by the use of anesthetics – this effect was countered by a concurrent use of hyperthermia (A). No attenuating effect of anesthetics was observed in NK-mediated cytotoxicity (B). Significant changes relative to non-treated mice are marked by asterisk (* p≤0.05; ** p≤0.01).

Results

Our results did not include the clinical parameters (tumor growth, survival), since the experiments were designed as short-term schedules after three courses of LHT treatment dedicated to the changes of immune parameters. We performed four consecutive experiments with 22 mice in the heat-treated group (HT), 17 mice in the anesthetized group (anest) and 16 animals in the untreated group (control) to evaluate LHT effects on the immune response of tumor-bearing animals and the distribution of leukocytes in different compartments (spleen, tumor). The subpopulation specific and activation markers were estimated using polychromatic FACS analysis for determination of the LHT effects on the immune cells proportion, and activation. Functional activities of cytotoxic cells (NK, CTL) were measured by standard ^{51}Cr-release assay in both *in vivo* and *in vitro* arrangements.

LHT-evoked changes in tumor microenvironment

We have determined the distribution of tumor infiltrating leukocytes (TIL) in tumors using FACS. We did not find any significant changes between the control, anesthetized and the LHT groups in proportion of CTLs, NK or APC cells in tumor microenvironment.

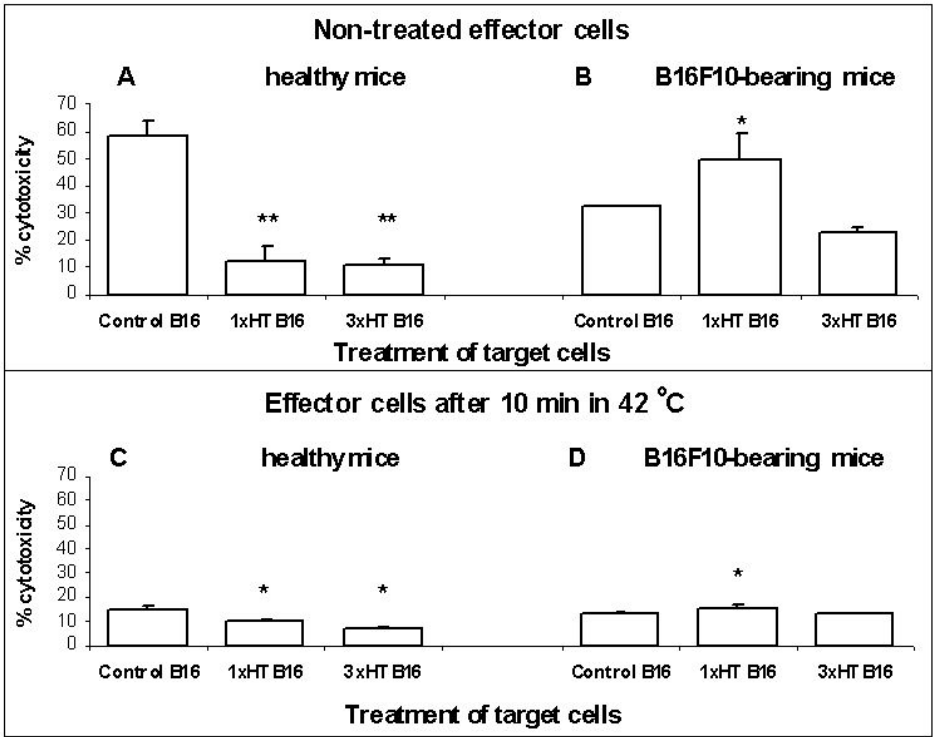

Fig. 5. Splenocyte cytotoxicity against B16F10 melanoma targets after *in vitro* applied HT to effectors and/or target cells. Cytotoxicity of splenocytes isolated from healthy (A, C) or B16F10 melanoma-bearing (B, D) mice against pretreated syngeneic B16F10 cell line: Control - untreated, 1 x HT B16 or 3 x HT B16 - hyperthermed B16F10 cells one or three times, respectively (10 min at 42 °C). Effector cells were incubated for 10 min in either 37 °C (A, B) or 42 °C (C, D). Cytotoxic assay was performed in E:T ratio 32:1, data represent mean ± S.D. of three experiments done in quintuplicates for each sample. Significant changes relative to non-treated mice are marked by asterisk (*p≤0.05; **p≤0.01).

Further we have investigated the changes of very early activation antigen CD69 on different TIL subpopulations – NK, CTL, APC, DC (Fig. 1E, 1F, 1G). Our results (Fig. 2) demonstrated enhanced expression of CD69 only in the monocyte population (CD8-/CD49b-/CD11b+/CD11c-). The counts of activated monocyte (CD11b+/CD69+) in both control and anesthetized mice were similar, 12±1.7 %, while the LHT-treated group showed a 40 % increase (17±2.6 %) in the TIL fraction.

LHT effect on distribution of immune cells in the spleen

Our study revealed changes in the occurrence of cell subpopulations in secondary lymphoid organ, the spleen, after the LHT application. The parameters of detected surface markers were similar as for the analysis of TILs (Fig. 1) without CD45 staining. Cytotoxic T lymphocytes (CD3+/CD8+) increased their counts by 22 %, natural killer cells (CD49b+/NK1.1+) increased by

Direct effect of heat treatment on melanoma and/or effector cells in vitro

To omit the effect of anesthesia, and to distinguish the role of hyperthermia on either tumor or lymphoid cell populations, we performed an *in vitro* modification of the experiments. In this procedure, we used splenocytes from healthy or B16F10 melanoma-bearing mice as effectors and B16F10 melanomas from *in vitro* cultures as targets. Hyperthermia was applied to B16F10 cells in one or three courses of 10-min incubation in 42 °C, 5 % CO_2 atmosphere in the same time schedule as was done during *in vivo* treatment (3 x HT on days 0, 4, and 7). The non-treated cells were kept under the same conditions in 37 °C. Freshly isolated spleen cells of either tumor-bearing or healthy animals were heated for 10 min at 42 °C (Fig. 5C, 5D) immediately before the experiment, while non-treated effector cells were kept in 37 °C (Fig.5A,B) in a round-bottomed 96 well plate. ^{51}Cr-labeled B16F10 target cells after HT treatment (none, 1 x HT and 3 x HT as indicated in Fig. 5) were washed and seeded onto splenocytes in E:T ratio 32:1. The cytotoxicity was measured in a standard 4-hour ^{51}Cr-release assay.

Heat treatment of effector cells exhibited a strong inhibition of cytotoxicity against untreated B16F10 targets that was more pronounced in healthy animals (down to 26 %, Fig. 5A *vs*. 5C) than in tumor-bearing ones (to 41 %, Fig. 5B *vs*. 5D). Further significant suppression was noted in cytotoxic activity of healthy splenocytes, when heat-treated melanoma cells were used as targets (Fig. 5A). No marked difference was seen between the 1 or 3 courses of HT. On the other hand, splenocyte cytotoxicity of tumor-bearing animals responded to 1 x HT B16F10 melanoma target cells by significant increase of cytotoxic effector function, not present in 3 x HT (Fig. 5B).

The presented results demonstrate an inhibitory

influence of HT on effector cells, which is well known in the case of tumoricidal temperature ranges (T≥42 ºC). However, the response of effectors to heat-treated melanoma cells evoke an opposite cytotoxicity effect in healthy (remains suppressed – Fig. 5A, 5C) and tumor-bearing animals (is stimulated – Fig. 5B, 5D). Moreover, the results in Figures 5B and 5D showed preferable use of one course of hyperthermia.

Discussion

One of the causes of cancer progression is the failure of tumor cells recognition by the immune system. In this study we revealed an increased count of activated monocytes in B16F10 melanoma microenvironment, which is poorly recognized by the immune system. These monocytes are potent antigen presenting cells (APCs), facilitating more effective identification of tumors by other immunocompetent cells. Here we showed an increase of cytotoxicity against the melanoma cells (Fig. 4), which we also observed *in vitro* in the case of splenocytes, derived from melanoma-bearing animals (Fig. 5B). The lack of antigen presentation accounts for the decreased cytotoxicity from our *in vitro* studies, where splenocytes from healthy animals were not primed for the killing of target cells by the shedded antigens (Davies and Lindmo 1990) (Fig. 5A, 5C). The prior contact with melanoma cells and subsequent priming of the immune system seems to be crucial for effector function of cytotoxic cells.

Ex vivo functional assays using B16F10 cell line as target demonstrated an attenuation of cytotoxicity by anesthetics, which returned to the control level after LHT application (Fig. 4A). On the other hand, the natural cytotoxicity against YAC-1 targets was not impaired by the use of anesthetics (Fig. 4B). Assuming that the total cytotoxicity against B16F10 targets involves both the natural and specific components, we have found the specific immunity (CTLs) to be predominant in B16F10 melanoma killing. Thus, the anesthetics affect either the specific immunity itself, or the antigen presentation, which is required for its proper function.

According to the literature, HT-induced changes involve an increase of tumor immunogenicity *via* induction of hsp70 expression (Clark and Menoret 2001), MHC II- (Michalek *et al*. 1992) and MHC I-mediated antigen presentation (Ito *et al*. 2001). Our results showing the tumor infiltrating monocyte activation, increase in CTL, and NK cell numbers in the spleen and stimulation of specific and natural cytotoxic activity under local hyperthermia are a contribution to the data on the involved cell subpopulations.

In conclusion, our study demonstrates significant changes in the distribution, phenotype, activation, and effector function of immune cell subpopulations in tumors and spleens of experimental animals after LHT. We suggest that the hyperthermia enhances tumor cell antigenicity, thus leading to improved recognition of these cells by the infiltrating monocytes. Activated monocytes then presumably present antigens to further cell subpopulations (Th, CTL), priming them for the effector function, as reflected in the increased counts of NK cells and CTLs in the spleen and their cytotoxic activity. As presented in the *in vitro* studies, the prior contact with tumor cells seems to be crucial for mounting this response. There are probably several pathways involved in the immunostimulatory effects of hyperthermia. The exact mechanisms and involved subpopulations require further investigation.

Conflict of Interest

There is no conflict of interest.

Acknowledgements

The study was supported by GAUK 92/2004/C, and GAAVCR-5020403, 500200620, and Institutional Research Concept AV0Z50200510.

References

ATANACKOVIC D, NIERHAUS A, NEUMEIER M, HOSSFELD DK, HEGEWISCH-BECKER S: 41.8 °C whole body hyperthermia as an adjunct to chemotherapy induces prolonged T cell activation in patients with various malignant diseases. *Cancer Immunol Immunother* **51**: 603-613, 2002.

BARONZIO G, GRAMAGLIA A, FIORENTINI G: Hyperthermia and immunity. A brief overview. *In Vivo* **20**: 689-695, 2006.

BASU S, SRIVASTAVA PK: Fever-like temperature induces maturation of dendritic cells through induction of hsp90. *Int Immunol* **15**: 1053-1061, 2003.

CLARK PR, MENORET A: The inducible Hsp70 as a marker of tumor immunogenicity. *Cell Stress Chaperones* **2**: 121-125, 2001.

DAVIES CD, LINDMO T: Hyperthermia-induced shedding and masking of melanoma-associated antigen. *Int J Hyperthermia* **6**: 1053-1064, 1990.

EMAMI B, NUSSBAUM GH, TENHAKEN RK, HUGHES WL: Physiological effects of hyperthermia: response of capillary blood flow and structure to local tumor heating. *Radiology* **137**: 805-809, 1980.

FIŠEROVÁ A, KOVÁŘŮ H, HAJDUOVÁ Z, MAREŠ V, STAREC M, KŘEN V, FLIEGER M, POSPÍŠIL M: Neuroimmunomodulation of natural killer (NK) cells by ergot alkaloid derivatives. *Physiol Res* **46**: 119-125, 1997.

HILDEBRANDT B, WUST P, AHLERS O, DIEING A, SREENIVASA G, KERNER T, FELIX R, RIESS H: The cellular and molecular basis of hyperthermia. *Crit Rev Oncol Hematol* **43**: 33-56, 2002.

HUANG YH, HAEGERSTRAND A, FROSTEGARD J: Effects of in vitro hyperthermia on proliferative responses and lymphocyte activity. *Clin Exp Immunol* **103**: 61-66, 1996.

ITO A, SHINKAI M, HONDA H, WAKABAYASHI T, YOSHIDA J, KOBAYASHI T: Augmentation of MHC class I antigen presentation via heat shock protein expression by hyperthermia. *Cancer Immunol Immunother* **50**: 515-522, 2001.

KAMPINGA HH, DYNLACHT JR, DIKOMEY E: Mechanism of radiosensitization by hyperthermia (≥43 ºC) as derived from studies with DNA repair defective mutant cell lines. *Int J Hyperthermia* **20**: 131-139, 2004.

MICHALEK MT, BENACERRAF B, ROCK KL: The class II MHC-restricted presentation of endogenously synthesized ovalbumin displays clonal variation, requires endosomal/lysosomal processing and is up-regulated by heat shock. *J. Immunol* **148**: 1016-1024, 1992.

MILANI V, NOESSNER E: Effects of thermal stress on tumor antigenicity and recognition by immune effector cells. *Cancer Immunol Immunother* **55**: 312-319, 2006.

OSTAPENKO VV, TANAKA H, MIYANO M, NISHIDE T, UEDA H, NISHIDE I, TANAKA Y, MUNE M, YUKAWA S: Immune-related effects of local hyperthermia in patients with primary liver cancer. *Hepatogastroenterology* **52**: 1502-1506, 2005.

SHEN R-N, LU L, YOUNG P, SHIDNIA H, HORNBACK NB, BROXMEYER HE: Influence of elevated temperature on natural killer cell activity, lypmhocyte-activated killer cell activity and lectin dependent cytotoxicity of human umbilical cord blood and adult blood cells. *Int J Radiation Oncol Biol Phys* **29**: 821-826, 1994.

STAWARZ B, ZIELINSKI H, SZMIGIELSKI S, RAPPAPORT E, DEBICKI P, PETROVICH Z: Transrectal hyperthermia as palliative treatment for advanced adenocarcinoma of prostate and studies of cell-mediated immunity. *Urology* **41**: 548-553, 1993.

SZMIGIELSKI S, SOBCZYNSKI J, SOKOLSKA G, STAWARZ B, ZIELINSKI H, PETROVICH Z: Effects of local prostatic hyperthermia on human NK and T cell function. *Int J Hyperthermia* **7**: 869-880, 1991.

VAN DER ZEE J: Heating the patient: a promising approach? *Ann Oncol* **8**: 1173-1184, 2002.

VARTAK S, GEORGE KC, SINGH BB: Antitumor effect of pre-transplantation local hyperthermia and augmentation by dietary unsaturated fat. *Indian J Exp Biol* **34**: 825-832, 1996.

Publication 7: MSH–coated ferritin–based nanoplatform is specific, non–toxic and modular.

Overview

Most immune modulators and mediators, whether synthetic or endogenous, have a pleiotropic effect and often influence cells that were not intended as primary targets. Even if a given agent has an exclusive specificity for certain receptor, it can be eliminated from the system before it reaches its target. Thus, development of targeted nanoparticles with selective targeting and enhanced retention is gaining wide popularity (140, 141).

Despite the large number of techniques available, the attainment of a suitable multifunctional platform with desired bioactivity, targeting specificity, stability, desired and defined structure and size remains a challenge. Protein–cage structures as of the ferritin family are novel and quite promising (142). Since they are DNA encoded, they are well defined, physiological, thus desirably bioactive and soluble, stable and have the ideal–range diameter to penetrate capillary fenestrations but avoid rapid clearance (143). Its 24–subunit structure (144) with distinct interfaces (internal and external both with distinct variety of functional groups) allows for multivalent chemical or genetic modifications, enhancing its targeting, imaging or therapeutic properties. Thus, genetic link for α–melanocyte–stimulating hormone (MSH) was added in our platform to target the particle into solid tumors and polyethylene glycol (PEG) molecules were added to mask the particle from its natural receptors to prolong its circulation.

Aims and methods

This study aims at the *in vitro* stability, affinity and specificity of melanoma–targeted nanoparticles, on their *in vivo* circulation and organ accumulation in the mouse C57BL/6 melanoma (B16F10) model. It was our goal to prove these particles stable, specific for the melanoma cells and having low accumulation in irrelevant organs with retained circulation. The particles were cloned, purified, PEGylated, fluorescently labeled and after structure and stability was confirmed, were introduced into *in vitro* cultures and living animals.

Results and discussion

The results shown a good stability and availability of the nanoplatform, with unique spectral properties, allowing fluorescent imaging (other molecules or magnetic/radioactive particles could be used to follow the fate of the particle). We further demonstrated its specificity for the targeted B16F10 melanomas both *in vitro* and *in vivo*. In addition, the PEG molecule masking increased its circulation in the system to several hours, when compared to minutes for the unmasked particle.

During *in vivo* imaging, we observed specific binding to melanocytes in the affected skin with intact (non–fluorescent) surrounding healthy tissue. Even single infiltrating melanoma–cells

were well discerned against the dark background. Increased but comparably lower accumulation of nanoparticles was observed in the liver Kupffer cells and in the kidney glomeruli. This accumulation was however much lower, than previously reported for unmasked construct with different targeting moiety (145).

In conclusion, we developed a rationally designed modified human ferritin–based multifunctional nanoplatform, with well–defined parameters and modularity in the targeting moiety, present on the surface of each of the 24 subunits. Thus, this platform can be equipped with specific ligands or monoclonal antibodies and loaded with mediators or heat–generating particles (139), achieving specifically targeted immune modulation in almost any system.

International Journal of Nanomedicine

Dovepress

open access to scientific and medical research

Open Access Full Text Article

ORIGINAL RESEARCH

Selective targeting of melanoma by PEG-masked protein-based multifunctional nanoparticles

This article was published in the following Dove Press journal:
International Journal of Nanomedicine
15 March 2012
Number of times this article has been viewed

Luca Vannucci[1,*]
Elisabetta Falvo[2,*]
Manuela Fornara[3]
Patrizio Di Micco[4]
Oldrich Benada[1]
Jiri Krizan[1]
Jan Svoboda[1]
Katarina Hulikova-Capkova[1]
Veronica Morea[3]
Alberto Boffi[4,5]
Pierpaolo Ceci[3]

[1]Institute of Microbiology, Academy of Sciences of the Czech Republic, VVI, Prague, Czech Republic; [2]Regina Elena Cancer Institute, Pharmacokinetic/Pharmacogenomic Unit, [3]National Research Council of Italy, Institute of Molecular Biology and Pathology, [4]Department of Biochemical Sciences "A Rossi Fanelli", University of Rome "Sapienza", [5]Center for Life Nano Science at Sapienza, Italian Institute of Technology, Rome, Italy

*These two authors contributed equally to this work

Video abstract

Point your smartphone at the QR code to the left. If you have a QR code reader the video abstract will appear. Or use: http://bit.ly/yZBwLu

Correspondence: Pierpaolo Ceci
National Research Council of Italy, Institute of Molecular Biology and Pathology, c/o Department of Biochemical Sciences "A Rossi Fanelli", University of Rome "Sapienza", P le Aldo Moro 5, Rome 00185, Italy
Tel +39 06 499 0910
Fax +39 06 444 0062
Email pierpaolo.ceci@cnr.it

Background: Nanoparticle-based systems are promising for the development of imaging and therapeutic agents. The main advantage of nanoparticles over traditional systems lies in the possibility of loading multiple functionalities onto a single molecule, which are useful for therapeutic and/or diagnostic purposes. These functionalities include targeting moieties which are able to recognize receptors overexpressed by specific cells and tissues. However, targeted delivery of nanoparticles requires an accurate system design. We present here a rationally designed, genetically engineered, and chemically modified protein-based nanoplatform for cell/tissue-specific targeting.

Methods: Our nanoparticle constructs were based on the heavy chain of the human protein ferritin (HFt), a highly symmetrical assembly of 24 subunits enclosing a hollow cavity. HFt-based nanoparticles were produced using both genetic engineering and chemical functionalization methods to impart several functionalities, ie, the α-melanocyte-stimulating hormone peptide as a melanoma-targeting moiety, stabilizing and HFt-masking polyethylene glycol molecules, rhodamine fluorophores, and magnetic resonance imaging agents. The constructs produced were extensively characterized by a number of physicochemical techniques, and assayed for selective melanoma-targeting in vitro and in vivo.

Results: Our HFt-based nanoparticle constructs functionalized with the α-melanocyte-stimulating hormone peptide moiety and polyethylene glycol molecules were specifically taken up by melanoma cells but not by other cancer cell types in vitro. Moreover, experiments in melanoma-bearing mice indicate that these constructs have an excellent tumor-targeting profile and a long circulation time in vivo.

Conclusion: By masking human HFt with polyethylene glycol and targeting it with an α-melanocyte-stimulating hormone peptide, we developed an HFt-based melanoma-targeting nanoplatform for application in melanoma diagnosis and treatment. These results could be of general interest, because the same strategy can be exploited to develop ad hoc nanoplatforms for specific delivery towards any cell/tissue type for which a suitable targeting moiety is available.

Keywords: multifunctional nanoparticles, ferritin, nanoplatform, cancer-targeting, melanoma

Introduction

Development of multifunctional nanoparticles for nanomedicine applications, such as cell/tissue-specific delivery, biomedical imaging and therapy, has recently gained wide popularity.[1–4] Various types of materials, including synthetic polymers and lipids, have been increasingly utilized as platforms for nanoparticle synthesis.[1,5] Despite the large number of bioconjugation techniques available, the attainment of multifunctional nanoprobes endowed with desired bioactivity, targeting specificity,

and stability remains a challenge. Approaches using protein-cage structures, such as proteins belonging to the ferritin family, are novel and very promising.[6,7] Apoferritin is a highly symmetrical multimeric protein consisting of 24 subunits that self-assemble into a shell-like molecule enclosing a hollow cavity, with external and internal diameters of 12 nm and 8 nm, respectively.[8,9] Ferritin structure and size are precisely controlled at the atomic level, because ferritin monomers are gene products. As a consequence, ferritin proteins guarantee excellent size and shape control in metal nanoparticle synthesis, and several materials, such as Fe_3O_4, Co_3O_4, Mn_3O_4, Pt, CoPt, Pd, CdS, CdSe, ZnSe, $CaCO_3$, Ag, and Au have been produced within the internal cavity of ferritin proteins.[10–18] The small size of ferritins (<20 nm) increases the chances of larger nanoparticles passing human body barriers and reaching specific targets. Indeed, the dimensions of the nanoparticles, which must be small enough to penetrate capillary fenestrations and large enough to avoid rapid clearance through the kidney (the ideal diameter being lower than 50–60 nm and greater than 6–8 nm, respectively),[19,20] are one of the key prerequisites for efficient targeted delivery, together with a long-circulating capability of the carrier and high specificity of the selector towards the target receptor. Additionally, the exceptional stability of the ferritin cage structure over a wide range of temperatures (up to 80°C–100°C) and pH conditions (3–10) and high expression levels as a recombinant protein in efficient heterologous systems like *Escherichia coli* cells (100–200 mg/L in laboratory scale) allow the apoferritin protein to be produced on a large-scale, at high yield (gram or even kilogram) and at low cost, which is useful for industrial scaleup purposes. Further, human ferritin is a physiological protein that has high solubility and stability in water, blood, and buffers, as well as low toxicity, all of which are desirable features for in vivo applications in humans.[21,22] Several groups have reported that ferritins are effective templates for loading either imaging agents for magnetic resonance imaging or positron emission tomography (PET),[21–24] as well as metal-based drugs in their internal cavity.[25] Finally, ferritin proteins possess distinct interfaces (ie, an internal one facing the cavity and an external one facing the solvent) endowed with a variety of chemical groups, eg, primary amines, carboxylates, and thiols, which can be linked either genetically and/or chemically with different functionalities for targeted delivery of imaging and/or therapeutic agents.[22,24] For all these reasons, there has been widespread interest in the possibility of using ferritin-based nanoplatforms for selective targeting.

In previous reports, the heavy chain of human ferritin (HFt) has been genetically conjugated with an arginine-glycine-aspartate (RGD)-containing tumor targeting peptide, which is recognized by a large number of integrin molecules expressed by melanoma, glioma, and other tumors, as well as by normal cells.[24,26] These RGD-containing HFt constructs have shown promising selectivity towards melanoma in in vitro experiments because compared with unconjugated HFt they have a threefold higher ability to bind melanoma cells, but show no difference in T lymphocyte binding.[26] In spite of these encouraging results, only one study has reported on the application of HFt-based constructs bearing a targeting moiety for a physiological receptor in vivo.[24] In this study, the localization of an RGD-containing HFt in an animal model of glioma was approximately 6% of the injected dosage, 2% of which was ascribed to the presence of the RGD targeting moiety and 4% to the enhanced permeability and retention effect of the tumor tissue. However, massive accumulation of the construct was observed in the liver, which appeared to be significantly greater than in the tumor.[26]

The enhanced permeability and retention effect has been shown to allow nanoparticles to accumulate at tumor sites in concentrations 5–10 times higher than in normal tissue within 1–2 days.[27] However, this effect is counteracted both by fast clearance from plasma (10–60 minutes), which has been observed in rats, dogs, and rabbits after intravenous injection of liver ferritin, and by the presence of ferritin receptors on several cell types, including macrophages,[21,28–32] which determines ferritin removal from the circulation by the reticuloendothelial or mononuclear phagocytic systems.

To overcome these limitations and increase the circulation time of ferritin, as well as target specificity with respect to previously reported HFt constructs, we developed chemically and genetically engineered HFt-based nanoparticles aimed at specifically targeting melanoma cancer cells and tissues, while minimizing nonspecific binding versus other human cells (Scheme 1). To achieve these goals, the following strategy was adopted. First, HFt nanoparticles were genetically linked to α-melanocyte-stimulating hormone (α-MSH), which had not been exploited previously as a targeting moiety for HFt constructs. The MSH peptide binds to melanocortin receptors that are overexpressed by melanoma cells and metastases, and expressed to a lower extent only by melanocytes. As a consequence, it is expected to be significantly more selective than the RGD peptide

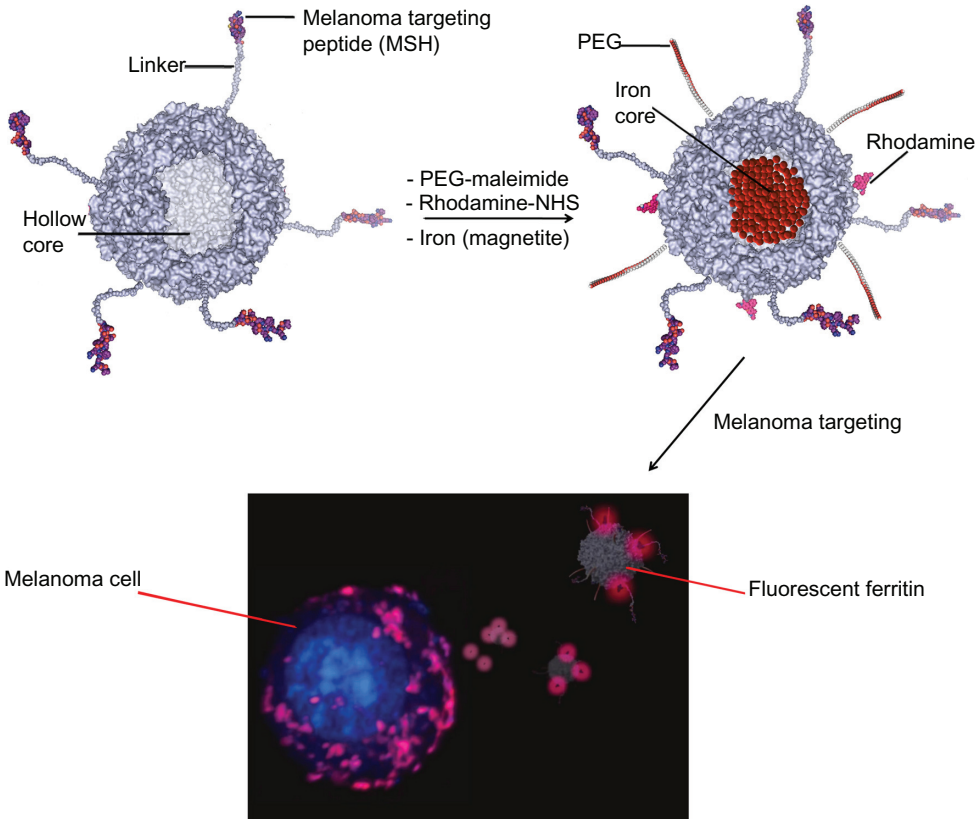

Scheme 1 Top: design of an HFt-based nanoplatform for melanoma targeting. The HFt protein has been genetically functionalized (left) with a melanocyte-stimulating hormone peptide joined to the N-terminus of each of the 24 subunits by a linker peptide (only five of the 24 derivatized N-termini are shown, for clarity). Additionally, chemical derivatization (right) has been performed to provide the HFt protein with novel functionalities for targeted delivery of imaging and therapeutic agents (polyethylene glycol, rhodamine, metal iron). Bottom: analysis of melanoma cells by confocal laser scanning microscopy. The shown confocal image demonstrates binding and uptake of HFt-based nanoparticles after in vitro incubation (60 minutes).
Abbreviation: HFt, human protein ferritin.

linked to HFt in previous studies, in that the RGD moiety is recognized by a large number of integrin molecules, which are expressed by both normal and tumor cells. Additionally, polyethylene glycol (PEG) molecules were conjugated with the HFt surface, with the aim of masking the protein from its physiological receptors. HFt masking by PEGylation, which has not been implemented in previous studies of HFt-based constructs, is aimed at decreasing uptake of HFt by the reticuloendothelial and mononuclear phagocytic systems, resulting in an increased blood circulation time.[27] Moreover, PEGylation is an effective method for preventing putative responses by the immune system, which would be elicited if the nanoparticles were sensed as foreign agents, in spite of the fact that both the HFt protein and MSH peptide components are extracellular and of human origin.

To assess the targeting specificity of our HFt-MSH-PEG constructs, we carried out in vitro experiments using both melanoma and control cells, with wild-type HFt and HFt-PEG as controls. Additionally, we investigated the specificity and circulation time of the HFt-MSH-PEG constructs in melanoma-bearing mice, using wild-type HFt as a control.

The data reported herein demonstrate that the HFt-MSH-PEG constructs were specifically taken up by melanoma cells but not by other tumor cells in vitro, and that the ability of HFt-MSH-PEG to bind to, and be internalized by melanoma cells is significantly higher than that of HFt-PEG nanoparticles, which are devoid of the targeting MSH moiety, and of wild-type HFt. If the MSH moiety endows HFt with melanoma-targeting ability, the presence of PEG efficiently shields HFt from its cell receptors, because the uptake of both HFt-PEG and HFt-MSH-PEG by colon cancer cells is significantly lower than that of wild-type HFt.

In agreement with our in vitro results, studies performed using a melanoma animal model in vivo showed that the HFt-MSH-PEG nanoparticles accumulated to a large extent at the tumor sites whereas accumulation of wild-type HFt was negligible, and that this accumulation effect appears

to be specific for the tumor when compared with the other tissues analyzed. Further, HFt-MSH-PEG had a higher circulation time than wild-type HFt, most likely because of the presence of PEG.

Thus, the strategy adopted to develop melanoma-targeting HFt-MSH-PEG nanoparticles appears to be suitable for the development of targeted imaging agents for magnetic resonance imaging, PET, and fluorescence imaging, as well as for targeted delivery of therapeutic agents in cancer therapy.

Materials and methods

Cloning, overexpression, and purification of HFt-based nanoparticles

The expression vector, pET-17b, containing the *HFt-MSH* gene, was purchased from GeneArt AG (Bavaria, Germany). Gene synthesis was performed taking into consideration the codon optimization for high level expression in *E. coli*. *E. coli* BL21 (DE3) cells harboring the recombinant *HFt-MSH* plasmid were grown to OD_{600} 3.0 at 30°C in 1 L of ampicillin-containing liquid Luria-Bertani broth medium (Sigma-Aldrich, Milan, Italy). The cells were harvested by centrifugation at 16,000 rpm for 20 minutes and suspended in 50 mM Tris-HCl, 0.5 mM dithiothreitol, 1 mM ethylenediamine tetra-acetic acid, and 300 mM NaCl at pH 7.5, and disrupted by sonication in the presence of 1 mM phenylmethylsulfonyl fluoride. The lysate was then centrifuged at 16,000 rpm for 40–45 minutes at 6°C. The pellet was washed twice with 100 mM *N*-cyclohexyl-3-aminopropanesulfonic acid (pH 10.5) and then centrifuged at 16,000 rpm for 10 minutes at 6°C to recover the HFt-MSH protein from the membrane-containing fraction. After each centrifugation step, the supernatants were collected and combined with each other. The solution obtained was dialyzed overnight against Tris 30 mM, 0.6 M NaCl, pH 7.8 at room temperature. HFt-MSH precipitates under these high salt conditions. The pellet was resuspended in Milli-Q water (Millipore, Billerica, MA), sterile-filtered, and stored at 4°C. Typical yields were 150–200 mg of pure protein per liter of culture. Human apo-HFt was provided by MoLiRom (Rome, Italy).

Protein stability measurements

The thermal stability of wild-type HFt and HFt-MSH was assessed in the temperature range of 30°C–100°C by following the circular dichroism signal at 222 nm to monitor the thermal unfolding process. A Jasco J-715 spectropolarimeter was used. Temperature was varied in steps of 1°C per minute. The protein, at 1 mg/mL in Milli-Q water, was kept in stoppered 0.1 cm quartz cells.

The ability of HFt-MSH to dissociate and reassociate reversibly as a function of pH was also assessed. The protein solution was adjusted to pH 2.0 by addition of HCl 0.1 M, and the pH was kept constant for about 15 minutes to ensure that dissociation of HFt-MSH was complete. The pH value was then adjusted to 7.5 by adding NaOH 0.1 M. The resulting solution was stirred at room temperature for 1 hour and checked for HFt-MSH oligomerization by size exclusion chromatography. The size exclusion chromatography experiments were performed using a Superose 6 gel filtration column connected to a GE Healthcare FPLC system Unicorn Akta purifier (GE Healthcare, Milan, Italy) equilibrated with phosphate-buffered saline at pH 7.5.

Preparation of PEGylated proteins

HFt and HFt-MSH solutions (2 mg/mL) were incubated with 1.0 mM of 5 kDa methoxypolyethylene glycol maleimide (Sigma-Aldrich), in 20 mM Tris-HCl at pH 7.2 and room temperature for about 2 hours under stirring. Subsequently, samples were filtered and exchanged 4–5 times with H_2O_{dd} using 30 kDa Amicon Ultra-15 centrifugal filter devices (Millipore) to remove the excess reagents. The PEGylated samples were sterile-filtered and stored at 4°C.

Size exclusion chromatography and dynamic light scattering

The size exclusion chromatography experiments were performed using a Superose 6 gel filtration column equilibrated with phosphate-buffered saline at pH 7.5. Dynamic light scattering experiments were carried out using a Zetasizer Nano S (Malvern Instruments, Worcestershire, UK) equipped with a 4 mW He-Ne laser (633 nm). Measurements were performed at 25°C, with an angle of 173° from the incident beam. Peak intensity analyses were used to determine the average hydrodynamic diameters (*Z*-average diameter) of the scattering particles. Results are the average of at least five measurements. All samples were prepared at 1 mg/mL in filtered H_2O_{dd}. All traces for the size exclusion chromatography and dynamic light scattering experiments were analyzed using Origin 8.0 (Originlab Corporation, Northampton, MA).

Mass spectrometric analysis and sample preparation

HFt-MSH and HFt-MSH-PEG samples at a concentration of 1 mg/mL were used in a native form and digested using trypsin enzyme (sequencing grade, Promega, Madison, WI). Trypsin digestion was performed overnight at 37°C in 25 mM ammonium bicarbonate at a pH of 8.0, with a trypsin:HFt

construct molar ratio of 1:50. The digested HFt construct was loaded onto the target plate and mixed immediately with an equal volume of α-cyanohydroxycinnamic acid in 50% acetonitrile and 0.1% trifluoroacetic acid (Sigma-Aldrich). The samples were analyzed using a matrix-assisted laser desorption/ionization (MALDI) time-of-flight Applied Biosystems/MDS Sciex 4800 Plus MALDI TOF/TOF™ analyzer (Monza, Italy). The base peak in the MALDI TOF mass spectrum (m/z 1056.5) was isolated and fragmented in the TOF/TOF mass spectrometer. Analysis of the tandem mass spectrum showed product ions (b and y series). Data analysis was carried out using the Data Explorer 4.0 software (Applied Biosystems).

Fourier transform infrared spectroscopic analysis

HFt-MSH and HFt-MSH-PEG samples for Fourier transform infrared spectroscopic measurements were used at 3 mg/mL in H_2O_{dd} and layered upon the ZnSe crystal. The protein solutions (250 μL) were layered on the ZnSe plate, dried under a nitrogen stream, and placed in an atmosphere saturated with water vapor in a glove box for 24 hours in order to obtain a fully hydrated sample. Attenuated total reflectance–Fourier transform infrared spectroscopic measurements were carried out on a Magna 760 Nicolet instrument equipped with an MCT/A detector (ThermoFisher Scientific Inc, Illkirch Cedex, France). ZnSe ARK plates equipped with a thermal ARK temperature controller (ThermoFisher Scientific Inc) were used as internal reflection elements. A sealed, volatile solvent cover was used during the measurements in order to maintain constant hydration of the sample. Typically, 128 scans were acquired at 4 cm^{-1} resolution, two levels of zero filling, and 25°C. For each spectrum, the background was acquired on the empty attenuated total reflectance plate.

Magnetic HFt preparation and transmission electron microscopic analysis

Magnetite (or maghemite) was incorporated into the HFt-MSH using a method described elsewhere.[34] Briefly, iron incorporation experiments were carried out at 65°C on 1 mg/mL HFt-MSH samples in 5 mM Hepes–NaOH at a pH of 8.5. Solutions of $FeSO_4$ dissolved in 0.5 mM HCl were used as an iron source. During the course of the experiment, the reaction vessel was kept at 65°C under a positive nitrogen pressure, and pH was maintained dynamically at 8.5 with 100 mM NaOH using an automatic titrator (Titrino; Metrohm AG, Herisau, Switzerland). Solutions of $FeSO_4$ 15 mM and H_2O_2 5 mM were added simultaneously at a constant rate (0.5 mL/minute) using two peristaltic pumps. The theoretical iron loading factor was 4500 Fe(II)/protein. The protein and iron contents in the samples containing the magnetic nanoparticles were assessed by means of native electrophoresis on 1% agarose gels and inductively-coupled plasma atomic emission spectroscopy.

HFt-MSH-enclosed magnetite/maghemite samples, in PEGylated or non-PEGylated form (0.1 mg/mL) were negatively stained (0.1% of trehalose into 1% ammonium molybdate) on glow discharge-activated carbon-coated grids.[35] Samples were viewed under a Philips CM100 electron microscope (Eindhoven, The Netherlands) at 80 kV. Digital images were recorded using a MegaView II slow scan camera at a primary magnification of 92,000×.

Protein structure analysis and modeling

The atomic structure of HFt was downloaded from the Protein Data Bank (http://www.pdb.org).[36] Protein structure visualization and modeling of the PEG chains, MSH peptide, and Gly/Ser-rich linker were performed using Insight II software (Accelrys Inc, San Diego, CA).

Fluorescent labeling of proteins

HFt-PEG and HFt-MSH-PEG solutions (2 mg/mL) were incubated with 1 mM of 5(6)-carboxytetramethylrhodamine N-succinimidyl ester (λ_{ex} 552 nm, λ_{em} 575 nm; Thermo Scientific, Milan, Italy) in phosphate-buffered saline for 2 hours at pH 7.5 and room temperature, with stirring in the dark. Subsequently, the samples were filtered, dialyzed, and exchanged with H_2O_{dd} and phosphate-buffered saline, using 30 kDa Amicon Ultra-15 centrifugal filter devices to remove excess reagents. The samples were sterile-filtered and stored at 4°C in the dark. The number of dye molecules linked per protein was determined by absorbance spectroscopy, in accordance with the manufacturer's instructions, applying the Beer-Lambert law. Briefly, the measurement was carried out using a 0.1 cm path length quartz cuvette at room temperature. The concentration of bound dye was calculated using the following equation: $c(dye) = A_{552\,nm}/(\varepsilon_{max} \times d)$, where ε_{max} is 80,000 for rhodamine dye. The protein concentration is obtained in the same way from its absorbance value at 280 nm, using an ε of 25,900 and 18,910 M^{-1} cm^{-1} for HFt-MSH and wild-type HFt, respectively. Because rhodamine shows some absorption at 280 nm, the measured absorbance A_{280} was corrected for the contribution of this dye (correction factor = 0.34).

Cell culture and confocal microscopy on tumor cells in vitro

The murine melanoma B16F10 cell line of C57BL/6 (*H-2*^{b}/*H-2*^{b}) origin (ATCC, Manassas, VA) as well as human colorectal carcinoma HT29 cell line (ATCC) were cultivated in RPMI-1640 medium (Institute of Molecular Genetics, Prague, Czech Republic), supplemented with 0.05 mg/mL gentamicin, 2 mM L-glutamine, 1 mM sodium pyruvate, 0.05 mM 2-mercaptoethanol, and 10% heat-inactivated fetal calf serum (Gibco, Grand Island, NY), at 37°C in a 5% CO_2 humidified atmosphere.

B16F10 melanoma or HT29 human colorectal carcinoma cells in suspension (1×10^6 cells/100 µL) were incubated with fluorescent wild-type HFt, HFt-PEG, or HFt-PEG-MSH in H-MEMD culture medium. The HFt nanoparticle solutions (100 µL) were added to 100 µL of cell solution. The final concentration of HFt nanoparticles was 0.007 mg/mL. The controls received only addition of medium without HFt nanoparticles. The cells were incubated at 37°C in 5% CO_2 for 10 and 60 minutes. After incubation, the cells were fixed in 3.7% formaldehyde for 30 minutes and then washed three times with Dulbecco's phosphate-buffered saline. The cell nuclei were stained using Draq5. The confocal microscopy apparatus comprised a confocal laser scanning system (1-photon) Olympus FV1000 with an IX 81 inverted microscope, a Hamamatsu C9 100/13 EM-CCD digital camera, and an imaging analysis program (Flowview 10; Olympus, Tokyo, Japan). Confocal microscopy was performed at 20× and 40× original magnification and all images, obtained using FluoView FV1000 software (Olympus), were background-subtracted and normalized to maximal intensities of the fluorescent HFt nanoparticles. Uptake of HFt nanoparticles by the cells was assessed from the average of the percentages of positive cells in three randomly evaluated fields per sample at 20× magnification, using four samples for each type of treatment and cells.

In vivo administration of HFt nanoparticles and confocal evaluation

Male C57BL/6 mice aged 7–8 weeks were purchased from AnLab (Prague, Czech Republic) and housed in conventional conditions in our experimental animal facility, and adapted to the local conditions over 10 days with a standard diet and access to water ad libitum before inoculation with the melanoma cells. The mice were intradermally/subcutaneously inoculated in the lower back with 1×10^6 B16F10 melanoma cells per mouse suspended in 0.1 mL of culture medium. Ten days after inoculation with the melanoma cells, the animals developed bulky tumors at the site of injection (5–7 mm diameter). Under general anesthesia, slow intracardiac injection of 0.1 mL of the experimental fluorescent wild-type HFt or HFt-PEG-MSH (0.5 mg) solution was performed. The animals were maintained for one hour under observation for possible secondary effects after awakening. The mice were sacrificed 24 hours after inoculation. A skin flap including the tumor and a liver sample were harvested. A thick tumor section, a sample of skin, and a thick liver section were mounted on a large coverglass for direct observation of rhodamine fluorescence in the tissue by confocal laser scanning microscopy (excitation filter 530–550 nm) at 40× original magnification, as described earlier.

Effect of HFt nanoparticles on immune cells in vivo

Healthy mice were sacrificed 24 hours after injection of the HFt nanoparticles. Their spleens were collected and gently dissociated through a nylon mesh in H-MEMD medium to prepare single cell suspensions, and splenocytes were not gradient-separated to collect all leukocytes. Complete blood samples were pretreated with ACK lysing buffer to lyse the erythrocytes before specific staining. Leukocytes were characterized by fluorescence-activated cell sorting analysis using an antibody against the CD45 common marker. CD69 positive cells were evaluated by gating the leukocyte population into granulogates, lymphogates, and monogates, respectively, on an FSc–SSc plot.

The experiments had the approval of the ethics committee at the Institute of Microbiology, according to the Animal Protection Act of the Academy of Sciences of the Czech Republic and the European Convention for the Care and Use of Laboratory Animals.

Plasma stability and circulation time of HFt nanoparticles

The stability of the iron-containing wild-type HFt and HFt-MSH-PEG in mouse plasma was determined by size exclusion chromatography. Samples of the HFt nanoparticles (0.20 mL, 10 mg/mL) were incubated at 37°C with mouse plasma (1.8 mL) and collected as follows. Samples were withdrawn at hours 1, 6, 18, 24, and 48, centrifuged at 13,000 rpm for 30 minutes, and loaded onto a Superose 6 gel filtration column connected to a GE Healthcare FPLC system Unicorn Akta purifier in phosphate-buffered saline at a flow rate of 0.5 mL/minute. The presence of intact HFt nanoparticles was determined by simultaneously following the protein signal (absorbance at 280 nm) and the iron cluster (absorbance

at 405 nm), and calculating the area of the elution peaks typical of HFt 24-mers using Unicorn 5.01 software (GE Healthcare).

To evaluate the circulation time of the wild-type HFt and HFt-MSH-PEG nanoparticles, 0.1 mL of nanoparticles (1.0 mg) was injected into the tail veins of the mice. Blood (0.5 mL) was collected from each mouse before injection and at 3 minutes and 1, 3, 6, and 24 hours following injection. Plasma was obtained by centrifugation of the fresh blood, containing heparin as an anticoagulant, at 13,000 rpm for 45 minutes. Presence of HFt nanoparticles was quantified by Western blotting using both anti-MSH and anti-HFt antibodies. Polyacrylamide gel electrophoresis was performed under denaturing and reducing conditions. Plasma was diluted 2× in sample buffer to prevent precipitation of serum proteins during boiling. Diluted samples were then boiled for 5 minutes. Thereafter, 12% sodium dodecyl sulfate gels were run at 150 V for one hour. Gel electrophoresis proteins were transferred to polyvinyl difluoride membranes in transfer buffer (25 mM Tris-HCl, 192 mM glycine, and 20% methanol, pH 8.3) at 100 mA for 45 minutes. Thereafter, membranes were blocked overnight at 4°C in 10% blocking reagent (Boehringer Mannheim, Ludwigshafen, Germany). Subsequently, the membranes were incubated in 1% gelatin in Tris-buffered saline with a rabbit monoclonal antibody, anti-HFt (Abcam, Cambridge, UK) or a rabbit polyclonal antibody anti-MSH (Abcam). Both antibodies were diluted 1000×. Primary antibodies were detected with horseradish peroxidase-conjugated rabbit antigoat IgG (Sigma-Aldrich), and signals were visualized using a luminol-based chemiluminescent substrate designed for use with peroxidase-labeled reporter molecules (LumiGlo®, KPL, Gaithersburg, MD) and Kodak Scientific Imaging Film (Eastman Kodak Company, Rochester, NY).

Results and discussion

Our main aim was to obtain an HFt-based construct that was shielded against nonspecific uptake by human cells and possessed a satisfactory circulation time in the bloodstream, which is a key property for in vivo applications. Derivatization using an inert and uncharged material such as PEG appeared to be an adequate strategy, both to reduce nonspecific cell binding and prolong the circulation time in serum. Based on previous reports, we set the size of the PEG molecules at 5 kDa.[37] Following observation of the three-dimensional structure of human HFt, we decided to link PEG molecules to the thiol groups of the cysteine residues, given that the location of the exposed cysteine thiols on the surface of HFt is such that their PEGylation is not expected to interfere with subsequent derivatization of the N-terminal region, and given that HFt has a relatively small number of cysteine side chains on the external surface (two per subunit, ie, 48 for the whole assembly), compared with other solvent-exposed reactive groups (ie, amines and carboxylates), allowing us to have tight control over the number of PEG molecules conjugated to the HFt shell. To obtain covalently bound HFt construct-PEG complexes, the HFt constructs were reacted with functionalized maleimide-PEG 5 kDa.

The PEGylation reaction was performed using both wild-type HFt and the HFt construct containing the melanoma-binding peptide sequence, α-MSH, genetically linked to the N-terminal region of HFt (HFt-MSH). The α-MSH peptide was chosen for a number of reasons. Short amino acid polymers (peptides) have a target-binding ability comparable with that of larger molecules, such as antibodies. Due to their small size, peptides are also ideal for multiple modifications of nanoparticle constructs and generation of pluripotent nanoparticles.[38] Moreover, α-MSH binds to melanocortin receptors and, in particular, is a potent agonist of the melanocortin type 1 receptor (MCR1, overexpressed by many melanoma cells[39]) and binds to MCR1 with high affinity (IC_{50} 0.21 nmol/L).[40] Importantly, more than 80% of human metastatic melanoma samples have been found to display MCR1.[41] Melanoma metastases are very aggressive, with a patient survival time of 3–15 months on average, and are the actual cause of mortality in patients with melanoma.[42] Therefore, the development of a system containing a targeting peptide able to bind melanoma metastases is of critical importance. Gold nanoparticles linked onto an analogous synthetic peptide were recently shown to have reasonably selective tumor localization compared with the nonspecific PEGylated form.[43] However, because of the synthetic peptide origin, a very long and expensive procedure including peptide synthesis and chemical conjugation to the nanoparticles was required to obtain the final constructs. In our case, a simple cost-effective genetic engineering approach was used to link the α-MSH peptide (SYSMEHFRWGKPV) to the N-terminus of the HFt subunit, resulting in production of an HFt assembly containing 24 peptide copies. This HFt nanocage should, in principle, have increased affinity for the corresponding receptor compared with a molecule containing a single peptide unit (ie, the multivalence effect).

Each α-MSH peptide was spatially separated from the HFt subunit N-terminus by an inert and flexible Gly/Ser-containing sequence linker. The length of the linker was designed based on analysis of the crystal structure of human HFt (PDB ID: 3AJO) and modeling of PEG molecules of

the chosen length to guarantee sufficient exposure of the targeting α-MSH peptide on the HFt external surface in the presence of PEG.

The yields of purified recombinant HFt-MSH and wild-type HFt from *E. coli* cultivation were in the ranges of 150–200 mg/L and 80–100 mg/L, respectively. The purification procedures used for HFt-MSH were much easier and faster with respect to HFt, and allowed us to obtain large amounts of pure and fully assembled protein within two days. The integrity of the HFt-MSH N-termini after protein purification and PEGylation was checked by MALDI mass spectrometry, which confirmed that the full-length amino acid sequence corresponding to the α-MSH peptide plus linker was present at the protein N-termini (Supplementary Figure S1). The mass spectra also highlighted the presence of PEG molecules linked to the cysteine residues of the protein (Supplementary Figure S2). Effective protein PEGylation was also monitored by Fourier transform infrared spectroscopy. Typical PEG signals relative to the (CH2–O–CH2) moiety and to the methylene stretching modes were detected only in the PEGylated HFt-MSH-PEG sample (see Supplementary Figure S3). In turn, amide bands at 1952 cm^{-1}, typical of alpha helical structures, were almost super imposable on the native and PEGylated proteins.

After incorporation of magnetite/maghemite, the HFt-MSH was analyzed by transmission electron microscopy, which showed that the HFt-MSH construct retained the ability of wild-type HFt to encapsulate magnetic iron and adopted the expected spherical cage-like structures with an external diameter of 13 ± 2.1 nm, typical of wild-type HFt (Supplementary Figure S4). As expected, the shape of the PEGylated HFt constructs did not appear to be perfectly spherical due to the flexibility of the PEG molecules present on the protein surface (Figure 1).

The magnetic properties of the HFt-MSH construct, evaluated by zero-field-cooled and field-cooled magnetization experiments (data not shown), were very similar to those previously reported for magnetite/maghemite nanoparticles

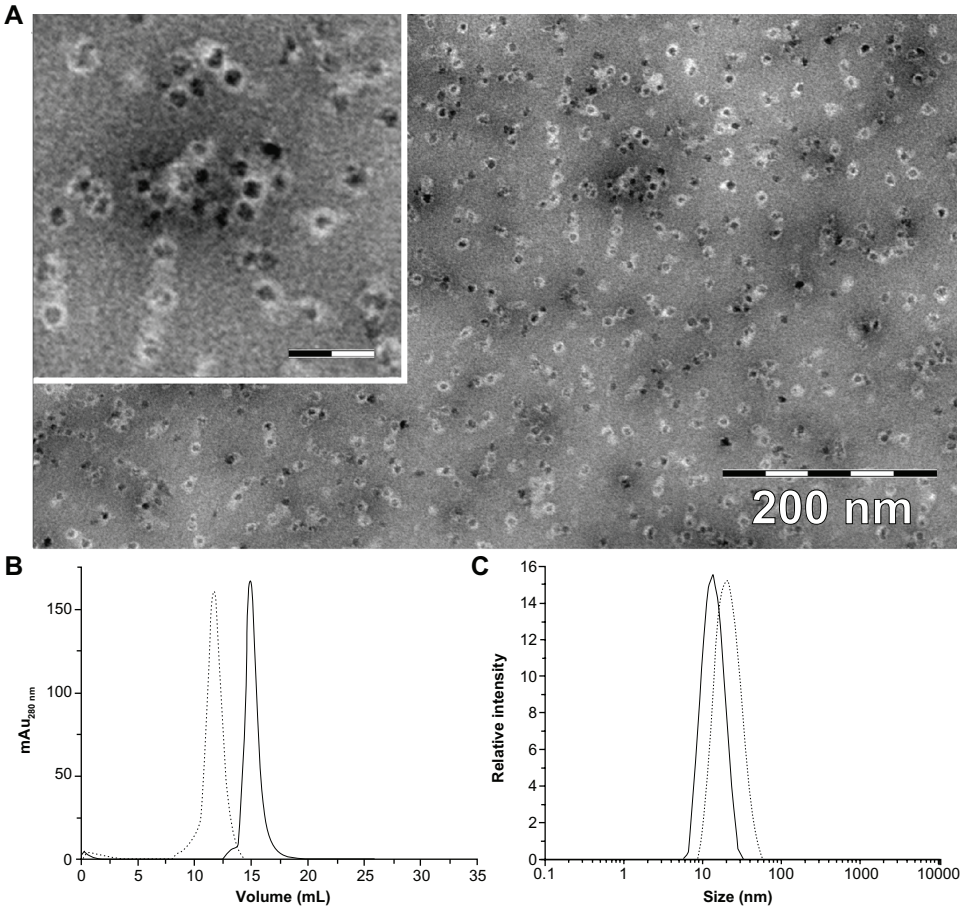

Figure 1 (**A**) Transmission electron microscopic image of magnetite/maghemite-containing HFt-MSH-PEG showing the metallic core (black) surrounded by the HFt shell (white). Inset: 2.5× magnified image, the scale bar represents 32 nm. (**B**) Size-exclusion chromatography and (**C**) dynamic light scattering profiles of HFt-MSH before (solid line) and after (dotted lines) the PEGylation reaction.

Abbreviations: HFt, human protein ferritin; PEG, polyethylene glycol; MSH, melanocyte-stimulating hormone peptide.

enclosed in different ferritin cages.[37] The HFt-MSH sample had a loading factor of 3900 metal atoms per protein molecule, as assessed by inductively coupled plasma analysis. This number is close to the maximum loading capacity of the protein, which is around 4000 atoms, and is relevant in view of the potential uses of HFt-based nanoparticles as magnetic resonance imaging agents, which require a high enough amount of iron atoms to provide a detectable signal.

Size exclusion chromatography and dynamic light scattering was performed to estimate the diameter and polydispersity of the PEGylated (HFt-PEG and HFt-MSH-PEG) samples. All samples were found to be quite monodispersed in solution (Figure 1B and C, and Supplementary Figure S5). Both experiments indicate that non-PEGylated and PEGylated samples have a significant difference in size (mean diameters 13.0 and 20.0 nm, respectively), implying elevated efficiency of the PEGylation reaction.

The aforementioned results indicate that, even after the addition of more than 30 amino acids to the N-terminal region of each protein subunit, HFt maintained the characteristic 24-mer cage architecture, the ability to incorporate iron derivatives, the ability to undergo pH-induced dissociation and reassembly (Supplementary Figure S6), and high thermal stability. Indeed, HFt-MSH showed even higher thermal stability than wild-type HFt in circular dichroism experiments (Supplementary Figure S7).

The PEGylated derivatives, HFt-PEG and HFt-MSH-PEG, were labeled with NHS–rhodamine, an amine-reactive fluorescent reagent that absorbs green visible light (552 nm) and emits orange-red visible light (575 nm). This permitted us to trace the localization of our constructs on the surface of and inside the target cells (see below). Rhodamine-labeled HFt nanoparticles were purified from free dye by dialysis and centrifugal filter devices. The number of dye molecules linked per protein was determined to be about 0.9/subunits (22.0/protein cage) for both HFt-PEG and HFt-MSH-PEG by absorbance spectroscopy (see Materials and methods section).

To investigate the targeting efficacy of the HFt-MSH-PEG constructs and to verify whether we succeeded in reducing their nonspecific binding to cancer cells, we compared their ability to target B16F10 melanoma cells versus a different type of cancer cells.

Cells incubated at different times with either 10 nM rhodamine-labeled wild-type HFt, HFt-PEG, or HFt-MSH-PEG were imaged using confocal microscopy. In agreement with previous findings,[25,36] wild-type human HFt bound both melanoma cells and human HT29 colon carcinoma cells, as shown by the presence of a number of red particle clusters on the cell surface (Supplementary Figures S8 and S9), indicating that it was recognized nonspecifically by different cell types. Conversely, none or very few of these clusters were observed in the case of HFt-PEG (Figure 2B), indicating that derivatization with PEG molecules effectively shields the HFt molecule from its receptors on melanoma cells. Remarkably, in the presence of HFt-MSH-PEG, large numbers of clusters of small red particles were easily detected on both the surface and in the cytoplasm of melanoma cells (Figure 2A) whereas none or very few fluorescent clusters were present inside or on the surface of HT29 cells (Figure 2C). The relative percentages of cancer cells positive to binding/internalization of HFt-MSH-PEG or HFt-PEG were evaluated in three randomly evaluated fields per sample at 20× magnification, and the average values are reported in Figure 2D. Four samples were examined for each type of construct and cells.

These results indicate that the α-MSH targeting moiety effectively overcomes PEG masking and allows the HFt-MSH-PEG constructs to recognize their target melanocortin receptors on melanoma cells specifically and that PEG molecules of the chosen length provide the HFt-MSH-PEG constructs with an effective shield against recognition by other cell types. It is important to point out that the HFt-MSH-PEG derivatives were also able to be internalized by the target melanoma cells, which is a necessary property for potential therapeutic application. In contrast, in the lone previous report on HFt derivatives bearing an RGD peptide as a targeting moiety, evidence of construct internalization was not provided.[26] Given that internalization is likely to be mediated by interaction of the exposed α-MSH ligand with its cognate melanocortin receptor, the choice of tumor selector appears to be an essential factor to take into account in the rational design of nanoparticles for targeted delivery.

Finally, we performed a series of in vivo experiments using melanoma-bearing mice. Twenty-four hours after intracardiac injection, confocal microscopy performed on freshly harvested skin flaps, including tumor tissue, demonstrated marked accumulation of HFt-MSH-PEG constructs inside the melanoma tissue in all the skin layers examined, ie, epidermal, dermal, subdermal, and subcutaneous (Figure 3 and Supplementary Figure S10). Only an occasional weak signal from a few cells in the dermal/subcutaneous layers was observed, most likely from phagocytes. In contrast, wild-type HFt did not accumulate at tumor sites (Figure 3). As expected, some accumulation of HFt-MSH-PEG constructs was found also in Kupffer cells in the liver, but not

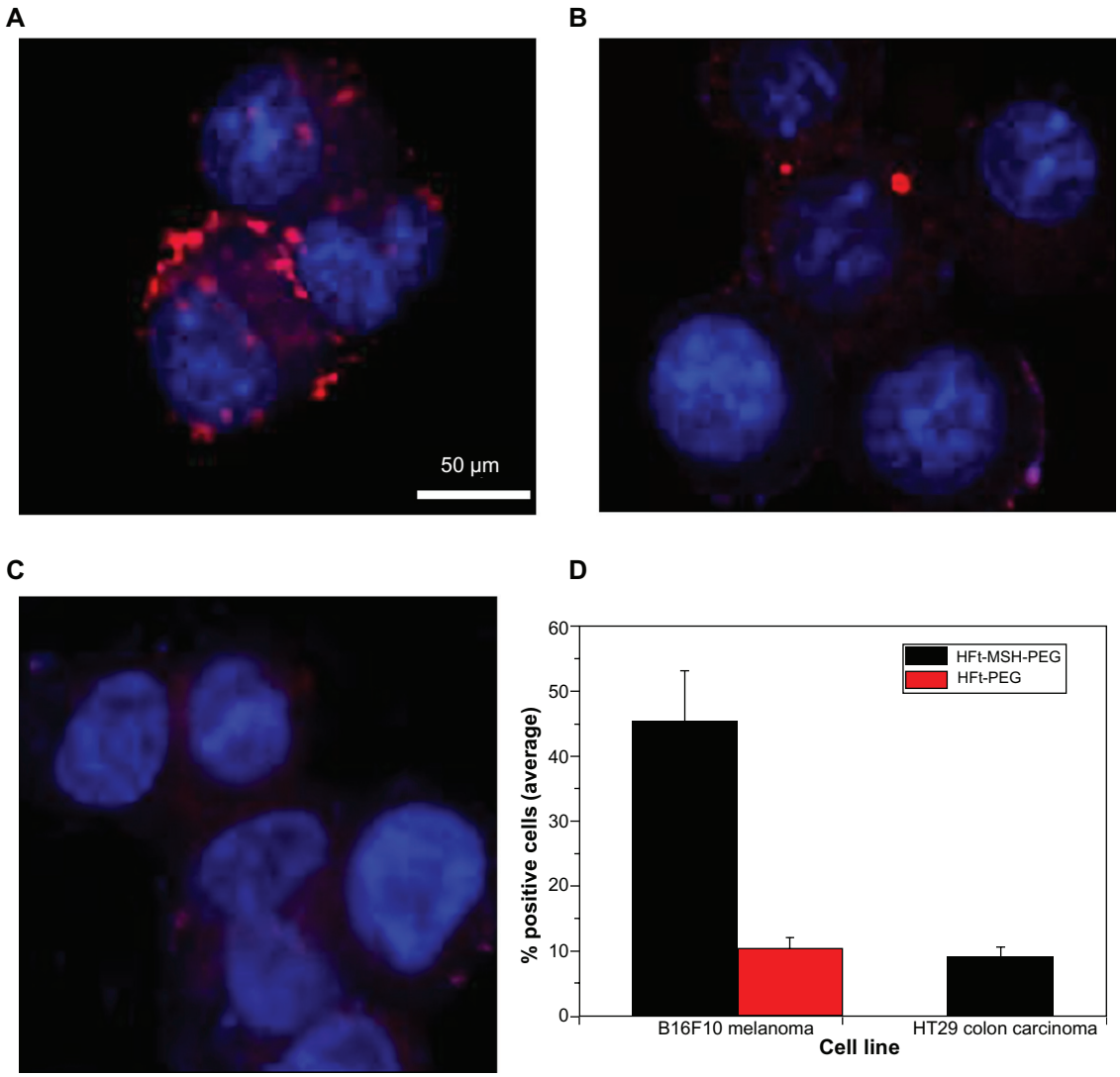

Figure 2 Laser-scanning confocal microscopy of mouse B16F10 melanoma (**A** and **B**) and human HT29 colon carcinoma (**C**) cells after one hour of incubation with HFt-MSH-PEG (**A** and **C**) or HFt-PEG (**B**) nanoparticles. Both types of nanoparticles were rhodamine-labeled. Clusters of HFt-based nanoparticles with rhodamine fluorescence appear in red. Original magnification 40×. Scale bar corresponds to all images. (**D**) Cell binding/internalization percentages assessed from the in vitro results. Average of positive cells in three randomly evaluated fields per sample at 20× magnification (four samples for each type of treatment and cells).
Abbreviations: HFt, human protein ferritin; PEG, polyethylene glycol; MSH, melanocyte-stimulating hormone peptide.

in hepatocytes. This result indicates that the HFt-MSH-PEG constructs have significantly higher target selectivity with respect to the previously reported HFt construct bearing an RGD peptide as the targeting moiety, accumulation of which was far greater in the liver than in the target glioma tumor.[24] To our knowledge, this is the only HFt-based construct that has been previously studied in vivo.

We then investigated the in vitro plasma stability and in vivo circulation time of the HFt-based nanoparticles. For the plasma stability test, a size exclusion chromatography experiment using a GE Healthcare FPLC system Unicorn Akta purifier was undertaken to monitor the presence of intact nanoparticles after incubation in mouse plasma. The data reported in Table S1 demonstrate that both wild-type HFt and HFt-MSH-PEG nanoparticles have very high in vitro plasma stability, because they undergo very little degradation over 48 hours of incubation in mouse plasma (about 92% and 98% of intact protein, respectively). Clearance of HFt and HFt-MSH-PEG nanoparticles from the blood was investigated in vivo using Western blot analysis in healthy mice. HFt-MSH-PEG nanoparticles showed a significantly higher concentration and longer residence time in blood compared with wild-type HFt nanoparticles (Figure 4). In particular, HFt was absent after one hour, in accordance with previously reported data indicating clearance of HFt from the circulation in the 10–60 minutes following injection.[28] In contrast,

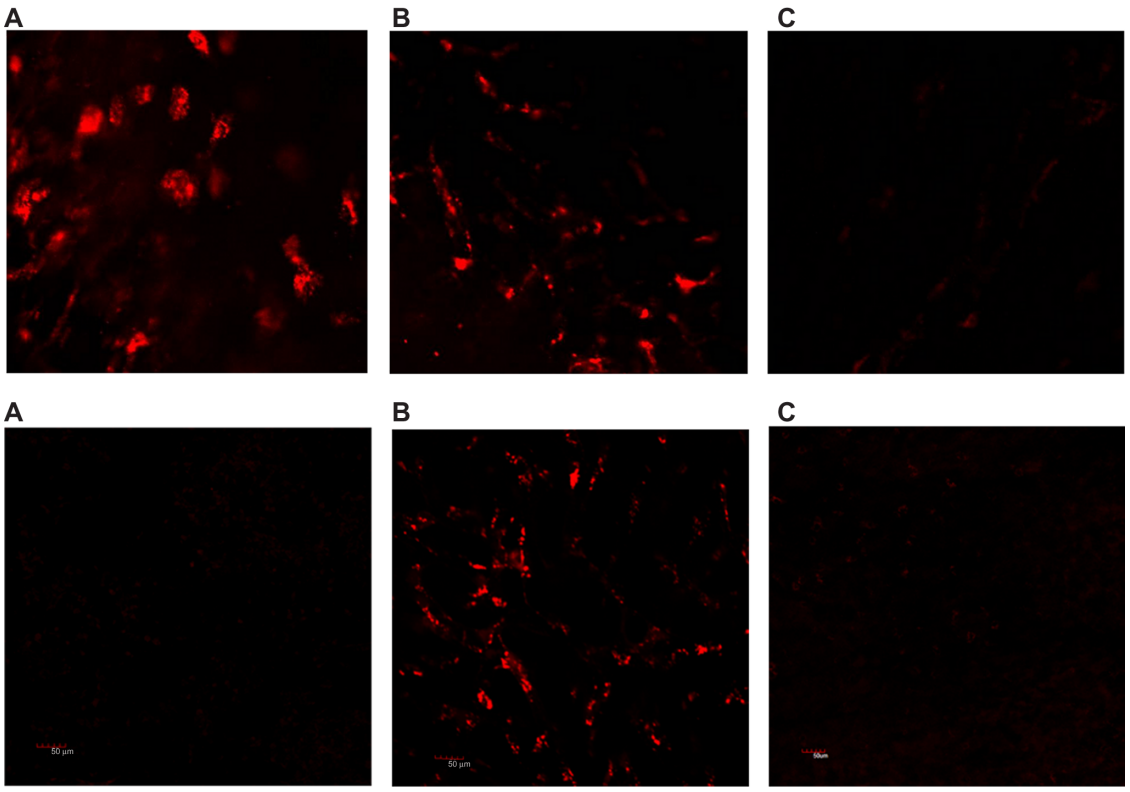

Figure 3 Laser scanning confocal microscopy on the freshly removed tumor (**A**), liver (**B**), and skin (**C**) 24 hours after intracardiac administration of rhodamine-labeled HFt-MSH-PEG (top) and wild-type HFt (bottom) nanoparticles. Melanoma B16F10 developed in mouse C57BL/6 with a 6 mm diameter. Original magnification 20×.
Abbreviations: HFt, human protein ferritin; PEG, polyethylene glycol; MSH, melanocyte-stimulating hormone peptide.

HFt-MSH-PEG showed significantly greater persistence in the circulation, being clearly visible for up to 6 hours and still detectable at 24 hours. Such differential blood kinetics are likely to contribute to the different biodistribution patterns observed for wild-type HFt and HFt-MSH-PEG.

In addition, very preliminary in vivo tests were performed to investigate the effect of HFt nanoparticles on immune cells. No significant changes in the percentages of immune cells present at 23–24 hours after in vivo administration of the nanoparticles in the murine model were observed. However, we found increased expression of the early activation marker, CD69, on all the leukocyte populations investigated (see Supplementary Figure S11). Activation by both HFt nanoparticles resulted to be generally higher in the spleen than in the blood, especially in the granulogate cells. Interestingly, activation of all groups of cells following administration of wild-type HFt was stronger than that induced by HFt-PEG-MSH nanoparticles. Although very preliminary, our results suggest that HFt nanoparticles exert some direct functional effects on leukocytes, possibly due to activation of phagocytosis, and that PEGylated HFt-MSH-PEG constructs have a weaker primary immunological stimulatory effect than wild-type HFt, supporting the hypothesis that PEG molecules are an effective shield for the HFt protein. However, it is worth bearing in mind that while α-MSH is completely conserved in humans and mice, murine HFt is not identical to the human homolog. Therefore, nanoparticles containing human HFt are expected to be more immunogenic in the mouse than in humans.

The high target selectivity, plasma stability, and a long circulation time observed for the HFt-MSH-PEG nanoparticles developed in this experiment indicate that these constructs can be exploited to develop HFt derivatives for application in the diagnosis and/or treatment of melanoma. For example, the HFt-MSH-PEG nanoparticles could be further engineered by chemically conjugating reactive groups on the external surface using temozolomide or dacarbazine by means of reversible cross-linkers, the bonding of which with the drug would be expected to be broken in the cytoplasm. Additionally, the internal cavity of HFt could be loaded with cisplatin, which has been shown to have cytotoxic activity when incorporated within commercial horse apoferritin,[25] or ^{64}Cu, which may be used for detection by PET.[24] HFt-based constructs bearing these functionalities are currently being developed in our laboratory.

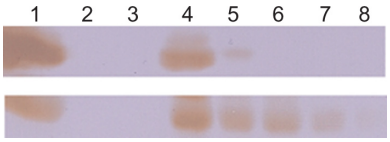

Figure 4 In vivo circulation time of HFt-based nanoparticles. HFt nanoparticles have been quantified by Western blot using an anti-MSH (bottom) and anti-HFt (top) antibody (see Materials and methods section). Lane 1, reference proteins HFt-MSH-PEG (bottom) and HFt (top), 1 mg/mL; lane 2, empty; lane 3, plasma before HFt-nanoparticle injection; lanes 4–8, plasma at 3 minutes and 1, 3, 6, and 24 hours following intracardiac injection.
Abbreviations: HFt, human protein ferritin; PEG, polyethylene glycol; MSH, melanocyte-stimulating hormone peptide.

Further, the rational design of HFt-based nanoparticles as reported here is amenable to exploitation for selective delivery to a large number of different cell types, provided that a suitable targeting moiety is available. Targeting moieties that can be loaded onto the HFt nanoplatform include not only peptides, which can be genetically linked to the protein, but also molecules endowed with reactive groups, which can be conjugated with reactive amino and/or carboxylate groups exposed on the HFt surface.

To evaluate the actual potential of targeted HFt-PEG constructs for clinical application and to assess whether PEGylation affects the main routes of ferritin protein excretion in the body (ie, the kidney and/or liver),[33] further in vivo studies, including biodistribution in other relevant tissues, body clearance, toxicity, immunological effects, and the immunogenicity of our constructs will be performed.

Conclusion

In this work, we developed a rationally designed, genetically engineered, and chemically modified HFt-based multifunctional nanoplatform (HFt-MSH-PEG). These constructs were extensively characterized by taking advantage of an array of physicochemical techniques, and their targeting selectivity and plasma stability were assessed by in vitro and in vivo experiments, HFt-MSH-PEG were recognized and internalized specifically by melanoma cells, but not by other human tumor cells or mouse tissues (except for expected uptake by dedicated phagocytes), and were present for up to 24 hours in the bloodstream. The high target specificity of HFt-MSH-PEG is determined by the following: choice of a selective targeting moiety, namely the α-MSH peptide, sufficiently exposed on the protein surface because of the presence of a peptide linker which binds receptors expressed only by melanoma cells and to a lesser extent by melanocytes; controlled modification of the HFt protein surface with PEG molecules of appropriate length, which mask the whole construct, except for the targeting α-MSH peptide, from its physiological receptors; and significant reduction in nonspecific recognition and reduced uptake by the reticuloendothelial and mononuclear phagocytic systems.

The targeting strategy adopted in this work to produce HFt-MSH-PEG constructs can be implemented to develop HFt-based PEGylated nanoparticles containing targeted molecules for different cells and tissues. Further modification with cytotoxic and/or imaging agents would be required to produce molecules amenable to theragnostic applications. Selective nanoparticle accumulation at the sites of disease, as observed in this work, would allow tumors to be visible in the earlier stages, enabling improved diagnostic possibilities, and contribute to reduction of toxic side effects in normal tissue, thereby increasing the efficacy of chemotherapy. Indeed, we expect that the HFt functionalization strategy presented here will help overcome many of the current difficulties in the use of ferritin-based assemblies for in vivo applications and advance towards the development of protein-based nanoplatforms for effective diagnostic and therapeutic applications.

Acknowledgments

PC thanks the Associazione Italiana per la Ricerca sul Cancro, Milan, for funding under grant agreement MFAG10545 and the Italian Ministry of Economy and Finance for funding the Project "FaReBio di Qualità". LV acknowledges Fondazione Anna Villa e Felice Rusconi, Varese, for funding and IRC MBU AV0Z50200510. The authors thank Giovanni Luca Scaglione at the Università Cattolica del Sacro Cuore of Rome for the dynamic light scattering experiments and Zaneta Ruzickova at the Institute of Microbiology VVI, Academy of Sciences of the Czech Republic, in Prague (CZ) for technical assistance in confocal microscopy.

Disclosure

The authors report no conflicts of interest in this work.

References

1. Poon Z, Chang D, Zhao X, Hammond PT. Layer-by-layer nanoparticles with a pH-sheddable layer for in vivo targeting of tumor hypoxia. *ACS Nano*. 2011;5(6):4284–4292.
2. Kateb B, Chiu K, Black KL, et al. Nanoplatforms for constructing new approaches to cancer treatment, imaging, and drug delivery: what should be the policy? *Neuroimage*. 2011;54 Suppl 1:S106–S124.
3. Nie S. Understanding and overcoming major barriers in cancer nanomedicine. *Nanomedicine*. 2010;5(4):523–528.
4. Armstead AL, Li B. Nanomedicine as an emerging approach against intracellular pathogens. *Int J Nanomedicine*. 2011;6(1):3281–3293.
5. Tzeng SY, Yang PH, Grayson WL, Green JJ. Synthetic poly(ester amine) and poly(amido amine) nanoparticles for efficient DNA and siRNA delivery to human endothelial cells. *Int J Nanomedicine*. 2011;6(1):3309–3322.
6. Bode SA, Minten IJ, Nolte RJ, Cornelissen JJ. Reactions inside nanoscale protein cages. *Nanoscale*. 2011;3(6):2376–2389.

7. Heddle JG. Protein cages, rings and tubes: useful components of future nanodevices? *Nanotechnol Sci Appl*. 2008;1:67–78.
8. Chiancone E, Ceci P, Ilari A, Ribacchi F, Stefanini S. Iron and proteins for iron storage and detoxification. *Biometals*. 2004;17(3):197–202.
9. Watt RK. The many faces of the octahedral ferritin protein. *Biometals*. 2011;24(3):489–500.
10. Niemeyer CM, Ceyhan B. DNA-directed functionalization of colloidal gold with proteins. *Angew Chem Int Ed Engl*. 2001;40(19):3685–3688.
11. Uchida M, Kang S, Reichhardt C, Harlen K, Douglas T. The ferritin superfamily: supramolecular templates for materials synthesis. *Biochim Biophys Acta*. 2010;1800(8):834–845.
12. Dominguez-Vera JM, Fernandez B, Galvez N. Native and synthetic ferritins for nanobiomedical applications: recent advances and new perspectives. *Future Med Chem*. 2010;2(4):609–618.
13. Kasyutich O, Ilari A, Fiorillo A, Tatchev D, Hoell A, Ceci P. Silver ion incorporation and nanoparticle formation inside the cavity of Pyrococcus furiosus ferritin: structural and size-distribution analyses. *J Am Chem Soc*. 2010;132(10):3621–3627.
14. Li M, Viravaidya C, Mann S. Polymer-mediated synthesis of ferritin-encapsulated inorganic nanoparticles. *Small*. 2007;3(9):1477–1481.
15. Ueno T, Suzuki M, Goto T, Matsumoto T, Nagayama K, Watanabe Y. Size-selective olefin hydrogenation by a Pd nanocluster provided in an apo-ferritin cage. *Angew Chem Int Ed Engl*. 2004;43(19):2527–2530.
16. Yoshimura H. Protein-assisted nanoparticle synthesis. *Colloids Surf A*. 2006;282–283(0):464–470.
17. Yamashita I. Biosupramolecules for nano-devices: biomineralization of nanoparticles and their applications. *J Mater Chem*. 2008;18(32):3813–3820.
18. Kostiainen MA, Ceci P, Fornara M, et al. Hierarchical self-assembly and optical disassembly for controlled switching of magnetoferritin nanoparticle magnetism. *ACS Nano*. 2011;5(8):6394–6402.
19. Bakoush O, Tencer J, Tapia J, Rippe B, Torffvit O. Higher urinary IgM excretion in type 2 diabetic nephropathy compared to type 1 diabetic nephropathy. *Kidney Int*. 2002;61(1):203–208.
20. Jain RK. Delivery of molecular and cellular medicine to solid tumors. *Adv Drug Deliv Rev*. 2001;46(1–3):149–168.
21. Uchida M, Willits DA, Muller K, et al. Intracellular distribution of macrophage targeting ferritin-iron oxide nanocomposite. *Adv Mater*. 2009;21(4):458–462.
22. Valero E, Tambalo S, Marzola P, et al. Magnetic nanoparticle-templated assembly of protein subunits: a new platform for carbohydrate-based MRI nanoprobes. *J Am Chem Soc*. 2011;133(13):4889–4895.
23. Geninatti CS, Crich S, Bussolati B, et al. Magnetic resonance visualization of tumor angiogenesis by targeting neural cell adhesion molecules with the highly sensitive gadolinium-loaded apoferritin probe. *Cancer Res*. 2006;66(18):9196–9201.
24. Lin X, Xie J, Niu G, et al. Chimeric ferritin nanocages for multiple function loading and multimodal imaging. *Nano Lett*. 2011;11(2):814–819.
25. Xing R, Wang X, Zhang C, et al. Characterization and cellular uptake of platinum anticancer drugs encapsulated in apoferritin. *J Inorg Biochem*. 2009;103(7):1039–1044.
26. Uchida M, Flenniken ML, Allen M, et al. Targeting of cancer cells with ferrimagnetic ferritin cage nanoparticles. *J Am Chem Soc*. 2006;128(51):16626–16633.
27. Barreto JA, O'Malley W, Kubeil M, Graham B, Stephan H, Spiccia L. Nanomaterials: applications in cancer imaging and therapy. *Adv Mater*. 2011;23(12):H18–H40.
28. Worwood M, Cragg SJ, Williams AM, Wagstaff M, Jacobs A. The clearance of 131I-human plasma ferritin in man. *Blood*. 1982;60(4):827–833.
29. Chen TT, Li L, Chung DH, et al. TIM-2 is expressed on B cells and in liver and kidney and is a receptor for H-ferritin endocytosis. *J Exp Med*. 2005;202(7):955–965.
30. Uchida M, Terashima M, Cunningham CH, et al. A human ferritin iron oxide nano-composite magnetic resonance contrast agent. *Magn Reson Med*. 2008;60(5):1073–1081.
31. Mack U, Storey EL, Powell LW, Halliday JW. Characterization of the binding of ferritin to the rat liver ferritin receptor. *Biochim Biophys Acta*. 1985;843(3):164–170.
32. Fisher J, Devraj K, Ingram J, et al. Ferritin: a novel mechanism for delivery of iron to the brain and other organs. *Am J Physiol Cell Physiol*. 2007;293(2):C641–C649.
33. Anderson JG, Ramm GA, Halliday WJ, Powell WL. Ferritin metabolism in hemochromatosis. In: Barton JC, Edwards CQ, editors. *Hemochromatosis: Genetics, Pathophysiology, Diagnosis and Treatment*. Cambridge, UK: Cambridge University Press; 2000.
34. Fittipaldi M, Innocenti C, Ceci P, et al. Looking for quantum effects in magnetic nanoparticles using the molecular nanomagnet approach. *Physical Review B*. 2011;83(10):104409.
35. Benada O, Pokorny V. Modification of the Polaron sputter-coater unit for glow-discharge activation of carbon support films. *J Electron Microsc Tech*. 1990;16(3):235–239.
36. Berman HM, Westbrook J, Feng Z, et al. The protein data bank. *Nucleic Acids Res*. 2000;28(1):235–242.
37. Ballou B, Lagerholm BC, Ernst LA, Bruchez MP, Waggoner AS. Noninvasive imaging of quantum dots in mice. *Bioconjug Chem*. 2004;15(1):79–86.
38. Raha S, Paunesku T, Woloschak G. Peptide-mediated cancer targeting of nanoconjugates. *Wiley Interdiscip Rev Nanomed Nanobiotechnol*. 2011;3(3):269–281.
39. Miao Y, Whitener D, Feng W, Owen NK, Chen J, Quinn TP. Evaluation of the human melanoma targeting properties of radiolabeled alpha-melanocyte stimulating hormone peptide analogues. *Bioconjug Chem*. 2003;14(6):1177–1184.
40. Tatro JB, Atkins M, Mier JW, et al. Melanotropin receptors demonstrated in situ in human melanoma. *J Clin Invest*. 1990;85(6):1825–1832.
41. Miao Y, Quinn TP. Peptide-targeted radionuclide therapy for melanoma. *Crit Rev Oncol Hematol*. 2008;67(3):213–228.
42. Balch CM, Soong SJ, Gershenwald JE, et al. Prognostic factors analysis of 17,600 melanoma patients: validation of the American Joint Committee on Cancer melanoma staging system. *J Clin Oncol*. 2001;19(16):3622–3634.
43. Lu W, Xiong C, Zhang G, et al. Targeted photothermal ablation of murine melanomas with melanocyte-stimulating hormone analog-conjugated hollow gold nanospheres. *Clin Cancer Res*. 2009;15(3):876–886.

Supplementary figures

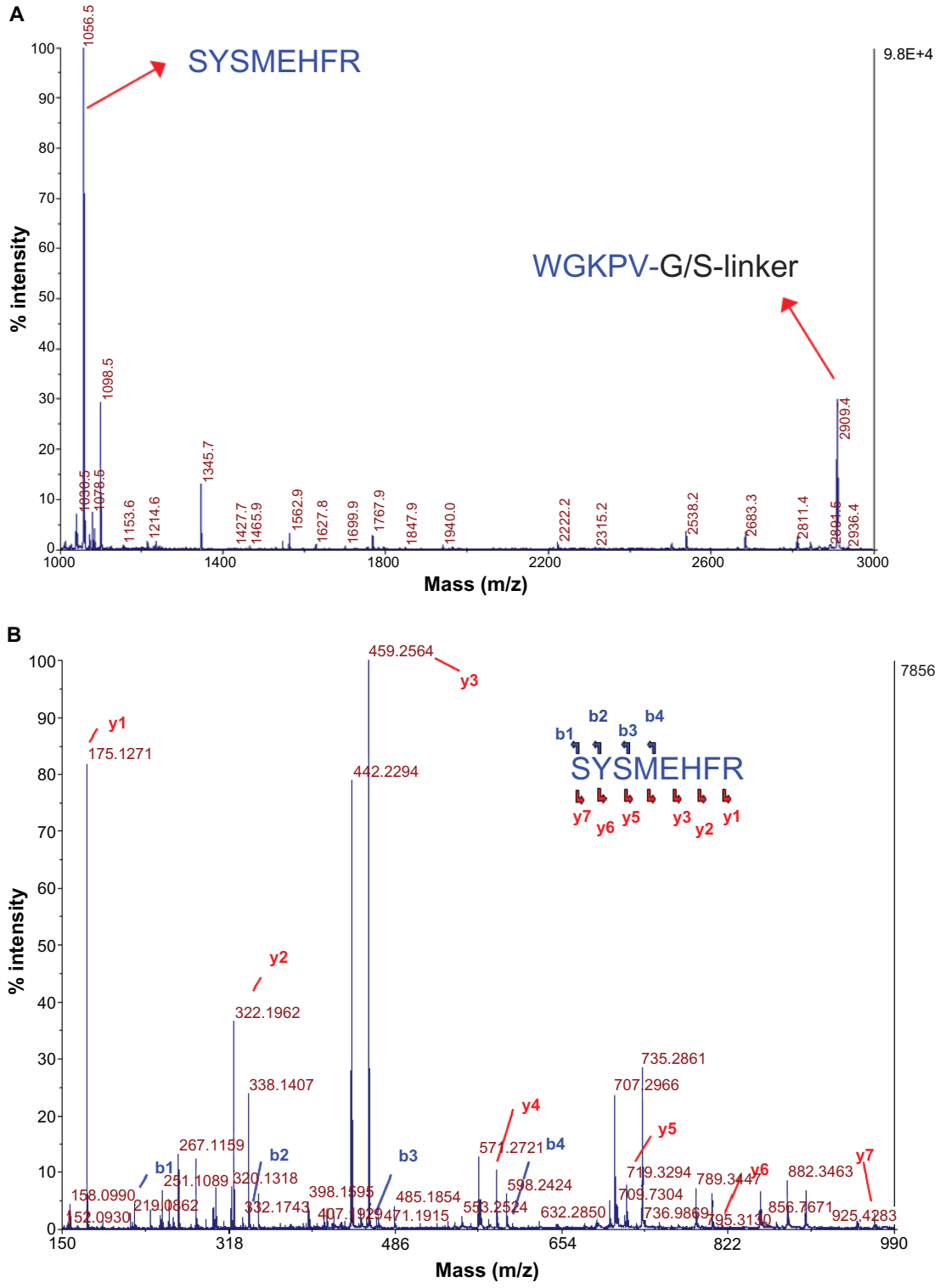

Figure S1 (A) MALDI-MS spectrum of the native HFt-MSH-PEG trypsin digests. Peaks corresponding to the MSH and linker amino acid sequences at the protein N-termini are indicated with red arrows. (**B**) MALDI-MS/MS spectrum of the m/z 1056.5 peak reported in (**A**).

Notes: The fragmentation sites along the peptide (SYSMEHFR) backbone corresponding to the observed peaks are indicated by arrows, and the arrow direction indicates the charge-retaining portion. Peaks corresponding to the expected masses for the y and b ions are indicated by the relative ion name.

Abbreviations: HFt, human protein ferritin; PEG, polyethylene glycol; MSH, melanocyte-stimulating hormone peptide; MALDI, matrix-assisted laser desorption ionization; MS, mass spectrometry.

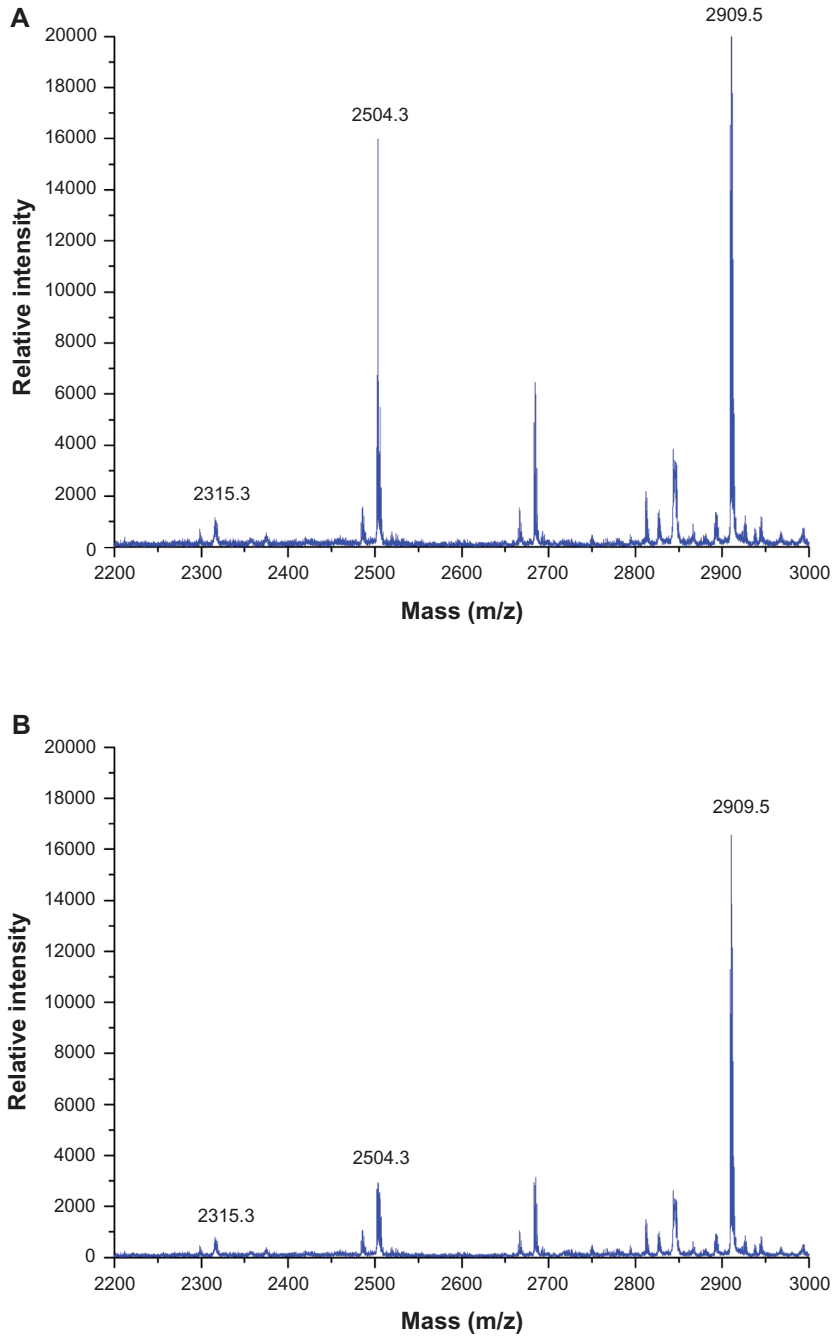

Figure S2 MALDI-MS spectrum (range 2200–3000 m/z) of the native HFt-MSH (**A**) and HFt-MSH-PEG (**B**) trypsin digests.
Notes: Peaks matching to the protein sequences are reported. The m/z 2504.3 peak corresponds to the KPDCDDWESGLNAMECALHLEK sequence and it is expected to react with and bind to PEG-maleimide molecules due to the presence of two cysteine residues. From mass analysis, a decrease of the peak corresponding to this peptide was observed, but a heavier peak at about 12,000–13,000 m/z did not appear, likely because of poor flying ability due to the conjugation with PEG molecules.
Abbreviations: HFt, human protein ferritin; PEG, polyethylene glycol; MSH, melanocyte-stimulating hormone peptide; MALDI, matrix-assisted laser desorption ionization; MS, mass spectrometry.

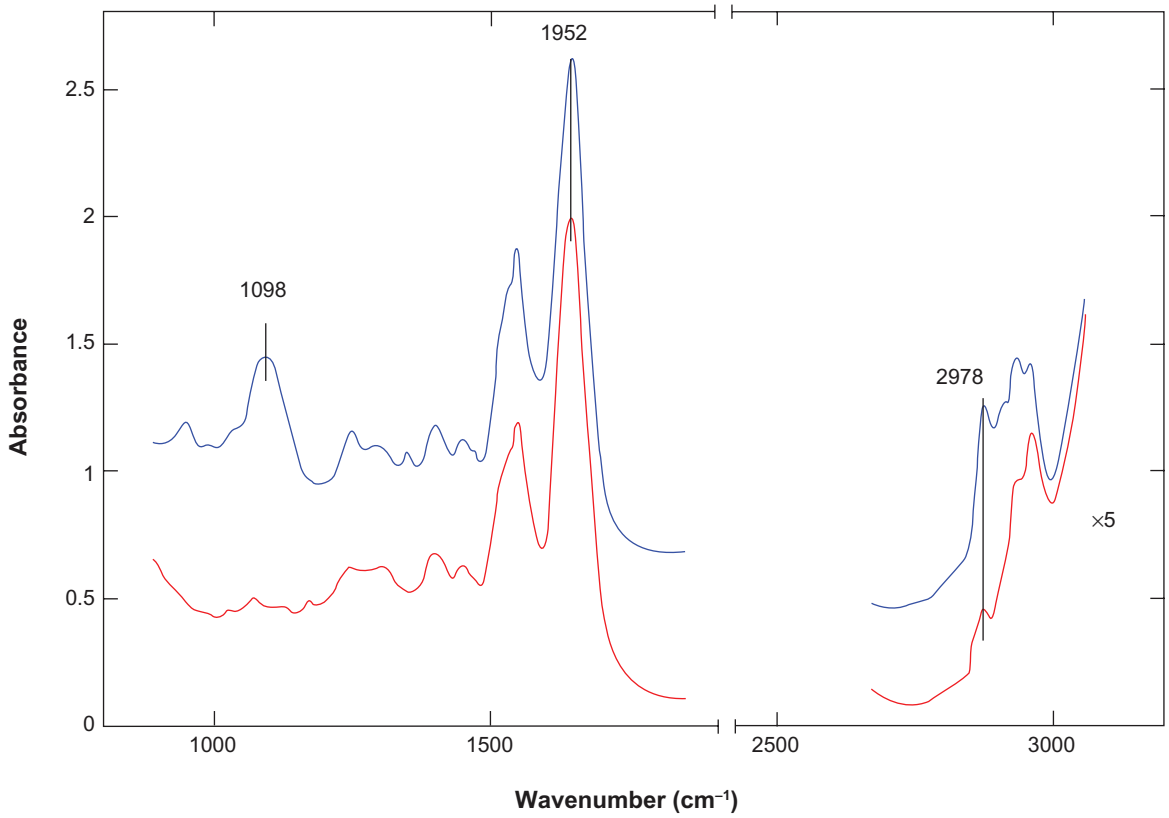

Figure S3 Attenuated total reflectance-Fourier transform infrared spectra of apo-HFt-MSH (red) and PEGylated apo-HFt-MSH-PEG (blue).
Notes: The spectra have been obtained on fully hydrated samples in attenuated total reflectance mode on a ZnSe plates at 4 cm^{-1} resolution and 25°C. Spectra were subtracted by the contribution of the clean and empty attenuated total reflectance plates. Details of the low frequency region highlight the presence of the PEG (CH_2–O–CH_2) stretching modes at 1098 cm^{-1} (top spectrum) in the PEGylated apo HFt-MSH. The contribution of the PEG (H–C–H) stretching modes is also manifest in the increased absorbance at 2978 cm^{-1} in the PEGylated protein (top spectrum).
Abbreviations: HFt, human protein ferritin; PEG, polyethylene glycol; MSH, melanocyte-stimulating hormone peptide; MALDI, matrix-assisted laser desorption ionization.

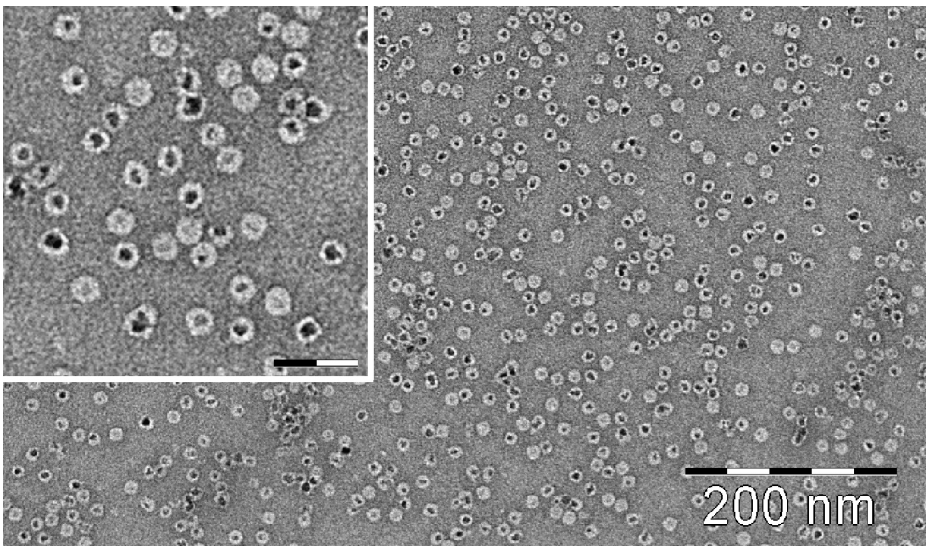

Figure S4 TEM image of magnetite/maghemite-containing HFt-MSH showing the metallic core (black) surrounded by the HFt shell (white). Inset: 2.5× magnified image, scale bar 32 nm.
Abbreviations: HFt, human protein ferritin; MSH, melanocyte-stimulating hormone peptide.

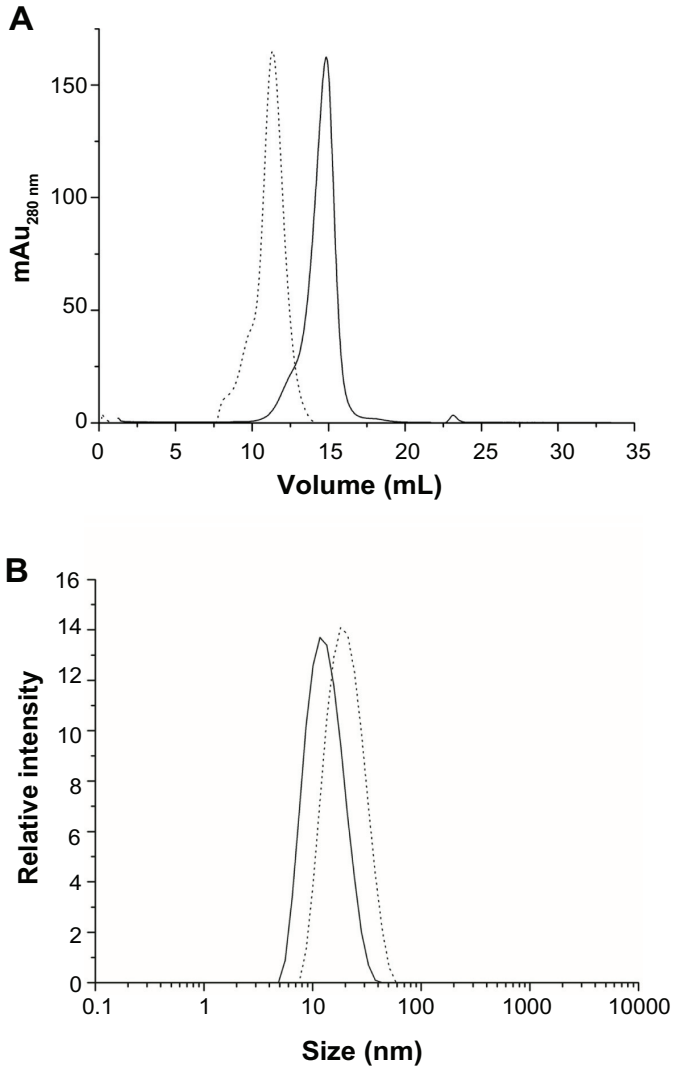

Figure S5 (**A**) Size exclusion chromatography and (**B**) dynamic light scattering profiles of HFt before (solid line) and after (dotted lines) the PEGylation reaction.
Abbreviations: HFt, human protein ferritin; PEG, polyethylene glycol.

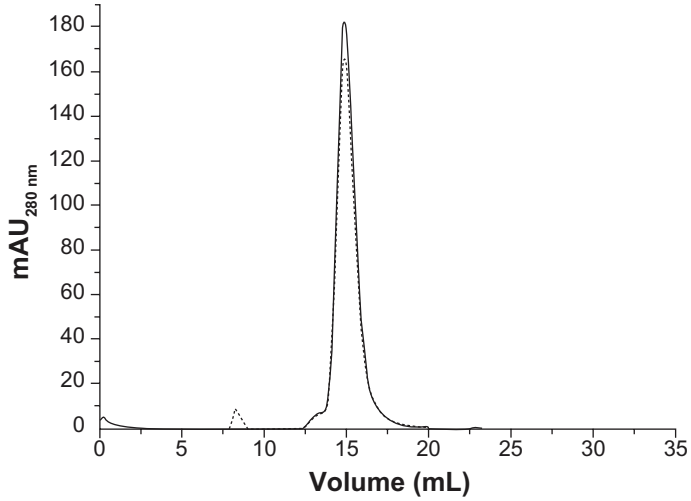

Figure S6 Size exclusion chromatography profiles of HFt-MSH before (solid line) and after (dotted lines) the pH jump experiment (see Material and methods section).
Abbreviations: HFt, human protein ferritin; MSH, melanocyte-stimulating hormone peptide.

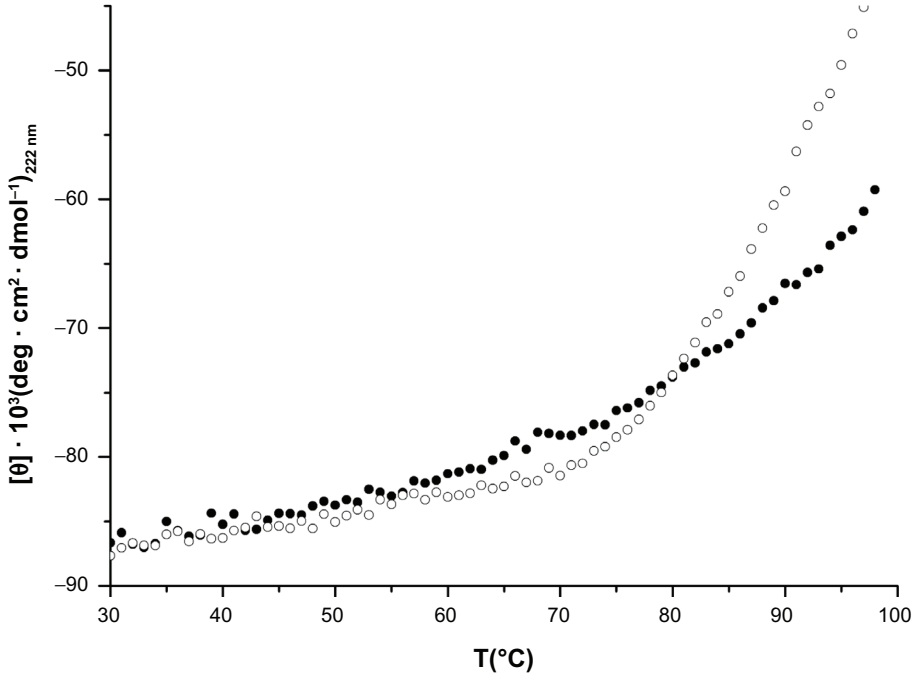

Figure S7 Thermal denaturation of HFt (open circle) and HFt-MSH (black circle).
Notes: Spectra were recorded at 222 nm in 0.1 quartz cuvettes. Protein concentration was 1 mg/mL in H_2O_{dd}.
Abbreviations: HFt, human protein ferritin; MSH, melanocyte-stimulating hormone peptide.

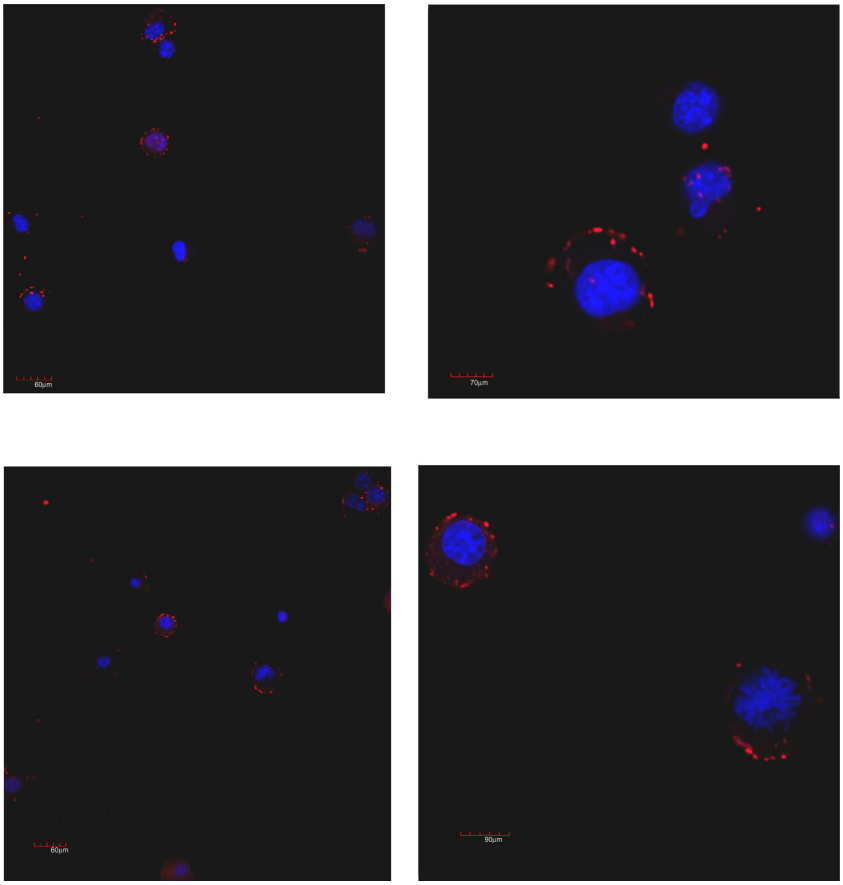

Figure S8 Laser-scanning confocal microscopy of mouse B16F10 melanoma cells after 10 (top) and 60 (down) minutes of incubation with HFt rhodamine-labeling.
Notes: Clusters of HFt-based nanoparticles with rhodamine fluorescence appear in red. Original magnification 40× (left) and zoom 3× (120×, right) were used.
Abbreviations: HFt, human protein ferritin; MSH, melanocyte-stimulating hormone peptide.

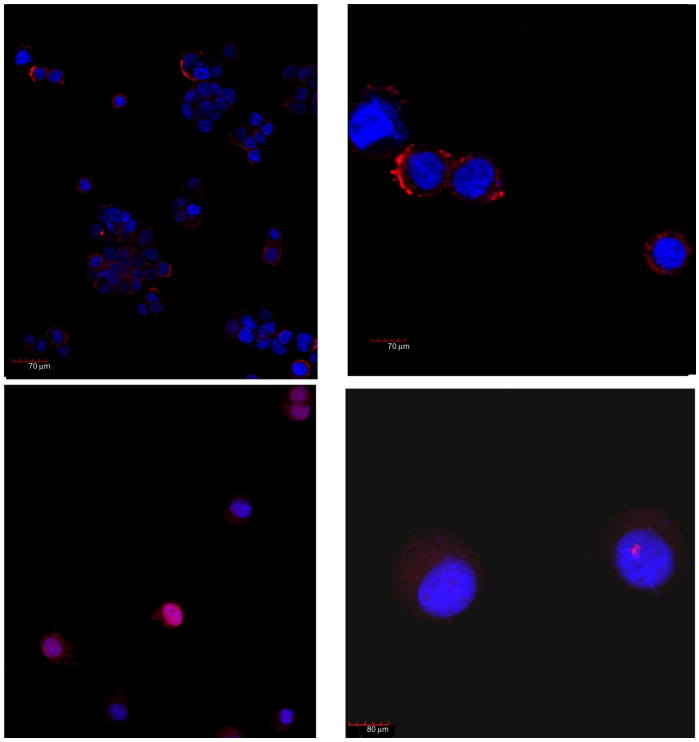

Figure S9 Laser scanning confocal microscopy of human HT29 colon carcinoma cells after 10 (top) and 60 (down) minutes of incubation with HFt rhodamine-labeling. Clusters of HFt-based nanoparticles with rhodamine fluorescence appear in red.
Note: Original magnification 40× (left) and zoom 3× (120×, right) were used.
Abbreviation: HFt, human protein ferritin.

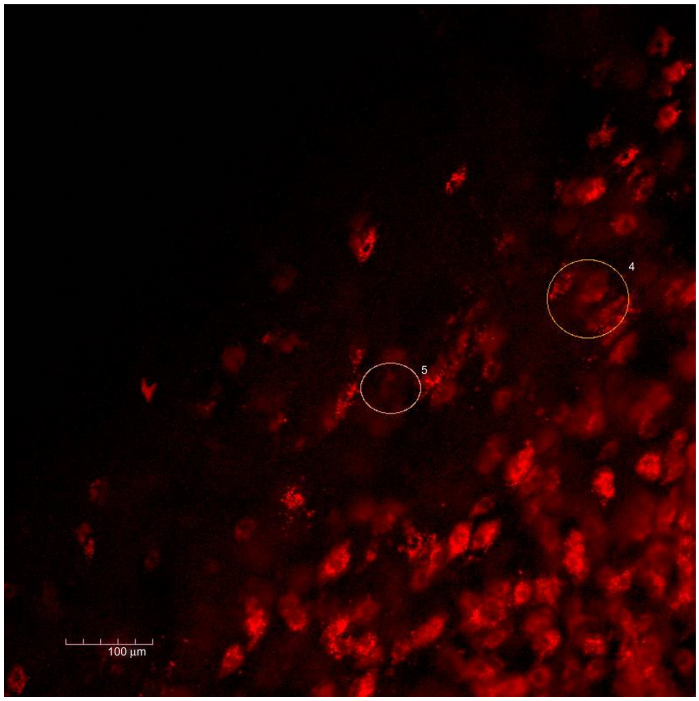

Figure S10 Melanoma and skin.
Notes: Representative image from a Z series of 46 images, 0.8 µm space, taken at the border of the tumor. The specific uptake of HFt-MSH-PEG nanoparticles by the tumor cells but not by the surrounding tissue was evident in all images. The tumor was initially sectioned to be leveled to the surrounding tissue and allow effective evaluation of both tissues on the same layer (confocal microscopy, 20× original magnification, nanoparticles fluorescence in red, numbers indicate areas that were selected for further imaging analysis, first image).
Abbreviations: HFt, human protein ferritin; PEG, polyethylene glycol; MSH, melanocyte-stimulating hormone peptide.

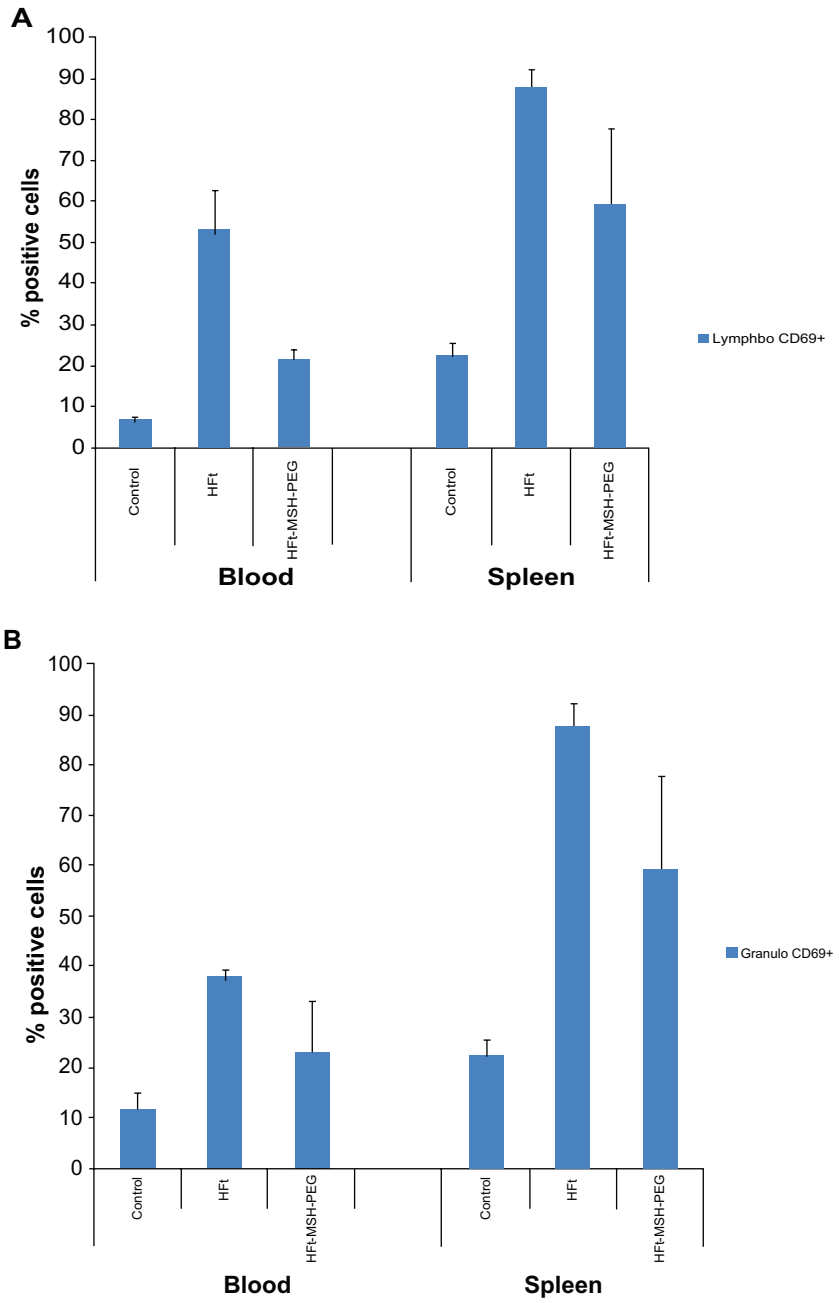

Figure S11 Percentages of CD69-positive cells in two gated populations of leukocytes (granulogates, lymphogates, and monogates) from peripheral blood and spleen cells, evaluated at 23 hours after administration of HFt-nanoparticles in healthy mice (three animals per group).
Abbreviation: HFt, human protein ferritin.

Table S1 Stability of HFt and HFt-MSH-PEG nanoparticles in human plasma

Time (hours)	HFt	HFt-MSH-PEG
% of intact protein		
Initial	100	100
1	93	99
6	92	98
18	92	98
24	92	98
48	92	98

Abbreviations: HFt, human protein ferritin; PEG, polyethylene glycol; MSH, melanocyte-stimulating hormone peptide.

Discussion

One of the goals of this thesis was to describe the NK cell reaction to glycans. The role of glycosylation and protein–glycan recognition in autoimmune diseases had been proven in the past and is being intensively studied in the present (98, 146). Aberrant glycosylation was also repeatedly reported during malignant tumor growth and was associated with metastatic potential (89), while other, bacterial LPS–derived glycans are long known to act in cellular activation and immune response enhancement (147, 148). Octavalent GlcNAc mimetic, GN8P, was used in the studies herein to simulate branched glycan structures, appearing during autoimmune disorders or malignant growth. According to the latest findings, there is no clear evidence about the direct binding of glycan (GlcNAc–terminated) structures to NKR–P1 receptor; nevertheless, it is important for NK, and subsequently other type of immune cells activation. CD161, a member of the C–type lectin–like receptor family, was reported previously to bind LacNAc (*N*–acetyl–lactosamine) epitopes and could thus be involved in the GN8P mimetic recognition probably in cooperation with other receptors. As shown in this thesis, RA patients with increased CD161 surface and mRNA expression on/in NK cells responded to the glycomimetic by attenuated NK cell–mediated cytotoxicity. Since similar effect can be achieved with CD161 natural ligand LLT1 (80), we can hypothesize a similar mechanism of action. Further study with LLT1 as a binding competitor in GN8P–CD161 interaction investigation is needed to test this hypothesis as well as to ascertain the involvement of other, CD161–associated co–receptors. In mice, there are several orthologs of CD161, NKR–P1A, B, C, D and F (59). While B and D isoforms contain an ITIM motif and are considered inhibitory, A, C and F lack it and were reported to associate with FcεRIγ and to have activation potential (59). In this thesis, it was presented that serum levels of IgG2a specific for both T–independent and T–dependent antigens were elevated after GN8P administration in C57Bl/6 mice. Since resting NK cells fail to modulate antibody responses, but if activated, preferentially upregulate IgG2a formation (7, 149), we can attribute this elevation to NK cells. In addition, we presented results that only NK1.1–positive C57Bl/6 mice responded to GN8P administration, while NK1.1–negative strains (Balb/c and DBA/2) were unresponsive. Also NK1.1–depleted SMC did not exert increased response to the glycomimetic as undepleted cells in C57Bl/6 mice. Therefore, we suggest that GN8P effect on antibody formation in mice might be dependent on the presence of NKR–P1C isoform encoded by *Nkr–p1c(T)* gene form (present in C57Bl/6 strain). We do not expect involvement of NKR–P1A and NKR–P1F isoforms (activating receptors) as their genes are present in DBA/2 and BALB/c as well as in C57BL/6 mice. As for NKR–P1B and NKR–P1D isoforms, *Nkr–p1b* gene in DBA/2 and BALB/c mice exerted 94.9% homology with *Nkr–p1d* in C57BL/6 mice. In addition, they both have inhibitory function (20) and have a mutual ligand, Clr–b (78). The involvement of NK cells in the GN8P–mediated antibody formation was further studied in the melanoma–bearing C57Bl/6 mice, where the glycomimetic administration evoked tumor–specific IgG2a upregulation, NK cell–mediated IFNγ production and increased ADCC effector function (150). Since IFNγ promotes Ig class switch towards IgG2a (113) and IgG2a is one of the most potent

IgG subclass in mediating ADCC (8), the involvement of NK cells was further validated. Yet again, the exact mechanism of glycomimetic–NK cell interaction needs to be further studied with NKR–P1C(T) natural ligands as binding–competitors, but these are as of yet still unknown. The glycomimetic effect on NK cell function was well described in humans and mice and in both cases, NKR–P1 receptor was involved. In recent studies, more and more attention is being given to the tumor–associated carbohydrate antigens (TACA) and their use in the preparation of carbohydrate–based vaccines (90, 91). Our data on NK cell reaction to GlcNAc based glycomimetic may prove quite useful in the future design of such vaccines as well as other applications.

We have shown here, that the choice of species in the study of receptor–ligand interactions may be crucial in some cases. For instance, the synthetic immune glycomimetic, GN8P, proved to have quite the opposite effect on the function of NK cells when human and C57BL/6 murine systems were compared. This may be due to the fact, that there is only one NKR–P1A isoform in humans with both activation and inhibitory potency (80, 102, 104), while in mice, these functions are divided between individual activating/inhibitory isoforms (106). Moreover, some murine strains (DBA/2, BALB/c) were utterly unaffected, despite having only one amino acid substitution in their NKR–P1C receptor and expressing NKR–P1A, which is considered an ortholog of the human CD161.

Among widely used, endogenously present and well–described immune modulators belong the hormones. In further study presented here we have shown, that the widely used controlled ovarian hyperstimulation protocol implementing GnRH antagonist/hCG treatment significantly increases KIR2DL4 expression on the surface of NK cells. This receptor is known to activate IFNγ cytokine production, but only weak cytotoxicity (61, 62) in NK cells and can thus be used to further modulate the NK cell function. As most hormones, hCG also shows a degree of pleiotropy in its effect, influencing CD4 and CD8 T cells and their receptors as well as NK cells. Thus, this effect needs to be targeted to NK cells to achieve specific and accurate modulation of NK cell function. That is where the protein–based multifunctional nanoparticles presented here come into view and could be used for selective NK cell targeting with hCG load for KIR2DL4 upregulation. Further studies involving these nanoparticles need to be performed to make the use of hCG as NK cell modulator specific.

Another endogenous and well–described immunomodulator is the purine nucleoside adenosine, often released by transformed cells under the hypoxic conditions of the tumor microenvironment. It influences many physiological functions (*e.g.*, vasodilatation, lipolysis, *etc.*) (129), and its levels are dramatically increased during hypoxic conditions, tissue damage and inflammation. Adenosine inhibits inflammatory activity of neutrophils, macrophages and lymphocytes, protecting the ischemic tissues from massive damage (130). Adenosine receptors (AR) are also involved in the inhibition of cytotoxic activity and cytokine production by activated NK cells (84, 131). Here we have proven the synthetic A_{2A} adenosine receptor agonist CPCA to be a universal NK cell cytotoxicity attenuator in several mammalian species in both healthy and immunocompromised subjects. These findings could be applied in transplantation

immunology to prevent the host versus graft reaction in the early phases, but without effective targeting, the entire host immune system could become compromised. Thus, further studies with CPCA specific targeting to terminal tissues/populations need to be performed to achieve practical applications for NK cell–mediated lysis attenuation. Such specificity can be achieved either in conjunction with tissue–targeting saccharide structures (94) or with the ferritin–based nanoplatform presented in this thesis.

Stress inducible proteins, ligands of the activating NKG2D (39), present another possibility how to activate NK cells. Hyperthermia represents an elegant way of contact–less attenuation of tumor growth, while inducing the responsiveness of the immune system, by increased presentation of these proteins (74). Higher temperatures (≥42°C) have directly cytotoxic and immunogenic effect on malignant tissue (133), and if properly focused only on the tumor itself, can provide tumoricidal temperature in the affected site, while maintaining febrile temperature range in the surrounding. This could prove very beneficial, since such range was reported previously to activate spleen cells (135), NK cells (136), cytotoxic T cells and T helper cells (137, 138). On the other hand, implementation of hyperthermia can be used only seldomly on barely detectable metastatic cells, early neoplasia or leukemia. Again, if properly targeted to these cells by the abovementioned nanoplatform, the ferritin core can be loaded with microwave–inducible heat generating particles (139) and could thus ensure the targeted heating of circulating, metastatic, leukemic cells or in the case of inaccessible tumors. Further research as to the specific particle load, temperature ranges and targeting moieties need to be performed in order to achieve future clinical applications in this field as well.

Among recent trends in tumor–immunotherapy is the specific or passive targeting of tumor–suppressants or immune mediators into the tumor site (140, 141). The nanoparticle platform presented here stands out by its simple versatility – it could be applied not only in one specific, controlled system, but with proper targeting structure and immune mediator load can be used in almost any pathology. Its employment for targeted hyperthermia, when loaded with heat–generating particles (139), is also notable but further studies, using this versatile system, need to be performed before practical applications are achieved.

Result summary, conclusions and remarks.

In this work, NK cells and their receptors were intensively studied in several mammalian species in order to acquire new insights on their function. Particular attention was given to their response to glycan structures (GN8P), hormones (hCG), tumor evasion strategies (adenosines) and stress inducible proteins (hyperthermia). Together with a immune modulation via localized hyperthermia and modular targeting nanoplatform, these findings provide new tools for immune modulation via the regulation of NK cell functions.

Based on the work provided here, we came to the following conclusions:

- In humans, there is a subset of NK cells (~50%), which react to the synthetic glycomimetic GN8P by impaired cytotoxic effector function and this subpopulation can be identified by their higher levels of CD161 expression. This expression can be increased by mutated citrullinated vimentin (MCV) in both rheumatoid arthritis patients and in healthy donors on the mRNA level. In addition, these results make us believe, that the impaired NK cell cytotoxicity in autoimmune patients could involve the interaction with CD161.
- The synthetic glycomimetic – GN8P has shown a potential to modulate specific antibody formation via NK cell stimulation in the C57BL/6 murine model. This stimulation was shown to be dependent on the surface expression of NKR–P1C isoform encoded by C57BL/6 *Nkr–p1c(T)* gene allele. Glycomimetic–induced NK cells, via IFNγ production, potentiate tumor–specific Ig formation, triggering ADCC reaction as well as antigen presentation by B cells. These results illustrate the importance of carbohydrates in NK cell–mediated regulation of adaptive immunity, with benefit for specific anticancer immune responses.
- The commonly used GnRH antagonist/hCG ovulation stimulation protocol increases the expression of KIR2DL4 on NK cells, influences the CD4/CD8 index, promoting cytotoxic T cells. This immunological profile was associated with decreased implantation rates.
- A_{2A} adenosine receptor agonist, CPCA, used in our *in vitro* evaluation of cytotoxic effector cells derived from different mammalian species, indicates for a universal NK cell cytotoxicity attenuator.
- *In vivo* tumor–localized hyperthermia proved to have beneficial effect on NK cell–mediated lytic activity, despite the NK cell numbers or receptors repertoire remained unchanged.
- We have developed a melanoma-specific tailor made ferritin–based multifunctional nanoplatform, with well–defined parameters and modularity in the targeting moiety. This platform can be equipped with specific ligands on heat–inducible nanoparticles singly or combined with the above mentioned mediators, achieving immunotherapeutic procedures in various systems.

This work brought further knowledge in the possibilities of NK cell modulation, nevertheless, further research needs to be performed for practical applications. More studies with the combination of the herein studied modulators targeted to specific cell populations by the established nanoplatform are required.

List of references

1. Marcenaro, E., S. Carlomagno, S. Pesce, M. Della Chiesa, S. Parolini, A. Moretta, and S. Sivori. 2011. NK cells and their receptors during viral infections. *Immunotherapy-Uk* 3:1075-1086.
2. Waldhauer, I., and A. Steinle. 2008. NK cells and cancer immunosurveillance. *Oncogene* 27:5932-5943.
3. Gerosa, F., B. Baldani-Guerra, C. Nisii, V. Marchesini, G. Carra, and G. Trinchieri. 2002. Reciprocal activating interaction between natural killer cells and dendritic cells. *J Exp Med* 195:327-333.
4. Adam, C., S. King, T. Allgeier, H. Braumuller, C. Luking, J. Mysliwietz, A. Kriegeskorte, D. H. Busch, M. Rocken, and R. Mocikat. 2005. DC-NK cell cross talk as a novel CD4+ T-cell-independent pathway for antitumor CTL induction. *Blood* 106:338-344.
5. Malhotra, A., and A. Shanker. 2011. NK cells: immune cross-talk and therapeutic implications. *Immunotherapy-Uk* 3:1143-1166.
6. Trinchieri, G. 1989. Biology of Natural-Killer Cells. *Advances in Immunology* 47:187-376.
7. Amigorena, S., C. Bonnerot, W. H. Fridman, and J. L. Teillaud. 1990. Recombinant interleukin 2-activated natural killer cells regulate IgG2a production. *Eur J Immunol* 20:1781-1787.
8. Koh, C. Y., and D. Yuan. 2000. The functional relevance of NK-cell-mediated upregulation of antigen-specific IgG2a responses. *Cell Immunol* 204:135-142.
9. Hinds, L. B. D., M. S. Alexandre-Moreira, D. Decote-Ricardo, M. P. Nunes, and L. M. T. Pecanha. 2001. Increased immunoglobulin secretion by B lymphocytes from Trypanosoma cruzi infected mice after B lymphocytes-natural killer cell interaction. *Parasite Immunol* 23:581-586.
10. Lunemann, A., J. D. Lunemann, and C. Munz. 2009. Regulatory NK-cell functions in inflammation and autoimmunity. *Mol Med* 15:352-358.
11. Perricone, R., C. Perricone, C. De Carolis, and Y. Shoenfeld. 2008. NK cells in autoimmunity: a two-edg'd weapon of the immune system. *Autoimmun Rev* 7:384-390.
12. Moffett-King, A. 2002. Natural killer cells and pregnancy. *Nat Rev Immunol* 2:656-663.
13. Gill, R. G. 2010. NK cells: elusive participants in transplantation immunity and tolerance. *Curr Opin Immunol* 22:649-654.
14. Horowitz, A., K. A. Stegmann, and E. M. Riley. 2011. Activation of natural killer cells during microbial infections. *Front Immunol* 2:88.
15. Wilk, E., K. Kalippke, S. Buyny, R. E. Schmidt, and R. Jacobs. 2008. New aspects of NK cell subset identification and inference of NK cells' regulatory capacity by assessing functional and genomic profiles. *Immunobiology* 213:271-283.
16. Wendt, K., E. Wilk, S. Buyny, J. Buer, R. E. Schmidt, and R. Jacobs. 2006. Gene and protein characteristics reflect functional diversity of CD56(dim) and CD56(bright) NK cells. *J Leukocyte Biol* 80:1529-1541.
17. Hayakawa, Y., and M. J. Smyth. 2006. CD27 dissects mature NK cells into two subsets with distinct responsiveness and migratory capacity. *Journal of Immunology* 176:1517-1524.

18. Hayakawa, Y., N. D. Huntington, S. L. Nutt, and M. J. Smyth. 2006. Functional subsets of mouse natural killer cells. *Immunol Rev* 214:47-55.
19. Walzer, T., M. Blery, J. Chaix, N. Fuseri, L. Chasson, S. H. Robbins, S. Jaeger, P. Andre, L. Gauthier, L. Daniel, K. Chemin, Y. Morel, M. Dalod, J. Imbert, M. Pierres, A. Moretta, F. Romagne, and E. Vivier. 2007. Identification, activation, and selective in vivo ablation of mouse NK cells via NKp46. *Proc Natl Acad Sci U S A* 104:3384-3389.
20. Carlyle, J. R., A. Mesci, B. Ljutic, S. Belanger, L. H. Tai, E. Rousselle, A. D. Troke, M. F. Proteau, and A. P. Makrigiannis. 2006. Molecular and genetic basis for strain-dependent NK1.1 alloreactivity of mouse NK cells. *Journal of Immunology* 176:7511-7524.
21. Moretta, L., R. Biassoni, C. Bottino, M. C. Mingari, and A. Moretta. 2000. Human NK-cell receptors. *Immunol Today* 21:420-422.
22. Chambers, W. H., and C. S. Brissettestorkus. 1995. Hanging in the Balance - Natural-Killer-Cell Recognition of Target-Cells. *Chem Biol* 2:429-435.
23. Lanier, L. L. 2001. On guard - activating NK cell receptors. *Nat Immunol* 2:23-27.
24. Blery, M., L. Olcese, and E. Vivier. 2000. Early signaling via inhibitory and activating NK receptors. *Hum Immunol* 61:51-64.
25. Ravetch, J. V., and L. L. Lanier. 2000. Immune inhibitory receptors. *Science* 290:84-89.
26. Ljunggren, H. G., and K. Karre. 1990. In Search of the Missing Self - Mhc Molecules and Nk Cell Recognition. *Immunol Today* 11:237-244.
27. Garrido, F., F. Ruiz-Cabello, T. Cabrera, J. J. Perez-Villar, M. Lopez-Botet, M. Duggan-Keen, and P. L. Stern. 1997. Implications for immunosurveillance of altered HLA class I phenotypes in human tumours. *Immunol Today* 18:89-95.
28. Moretta, L., R. Biassoni, C. Bottino, C. Cantoni, D. Pende, M. C. Mingari, and A. Moretta. 2002. Human NK cells and their receptors. *Microbes Infect* 4:1539-1544.
29. Isakov, N. 1998. Role of immunoreceptor tyrosine-based activation motif in signal transduction from antigen and Fc receptors. *Adv Immunol* 69:183-247.
30. Lanier, L. L., G. Yu, and J. H. Phillips. 1991. Analysis of Fc gamma RIII (CD16) membrane expression and association with CD3 zeta and Fc epsilon RI-gamma by site-directed mutation. *J Immunol* 146:1571-1576.
31. Wu, J., H. Cherwinski, T. Spies, J. H. Phillips, and L. L. Lanier. 2000. DAP10 and DAP12 form distinct, but functionally cooperative, receptor complexes in natural killer cells. *J Exp Med* 192:1059-1068.
32. Perussia, B. 2000. Signaling for cytotoxicity. *Nat Immunol* 1:372-374.
33. Anegon, I., M. C. Cuturi, G. Trinchieri, and B. Perussia. 1988. Interaction of Fc receptor (CD16) ligands induces transcription of interleukin 2 receptor (CD25) and lymphokine genes and expression of their products in human natural killer cells. *J Exp Med* 167:452-472.
34. Azzoni, L., I. Anegon, B. Calabretta, and B. Perussia. 1995. Ligand binding to Fc gamma R induces c-myc-dependent apoptosis in IL-2-stimulated NK cells. *J Immunol* 154:491-499.
35. Takai, T., M. Li, D. Sylvestre, R. Clynes, and J. V. Ravetch. 1994. FcR gamma chain deletion results in pleiotrophic effector cell defects. *Cell* 76:519-529.
36. Clynes, R. A., T. L. Towers, L. G. Presta, and J. V. Ravetch. 2000. Inhibitory Fc receptors modulate in vivo cytotoxicity against tumor targets. *Nat Med* 6:443-446.

37. Jiang, K., B. Zhong, D. L. Gilvary, B. C. Corliss, E. Hong-Geller, S. Wei, and J. Y. Djeu. 2000. Pivotal role of phosphoinositide-3 kinase in regulation of cytotoxicity in natural killer cells. *Nat Immunol* 1:419-425.
38. Wu, J., Y. Song, A. B. Bakker, S. Bauer, T. Spies, L. L. Lanier, and J. H. Phillips. 1999. An activating immunoreceptor complex formed by NKG2D and DAP10. *Science* 285:730-732.
39. Bauer, S., V. Groh, J. Wu, A. Steinle, J. H. Phillips, L. L. Lanier, and T. Spies. 1999. Activation of NK cells and T cells by NKG2D, a receptor for stress-inducible MICA. *Science* 285:727-729.
40. Ingley, E. 2008. Src family kinases: regulation of their activities, levels and identification of new pathways. *Biochim Biophys Acta* 1784:56-65.
41. Tourdot, B. E., M. K. Brenner, K. C. Keough, T. Holyst, P. J. Newman, and D. K. Newman. 2013. Immunoreceptor Tyrosine-Based Inhibitory Motif (ITIM)-Mediated Inhibitory Signaling Is Regulated by Sequential Phosphorylation Mediated by Distinct Nonreceptor Tyrosine Kinases: A Case Study Involving PECAM-1. *Biochemistry-Us* 52:2597-2608.
42. Lowell, C. A. 2011. Src-family and Syk kinases in activating and inhibitory pathways in innate immune cells: signaling cross talk. *Cold Spring Harb Perspect Biol* 3.
43. Lanier, L. L. 1998. NK cell receptors. *Annu Rev Immunol* 16:359-393.
44. Ortaldo, J. R., L. H. Mason, T. A. Gregorio, J. Stoll, and R. T. Winkler-Pickett. 1997. The Ly-49 family: regulation of cytokine production in murine NK cells. *J Leukoc Biol* 62:381-388.
45. Leibson, P. J. 1997. Signal transduction during natural killer cell activation: inside the mind of a killer. *Immunity* 6:655-661.
46. Vivier, E., and M. Daeron. 1997. Immunoreceptor tyrosine-based inhibition motifs. *Immunol Today* 18:286-291.
47. Valiante, N. M., J. H. Phillips, L. L. Lanier, and P. Parham. 1996. Killer cell inhibitory receptor recognition of human leukocyte antigen (HLA) class I blocks formation of a pp36/PLC-gamma signaling complex in human natural killer (NK) cells. *J Exp Med* 184:2243-2250.
48. Brumbaugh, K. M., J. J. Perez-Villar, C. J. Dick, R. A. Schoon, M. Lopez-Botet, and P. J. Leibson. 1996. Clonotypic differences in signaling from CD94 (kp43) on NK cells lead to divergent cellular responses. *J Immunol* 157:2804-2812.
49. Binstadt, B. A., K. M. Brumbaugh, C. J. Dick, A. M. Scharenberg, B. L. Williams, M. Colonna, L. L. Lanier, J. P. Kinet, R. T. Abraham, and P. J. Leibson. 1996. Sequential involvement of Lck and SHP-1 with MHC-recognizing receptors on NK cells inhibits FcR-initiated tyrosine kinase activation. *Immunity* 5:629-638.
50. Nakamura, M. C., E. C. Niemi, M. J. Fisher, L. D. Shultz, W. E. Seaman, and J. C. Ryan. 1997. Mouse Ly-49A interrupts early signaling events in natural killer cell cytotoxicity and functionally associates with the SHP-1 tyrosine phosphatase. *J Exp Med* 185:673-684.
51. Ono, M., S. Bolland, P. Tempst, and J. V. Ravetch. 1996. Role of the inositol phosphatase SHIP in negative regulation of the immune system by the receptor Fc(gamma)RIIB. *Nature* 383:263-266.
52. Gupta, N., A. M. Scharenberg, D. N. Burshtyn, N. Wagtmann, M. N. Lioubin, L. R. Rohrschneider, J. P. Kinet, and E. O. Long. 1997. Negative signaling pathways of the

killer cell inhibitory receptor and Fc gamma RIIb1 require distinct phosphatases. *J Exp Med* 186:473-478.
53. Mandelboim, O., N. Lieberman, M. Lev, L. Paul, T. I. Arnon, Y. Bushkin, D. M. Davis, J. L. Strominger, J. W. Yewdell, and A. Porgador. 2001. Recognition of haemagglutinins on virus-infected cells by NKp46 activates lysis by human NK cells. *Nature* 409:1055-1060.
54. Bubic, I., M. Wagner, A. Krmpotic, T. Saulig, S. Kim, W. M. Yokoyama, S. Jonjic, and U. H. Koszinowski. 2004. Gain of virulence caused by loss of a gene in murine cytomegalovirus. *J Virol* 78:7536-7544.
55. Newman, K. C., and E. M. Riley. 2007. Whatever turns you on: accessory-cell-dependent activation of NK cells by pathogens. *Nat Rev Immunol* 7:279-291.
56. Humann, J., and L. L. Lenz. 2010. Activation of Naive NK Cells in Response to Listeria monocytogenes Requires IL-18 and Contact with Infected Dendritic Cells. *Journal of Immunology* 184:5172-5178.
57. Lanier, L. L., B. Corliss, and J. H. Phillips. 1997. Arousal and inhibition of human NK cells. *Immunol Rev* 155:145-154.
58. Cerwenka, A., J. L. Baron, and L. L. Lanier. 2001. Ectopic expression of retinoic acid early inducible-1 gene (RAE-1) permits natural killer cell-mediated rejection of a MHC class I-bearing tumor in vivo. *P Natl Acad Sci USA* 98:11521-11526.
59. Lanier, L. L. 2005. NK cell recognition. *Annual Review of Immunology* 23:225-274.
60. Faure, M., and E. O. Long. 2002. KIR2DL4 (CD158d), an NK cell-activating receptor with inhibitory potential. *Journal of Immunology* 168:6208-6214.
61. Rajagopalan, S., J. Fu, and E. O. Long. 2001. Cutting edge: induction of IFN-gamma production but not cytotoxicity by the killer cell Ig-like receptor KIR2DL4 (CD158d) in resting NK cells. *J Immunol* 167:1877-1881.
62. Kikuchi-Maki, A., S. Yusa, T. L. Catina, and K. S. Campbell. 2003. KIR2DL4 is an IL-2-regulated NK cell receptor that exhibits limited expression in humans but triggers strong IFN-gamma production. *Journal of Immunology* 171:3415-3425.
63. Chang, C. W., A. Rodriguez, M. Carretero, M. Lopezbotet, J. H. Phillips, and L. L. Lanier. 1995. Molecular Characterization of Human Cd94 - a Type-Ii Membrane Glycoprotein Related to the C-Type Lectin Superfamily. *European Journal of Immunology* 25:2433-2437.
64. Vance, R. E., J. R. Kraft, J. D. Altman, P. E. Jensen, and D. H. Raulet. 1998. Mouse CD94/NKG2A is a natural killer cell receptor for the nonclassical major histocompatibility complex (MHC) class I molecule Qa-1(b). *Journal of Experimental Medicine* 188:1841-1848.
65. Vance, R. E., A. M. Jamieson, and D. H. Raulet. 1999. Recognition of the class Ib molecule Qa-1(b) by putative activating receptors CD94/NKG2C and CD94/NKG2E on mouse natural killer cells. *Journal of Experimental Medicine* 190:1801-1812.
66. Lanier, L. L., B. Corliss, J. Wu, and J. H. Phillips. 1998. Association of DAP12 with activating CD94/NKG2C NK cell receptors. *Immunity* 8:693-701.
67. Carretero, M., C. Cantoni, T. Bellon, C. Bottino, R. Biassoni, A. Rodriguez, J. J. PerezVillar, L. Moretta, A. Moretta, and M. LopezBotet. 1997. The CD94 and NKG2-A C-type lectins covalently assemble to form a natural killer cell inhibitory receptor for HLA class I molecules. *European Journal of Immunology* 27:563-567.

68. Vales-Gomez, M., H. T. Reyburn, R. A. Erskine, M. Lopez-Botet, and J. L. Strominger. 1999. Kinetics and peptide dependency of the binding of the inhibitory NK receptor CD94/NKG2-A and the activating receptor CD94/NKG2-C to HLA-E. *Embo Journal* 18:4250-4260.
69. Lee, N., D. R. Goodlett, A. Ishitani, H. Marquardt, and D. E. Geraghty. 1998. HLA-E surface expression depends on binding of TAP-dependent peptides derived from certain HLA class I signal sequences. *Journal of Immunology* 160:4951-4960.
70. Ho, E. L., L. N. Carayannopoulos, J. Poursine-Laurent, J. Kinder, B. Plougastel, H. R. C. Smith, and W. M. Yokoyama. 2002. Costimulation of multiple NK cell activation receptors by NKG2D. *Journal of Immunology* 169:3667-3675.
71. Houchins, J. P., T. Yabe, C. Mcsherry, and F. H. Bach. 1991. DNA-Sequence Analysis of Nkg2, a Family of Related Cdna Clones Encoding Type-Ii Integral Membrane-Proteins on Human Natural-Killer-Cells. *Journal of Experimental Medicine* 173:1017-1020.
72. Lodoen, M., K. Ogasawara, J. A. Hamerman, H. Arase, J. P. Houchins, E. S. Mocarski, and L. L. Lanier. 2003. NKG2D-mediated natural killer cell protection against cytomegalovirus is impaired by viral gp40 modulation of retinoic acid early inducible 1 gene molecules. *Journal of Experimental Medicine* 197:1245-1253.
73. Groh, V., J. Wu, C. Yee, and T. Spies. 2002. Tumour-derived soluble MIC ligands impair expression of NKG2D and T-cell activation. *Nature* 419:734-738.
74. Kim, J. Y., Y. O. Son, S. W. Park, J. H. Bae, J. S. Chung, H. H. Kim, B. S. Chung, S. H. Kim, and C. D. Kang. 2006. Increase of NKAG2D ligands and sensitivity to NK cell-mediated cytotoxicity of tumor cells by heat shock and ionizing radiation. *Exp Mol Med* 38:474-484.
75. Galazka, G., A. Jurewicz, W. Orlowski, M. Stasiolek, C. F. Brosnan, C. S. Raine, and K. Selmaj. 2007. EAE tolerance induction with Hsp70-peptide complexes depends on H60 and NKG2D activity. *Journal of Immunology* 179:4503-4512.
76. Groh, V., A. Bruhl, H. El-Gabalawy, J. L. Nelson, and T. Spies. 2003. Stimulation of T cell autoreactivity by anomalous expression of NKG2D and its MIC ligands in rhe'umatoid arthritis. *P Natl Acad Sci USA* 100:9452-9457.
77. Plougastel, B., C. Dubbelde, and W. M. Yokoyama. 2001. Cloning of Clr, a new family of lectin-like genes localized between mouse NKrp1a and Cd69. *Immunogenetics* 53:209-214.
78. Carlyle, J. R., A. M. Jamieson, S. Gasser, C. S. Clingan, H. Arase, and D. H. Raulet. 2004. Missing self-recognition of Ocil/Clr-b by inhibitory NKR-P1 natural killer cell receptors. *P Natl Acad Sci USA* 101:3527-3532.
79. Iizuka, K., O. V. Naidenko, B. F. M. Plougastel, D. H. Fremont, and W. M. Yokoyama. 2003. Genetically linked C-type lectin-related ligands for the NKRP1 family of natural killer cell receptors. *Nat Immunol* 4:801-807.
80. Rosen, D. B., J. Bettadapura, M. Alsharifi, P. A. Mathew, H. S. Warren, and L. L. Lanier. 2005. Cutting edge: lectin-like transcript-1 is a ligand for the inhibitory human NKR-P1A receptor. *J Immunol* 175:7796-7799.
81. Kamishikiryo, J., H. Fukuhara, Y. Okabe, K. Kuroki, and K. Maenaka. 2011. Molecular Basis for LLT1 Protein Recognition by Human CD161 Protein (NKRP1A/KLRB1). *Journal of Biological Chemistry* 286:23823-23830.

82. Ryan, J. C., E. C. Niemi, M. C. Nakamura, and W. E. Seaman. 1995. NKR-P1A is a target-specific receptor that activates natural killer cell cytotoxicity. *J Exp Med* 181:1911-1915.
83. Kumar, V., and A. Sharma. 2009. Adenosine: An endogenous modulator of innate immune system with therapeutic potential. *Eur J Pharmacol* 616:7-15.
84. Raskovalova, T., X. J. Huang, M. Sitkovsky, L. C. Zacharia, E. K. Jackson, and E. Gorelik. 2005. G(S) protein-coupled adenosine receptor signaling and lytic function of activated NK cells. *Journal of Immunology* 175:4383-4391.
85. Harish, A., G. Hohana, P. Fishman, O. Arnon, and S. Bar-Yehuda. 2003. A3 adenosine receptor agonist potentiates natural killer cell activity. *International Journal of Oncology* 23:1245-1249.
86. Vivier, E., and S. Ugolini. 2011. Natural killer cells: from basic research to treatments. *Front Immunol* 2:18.
87. Buskas, T., P. Thompson, and G. J. Boons. 2009. Immunotherapy for cancer: synthetic carbohydrate-based vaccines. *Chem Commun*:5335-5349.
88. Astronomo, R. D., and D. R. Burton. 2010. Carbohydrate vaccines: developing sweet solutions to sticky situations? *Nat Rev Drug Discov* 9:308-324.
89. Li, M., L. J. Song, and X. Y. Qin. 2010. Glycan changes: cancer metastasis and anti-cancer vaccines. *J Biosciences* 35:665-673.
90. Yin, Z., M. Comellas-Aragones, S. Chowdhury, P. Bentley, K. Kaczanowska, L. Benmohamed, J. C. Gildersleeve, M. G. Finn, and X. Huang. 2013. Boosting Immunity to Small Tumor-Associated Carbohydrates with Bacteriophage Qbeta Capsids. *ACS Chem Biol*.
91. Huang, Y. L., J. T. Hung, S. K. Cheung, H. Y. Lee, K. C. Chu, S. T. Li, Y. C. Lin, C. T. Ren, T. J. Cheng, T. L. Hsu, A. L. Yu, C. Y. Wu, and C. H. Wong. 2013. Carbohydrate-based vaccines with a glycolipid adjuvant for breast cancer. *Proc Natl Acad Sci U S A* 110:2517-2522.
92. Gening, M. L., Y. E. Tsvetkov, G. B. Pier, and N. E. Nifantiev. 2007. Synthesis of beta-(1 -> 6)-linked glucosamine oligosaccharides corresponding to fragments of the bacterial surface polysaccharide poly-N-acetylglucosamine. *Carbohyd Res* 342:567-575.
93. Lindhorst, T. K., and C. Kieburg. 1996. Glycocoating of oligovalent amines: Synthesis of thiourea-bridged cluster glycosides from glycosyl isothiocyanates. *Angewandte Chemie-International Edition in English* 35:1953-1956.
94. Zhang, H. L., Y. Ma, and X. L. Sun. 2010. Recent Developments in Carbohydrate-Decorated Targeted Drug/Gene Delivery. *Med Res Rev* 30:270-289.
95. Bernardi, A., J. Jimenez-Barbero, A. Casnati, C. De Castro, T. Darbre, F. Fieschi, J. Finne, H. Funken, K. E. Jaeger, M. Lahmann, T. K. Lindhorst, M. Marradi, P. Messner, A. Molinaro, P. V. Murphy, C. Nativi, S. Oscarson, S. Penades, F. Peri, R. J. Pieters, O. Renaudet, J. L. Reymond, B. Richichi, J. Rojo, F. Sansone, C. Schaffer, W. B. Turnbull, T. Velasco-Torrijos, S. Vidal, S. Vincent, T. Wennekes, H. Zuilhof, and A. Imberty. 2013. Multivalent glycoconjugates as anti-pathogenic agents. *Chem Soc Rev* 42:4709-4727.
96. Sutlu, T., and E. Alici. 2009. Natural killer cell-based immunotherapy in cancer: current insights and future prospects. *J Intern Med* 266:154-181.

97. Konjevic, G., V. Jurisic, V. Jovic, A. Vuletic, K. Mirjacic Martinovic, S. Radenkovic, and I. Spuzic. 2012. Investigation of NK cell function and their modulation in different malignancies. *Immunol Res* 52:139-156.
98. Delves, P. J. 1998. The role of glycosylation in autoimmune disease. *Autoimmunity* 27:239-253.
99. Azzoni, L., O. Zatsepina, B. Abebe, I. M. Bennett, P. Kanakaraj, and B. Perussia. 1998. Differential transcriptional regulation of CD161 and a novel gene, 197/15a, by IL-2, IL-15, and IL-12 in NK and T cells. *J Immunol* 161:3493-3500.
100. Park, Y. W., S. J. Kee, Y. N. Cho, E. H. Lee, H. Y. Lee, E. M. Kim, M. H. Shin, J. J. Park, T. J. Kim, S. S. Lee, D. H. Yoo, and H. S. Kang. 2009. Impaired differentiation and cytotoxicity of natural killer cells in systemic lupus erythematosus. *Arthritis Rheum* 60:1753-1763.
101. Aust, J. G., F. Gays, K. M. Mickiewicz, E. Buchanan, and C. G. Brooks. 2009. The Expression and Function of the NKRP1 Receptor Family in C57BL/6 Mice. *Journal of Immunology* 183:106-116.
102. Lanier, L. L., C. W. Chang, and J. H. Phillips. 1994. Human Nkr-P1a - a Disulfide-Linked Homodimer of the C-Type Lectin Superfamily Expressed by a Subset of Nk and T-Lymphocytes. *Journal of Immunology* 153:2417-2428.
103. Poggi, A., P. Costa, L. Morelli, C. Cantoni, N. Pella, F. Spada, R. Biassoni, L. Nanni, V. Revello, E. Tomasello, M. C. Mingari, A. Moretta, and L. Moretta. 1996. Expression of human NKRP1A by CD34(+) immature thymocytes: NKRP1A-mediated regulation of proliferation and cytolytic activity. *European Journal of Immunology* 26:1266-1272.
104. Exley, M., S. Porcelli, M. Furman, J. Garcia, and S. Balk. 1998. CD161 (NKR-P1A) costimulation of CD1d-dependent activation of human T cells expressing invariant V alpha 24J alpha Q T cell receptor alpha chains. *Journal of Experimental Medicine* 188:867-876.
105. Richter, J., V. Benson, V. Grobarova, J. Svoboda, J. Vencovsky, R. Svobodova, and A. Fiserova. 2010. CD161 receptor participates in both impairing NK cell cytotoxicity and the response to glycans and vimentin in patients with rheumatoid arthritis. *Clin Immunol* 136:139-147.
106. Ljutic, B., J. R. Carlyle, D. Filipp, R. Nakagawa, M. Julius, and J. C. Zuniga-Pflucker. 2005. Functional requirements for signaling through the stimulatory and inhibitory mouse NKR-P1 (CD161) NK cell receptors. *J Immunol* 174:4789-4796.
107. Koo, G. C., and J. R. Peppard. 1984. Establishment of monoclonal anti-Nk-1.1 antibody. *Hybridoma* 3:301-303.
108. Ryan, J. C., J. Turck, E. C. Niemi, W. M. Yokoyama, and W. E. Seaman. 1992. Molecular cloning of the NK1.1 antigen, a member of the NKR-P1 family of natural killer cell activation molecules. *J Immunol* 149:1631-1635.
109. Carlyle, J. R., A. Martin, A. Mehra, L. Attisano, F. W. Tsui, and J. C. Zuniga-Pflucker. 1999. Mouse NKR-P1B, a novel NK1.1 antigen with inhibitory function. *J Immunol* 162:5917-5923.
110. Vannucci, L., A. Fiserova, K. Sadalapure, T. K. Lindhorst, M. Kuldova, P. Rossmann, O. Horvath, V. Kren, P. Krist, K. Bezouska, M. Luptovcova, F. Mosca, and M. Pospisil. 2003. Effects of N-acetyl-glucosamine-coated glycodendrimers as biological modulators in the B16F10 melanoma model in vivo. *Int J Oncol* 23:285-296.

111. Snapper, C. M., H. Yamaguchi, M. A. Moorman, R. Sneed, D. Smoot, and J. J. Mond. 1993. Natural killer cells induce activated murine B cells to secrete Ig. *J Immunol* 151:5251-5260.
112. Hulikova, K., V. Benson, J. Svoboda, P. Sima, and A. Fiserova. 2009. N-Acetyl-D-glucosamine-coated polyamidoamine dendrimer modulates antibody formation via natural killer cell activation. *Int Immunopharmacol* 9:792-799.
113. Wilder, J. A., C. Y. Koh, and D. Yuan. 1996. The role of NK cells during in vivo antigen-specific antibody responses. *Journal of Immunology* 156:146-152.
114. Caputo, M., M. Nicotra, and E. Gloria-Bottini. 2008. Fertility transition: forecast for demography. *Hum Biol* 80:359-376.
115. Giuliani, A., W. Schoell, J. Auner, and W. Urdl. 1998. Controlled ovarian hyperstimulation in assisted reproduction: effect on the immune system. *Fertil Steril* 70:831-835.
116. Karami, N., M. G. Boroujerdnia, R. Nikbakht, and A. Khodadadi. 2012. Enhancement of peripheral blood CD56(dim) cell and NK cell cytotoxicity in women with recurrent spontaneous abortion or in vitro fertilization failure. *J Reprod Immunol* 95:87-92.
117. Sacks, G., Y. Yang, E. Gowen, S. Smith, L. Fay, and M. Chapman. 2012. Detailed analysis of peripheral blood natural killer cells in women with repeated IVF failure. *Am J Reprod Immunol* 67:434-442.
118. Hunt, J. S., and D. L. Langat. 2009. HLA-G: a human pregnancy-related immunomodulator. *Curr Opin Pharmacol* 9:462-469.
119. Hunt, J. S., M. G. Petroff, R. H. McIntire, and C. Ober. 2005. HLA-G and immune tolerance in pregnancy. *FASEB J* 19:681-693.
120. Middleton, D., and F. Gonzelez. 2010. The extensive polymorphism of KIR genes. *Immunology* 129:8-19.
121. Miah, S. M., T. L. Hughes, and K. S. Campbell. 2008. KIR2DL4 differentially signals downstream functions in human NK cells through distinct structural modules. *J Immunol* 180:2922-2932.
122. Brown, D., J. Trowsdale, and R. Allen. 2004. The LILR family: modulators of innate and adaptive immune pathways in health and disease. *Tissue Antigens* 64:215-225.
123. Moysey, R. K., Y. Li, S. J. Paston, E. E. Baston, M. S. Sami, B. J. Cameron, J. Gavarret, P. Todorov, A. Vuidepot, S. M. Dunn, N. J. Pumphrey, K. J. Adams, F. Yuan, R. E. Dennis, D. H. Sutton, A. D. Johnson, J. E. Brewer, R. Ashfield, N. M. Lissin, and B. K. Jakobsen. 2010. High affinity soluble ILT2 receptor: a potent inhibitor of CD8(+) T cell activation. *Protein Cell* 1:1118-1127.
124. De Maria, A., F. Bozzano, C. Cantoni, and L. Moretta. 2011. Revisiting human natural killer cell subset function revealed cytolytic CD56(dim)CD16+ NK cells as rapid producers of abundant IFN-gamma on activation. *Proc Natl Acad Sci U S A* 108:728-732.
125. Saito, S., K. Nishikawa, T. Morii, M. Enomoto, N. Narita, K. Motoyoshi, and M. Ichijo. 1993. Cytokine production by CD16-CD56bright natural killer cells in the human early pregnancy decidua. *Int Immunol* 5:559-563.
126. Chaouat, G., S. Dubanchet, and N. Ledee. 2007. Cytokines: Important for implantation? *J Assist Reprod Genet* 24:491-505.
127. Lachapelle, M. H., R. Hemmings, D. C. Roy, T. Falcone, and P. Miron. 1996. Flow cytometric evaluation of leukocyte subpopulations in the follicular fluids of infertile patients. *Fertil Steril* 65:1135-1140.

128. Lukassen, H. G., A. van der Meer, M. J. van Lierop, E. J. Lindeman, I. Joosten, and D. D. Braat. 2003. The proportion of follicular fluid CD16+CD56DIM NK cells is increased in IVF patients with idiopathic infertility. *J Reprod Immunol* 60:71-84.
129. Fredholm, B. B., I. J. AP, K. A. Jacobson, K. N. Klotz, and J. Linden. 2001. International Union of Pharmacology. XXV. Nomenclature and classification of adenosine receptors. *Pharmacol Rev* 53:527-552.
130. Ohta, A., and M. Sitkovsky. 2001. Role of G-protein-coupled adenosine receptors in downregulation of inflammation and protection from tissue damage. *Nature* 414:916-920.
131. Lokshin, A., T. Raskovalova, X. Huang, L. C. Zacharia, E. K. Jackson, and E. Gorelik. 2006. Adenosine-mediated inhibition of the cytotoxic activity and cytokine production by activated natural killer cells. *Cancer Res* 66:7758-7765.
132. Atanackovic, D., A. Nierhaus, M. Neumeier, D. K. Hossfeld, and S. Hegewisch-Becker. 2002. 41.8 degrees C whole body hyperthermia as an adjunct to chemotherapy induces prolonged T cell activation in patients with various malignant diseases. *Cancer Immunol Immunother* 51:603-613.
133. Milani, V., and E. Noessner. 2006. Effects of thermal stress on tumor antigenicity and recognition by immune effector cells. *Cancer Immunol Immun* 55:312-319.
134. Shen, R. N., L. Lu, P. Young, H. Shidnia, N. B. Hornback, and H. E. Broxmeyer. 1994. Influence of elevated temperature on natural killer cell activity, lymphokine-activated killer cell activity and lectin-dependent cytotoxicity of human umbilical cord blood and adult blood cells. *Int J Radiat Oncol Biol Phys* 29:821-826.
135. Vartak, S., K. C. George, and B. B. Singh. 1996. Antitumor effect of pre-transplantation local hyperthermia and augmentation by dietary unsaturated fat. *Indian J Exp Biol* 34:825-832.
136. Szmigielski, S., J. Sobczynski, G. Sokolska, B. Stawarz, H. Zielinski, and Z. Petrovich. 1991. Effects of local prostatic hyperthermia on human NK and T cell function. *Int J Hyperthermia* 7:869-880.
137. Ostapenko, V. V., H. Tanaka, M. Miyano, T. Nishide, H. Ueda, I. Nishide, Y. Tanaka, M. Mune, and S. Yukawa. 2005. Immune-related effects of local hyperthermia in patients with primary liver cancer. *Hepatogastroenterology* 52:1502-1506.
138. Stawarz, B., H. Zielinski, S. Szmigielski, E. Rappaport, P. Debicki, and Z. Petrovich. 1993. Transrectal hyperthermia as palliative treatment for advanced adenocarcinoma of prostate and studies of cell-mediated immunity. *Urology* 41:548-553.
139. Porch, A., D. Slocombe, and P. P. Edwards. 2013. Microwave absorption in powders of small conducting particles for heating applications. *Phys Chem Chem Phys* 15:2757-2763.
140. Kateb, B., K. Chiu, K. L. Black, V. Yamamoto, B. Khalsa, J. Y. Ljubimova, H. Ding, R. Patil, J. A. Portilla-Arias, M. Modo, D. F. Moore, K. Farahani, M. S. Okun, N. Prakash, J. Neman, D. Ahdoot, W. Grundfest, S. Nikzad, and J. D. Heiss. 2011. Nanoplatforms for constructing new approaches to cancer treatment, imaging, and drug delivery: what should be the policy? *Neuroimage* 54 Suppl 1:S106-124.
141. Armstead, A. L., and B. Li. 2011. Nanomedicine as an emerging approach against intracellular pathogens. *Int J Nanomedicine* 6:3281-3293.
142. Dominguez-Vera, J. M., B. Fernandez, and N. Galvez. 2010. Native and synthetic ferritins for nanobiomedical applications: recent advances and new perspectives. *Future Med Chem* 2:609-618.

143. Jain, R. K. 2001. Delivery of molecular and cellular medicine to solid tumors. *Adv Drug Deliv Rev* 46:149-168.
144. Watt, R. K. 2011. The many faces of the octahedral ferritin protein. *Biometals* 24:489-500.
145. Lin, X., J. Xie, G. Niu, F. Zhang, H. Gao, M. Yang, Q. Quan, M. A. Aronova, G. Zhang, S. Lee, R. Leapman, and X. Chen. 2011. Chimeric ferritin nanocages for multiple function loading and multimodal imaging. *Nano Lett* 11:814-819.
146. Bianco, G. A., M. A. Toscano, J. M. Ilarregui, and G. A. Rabinovich. 2006. Impact of protein-glycan interactions in the regulation of autoimmunity and chronic inflammation. *Autoimmunity Reviews* 5:349-356.
147. Lengacher, S., C. V. Jongeneel, D. LeRoy, J. D. Lee, V. Kravchenko, R. J. Ulevitch, M. P. Glauser, and D. Heumann. 1996. Reactivity of murine and human recombinant LPS-binding protein (LBP) with LPS and gram negative bacteria. *J Inflamm* 47:165-172.
148. Monner, D. A., J. Gmeiner, and P. F. Muhlradt. 1981. Evidence from a Carbohydrate Incorporation Assay for Direct Activation of Bone-Marrow Myelopoietic Precursor Cells by Bacterial-Cell Wall Constitutents. *Infection and Immunity* 31:957-964.
149. De Arruda Hinds, L. B., M. S. Alexandre-Moreira, D. Decote-Ricardo, M. P. Nunes, and L. M. Pecanha. 2001. Increased immunoglobulin secretion by B lymphocytes from Trypanosoma cruzi infected mice after B lymphocytes-natural killer cell interaction. *Parasite Immunol* 23:581-586.
150. Hulikova, K., J. Svoboda, V. Benson, V. Grobarova, and A. Fiserova. 2011. N-Acetyl-d-glucosamine-coated polyamidoamine dendrimer promotes tumor-specific B cell responses via natural killer cell activation. *Int Immunopharmacol*.